



**ADDITIONAL MATERIALS AVAILABLE ON THE HEI WEBSITE**

**Research Report 210**

**Global Burden of Disease from Major Air Pollution Sources**

**(GBD MAPS): A Global Approach**

**Erin McDuffie et al.**

**Additional Materials 1: McDuffie EE, Smith SJ, O'Rourke P, Tibrewal K, Venkataraman C, Marais EA, et al. 2020. A global anthropogenic emission inventory of atmospheric pollutants from sector- and fuel-specific sources (1970–2017): An application of the Community Emissions Data System (CEDS). *Earth Syst Sci Data* 12:3413–3442; doi:10.5194/essd-12-3413-2020.**

Additional Materials 1 was not formatted or edited by HEI. It is distributed under the Creative Commons Attribution 4.0 License. This document was part of the HEI Special Review Panel's review process.

---

Correspondence concerning the Investigators' Report may be addressed to Dr. Michael Brauer, The University of British Columbia, School of Population and Public Health, 366A – 2206 East Mall, Vancouver, BC V6T1Z3, Canada; e-mail: [michael.brauer@ubc.ca](mailto:michael.brauer@ubc.ca), [guxens@isglobal.org](mailto:guxens@isglobal.org).

© 2021 Health Effects Institute, 75 Federal Street, Suite 1400, Boston, MA 02110



# A global anthropogenic emission inventory of atmospheric pollutants from sector- and fuel-specific sources (1970–2017): an application of the Community Emissions Data System (CEDs)

Erin E. McDuffie<sup>1,2</sup>, Steven J. Smith<sup>3</sup>, Patrick O'Rourke<sup>3</sup>, Kushal Tibrewal<sup>4</sup>, Chandra Venkataraman<sup>4</sup>,  
Eloise A. Marais<sup>5,a</sup>, Bo Zheng<sup>6</sup>, Monica Crippa<sup>7</sup>, Michael Brauer<sup>8,9</sup>, and Randall V. Martin<sup>2,1</sup>

<sup>1</sup>Department of Physics and Atmospheric Science, Dalhousie University, Halifax, NS, Canada

<sup>2</sup>Department of Energy, Environmental, and Chemical Engineering, Washington University in St. Louis,  
St. Louis, MO, USA

<sup>3</sup>Joint Global Change Research Institute, Pacific Northwest National Laboratory, College Park, MD, USA

<sup>4</sup>Department of Chemical Engineering, Indian Institute of Technology Bombay, Mumbai, Maharashtra, India

<sup>5</sup>School of Physics and Astronomy, University of Leicester, Leicester, UK

<sup>6</sup>Institute of Environment and Ecology, Tsinghua Shenzhen International Graduate School, Tsinghua  
University, Shenzhen 518055, China

<sup>7</sup>European Commission, Joint Research Centre (JRC), Via E. Fermi 2749 (T.P. 123), 21027 Ispra, Varese, Italy

<sup>8</sup>School of Population and Public Health, University of British Columbia, Vancouver, BC, Canada

<sup>9</sup>Institute for Health Metrics and Evaluation, University of Washington, Seattle, WA, USA

<sup>a</sup>now at: Department of Geography, University College London, London, UK

**Correspondence:** Erin E. McDuffie (erin.mcduffie@wustl.edu)

Received: 27 April 2020 – Discussion started: 3 June 2020

Revised: 4 October 2020 – Accepted: 27 October 2020 – Published: 15 December 2020

**Abstract.** Global anthropogenic emission inventories remain vital for understanding the sources of atmospheric pollution and the associated impacts on the environment, human health, and society. Rapid changes in today's society require that these inventories provide contemporary estimates of multiple atmospheric pollutants with both source sector and fuel type information to understand and effectively mitigate future impacts. To fill this need, we have updated the open-source Community Emissions Data System (CEDs) (Hoesly et al., 2019) to develop a new global emission inventory, CEDs<sub>GBD-MAPS</sub>. This inventory includes emissions of seven key atmospheric pollutants (NO<sub>x</sub>; CO; SO<sub>2</sub>; NH<sub>3</sub>; non-methane volatile organic compounds, NMVOCs; black carbon, BC; organic carbon, OC) over the time period from 1970–2017 and reports annual country-total emissions as a function of 11 anthropogenic sectors (agriculture; energy generation; industrial processes; on-road and non-road transportation; separate residential, commercial, and other sectors (RCO); waste; solvent use; and international shipping) and four fuel categories (total coal, solid biofuel, the sum of liquid-fuel and natural-gas combustion, and remaining process-level emissions). The CEDs<sub>GBD-MAPS</sub> inventory additionally includes monthly global gridded (0.5° × 0.5°) emission fluxes for each compound, sector, and fuel type to facilitate their use in earth system models. CEDs<sub>GBD-MAPS</sub> utilizes updated activity data, updates to the core CEDs default scaling procedure, and modifications to the final procedures for emissions gridding and aggregation. Relative to the previous CEDs inventory (Hoesly et al., 2018), these updates extend the emission estimates from 2014 to 2017 and improve the overall agreement between CEDs and two widely used global bottom-up emission inventories. The

CEDS<sub>GBD-MAPS</sub> inventory provides the most contemporary global emission estimates to date for these key atmospheric pollutants and is the first to provide global estimates for these species as a function of multiple fuel types and source sectors. Dominant sources of global NO<sub>x</sub> and SO<sub>2</sub> emissions in 2017 include the combustion of oil, gas, and coal in the energy and industry sectors as well as on-road transportation and international shipping for NO<sub>x</sub>. Dominant sources of global CO emissions in 2017 include on-road transportation and residential biofuel combustion. Dominant global sources of carbonaceous aerosol in 2017 include residential biofuel combustion, on-road transportation (BC only), and emissions from the waste sector. Global emissions of NO<sub>x</sub>, SO<sub>2</sub>, CO, BC, and OC all peak in 2012 or earlier, with more recent emission reductions driven by large changes in emissions from China, North America, and Europe. In contrast, global emissions of NH<sub>3</sub> and NMVOCs continuously increase between 1970 and 2017, with agriculture as a major source of global NH<sub>3</sub> emissions and solvent use, energy, residential, and the on-road transport sectors as major sources of global NMVOCs. Due to similar development methods and underlying datasets, the CEDS<sub>GBD-MAPS</sub> emissions are expected to have consistent sources of uncertainty as other bottom-up inventories. The CEDS<sub>GBD-MAPS</sub> source code is publicly available online through GitHub: [https://github.com/emcduffie/CEDS/tree/CEDS\\_GBD-MAPS](https://github.com/emcduffie/CEDS/tree/CEDS_GBD-MAPS) (last access: 1 December 2020). The CEDS<sub>GBD-MAPS</sub> emission inventory dataset (both annual country-total and monthly global gridded files) is publicly available under <https://doi.org/10.5281/zenodo.3754964> (McDuffie et al., 2020c).

## 1 Introduction

Human activities emit a complex mixture of chemical compounds into the atmosphere, impacting air quality, the environment, and population health. For instance, direct emissions of nitric oxide (NO) rapidly oxidize to form nitrogen dioxide (NO<sub>2</sub>) and can lead to net ozone (O<sub>3</sub>) production in the presence of sunlight and oxidized volatile organic compounds (VOCs) (e.g., Chameides, 1978; Crutzen, 1970). In addition, direct emissions of particles containing organic carbon (OC) and black carbon (BC) as well as secondary reactions involving gaseous sulfur dioxide (SO<sub>2</sub>), NO, ammonia (NH<sub>3</sub>), and VOCs can lead to atmospheric fine particulate matter less than 2.5 μm in diameter (PM<sub>2.5</sub>) (e.g., Mozurkewich, 1993; Jimenez et al., 2009; Saxena and Seigneur, 1987; Brock et al., 2002). PM<sub>2.5</sub> concentrations were estimated to account for nearly 3 million deaths worldwide in 2017 (GBD 2017 Risk Factor Collaborators, 2018), while surface O<sub>3</sub> concentrations were associated with nearly 500 000 deaths in 2017 (GBD 2017 Risk Factor Collaborators, 2018) and significant global crop losses, valued at USD 11 billion in 2000 (USD<sub>2000</sub>) (Avnery et al., 2011; Ainsworth, 2017). In addition, atmospheric O<sub>3</sub> and aerosol both impact earth's radiative budget (e.g., Bond et al., 2013; Haywood and Boucher, 2000; US EPA, 2018). Other pollutants, including carbon monoxide (CO), NO<sub>2</sub>, and SO<sub>2</sub>, are also directly hazardous to human health (US EPA, 2018), while NO<sub>2</sub> and SO<sub>2</sub> can additionally contribute to acid rain (Saxena and Seigneur, 1987; US EPA, 2018) and indirectly impact human health via their contributions to secondary PM<sub>2.5</sub> formation. In addition, NH<sub>3</sub> deposition and nitrification can also cause nutrient imbalances and eutrophication in terrestrial and marine ecosystems (e.g., Behera et al., 2013; Stevens et al., 2004). While these reactive gases and aerosol have both anthropogenic and natural sources, domi-

nant global sources of NO<sub>x</sub> (= NO + NO<sub>2</sub>), SO<sub>2</sub>, CO, and VOCs include fuel transformation and use in the energy sector, industrial activities, and on-road and off-road transportation (Hoesly et al., 2018). Global NH<sub>3</sub> emissions are predominantly from agricultural activities such as animal husbandry and fertilizer application (e.g., Behera et al., 2013), and OC and BC have large contributions from incomplete or uncontrolled combustion in residential and commercial settings (e.g., Bond et al., 2013). Emissions of these compounds and the distribution of their chemical products vary spatially and temporally, with atmospheric lifetimes that allow for their transport across political boundaries, continuously driving changes in the composition of the global atmosphere.

Global emission inventories of these major atmospheric pollutants, with both sectoral and fuel type information, are paramount (1) for understanding the range of emission impacts on the environment and human health and (2) for developing effective strategies for pollution mitigation. For example, spatially gridded emission inventories are used as inputs in general circulation climate (GCM) and chemical transport models (CTM), which are used to predict the evolution of atmospheric constituents over space and time. By perturbing emission sources or historical emission trends, such models can quantify the impact of emissions on the environment, economy, and human health (e.g., Mauzerall et al., 2005; Lelieveld et al., 2019; IPCC, 2013; Liang et al., 2018; Lacey and Henze, 2015); provide mitigation-relevant information for polluted regions (e.g., GBD MAPS Working Group, 2016, 2018; RAQC, 2019; Lacey et al., 2017); and anchor future projections (e.g., Shindell and Smith, 2019; Venkataraman et al., 2018; Gidden et al., 2019; Mickley et al., 2004).

Three global emission inventories have been widely used for these purposes, including the Emissions Database for

Global Atmospheric Research (EDGAR) from the European Commission Joint Research Centre (Crippa et al., 2018), the ECLIPSE (Evaluating the Climate and Air Quality Impacts of Short-Lived Pollutants) inventory from the Greenhouse Gas–Air Pollution Interactions and Synergies (GAINS) model at the International Institute for Applied Systems Analysis (IIASA) (Amann et al., 2011; Klimont et al., 2017), and the CEDS (v2016-07-26) inventory from the newly developed Community Emissions Data System (CEDS) from the Joint Global Change Research Institute at the Pacific Northwest National Laboratory and University of Maryland (Hoesly et al., 2018). All three inventories are derived using a bottom-up approach where emissions are estimated using reported activity data (e.g., amount of fuel consumed) and source- and region-specific (where available) emission factors (mass of emitted pollutant per mass of fuel consumed) for each emitted compound. All three inventories are similar in that they use this bottom-up approach to provide historical, source-specific gridded emission estimates of major atmospheric pollutants ( $\text{NO}_x$  (as  $\text{NO}_2$ );  $\text{SO}_2$ ;  $\text{CO}$ ; non-methane volatile organic compounds, NMVOCs;  $\text{NH}_3$ ;  $\text{BC}$ ; and  $\text{OC}$ ). Table 1 provides a comparison of the key features between these inventories, which provide emissions from multiple source sectors over the collective time period from 1750–2014. In contrast to EDGAR and GAINS, the CEDS system implements an increasingly utilized mosaic approach, which, in this case, incorporates activity and emission input data from other sources such as EDGAR, GAINS, and regional- and national-level inventories to produce global emissions that are both historically consistent and reflective of contemporary country-level estimates (Hoesly et al., 2018). The CEDS source code has been publicly released (<https://github.com/JGCRI/CEDS/tree/master>, last access: 1 December 2020), increasing both the reproducibility and public accessibility to quality emission estimates of global- and national-level air pollutants.

Due to the long development times of global bottom-up inventories, current versions of the EDGAR, ECLIPSE, and CEDS inventories are limited in their ability to capture emission trends over recent years (Table 1), particularly the last 6–10 years in regions undergoing rapid change such as China, North America, Europe, India, and Africa. For example, China implemented the Action Plan on the Prevention and Control of Air Pollution in 2013, which has targeted specific emission sectors, fuels, and species and resulted in reductions in ambient  $\text{PM}_{2.5}$  concentrations by up to 40 % in metropolitan regions between 2013 and 2017 (reviewed in Zheng et al., 2018). Similarly, over the past 10–20 years in the US and Europe, the reduction in coal-fired power plant emissions and phase-in of stricter vehicle emission standards have resulted in emission reductions in  $\text{SO}_2$  and  $\text{NO}_x$  across these regions (Krotkov et al., 2016; Duncan et al., 2013; Castellanos and Boersma, 2012; de Gouw et al., 2014). Over this same time period, however, oil and gas production in key regions in the US has more than tripled be-

tween 2007 and 2017 (EIA, 2020). In addition, the absence of widespread regulations targeting  $\text{NH}_3$  from agricultural practices has led to continuous increases in global  $\text{NH}_3$  emissions (Behera et al., 2013). Global energy consumption also increased by an average of 1.5 % each year between 2008 and 2018 (BP, 2019), and the global consumption of coal increased for the first time in 2017 since its peak in 2013 (BP, 2019). Many of these energy changes have been attributed to the growth of energy generation in rapidly growing regions, such as India (BP, 2019). Africa is also experiencing rapid growth, with increasing emissions from diffuse and inefficient combustion sources, which may not be accurately accounted for in current global inventories (Marais and Wiedinmyer, 2016). Therefore, to capture recent trends around the globe as well as quantify the resulting economic, health, and environmental impacts and mitigate future burdens, computational models require emission inventories with regionally accurate estimates, global coverage, and the most up-to-date information possible. Though global bottom-up inventories can lag in time due to data collection and reporting requirements, the incorporation of smaller regional inventories provides the opportunity to improve the timeliness and regional accuracy of global estimates.

To further increase the policy relevance of such data, it is also important that global emission inventories not only provide contemporary estimates but report emissions as a function of detailed source sector and fuel type. For example, the recent air quality policies in China have included emission reductions targeting coal-fired power plants within the larger energy generation sector (e.g., Zheng et al., 2018). Decisions to implement such policies require accurate predictions of the air quality benefits, which in turn depend on simulations that use accurate estimates of contemporary sector- and fuel-specific emissions. While the EDGAR, ECLIPSE, and CEDS inventories all provide varying degrees of sectoral information (Table 1), there are no global inventories to date that provide public datasets of multiple atmospheric pollutants with both detailed source sector and fuel type information. Crippa et al. (2019) do describe estimates of biofuel use from the residential sector in Europe using emissions from the EDGAR v4.3.2 inventory (EC-JRC, 2018) but do not report global estimates or regional emissions from other fuel types. Similarly, Hoesly et al. (2018) describe fuel-specific activity data and emission factors used to develop the global CEDS v2016-07-26 inventory but do not publicly report final global emissions as a function of fuel type. In contrast, a limited number of regional inventories have provided both fuel- and sector-specific emissions. These inventories, for example, have been applied to earth system models to attribute the mortality associated with outdoor air pollution to dominant sources of ambient  $\text{PM}_{2.5}$  mass, such as residential biofuel combustion in India and coal combustion in China (GBD MAPS Working Group, 2018, 2016). As countries undergo rapid changes that impact fluxes of their emitted pollutants, including population, emission capture technologies, and the

**Table 1.** Comparison of three historical, gridded, source-specific emission inventories of atmospheric pollutants (NO<sub>x</sub>, SO<sub>2</sub>, CO, NMVOCs, NH<sub>3</sub>, BC, OC).

Inventory name (version)	Temporal coverage	Number of reported gridded sectors	Detailed fuels	Spatial resolution	Reference
CEDS (v2016_07_26)	1750–2014	9	Total only	0.5° × 0.5°	Hoesly et al. (2018)
EDGAR (v4.3.2)	1970–2012	26	Biofuel (Europe only) <sup>b</sup>	0.1° × 0.1°	Crippa et al. (2018)
ECLIPSE (v5a)	1990, 1995, 2000, 2005, 2010 (projections to 2050) <sup>a</sup>	8	Total only	0.5° × 0.5°	Klimont et al. (2017), Amann et al. (2011)

<sup>a</sup> Projections assume current air pollution legislation (CLE) in the GAINS model. <sup>b</sup> Described in Crippa et al. (2019).

mix of fuels used, fuel- and source-specific estimates are vital for capturing these contemporary changes and understanding the air quality impacts across multiple scales.

As part of the Global Burden of Disease – Major Air Pollution Sources (GBD-MAPS) project, which aims to quantify the disease burden associated with dominant country-specific sources of ambient PM<sub>2.5</sub> mass (<https://sites.wustl.edu/acag/datasets/gbd-maps/>, last access: 1 December 2020), we have updated and utilized the CEDS open-source emissions system to produce a new global anthropogenic emission inventory (CEDS<sub>GBD-MAPS</sub>). CEDS<sub>GBD-MAPS</sub> includes country-level and global gridded (0.5° × 0.5°) emissions of seven major atmospheric pollutants (NO<sub>x</sub> (as NO<sub>2</sub>), CO, NH<sub>3</sub>, SO<sub>2</sub>, NMVOCs, BC, OC) as a function of 11 detailed emission source sectors (agriculture, energy generation, industry, on-road transportation, non-road and off-road transportation, residential energy combustion, commercial combustion, other combustion, solvent use, waste, and international shipping) and four fuel groups (emissions from the combustion of total coal, solid biofuel, liquid fuels and natural gas, plus all remaining process-level emissions) for the time period between 1970–2017. Similar to the prior CEDS inventory released for CMIP6 (Hoesly et al., 2018), CEDS<sub>GBD-MAPS</sub> provides surface-level emissions from all sectors, including fertilized soils, but does not include emissions from open burning. In the first two sections we provide an overview of the CEDS<sub>GBD-MAPS</sub> system and describe the updates that have allowed for the extension to the year 2017 and the added fuel type information. These include updates to the underlying activity data and input emission inventories used for default estimates and scaling procedures (including the use of two new inventories from Africa and India), the additional scaling of default BC and OC emissions, the use of updated spatial gridding proxies, and adjustments to the final gridding and aggregation steps that retain detailed sub-sector and fuel type information. The third section presents global CEDS<sub>GBD-MAPS</sub> emissions in 2017 and discusses historical trends as a function of compound, sector, fuel type, and world region. The final section provides a comparison of the global CEDS<sub>GBD-MAPS</sub> emissions with other global inventories as well as a discussion of the magnitude and sources of uncertainty associated with the CEDS<sub>GBD-MAPS</sub> products.

## 2 Methods

The 23 December 2019 full release of the Community Emissions Data System (Hoesly et al., 2019) provides the core system framework for the development of the contemporary CEDS<sub>GBD-MAPS</sub> inventory. The CEDS<sub>GBD-MAPS</sub> inventory is developed for the GBD-MAPS project and is not an updated release of the core CEDS emissions inventory. As detailed in Hoesly et al. (2018), the original version of the CEDS system was used to produce the first CEDS v2016-07-26 inventory (hereafter called CEDS<sub>Hoesly</sub>) (CEDS, 2017a, b), which provides global gridded (0.5° × 0.5°) emissions of atmospheric reactive gases (NO<sub>x</sub> (as NO<sub>2</sub>), SO<sub>2</sub>, NH<sub>3</sub>, NMVOCs, CO), carbonaceous aerosol (BC, OC), and greenhouse gases (CO<sub>2</sub>, CH<sub>4</sub>) from eight anthropogenic sectors (agriculture – AGR; transportation – TRA; energy – ENE; industry – IND; residential, commercial, other – RCO; solvents – SLV; waste – WST; international shipping – SHP) over the time period from 1750–2014. Here we provide a brief overview of the Community Emissions Data System with detailed descriptions of the major updates that have been implemented to produce the new CEDS<sub>GBD-MAPS</sub> inventory. This inventory has been extended to provide emissions from 1970–2017 for reactive gases and carbonaceous aerosol (NO<sub>x</sub>, SO<sub>2</sub>, NMVOCs, NH<sub>3</sub>, CO, BC, OC) with increased fuel and sectoral information relative to the CEDS<sub>Hoesly</sub> inventory (Sect. 2.2–2.3). Updates primarily include the use of updated input datasets (Sect. 2.1), new and updated global and regional scaling inventories (Sect. 2.2), added scaling of default BC and OC emissions (Sect. 2.3), and the disaggregation of emissions into contributions from additional source sectors and multiple fuel types (Sect. 2.4).

### 2.1 Overview of CEDS<sub>GBD-MAPS</sub> system

The CEDS system has five key procedural steps, illustrated in Fig. 1. After the collection of input data in Step 0, Step 1 calculates default global emission estimates (Em) for each chemical compound using a bottom-up approach shown in Eq. (1). In Eq. (1), emissions are calculated using relevant activity (A) and emission factor (EF) data for each country (c) and year (y) as a function of 52 detailed working sectors (s) (sub-sectors used for intermediate steps in the CEDS sys-

tem) and nine working fuel types (f) (Table 2). CEDS conducts these calculations for two types of emission categories: (1) fuel combustion sources (e.g., electricity production, industrial machinery, on-road transportation, etc.) and (2) process sources (e.g., metal production, chemical industry, manure management, etc.). We note that the distinction between these source categories is reflective of both sector definition and CEDS methodology, as described further in Sect. S2.1 in the Supplement. This results in some working sectors that include emissions from combustion, such as waste incineration and fugitive petroleum and gas emissions, to be characterized in the CEDS system as process-level sources (further details in Sect. S2.1). In contrast to CEDS combustion source emissions, which are calculated in Eq. (1) as a function of eight fuel types, emissions from CEDS process-level sources are combined into a single “process” category, as described in Sect. 2.4. Table 2 provides a complete list of CEDS<sub>GBD-MAPS</sub> working sectors and fuel types as well as source category distinctions.

$$Em_{\text{species}}^{\text{country, sector, fuel, year}} = A^{\text{c,s,f,y}} \times EF_{\text{species}}^{\text{c,s,f,y}} \quad (1)$$

For emissions from CEDS combustion sources, annual activity drivers in Eq. (1) primarily include country-, fuel-, and sector-specific energy consumption data from the International Energy Agency (IEA, 2019). Sector- and compound-specific emission factors are typically derived from energy use and total emissions reported from other inventories, including from the GAINS model (Klimont et al., 2017; IIASA, 2014; Amann et al., 2015), Speciated Pollutant Emission Wizard (SPEW) (Bond et al., 2007), and the US National Emissions Inventory (NEI) (NEI, 2013). For international shipping, IEA activity data are supplemented with consumption data and EFs from the International Maritime Organization (IMO), as described in Hoesly et al. (2018) and its supplement. In contrast, default emissions ( $Em$ ) for CEDS process sources are directly taken from other inventories, including from the EDGAR v4.3.2 global emission inventory (EC-JRC, 2018; Crippa et al., 2018). “Implied emission factors” are then calculated for these process sources in Eq. (1) using global population data (UN, 2019, 2018) or pulp and paper consumption (FAOSTAT, 2015) as the primary activity drivers. For years without available emissions, default estimates for CEDS process sources are calculated in Eq. (1) from a linear interpolation of the “implied emission factors” and available activity data ( $A$ ) for that year. Supplement Sects. S2.1 and S2.2 provide additional details regarding the input datasets for activity drivers and emission factors used for both CEDS combustion and process source categories.

While CEDS Step 1 is designed to provide a complete set of historical emission estimates, CEDS Step 2 scales these total default emission estimates to existing, authoritative global-, regional-, and national-level inventories. As described in Hoesly et al. (2018), CEDS uses a “mosaic” scaling approach to retain detailed fuel- and sector-specific information across different inventories while maintaining con-

sistent methodology over space and time. The development and use of mosaic inventories has been recently increasing as they provide a means to utilize detailed local emissions while harmonizing this information across large regional or global scales (C. Li et al., 2017; Janssens-Maenhout et al., 2015). The CEDS approach, however, differs from previous mosaic inventories (e.g., Janssens-Maenhout et al., 2015), in that local and regional inventories in CEDS<sub>GBD-MAPS</sub> are used to scale sectoral emissions at the national level rather than merge together spatially distributed gridded estimates.

The first step in the scaling procedure is to derive a time series of scaling factors (SFs) for each scaling inventory using Eq. (2), calculated as a function of chemical compound, country, sector, and fuel type (where available). Due to persistent differences and uncertainties in the underlying activity data and sectoral definitions in each scaling inventory, CEDS emissions are scaled to total emissions within aggregate scaling sectors (and fuels, where applicable). These aggregate scaling groups are defined for each scaling inventory and are chosen to be broad in order to improve the overlap between CEDS emission estimates and those reported in other inventories. For example, the sum of CEDS emissions from working sectors 1A4a\_Commercial-institutional, 1A4b\_Residential, and 1A4c\_agriculture-forestry-fishing are scaled to the aggregate 1A4\_energy-for-buildings sector in the EDGAR v4.3.2 inventory. Sections 2.2 and S2.3 provide further details about this scaling procedure and the scaling inventories used to develop the 1970–2017 CEDS<sub>GBD-MAPS</sub> inventory.

$$SF_{\text{species}}^{\text{c,s,f,y}} = \frac{\text{scaling inventory } Em_{\text{species}}^{\text{c,s,f,y}}}{\text{default CEDS } Em_{\text{species}}^{\text{c,s,f,y}}} \quad (2)$$

After SFs are calculated in Eq. (2), the second step in the scaling procedure is to extend these SFs forward and backward in time to fill years with missing data. For these time periods, the nearest available SF is applied. If a particular sector or compound is not present in a scaling inventory, default CEDS estimates are not scaled. For BC and OC emissions, the default procedure in the CEDS v2019-12-23 system was to retain all default BC and OC emission estimates due to limited availability of historical BC and OC emissions. In the CEDS<sub>GBD-MAPS</sub> inventory, these species are now scaled to available regional- and national-level inventories (further details in Sect. 2.2). For all other species, the CEDS<sub>GBD-MAPS</sub> system uses a sequential scaling methodology where total default emissions for each country are first scaled to available global inventories (primarily EDGAR v4.3.2) and then scaled to regional- and national-level inventories, many of which have been updated in this work (Sect. 2.2 and Table 3). This process results in final CEDS<sub>GBD-MAPS</sub> emissions that reflect the inventory last used to scale the emissions for that country (Fig. 2). Figure S2 in the Supplement provides a time series of implied emission factors after the scaling procedure for select sector and fuel combinations that dominate emis-

**Table 2.** CEDS sector and fuel type definitions. Aggregate sectors and fuel types in the CEDS<sub>Hoesly</sub> (bold) and CEDS<sub>GBD-MAPS</sub> (bold and italic) inventories as well as the system's intermediate gridding sectors (italic) and detailed working sectors and fuel types (consistent between CEDS<sub>Hoesly</sub> and CEDS<sub>GBD-MAPS</sub> inventories). CEDS working sectors are methodologically treated as two different categories: combustion sectors (c) and “process” sectors (p). As described in the text, combustion sector emissions are calculated as a function of CEDS working fuels, while process emissions are assigned to the single “process” fuel type.

CEDS emission sectors	
<b>Energy production (ENE)</b>	<b>Residential, commercial, other (RCO)</b>
<i>Energy production (ENE)</i>	<i>Residential (RCOR)</i>
<i>Electricity and heat production</i>	<i>Res., Comm., Other – Residential</i>
1A1a_Electricity-public (c)	1A4b_Residential (c)
1A1a_Electricity-autoproducer (c)	<b>Commercial (RCOC)</b>
1A1a_Heat-production (c)	<i>Res., Comm., Other – Commercial</i>
<i>Fuel Production and Transformation</i>	1A4a_Commercial-institutional (c)
1A1bc_Other-transformation (p)	<b>Other (RCOO)</b>
1B1_Fugitive-solid-fuels (p)	<i>Res., Comm., Other – Other</i>
<i>Oil and Gas Fugitive/Flaring</i>	1A4c_Agriculture-forestry-fishing (c)
1B2_Fugitive-petr-and-gas (p)	<b>Solvents (SLV)</b>
<i>Fuel Production and Transformation</i>	<i>Solvents (SLV)</i>
1B2d_Fugitive-other-energy (p)	<i>Solvents production and application</i>
<i>Fossil Fuel Fires</i>	2D_Degreasing-Cleaning (p)
7A_Fossil-fuel-fires (p)	2D3_Other-product-use (p)
<b>Industry (IND)</b>	2D_Paint-application (p)
<i>Industry (IND)</i>	2D3_Chemical-products-manufacture-processing (p)
<i>Industrial combustion</i>	<b>Agriculture (AGR)</b>
1A2a_Ind-Comb-Iron-steel (c)	<i>Agriculture (AGR)</i>
1A2b_Ind-Comb-Non-ferrous-metals (c)	<i>Agriculture</i>
1A2c_Ind-Comb-Chemicals (c)	3B_Manure-management (p)
1A2d_Ind-Comb-Pulp-paper (c)	3D_Soil-emissions (p)
1A2e_Ind-Comb-Food-tobacco (c)	3I_Agriculture-other (p)
1A2f_Ind-Comb-Non-metallic-minerals (c)	3D_Rice-Cultivation (p)
1A2g_Ind-Comb-Construction (c)	3E_Enteric-fermentation (p)
1A2g_Ind-Comb-transpequip (c)	<b>Waste (WST)</b>
1A2g_Ind-Comb-machinery (c)	<i>Waste (WST)</i>
1A2g_Ind-Comb-mining-quarrying (c)	<i>Waste</i>
1A2g_Ind-Comb-wood-products (c)	5A_Solid-waste-disposal (p)
1A2g_Ind-Comb-textile-leather (c)	5E_Other-waste-handling (p)
1A2g_Ind-Comb-other (c)	5C_Waste-incineration (p)
1A5_Other-unspecified (c)	5D_Wastewater-handling (p)
<i>Industrial process and product use</i>	<b>Shipping (SHP)</b>
2A1_Cement-production (p)	<i>Shipping (SHP)</i>
2A2_Lime-production (p)	<i>International shipping</i>
2A6_Other-minerals (p)	1A3di_International-shipping (c)
2B_Chemical-industry (p)	<i>Tanker Loading</i>
2C_Metal-production (p)	1A3di_Oil_Tanker_Loading (p)
2H_Pulp-and-paper-food-beverage-wood (p)	
2L_Other-process-emissions (p)	
6A_Other-in-total (p)	
<b>Transportation (TRA)</b>	<b>Transportation Cont. (TRA)</b>
<i>Road transportation (ROAD)</i>	<i>Non-road transportation (NRTR)</i>
<i>Road transportation</i>	<i>Non-road Transportation</i>
1A3b_Road (c)	1A3c_Rail (c)
	1A3dii_Domestic-navigation (c)
	1A3eii_Other-transp (c)
<b>CEDS fuels</b>	
<b>Total</b>	
<i>Coal</i>	<i>Liquid fuel and natural gas</i>
Brown coal	Heavy oil
Coal coke	Diesel oil
Hard coal	Light oil
<i>Biofuel</i>	Natural Gas
Biofuel	<b>Process</b>
	Process

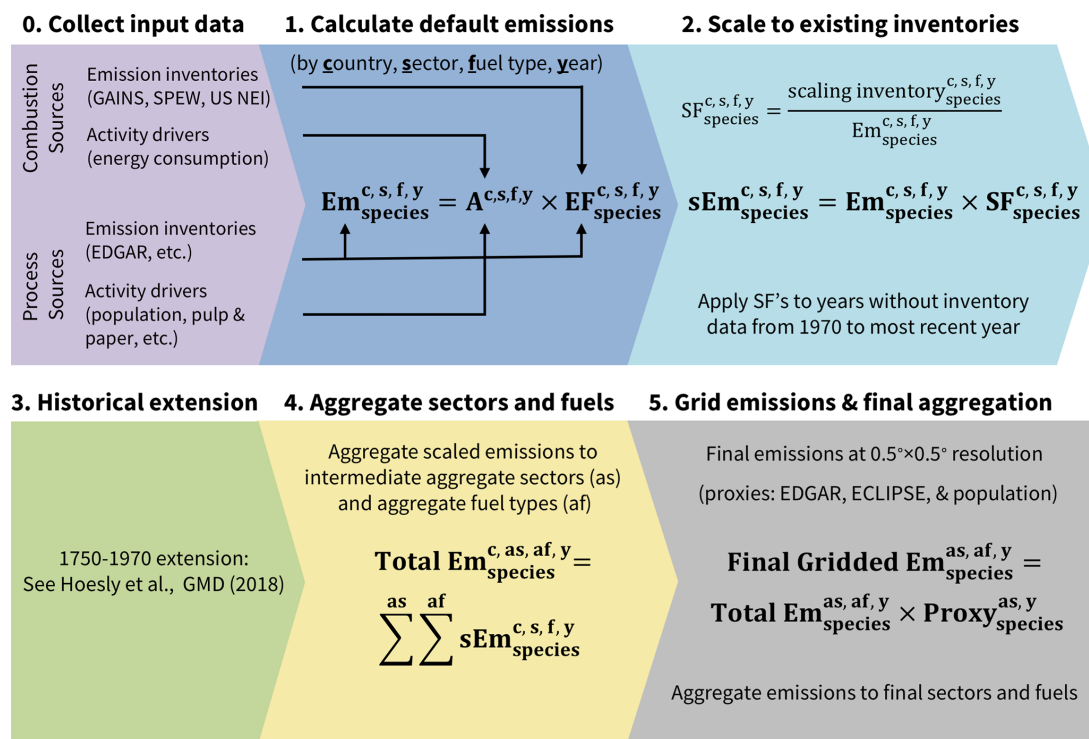


**Figure 1.** Default CEDS system summary, adapted from Fig. 1 in Hoesly et al. (2018). Key steps include (0) collecting activity driver (A) and emission factor (EF) input data for non-combustion and combustion emission sources; (1) calculating default emissions (Em) as a function of chemical species, country, emission sector, fuel type, and year; (2) calculating scaling factors (SFs) for overlapping years with existing inventories in order to scale default estimates (sEm) and extending SFs for non-overlapping years between 1970–2017 (for earlier emissions, see Hoesly et al., 2018); (4) aggregating scaled emissions to intermediate sectors and fuel types; and (5) using source- and compound-specific spatial proxies to calculate final gridded emissions and aggregate them to the final sectors and fuels. A list of intermediate and final sectors and fuels are in Table 2.

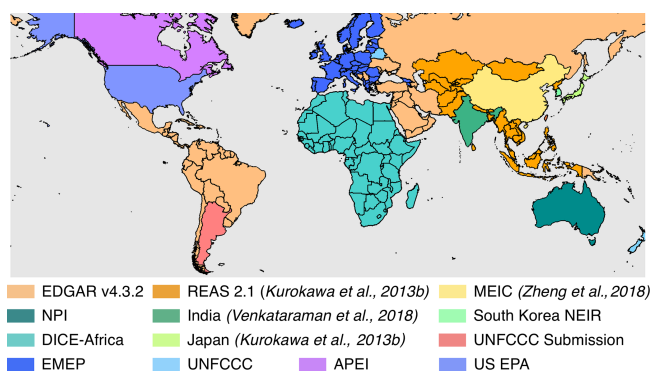


**Figure 2.** Final scaling inventories used for CEDS<sub>GBD-MAPS</sub> NO<sub>x</sub> emissions; inventory details in Table 3.

sions of each compound in the top 15 emitting countries. Sections 2.2 and S2.3 describe further details and updates to this scaling procedure.

CEDS Step 3 extends the scaled emission estimates from 1970 back in time to 1750. This process is necessary as reported emission estimates and energy data are not typically reported with the same level of sectoral and fuel type detail

prior to 1970. Hoesly et al. (2018) provide a detailed description of this historical extension procedure, which is used to derive pre-1970 emissions in the CEDS<sub>Hoesly</sub> inventory. The new CEDS<sub>GBD-MAPS</sub> inventory only reports more contemporary emissions after 1970 and therefore does not utilize this historical extension.

CEDS Step 4 aggregates the scaled country-level CEDS<sub>GBD-MAPS</sub> emissions into 17 intermediate gridding sectors (defined in Table 2). In the CEDS v2019-12-23 system, Step 4 additionally aggregated sectoral emissions from all fuel types. In contrast, the CEDS<sub>GBD-MAPS</sub> system retains sectoral emissions from the combustion of total coal (hard coal + coal coke + brown coal), solid biofuel, the sum of liquid oil (light oil + heavy oil + diesel oil) and natural gas, and all CEDS process-level emissions (Table 2). Sections 2.4 and 4.2.4 describe the CEDS<sub>GBD-MAPS</sub> fuel-specific emissions in further detail.

Lastly, CEDS Step 5 uses normalized spatial-distribution proxies to allocate annual country-level emission estimates onto a 0.5° × 0.5° global grid. Annual emissions from the 17 intermediate gridding sectors and four fuel groups are first distributed spatially using compound-, sector-, and year-specific spatial proxies, primarily from the gridded



**Table 3.** Scaling inventories.

Inventory name	Scaled inventory years	Scaled species	Reference
EDGAR v4.3.2	1992–2012	CO, NH <sub>3</sub> , NMVOCs, NO <sub>x</sub>	(EC-JRC, 2018)
EMEP NFR14	1990–2017	CO, NH <sub>3</sub> , NMVOCs, NO <sub>x</sub> , SO <sub>2</sub> , BC	EMEP (2019)
UNFCCC	1990–2017	CO, NMVOCs, NO <sub>x</sub> , SO <sub>2</sub>	UNFCCC (2019)
REAS 2.1 <sup>a</sup>	2000–2008	CO, NH <sub>3</sub> , NMVOCs, NO <sub>x</sub> , SO <sub>2</sub> , BC	Kurokawa et al. (2013)
APEI (Canada)	1990–2017	CO, NH <sub>3</sub> , NMVOCs, NO <sub>x</sub> , SO <sub>2</sub>	ECCC (2019)
US EPA	1970, 1975, 1980, 1985, 1990–2017	CO, NH <sub>3</sub> , NMVOCs, NO <sub>x</sub> , SO <sub>2</sub>	US EPA (2019)
MEIC (China)	2008, 2010–2017	CO, NH <sub>3</sub> , NMVOCs, NO <sub>x</sub> , SO <sub>2</sub> , BC, OC	Zheng et al. (2018), C. Li et al. (2017)
Argentina <sup>a</sup>	1990–1999, 2011–2009, 2011	CO, NMVOCs, NO <sub>x</sub> , SO <sub>2</sub>	Argentina UNFCCC Submission (2016)
Japan <sup>a</sup>	1960–2010	CO, NH <sub>3</sub> , NMVOCs, NO <sub>x</sub> , SO <sub>2</sub> , BC, OC	preliminary update from Kurokawa et al. (2013)
NEIR (South Korea) <sup>a</sup>	1999–2012	CO, NMVOCs, NO <sub>x</sub> , SO <sub>2</sub>	South Korea National Institute of Environmental Research (2016)
Taiwan <sup>a</sup>	2003, 2006, 2010	CO, NMVOCs, NO <sub>x</sub> , SO <sub>2</sub>	TEPA (2016)
NPI (Australia)	2000–2017	CO, NMVOCs, NO <sub>x</sub> , SO <sub>2</sub>	ADE (2019)
DICE-Africa <sup>b</sup>	2006, 2013	CO, NMVOCs, NO <sub>x</sub> , SO <sub>2</sub> , BC, OC	Marais and Wiedinmyer (2016)
SMoG-India <sup>b</sup>	2015	CO, NMVOCs, NO <sub>x</sub> , SO <sub>2</sub> , BC, OC	Venkataraman et al. (2018)

<sup>a</sup> Not updated from CEDS v2019-12-23; details in Hoesly et al. (2018). <sup>b</sup> Emissions scaled as a function of sector and fuel type.

EDGAR v4.3.2 inventory. Supplement Table S7 provides a complete list of sector-specific gridding proxies. Details about the general CEDS gridding procedure are provided in Feng et al. (2020), with additional details specific to the CEDS<sub>GBD-MAPS</sub> system in Sect. S2.5. Second, gridded emission fluxes (units: kg m<sup>-2</sup> s<sup>-1</sup>) are aggregated into 11 final sectors (Table 2) and distributed over 12 months using sectoral and spatially explicit monthly fractions from the ECLIPSE project (IIASA, 2015) and EDGAR inventory (international shipping only). Relative to CEDS v2019-12-23, the new CEDS<sub>GBD-MAPS</sub> inventory retains detailed sub-sector emissions from the aggregate RCO (now RCO-residential, RCO-commercial, and RCO-other) and TRA (now on-road and non-road) sectors; separate sectoral emissions from process sources; and combustion sources that utilize coal, solid biofuel, and the sum of liquid fuels and natural gas. Table 2 contains a complete breakdown of the definitions of CEDS working, intermediate gridding, and final sectors. Gridded total NMVOCs are additionally disaggregated into 25 VOC classes following sector- and country-specific VOC speciation maps from the RETRO project (HTAP2, 2013), which are different from those used in the recent EDGAR v4.3.2 inventory (Huang et al., 2017). Similar to the gridding procedure, the same VOC speciation and monthly distributions are applied to sectoral emissions associated with each fuel category.

Final products from the CEDS<sub>GBD-MAPS</sub> system include total annual emissions from 1970–2017 for each country as well as monthly global gridded (0.5° × 0.5°) emission fluxes, both as a function of 11 final source sectors and four fuel categories (total coal, solid biofuel, liquid fuel + natural gas, and remaining process sources). Section 5 provides additional details on the dataset availability and file formats.

## 2.2 Default emission-scaling procedure – CEDS<sub>GBD-MAPS</sub> update details

As described above, default emission estimates for each compound are scaled in CEDS Step 2 to existing authoritative inventories as a function of emission sector and fuel type (where available). In the scaling procedure, annual emissions and EFs for each country are first scaled to available global inventories, then to available regional- and national-level inventories, assuming that the latter use local knowledge to derive more accurate regional estimates. Final CEDS<sub>GBD-MAPS</sub> emission totals for each country therefore reflect the inventory last used to scale each compound and sector. Many of these inventories are updated annually and, where available, have been updated in this work relative to the CEDS v2019-12-23 system (Table 3). For example, global CEDS<sub>GBD-MAPS</sub> combustion source emissions of NO<sub>x</sub>, total NMVOCs, CO, and NH<sub>3</sub> are first scaled to EDGAR v4.3.2 country-level emissions as a means to incorporate additional country-specific information relative to default estimates derived using more regionally aggregate EFs from GAINS. CEDS<sub>GBD-MAPS</sub> emissions from European countries are then scaled to available EMEP (European Monitoring and Evaluation Programme) (EMEP, 2019) and UNFCCC (United Nations Framework Convention on Climate Change) (UNFCCC, 2019) inventories that extend to 2017, while CO, NMVOCs, NO<sub>x</sub> and SO<sub>2</sub> emissions from the US, Canada, and Australia are scaled to emissions that extend to 2017 from the US NEI (US EPA, 2019), Canadian APEI (Air Pollutant Emissions Inventory) (ECCC, 2019), and Australian NPI (National Pollutant Inventory) (ADE, 2019), respectively. In addition, emissions of all seven compounds from China are scaled to emissions for 2008, 2010, and 2012 from C. Li et al. (2017), followed by subsequent scaling to emissions between 2010 and 2017 from Zheng et al. (2018). Relative to the CEDS v2019-12-23 system, regional inventories have also been added to scale CEDS<sub>GBD-MAPS</sub> emissions

from India and Africa as described below. Updates to additional regional scaling inventories, including South Korea, Japan, and other European and Asian countries, are not available relative to those used in the CEDS v2019-12-23 system. Table 3 provides a complete list of the inventories used to scale CEDS<sub>GBD-MAPS</sub> default emissions, with additional details in Sect. S2.3.

Relative to the CEDS v2019-12-23 system, the CEDS<sub>GBD-MAPS</sub> system adds scaling inventories for two rapidly changing regions, Africa and India. First, CEDS<sub>GBD-MAPS</sub> emissions from Africa for select sectors are now scaled to the Diffuse and Inefficient Combustion Emissions in Africa (DICE-Africa) inventory from Marais and Wiedinmyer (2016). This inventory provides gridded ( $0.1^\circ \times 0.1^\circ$ ) emissions for  $\text{NO}_x$  ( $= \text{NO} + \text{NO}_2$ ),  $\text{SO}_2$ , 25 speciated VOCs,  $\text{NH}_3$ , CO, BC, and OC for 2006 and 2013 for select anthropogenic sectors and fuels. In this work, default CEDS emissions are scaled to total DICE-Africa emissions from each country and later re-gridded in CEDS Step 5 using source-specific spatial proxies described in Sect. 2.1. Following the CEDS v2019-12-23 scaling procedure (Supplement Sect. S2.3), a set of aggregate scaling sectors and fuels are defined to ensure that CEDS<sub>GBD-MAPS</sub> emissions are scaled to emissions from consistent sectors and fuel types within the DICE-Africa inventory (Table S3). Briefly, CEDS<sub>GBD-MAPS</sub> 1A3b\_Road and 1A4b\_Residential emissions are scaled to DICE-Africa emissions from diesel- and gasoline-powered cars and motorcycles as well as biomass and oil combustion associated with residential charcoal, crop residue, fuelwood, and kerosene use. The DICE-Africa inventory also includes emission estimates from gas flares across Africa and ad hoc oil refining in the Niger Delta, fuelwood use for charcoal production and other commercial enterprises, and gas and diesel use in residential generators. Marais and Wiedinmyer (2016) state that these particular sources are missing or not adequately captured in existing global inventories. Therefore, depending on the source sector and inventory details, they recommend that these emissions be added to existing global inventories for formal industry and on-grid energy production in Africa (DICE-Africa, 2016). Due to uncertainties in the representation of these sectors in the default CEDS Africa emissions, these sources are not included in the scaling process here. Default CEDS<sub>GBD-MAPS</sub> emissions from the 1B2\_fugitive\_pert\_gas (gas flaring) sector (derived from the ECLIPSE and EDGAR inventories) are larger than DICE-Africa gas flaring emissions in 2013, suggesting that this source may be accurately represented in the default CEDS<sub>GBD-MAPS</sub> estimates. As described in Sect. S2.3.2, however, residential generator and fuelwood use for charcoal production and other commercial activities are not explicitly represented in CEDS and will be accounted for only to the extent that these sources are included in the underlying IEA activity data and EDGAR process emission estimates. In the event that the DICE-Africa emissions from these sources

are missing in the default CEDS estimates, total 2013 CEDS<sub>GBD-MAPS</sub> emissions from Africa for each compound may be underestimated by up to 11 % (Sect. S2.3, Table S5). These values range from 0.7 % for  $\text{SO}_2$  to 11 % for CO (Table S5) and all fall within the range of uncertainties typically reported from regional bottom-up inventories ( $> 20\%$ ; Sect. 4.2.3). Final emissions from additional sectors or species in CEDS that are not included in the DICE-Africa inventory are set to CEDS<sub>GBD-MAPS</sub> default values.

Second, emissions from India for select sectors are now scaled to the Speciated Multi-pollutant Generator Inventory described by Venkataraman et al. (2018) (hereafter called SMOG-India). This inventory includes gridded emissions ( $0.25^\circ \times 0.25^\circ$ ) of  $\text{NO}_x$  (as  $\text{NO}_2$ ),  $\text{SO}_2$ , total NMVOCs, CO, BC, and OC for the year 2015 from select anthropogenic sectors and fuels (SMoG-India, 2019). Similar to DICE-Africa emissions, the final spatial distribution in the SMOG-India and CEDS<sub>GBD-MAPS</sub> inventories will differ as country-level emissions are scaled to country totals and spatially re-allocated using CEDS proxies in Step 5. SMOG-India emissions for each compound are available for 17 sectors and nine fuel types (coal, fuel oil, diesel, gasoline, kerosene, naphtha, gas, biomass, and fugitive or process). Similar to the DICE-Africa inventory, aggregate scaling groups have been defined to scale consistent sectors and fuels between inventories, as described in Sect. S2.3. Briefly, default CEDS<sub>GBD-MAPS</sub> emissions for the 1A4c\_Agriculture-forestry-fishing sector are scaled to the sum of SMOG-India emissions for agricultural pumps and tractors; 1A4b\_Residential emissions are scaled to the sum of SMOG-India emissions from residential lighting, cooking, diesel generator use, and space and water heating; 1A1a\_electricity and heat generation sectors are scaled to SMOG-India thermal power plant emissions; 1A3b\_road and rail sectors are scaled to the respective SMOG-India road and rail emissions; and CEDS<sub>GBD-MAPS</sub> industrial working sectors are allocated and scaled to four SMOG-India industrial sectors: light industry (e.g., mining and chemical production), heavy industry (e.g., iron and steel production), informal industry (e.g., food production), and brick production. Calculated scaling factors for these sectors are held constant before and after 2015. CEDS<sub>GBD-MAPS</sub> emissions do not include contributions from open burning and are not scaled to SMOG-India open burning emissions. In cases where SMOG-India emissions are not reported (e.g., power generation from oil combustion), default CEDS<sub>GBD-MAPS</sub> emissions are retained. Section S2.3.3 provides additional details.

To examine the changes in CEDS<sub>GBD-MAPS</sub> emissions associated with the incorporation of the SMOG-India and DICE-Africa scaling inventories as well as the updated underlying input datasets, Fig. 3 compares the total and sectoral distribution of CEDS<sub>GBD-MAPS</sub> and CEDS<sub>Hoesly</sub> emissions for these two regions in 2014 (year with latest overlapping data). For the Africa comparison, panel a in Fig. 3 shows that total  $\text{NO}_x$ , BC, and OC emissions are generally

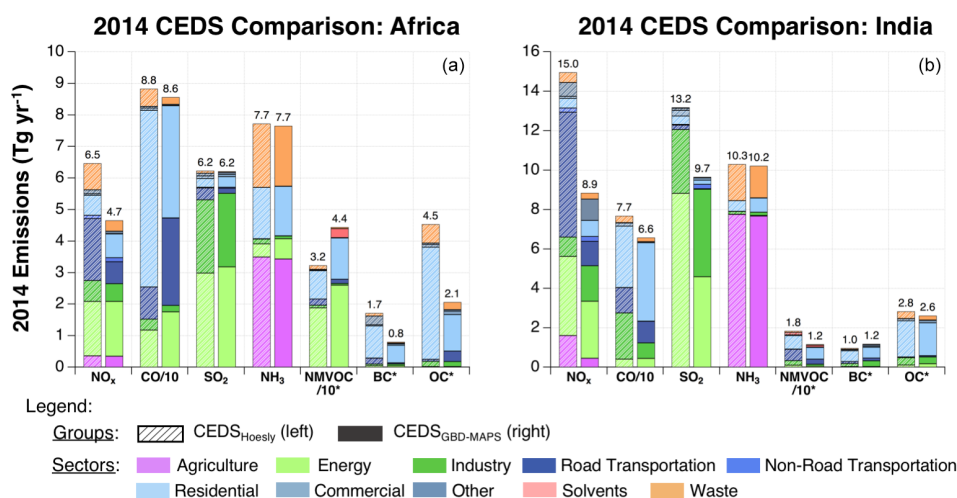


**Figure 3.** Sectoral contributions to total annual emissions for 2014 of CEDS<sub>Hoesly</sub> (a) and CEDS<sub>GBD-MAPS</sub> (b) emissions after scaling to DICE-Africa and SMOG-India regional inventories. The total annual emissions are given by the values above each bar; bar colors represent absolute sectoral contributions to emissions of each chemical compound. CO and NMVOC emissions are divided by 10 for clarity. Stars indicate that NMVOC, BC, and OC emissions are in units of Tg C yr<sup>-1</sup>. NO<sub>x</sub> is in units of Tg NO<sub>2</sub> yr<sup>-1</sup>.

lower in the CEDS<sub>GBD-MAPS</sub> inventory than in CEDS<sub>Hoesly</sub>. Lower NO<sub>x</sub> and OC emissions are largely associated with smaller contributions from on-road transport and residential combustion, respectively, while lower BC emissions are associated with both lower residential and on-road transport contributions. Lower emissions of NO<sub>x</sub> from the transport sector result from the lower EF used for diesel vehicles in the DICE-Africa inventory (Marais et al., 2019). Compared to GAINS (2010) and EDGAR v4.3.2 (2012), on-road emissions from African countries in CEDS<sub>GBD-MAPS</sub> are up to 2.5 Tg lower for NO<sub>x</sub> but within 0.1 Tg for BC. In contrast to NO<sub>x</sub>, larger EFs in the DICE-Africa inventory for on-road emissions of CO and OC result in CEDS<sub>GBD-MAPS</sub> emissions from this sector that are up to 14.8 and 0.3 Tg higher than previous estimates. Figure S2 shows that after scaling, the implied emission factors of CO from oil and gas combustion in the on-road transport sector for four African countries range from 0.19–0.28 g g<sup>-1</sup>, slightly smaller than the range of 0.029–0.380 g g<sup>-1</sup> used in the DICE-Africa inventory. Emissions from the residential and commercial sectors in Africa are generally lower in CEDS<sub>GBD-MAPS</sub> than in CEDS<sub>Hoesly</sub> due to both lower biofuel consumption and a lower assumed EF in the DICE-Africa inventory (Marais and Wiedinmyer, 2016). Residential BC and OC emission estimates are also lower than those from GAINS (Klimont et al., 2017). The difference in biofuel consumption is due to different data sources. The DICE-Africa inventory uses residential wood fuel consumption estimates from the UN, while CEDS<sub>Hoesly</sub> uses data from the IEA. Both of these sources consist largely of estimates for African countries because there is little country-reported biofuel consumption data available. The estimation methodologies for both the UN and IEA estimates are not well documented, which adds

to the uncertainty in these values (Sect. 4.2). After scaling, the implied EFs for residential biofuel emissions of OC are ~0.001–0.002 g g<sup>-1</sup> in three African countries (Fig. S2), within the range of EFs of 0.0007–0.003 g g<sup>-1</sup> implemented in the DICE-Africa inventory. Total CEDS<sub>GBD-MAPS</sub> emissions of NMVOCs are larger, primarily due to increased contributions from solvent use in the energy sector associated with changes in the EDGAR v4.3.2 inventory, while total emissions of CO, SO<sub>2</sub>, and NH<sub>3</sub> are relatively consistent between the two CEDS versions.

For the India comparison, panel b of Fig. 3 shows that total emissions of NO<sub>x</sub>, CO, SO<sub>2</sub>, NMVOCs, and OC are lower in CEDS<sub>GBD-MAPS</sub>. Relative reductions in NO<sub>x</sub> emissions are largely associated with on-road transport. Scaled CEDS<sub>GBD-MAPS</sub> transport emissions are 5 Tg smaller than NO<sub>x</sub> emissions in CEDS<sub>Hoesly</sub>, largely as a result of lower fuel consumption levels for gas, diesel, and compressed natural gas (CNG) on-road vehicles used to develop SMOG-India estimates (Sadavarte and Venkataraman, 2014). Figure S2 shows that the implied emission factor for NO<sub>x</sub> emissions from oil and gas combustion in the on-road transport sector in India is ~0.015 g g<sup>-1</sup> in 2015, which falls within the range of values of 0.0026–0.046 g g<sup>-1</sup> used for various vehicles and fuel type in Venkataraman et al. (2018). Similarly, NO<sub>x</sub> transport emissions are also lower in CEDS<sub>GBD-MAPS</sub> relative to the EDGAR and GAINS inventories. Causes of other reductions relative to the CEDS<sub>Hoesly</sub> are mixed. For example, lower emissions of SO<sub>2</sub> and NMVOCs are largely associated with the energy sector, while reductions in the industry sector contribute to reduced CO emissions. For SO<sub>2</sub>, Fig. S2 shows that the implied EF for coal combustion in the energy sector is ~0.004 g g<sup>-1</sup>, slightly lower than the range of 0.0049–0.0073 g g<sup>-1</sup> used for the SMOG-India inventory.

To further examine the CEDS<sub>GBD-MAPS</sub> inventory in these regions, Fig. 4 compares final CEDS<sub>GBD-MAPS</sub> and CEDS<sub>Hoesly</sub> emissions for India and Africa to total emissions from two widely used global inventories: GAINS (ECLIPSE v5a) and EDGAR (v4.3.2). First, Fig. 4 shows the percent difference between the CEDS<sub>GBD-MAPS</sub> inventory and the GAINS and EDGAR inventories on the y axis against the percent difference between the CEDS<sub>Hoesly</sub> inventory and GAINS and EDGAR emissions on the x axis. Percent differences are calculated from total emissions from Africa (left) and India (right) for the year 2012 for the comparison with EDGAR and for 2010 for the comparison with GAINS (most recent years with overlapping data). The green shaded areas indicate regions where the updated CEDS<sub>GBD-MAPS</sub> inventory has improved agreement with EDGAR or GAINS relative to the CEDS<sub>Hoesly</sub> inventory. This comparison shows that the additional scaling of CEDS<sub>GBD-MAPS</sub> emissions to the SMOG-India inventory generally improves agreement with both the EDGAR and GAINS inventories relative to CEDS<sub>Hoesly</sub> for all species except black carbon (BC). Scaling to the DICE-Africa inventory generally improves CEDS<sub>GBD-MAPS</sub> agreement with the EDGAR inventory but not with GAINS (except for OC). Further comparisons to these two inventories are discussed in Sect. 4. While uncertainties in emissions from these inventories are expected to be at least 20 % for each compound (discussed in Sect. 3.3), this comparison provides an illustration of the changes between the two CEDS versions relative to two widely used global inventories.

### 2.3 Default BC- and OC-scaling procedure – CEDS<sub>GBD-MAPS</sub> update details

Relative to the CEDS v2019-12-23 system, the second-largest change to the CEDS<sub>GBD-MAPS</sub> system is the added scaling of BC and OC emissions in CEDS Step 2. In the v2019-12-23 system, OC and BC were not scaled due to a lack of historical BC and OC emission estimates in regional and global inventories. Due to the focus of the CEDS<sub>GBD-MAPS</sub> inventory on more recent years, these two compounds are now scaled to available regional- and country-level estimates (Table 3) following the same scaling procedure described above for the reactive gases. Unlike the reactive gases, however, BC and OC emissions are not scaled to the global EDGAR v4.3.2 inventory due to the large reported uncertainties in this inventory (ranging from 46.8 % to 153.2 %; Crippa et al., 2018).

To examine the impact of the new BC and OC emissions scaling, in addition to the updated IEA energy consumption data, Figs. 5 and S3–S4 show time series of global BC and OC emissions from CEDS<sub>GBD-MAPS</sub> compared to emissions from the CEDS<sub>Hoesly</sub> inventory. In 2014, respective global annual emissions of BC and OC are 21 % and 28 % lower than the CEDS<sub>Hoesly</sub> inventory and have total global annual emissions in 2017 of 6 and 13 Tg C yr<sup>-1</sup> for BC and

OC, respectively. These reductions in global emissions are largely due to the added scaling of emissions from China, Africa, Japan, and other countries in Asia included in the REAS inventory (Figs. S3–S4). Figures 5 and S3–S4 additionally compare CEDS<sub>GBD-MAPS</sub> emissions to those from the GAINS (ECLIPSE v5a) and EDGAR (v4.3.2) inventories, which generally show improved agreement in BC and OC emissions with the GAINS inventory. CEDS<sub>GBD-MAPS</sub> emissions between 1990 and 2015 are now 7 %–14 % lower than GAINS BC emissions, while CEDS<sub>GBD-MAPS</sub> emissions of OC remain 12 %–25 % higher than GAINS estimates. Further discussion of CEDS<sub>GBD-MAPS</sub> BC and OC emissions and comparisons to EDGAR and GAINS inventories are below in Sect. 4.1.2. As an additional point of comparison, Bond et al. (2013) report global BC and OC values for the year 2000, derived from averages of energy-related burning emissions from SPEW and GAINS. Reported global estimates of BC and OC are 5 and ~11–14 Tg C (16 Tg organic aerosol reported; organic-mass-to-organic-carbon ratio = 1.1–1.4), respectively (Bond et al., 2013). These also have improved agreement with the CEDS<sub>GBD-MAPS</sub> estimates of BC and OC in 2000 relative to those in the CEDS<sub>Hoesly</sub> inventory. Lastly, we note plans for an upcoming update to the core CEDS system to improve historical trends in carbonaceous aerosol by incorporating reported inventory values for total PM<sub>2.5</sub> and its ratio with BC and OC emissions.

### 2.4 Fuel-specific emissions – CEDS<sub>GBD-MAPS</sub> update details

Prior to gridding, CEDS<sub>GBD-MAPS</sub> Step 4 combines total country-level emissions for each of the 52 working sectors and nine fuel groups into 17 aggregate sectors and four fuel groups: total coal (hard coal + brown coal + coal coke), solid biofuel, the sum of liquid fuels (heavy oil + light oil + diesel oil) and natural gas, and all remaining “process” emissions (Table 2). In contrast, the CEDS v2019-12-23 system aggregates all fuel-specific emissions and reports inventory values as a function of sector only. In CEDS<sub>GBD-MAPS</sub>, country-total emissions from these aggregate sectors and fuel groups are distributed across a 0.5° × 0.5° global grid using spatial gridding proxies, as discussed in Sect. 2.1 (Table S7). During gridding, the same spatial proxies are applied to all fuel groups within each sector. In practice, this requires that the gridding procedure be repeated 4 times for each of the fuel groups. After gridding in CEDS Step 5, both annual country-total and gridded emission fluxes from each fuel group are aggregated to 11 final sectors. Figure S5 demonstrates the level of detail available in the new CEDS<sub>GBD-MAPS</sub> gridded emission inventory by illustrating global BC emissions in 2017 from (1) all source sectors, (2) the residential sector only, (3) residential biofuel use only, and (4) residential coal use only. Additional uncertainties associated with the CEDS<sub>GBD-MAPS</sub> fuel-specific emissions in both the country-

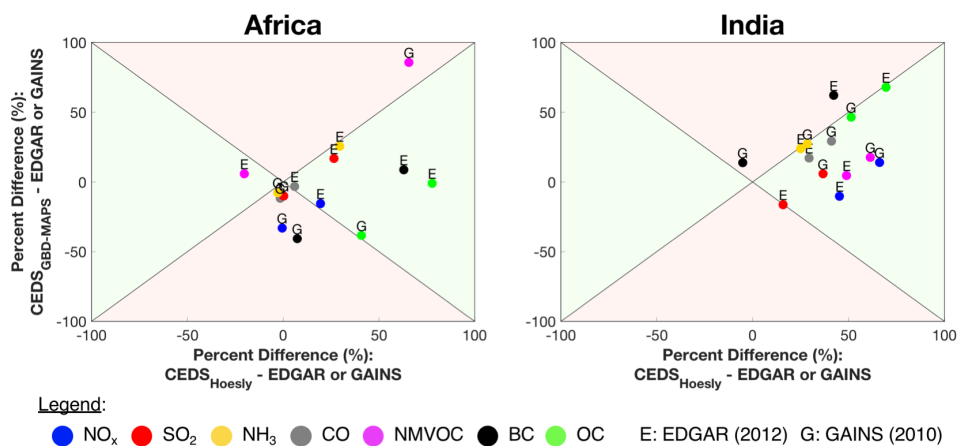


**Figure 4.** The  $x$  and  $y$  axes show the percent difference between CEDS emissions in India and Africa ( $y$  axis:  $\text{CEDS}_{\text{GBD-MAPS}}$ ;  $x$  axis:  $\text{CEDS}_{\text{Hoesly}}$ ) and those from the GAINS (ECLIPSE v5a) and EDGAR v4.3.2 inventories (i.e.,  $100 \times (\text{CEDS} - \text{EDGAR}) / ((\text{CEDS} - \text{EDGAR}) / 2)$ ). Comparisons are conducted with the most recent available year, 2010, for the comparison with GAINS and 2012 for the comparison with EDGAR. Green regions indicate where the  $\text{CEDS}_{\text{GBD-MAPS}}$  emissions have improved agreement with EDGAR and GAINS relative to the  $\text{CEDS}_{\text{Hoesly}}$  inventory. Red regions indicate where  $\text{CEDS}_{\text{GBD-MAPS}}$  emissions have worse agreement with EDGAR or GAINS relative to the  $\text{CEDS}_{\text{Hoesly}}$  inventory. The color of each point represents the chemical compound, and each point is labeled with an “E” or “G”, indicating that the percent difference was calculated using EDGAR or GAINS, respectively.

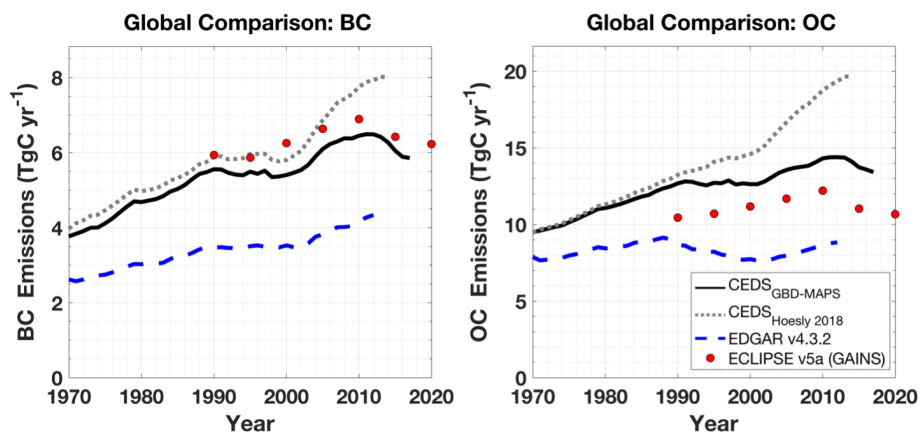


**Figure 5.** Comparison of global inventories of BC and OC emissions. Total EDGAR v4.3.2 and GAINS (ECLIPSE v5a) emission inventories shown without agricultural waste burning and aviation emissions.  $\text{CEDS}_{\text{GBD-MAPS}}$  emissions of BC and OC are not scaled to EDGAR or GAINS estimates.

total and annual gridded products are discussed further in Sect. 4.2.4

### 3 Results

The new  $\text{CEDS}_{\text{GBD-MAPS}}$  inventory provides global emissions of  $\text{NO}_x$ ,  $\text{SO}_2$ , NMVOCs,  $\text{NH}_3$ , CO, OC, and BC for 11 anthropogenic sectors (agriculture, energy, industry, on-road, non-road transportation, residential, commercial, other, waste, solvents, international shipping) and four fuel groups (combustion of total coal, solid biofuel, liquid fuels and natural gas, and process sources) over the time period between 1970–2017. Final country-level emissions are provided as annual time series in units of metric kilotons per

year ( $\text{kt yr}^{-1}$ ) for each sector and fuel type and include  $\text{NO}_x$  as emissions of  $\text{NO}_2$ . Final global gridded ( $0.5^\circ \times 0.5^\circ$ ) emissions for each compound, sector, and fuel group have been converted to emission fluxes ( $\text{kg m}^{-2} \text{s}^{-2}$ ), distributed over 12 months, and represent  $\text{NO}_x$  as NO to facilitate use in earth system models. Total NMVOCs in gridded products are additionally separated into 25 sub-VOC classes. Using a combination of updated energy consumption data and scaling procedures,  $\text{CEDS}_{\text{GBD-MAPS}}$  provides the most contemporary bottom-up global emission inventory to date and is the first inventory to report global emissions of multiple atmospheric pollutants from multiple fuel groups and sectors using consistent methodology. The following results section presents an overview of the  $\text{CEDS}_{\text{GBD-MAPS}}$  emission inven-

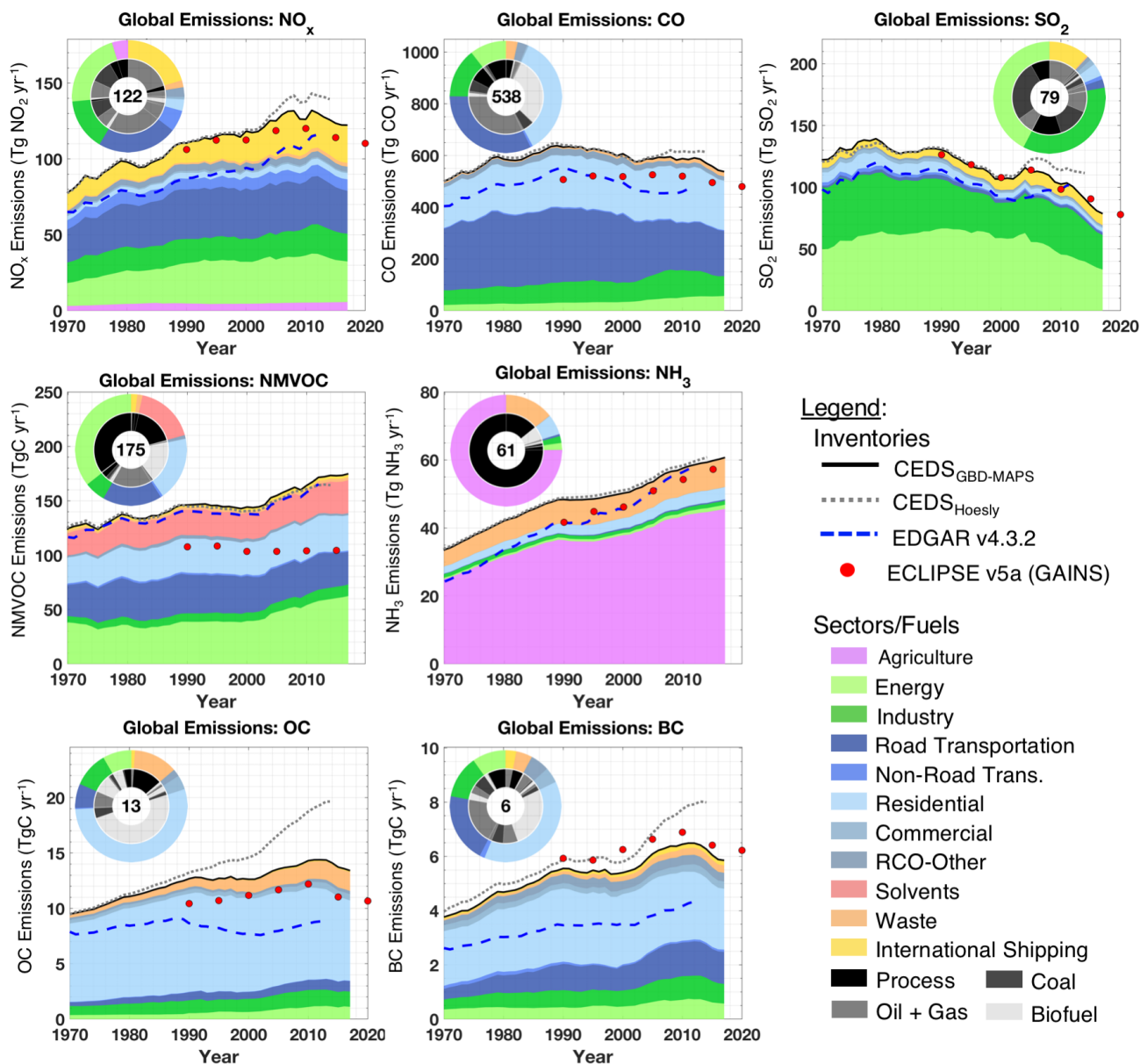


**Figure 6.** Time series of global annual emissions of  $\text{NO}_x$  (as  $\text{NO}_2$ ), CO,  $\text{SO}_2$ , NMVOCs,  $\text{NH}_3$ , BC, and OC for all sectors and fuel types. Solid black lines are the  $\text{CEDS}_{\text{GBD-MAPS}}$  inventory, with fractional sector contributions indicated by colors. Dashed gray lines are the  $\text{CEDS}_{\text{Hoesly}}$  inventory. Dashed blue lines are the EDGAR v4.3.2 global inventory. Red markers are ECLIPSE v5a baseline “current legislation” (CLE) emissions (from the GAINS model) with data in 2015 and 2020 from GAINS CLE projections. All inventories include international shipping but exclude aircraft emissions. Pie chart inserts show fractional contributions of emission sectors to total 2017 emissions (outer) and fuel type contributions to each sector (inner). Emission totals for 2017 (units:  $\text{Tg yr}^{-1}$ ;  $\text{Tg C yr}^{-1}$  for NMVOCs, OC, BC) are given inside each pie chart.

tory, with particular focus on emissions in 2017 and historical trends as a function of compound, sector, fuel type, and world region. Section 4 compares these results to other global emission inventories and discusses the magnitudes and sources of inventory uncertainties. Known issues in the inventory data at the time of submission are detailed in Sect. S4.

### 3.1 Global annual total emissions in 2017

Figures 6 and 7 show time series from 1970–2017 of global annual  $\text{CEDS}_{\text{GBD-MAPS}}$  emissions for each emitted compound. Global  $\text{CEDS}_{\text{GBD-MAPS}}$  emissions for reactive gases in 2017 are 122 Tg for  $\text{NO}_x$  (as  $\text{NO}_2$ ), 538 Tg for CO, 79 Tg for  $\text{SO}_2$ , 175 Tg C for total NMVOCs, and 61 Tg for  $\text{NH}_3$ . Global 2017 emissions of carbonaceous aerosol are 13 and

6 Tg C for OC and BC, respectively. The time series in Figs. 6 and 7 additionally show the contributions to global emissions from each of the 11 source sectors (Fig. 6) and four fuel groups (Fig. 7). Each panel in Fig. 6 additionally shows a pie chart with the fractional contribution of each sector to total global emissions in 2017 (outside), while the inner pie chart shows the fractional contributions from each of the fuel groups to each source sector. Numerical values for these fractional contributions are in Table S8. Global totals for 2017 are provided in the center of each pie chart. Global emissions from each compound are additionally split into contributions from 11 world regions (defined in Table S9) in Fig. 8 to aid in the interpretation of global trends below.

For global 2017 emissions of  $\text{NO}_x$ , Fig. 6 and Table S8 show that 60 % of  $\text{NO}_x$  emissions are associated with the energy generation (22 %), industry (15 %), and on-road transportation (23 %) sectors. These sectors have the largest contributions from emissions from coal combustion (> 46 % for the energy and industry emissions) and the combined combustion of liquid fuels (oil) and natural gas (with these two fuels accounting for 100 % of  $\text{NO}_x$  on-road emissions). Time series of regional contributions to global emissions in Fig. 8 additionally show that 50 % of global 2017  $\text{NO}_x$  emissions are from the combined Other Asia/Pacific region (Table S9) (13 Tg), China (24 Tg), and international shipping (25 Tg). For global 2017 emissions of remaining gas-phase pollutants, 67 % of CO emissions are from the on-road (100 %: oil + gas) and residential (86 %: biofuel) sectors; 78 % of  $\text{SO}_2$  emissions are from the energy generation (63 %: coal) and industry (38 % coal, 36 % process, 25 % oil + gas) sectors; 89 % of  $\text{NH}_3$  emissions are from the agriculture (100 %: process) and waste (100 %: process) sectors; and emissions of NMVOCs have the largest single contribution (36 %) from the energy sector, 99 % of which are associated with CEDS<sub>GBD-MAPS</sub> process sources (Table 2). For carbonaceous aerosol in 2017, 58 % of global BC emissions are from the residential (70 %: biofuel) and on-road (100 %: oil + gas) sectors, while 67 % of global OC emissions are from the residential (92 %: biofuel) and waste (100 %: process) sectors. Figure 8 shows that in 2017, China is the dominant source of global CO (144 Tg, 27 % of global total),  $\text{SO}_2$  (12 Tg, 15 % of global total),  $\text{NH}_3$  (12 Tg, 20 % of global total), OC (2.7 Tg C, 20 % of global total), and BC (1.4 Tg C, 24 % of global total). In contrast, Africa is the dominant source of global NMVOCs in 2017 (48 Tg C, 27 % of global total), and international shipping is the dominant source of global  $\text{NO}_x$  emissions (25 Tg, 20 % of global total).

As discussed above in Sect. 2 and below in Sect. 4.2.4, the distinction between CEDS combustion- and process-level source categories for all species may result in the underrepresentation of emissions from combustion sources relative to those from CEDS process-level sectors. As shown in Table 2, for example, some combustion emissions from the energy, industry, and waste sectors, such as fossil fuel fires and waste incineration, are categorized as CEDS “process-level” source

categories (Table 2). These emissions are allocated to the final CEDS process category rather than the CEDS total coal, biofuel, or oil and gas categories.

### 3.2 Historical trends in annual global emissions

Historical emission trends between 1970 and 2017 in Figs. 6 and 7 indicate that global emissions of each compound generally follow three patterns: (1) global CO and  $\text{SO}_2$  emissions peak prior to 1990 and generally decrease until 2017; (2) global emissions of  $\text{NO}_x$ , BC, and OC peak much later, around 2010, and then decrease until 2017; and (3) global emissions of  $\text{NH}_3$  and NMVOCs continuously increase throughout the entire time period. These trends generally reflect the sector-specific regulations implemented in dominant source regions around the world. For example, global emissions of CO generally decrease after the incorporation of catalytic converters in North America and Europe around 1990 (Figs. S7 and S8). Despite, however, continued reductions in these regions, global emissions of CO slightly increase between 2002 and 2012 due to simultaneous increases among the energy, industry, and residential sectors in China, India, Africa, and the Other Asia/Pacific region (Figs. S9–S12). Global CO emissions then decrease by 9 % between 2012 and 2017, largely due to reductions in industrial coal, residential biofuel, and process energy sector emissions in China (Figs. S9, S17–S18, S20), associated with the implementation of emission control strategies (reviewed in Zheng et al., 2018) as well as continued reductions in on-road transport emissions in North America and Europe (Figs. S7–S8). Similarly, global  $\text{SO}_2$  emissions decrease after peaking in 1979, largely due to emission control policies in the energy and industry sectors in North America and Europe (Figs. S7–S8). While simultaneous increases in emissions from coal use in the energy and industry sectors in China result in a brief increase in global  $\text{SO}_2$  emissions between 1999 and 2004 (Figs. 6, S9), global  $\text{SO}_2$  emissions decline by 32 % between 2004 and 2017 due to the implementation of stricter emission standards for the energy and industry sectors after 2010 in China (Zheng et al., 2018) as well as continued reductions in North America and Europe (Figs. S7–S8). Regional  $\text{SO}_2$  emission trends are particularly large with a factor of 9.5 decrease in total  $\text{SO}_2$  emissions in North America between 1973 and 2017, a factor of 6.9 decrease in Europe between 1979 and 2017, and a factor of 5.9 increase in China between 1970 and 2004, followed by a factor of 2.6 decrease after 2011 (Fig. 8). While China is the largest global contributor to  $\text{SO}_2$  emissions between 1994 and 2017, these large regional reductions, coupled with increasing  $\text{SO}_2$  emissions in the Other Asia/Pacific region, African countries, and India (Fig. 8), indicate that future global  $\text{SO}_2$  emissions will increasingly reflect activities in these other rapidly growing regions.

In contrast to historical emissions of  $\text{SO}_2$  and CO, global emissions of  $\text{NO}_x$ , BC, and OC peak later, between 2011

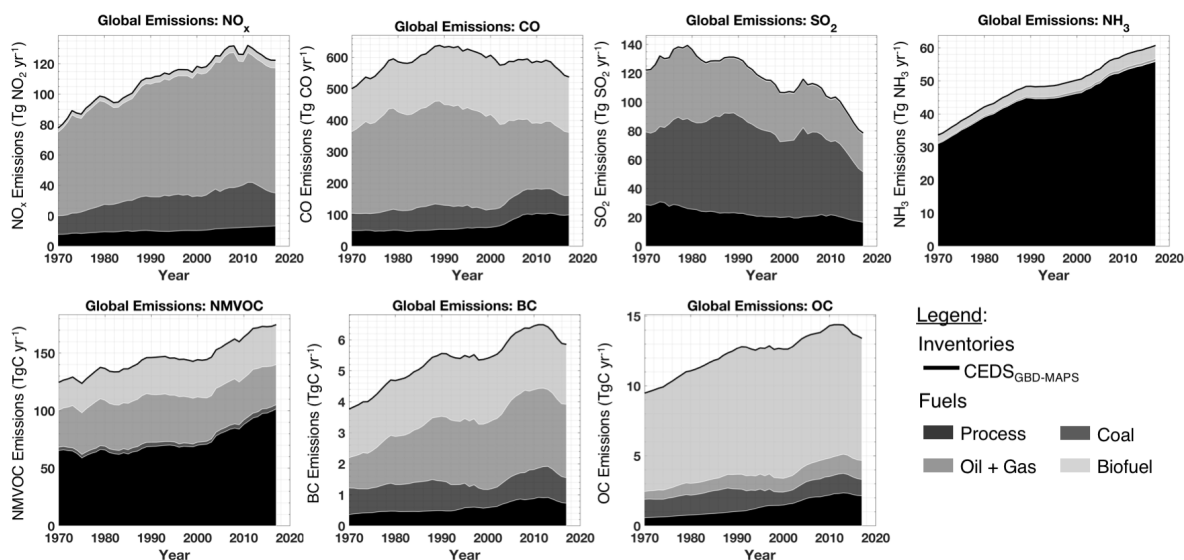


**Figure 7.** Time series of global annual emissions of  $\text{NO}_x$ , CO,  $\text{SO}_2$ ,  $\text{NH}_3$ , NMVOCs, BC, and OC for all sectors, colored by fuel group.

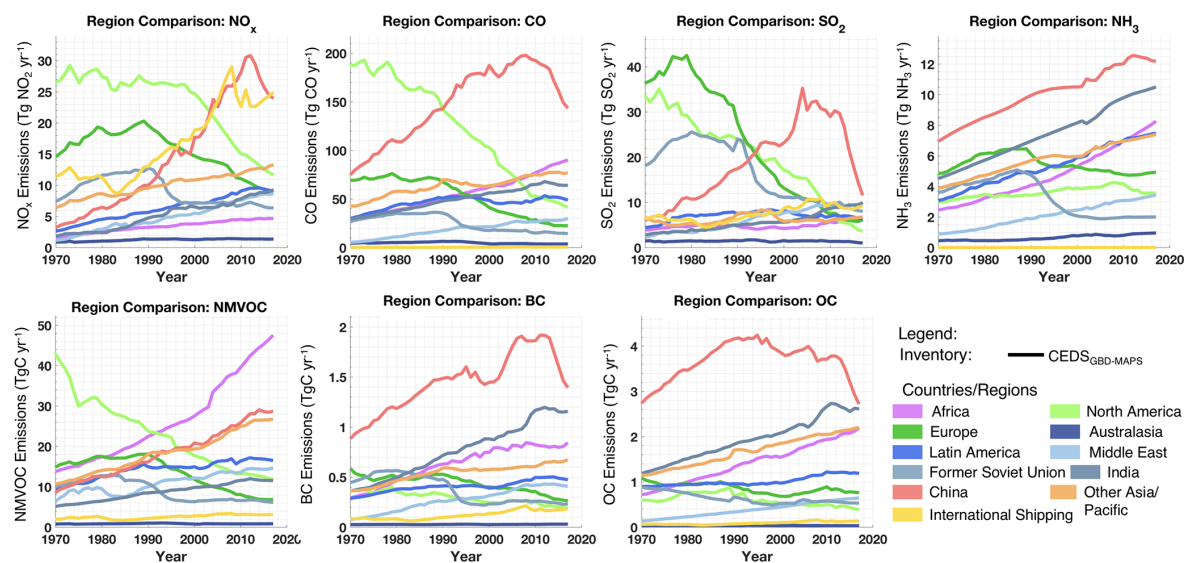


**Figure 8.** Time series of global annual  $\text{CEDS}_{\text{GBD-MAPS}}$  emissions of  $\text{NO}_x$ , CO,  $\text{SO}_2$ ,  $\text{NH}_3$ , NMVOCs, BC, and OC for all sectors and fuel types, split into 11 regions and countries (defined in Table S9).

and 2013. Global emissions then decrease by 7%, 9%, and 7%, respectively, by 2017 (Fig. 6). These trends also reflect the sector-specific regulations implemented in dominant source regions. For  $\text{NO}_x$  for example, global emissions between 1970 and 2017 are dominated by the combustion of coal, oil, and gas in the on-road transportation, energy generation, industry, and international shipping sectors (Figs. 6, 8). Global on-road transportation emissions are generally flat between 1988 and 2013 due to competing trends across world regions. While more stringent vehicle emission standards result in more than a factor of 2 decrease in on-road transportation  $\text{NO}_x$  emissions in North America and Europe be-

tween 1992 and 2017 (Figs. S7–S8), on-road transport emissions in China, India, and the Other Asia/Pacific region simultaneously experience between a factor of 1.3 and 2.8 increase (Figs. S9–S11). Subsequent reductions between 2013 and 2017 in global on-road emissions correspond to a 12% reduction in on-road transportation emissions in China due to the phase-in of stricter emission standards (Zheng et al., 2018), coupled with a continued decrease in emissions from North America and Europe. Global  $\text{NO}_x$  emissions from the energy and industry sectors increase by up to a factor of 6 between 1970 and 2011 due to regional increases in China, India, the Other Asia/Pacific region, and African countries,



with reductions between 2011 and 2017, again largely from reductions in China from stricter emissions control policies for coal-fired power plants and coal use in industrial processes (Zheng et al., 2018; Liu et al., 2015). Global emissions of  $\text{NO}_x$  from waste combustion and agricultural activities also increased by 2 % and 65 %, respectively, between 1970 and 2017, also contributing to the offset of recent reductions in emissions from regulated combustion sources (Fig. 6). Similar to global  $\text{NO}_x$  emissions, trends in historical BC and OC emissions reflect a balance between emission trends in North America, Europe, and other world regions, with reduction between 2010 and 2017 largely driven by reductions in emissions from China (Figs. 8, S9). In contrast to  $\text{NO}_x$  emissions, however, BC and OC emissions are dominated by contributions from biofuel combustion in the residential sector as well as on-road transportation, industry, and energy sectors for BC and the waste sector for global OC (Fig. 6). Though emissions of BC and OC have a higher level of uncertainty relative to other compounds (Sect. 4), emissions from African countries and the Other Asia/Pacific region experience growth in BC and OC emissions from these sectors. The exceptions are in China and India, both of which experience a plateau or reduction in BC and OC emissions from the residential, energy (China only), industry, and on-road transportation sectors between 2010 and 2017. In India, reductions in BC and OC emissions from the residential and informal industry sectors are expected to continue under policies to switch to cleaner residential fuels and energy sources, while BC emissions from on-road transport may increase due to increased transport demand (Venkataraman et al., 2018). Similar to trends in  $\text{SO}_2$  emissions, increasing trends in total OC and BC emissions from Africa, India, Latin America, the Middle East, and the Other Asia/Pacific region, coupled with large decreases in emissions from China, North America, and Europe (Fig. 8), indicate that global emissions will increasingly reflect activities in these rapidly growing regions.

Trends in historical emissions of NMVOCs and  $\text{NH}_3$  differ from other pollutants in that they continuously increase between 1970 and 2017. Global emissions of  $\text{NH}_3$  increase by 81 % between 1970 and 2017 and are largely associated with emissions from agricultural practices (75 % in 2017) and waste disposal and handling (14 % in 2017) (Fig. 6, Table S8). Unlike emissions from combustion sources, there are no large-scale regulations outside of Europe targeting  $\text{NH}_3$  emissions from agricultural activities, such as livestock manure management. As a result, global agricultural emissions of  $\text{NH}_3$  increase between 1970 and 2017 by 82 %, driven by increases in all regions other than Europe (Figs. 6, S6–S12). Similarly, global  $\text{NH}_3$  emissions from the waste sector increase by 77 % between 1970 and 2017, driven by increases in Latin America, the Other Asia/Pacific region, Africa, and India (Figs. S10–S12). Global emissions of NMVOCs increase by 40 % between 1970 and 2017 and are largely associated with emissions from the on-road transport, residential, energy, industry, and solvent use sectors (Fig. 6).

In contrast to other emitted pollutants, Africa is the largest global source of NMVOC emissions between 2010 and 2017, largely due to large contributions and continued increases in emissions from the residential (factor of 2.7) and energy (factor of 4) sectors (Fig. S12). Increases in energy sector emissions after 2003 are largely driven by increases in fugitive emissions from select African countries, including Nigeria, Kenya, Angola, and Mozambique. Emissions from China are the second-largest global NMVOC source between 1996 and 2017 (Fig. 8), while the Other Asia/Pacific region is the third-largest source between 1999 and 2017. Total NMVOCs in China increase by a factor of 3.4 between 1970 and 2017 due to activity increases in the solvent, energy, and industry sectors (Zheng et al., 2018), while targeted emission controls for the residential and on-road transport sectors result in their reduced contributions to NMVOC emissions between 2012 and 2017 (Fig. S9). Total emissions of NMVOCs in Europe and North America decrease by up to a factor of 2.4 between 1970 and 2017 due to reductions in all source sectors, except for energy emissions in North America, which increase between 2007 and 2011 and remain flat through 2017 (Fig. S7).

To provide a fuel-centric perspective of global historical emissions trends, Fig. 7 illustrates the contributions from the combustion of coal, solid biofuel, the sum of liquid fuel and natural gas, and all remaining CEDS “process-level” sources (Table 2) to total global emissions between 1970 and 2017. Reductions discussed above between 2010 and 2017 for global emissions of  $\text{NO}_x$ , CO,  $\text{SO}_2$ , BC, and OC are largely associated with reductions in coal combustion from the energy, industry, and residential sectors associated with emission control policies and residential fuel replacement in China as well as coal-fired power plant reductions in North America and Europe (Figs. 7, S13, S17–S18). Despite large reductions in emissions, China is still the single largest source of global emissions from coal combustion in 2017 (23 %–64 % for each compound except  $\text{NH}_3$ ). Figure S17, however, also shows that emissions from coal combustion are simultaneously increasing in India, the Other Asia/Pacific region, and Africa. Specifically,  $\text{SO}_2$  emissions from coal combustion in India are set to surpass those from China by 2018 if recent CEDS<sub>GBD-MAPS</sub> trends hold. For solid biofuel combustion, global emissions of all compounds are primarily associated with the residential sector (Fig. S14), with recent reductions in biofuel CO,  $\text{SO}_2$ , BC, and OC emissions largely from reductions in China (Fig. S18). In contrast, biofuel emissions from all other regions remain relatively flat or increase between 1970 and 2017, though biofuel emissions of NMVOCs, CO,  $\text{SO}_2$ , and OC in India as well as  $\text{SO}_2$  emissions in North America both decrease between 2010 and 2017 (Fig. S18). In 2017, biofuel emissions of all compounds are dominated by emissions from either Africa ( $\text{NO}_x$ ,  $\text{SO}_2$ ,  $\text{NH}_3$ , NMVOC, BC) or India (OC). For oil and gas combustion, global emissions of all compounds are primarily associated with on-road transportation, international shipping, and energy and industry ( $\text{SO}_2$  only) sec-

tors, with general decreases in associated emissions in North America and Europe between 1970 and 2017 and increases in other regions (Fig. S19). In contrast to other combustion sectors and fuels, emissions of  $\text{NO}_x$ , CO, NMVOCs, BC, and OC from the combustion of liquid fuels and natural gas in China remain relatively flat or slightly decrease between 2010 and 2017. Dominant global regions vary by compound (Fig. S19) and include international shipping ( $\text{NO}_x$ ,  $\text{SO}_2$ ), Africa (OC), India (BC), North America (CO,  $\text{NH}_3$ ), and the Other Asia/Pacific region (NMVOCs). Global CEDS process source emissions, which include contributions from some fuel combustion processes (Table 2), decrease between 2010 and 2017 for CO,  $\text{SO}_2$ , BC, and OC. These trends are primarily associated with reductions in emissions from the energy and industry sectors. In contrast, process source contributions to  $\text{NO}_x$ ,  $\text{NH}_3$ , and NMVOCs increase over this same time period due to increases in non-combustion agricultural and solvent use emissions as well as emissions from waste disposal and energy generation and transformation (Fig. S16). Increases in emissions from these sectors between 1970–2017 drive the continuous increases in global  $\text{NH}_3$  and NMVOCs, discussed above. Dominant source regions in 2017 of these process-level emissions include China ( $\text{NO}_x$ , CO,  $\text{NH}_3$ , BC, OC), India ( $\text{SO}_2$ ), and African countries (NMVOCs) (Fig. S20).

## 4 Discussion

### 4.1 Comparison to global inventories

#### 4.1.1 Comparison to CEDS<sub>Hoesly</sub> inventory

As a result of the similar methodologies, Fig. 6 shows that CEDS<sub>GBD-MAPS</sub> and CEDS<sub>Hoesly</sub> emission inventories predict similar magnitudes and historical trends in global emissions of each compound between 1970 and 2014. The two inventories, however, diverge in recent years due to the incorporation of updated activity data and both updated and new scaling emission inventories included in the CEDS<sub>GBD-MAPS</sub> system. For global emissions of  $\text{NO}_x$ , CO, and  $\text{SO}_2$ , the CEDS<sub>GBD-MAPS</sub> emissions are smaller than the CEDS<sub>Hoesly</sub> emissions after 2006 and show a faster decreasing trend. By 2014, global emissions of these compounds are between 7 % and 21 % lower than previous CEDS<sub>Hoesly</sub> estimates. These differences are largely associated with large emission reductions in China as a result of the updated national-level scaling inventory from Zheng et al. (2018), along with the added DICE-Africa (Marais and Wiedinmyer, 2016) and SMoG-India (Venkataraman et al., 2018) scaling inventories. Differences in emissions from India and Africa in the two CEDS inventories are discussed in Sect. 2 (Fig. 3) and, combined, account for ~ 60 % of the reduction in global  $\text{NO}_x$  emissions, 23 % of the reduction in global CO, and 14 % of the reduction in global  $\text{SO}_2$ . The largest differences between these two inventories in India and Africa are the reduced  $\text{NO}_x$  emissions

from the transport sector as well as reduced energy emissions of  $\text{SO}_2$  in India. Remaining differences between  $\text{NO}_x$  and  $\text{SO}_2$  emissions in the two CEDS inventories are largely associated with the updated China emission inventory from Zheng et al. (2018), which reports lower emissions in 2010 and 2012 than a previous version of the MEIC inventory that was used to scale China emissions in the CEDS<sub>Hoesly</sub> inventory (C. Li et al., 2017). These emission reductions are largely associated with the industrial and residential sectors in China and are partially offset by a simultaneous increase in transportation emissions of all compounds relative to CEDS<sub>Hoesly</sub>.

For global emissions of  $\text{NH}_3$  and NMVOCs, these species remain relatively unchanged between the CEDS<sub>Hoesly</sub> and CEDS<sub>GBD-MAPS</sub> inventories. In 2014 CEDS<sub>GBD-MAPS</sub> emissions are 5 % higher than CEDS<sub>Hoesly</sub> emissions for NMVOCs and 2 % lower than CEDS<sub>Hoesly</sub> global  $\text{NH}_3$  emissions. Emissions of  $\text{NH}_3$  remain relatively unchanged (within < 2 %) from dominant source regions, including India, Africa (Fig. 3), and China. In contrast, emissions of NMVOCs from Africa and China in the DICE-Africa and Zheng et al. (2018) scaling inventories are larger than those in the CEDS<sub>Hoesly</sub> inventory. Global emissions of NMVOCs are also higher in the EDGAR v4.3.2 inventory relative to the previous version used in the CEDS<sub>Hoesly</sub> inventory. NMVOCs are particularly large from the process energy sector emissions in Africa (Fig. S12), which primarily include fugitive emissions from oil and gas operations (Table 2). Default energy sector emissions from “non-combustion” processes are taken from the EDGAR inventory and are not scaled to the DICE-Africa inventory. Therefore, the large increase in these emissions in Africa relative to CEDS<sub>Hoesly</sub> is largely driven by changes in the EDGAR v4.3.2 inventory, with emissions from the 1B2\_Fugitive\_Fossil fuels sector increasing for example by a factor of 5 in Nigeria between 2003 and 2017.

Global emissions of OC and BC have the largest differences between the two CEDS inventories, with CEDS<sub>GBD-MAPS</sub> emissions consistently smaller than CEDS<sub>Hoesly</sub> emissions between 1970 and 2014. By 2014, CEDS<sub>GBD-MAPS</sub> emissions of BC and OC are 24 % and 33 % smaller than corresponding CEDS<sub>Hoesly</sub> emissions. In the CEDS<sub>Hoesly</sub> inventory, default emissions of BC and OC are not scaled, and therefore these differences are largely associated with the added scaling inventories, discussed in Sect. 2 and shown in Table 3. As shown in Figs. S3–S4, the added scaling of BC and OC emissions leads to a reduction in global CEDS<sub>GBD-MAPS</sub> emissions of OC in all scaled regions and a reduction in BC emissions in all regions other than India. In India, increases in industry and residential BC emissions from the SMoG-India scaling inventory result in a slight increase in BC emissions relative to the CEDS<sub>Hoesly</sub> inventory (Fig. 3). Waste emissions of OC and BC are also reduced in the CEDS<sub>GBD-MAPS</sub> inventory due to updated assumptions for the fraction of waste burned (Sect. S1.1).

As discussed in Hoesly et al. (2018) and further below, BC and OC emissions typically have the largest uncertainties of all the emitted species, and their recent changes in the residential and waste sectors are particularly uncertain.

The relative contributions of each source sector to emissions in the two CEDS versions are additionally shown in Fig. S21. This comparison shows that the fractional sectoral contributions to global emissions in 2014 are the same to within 10 % in the two CEDS inventories. The largest differences are a 9 % increase in the relative contribution of on-road transportation emissions of CO and reductions in the relative contribution of waste emissions across all compounds. These trends reflect the large update to default waste emissions described above as well as changes associated with the DICE-Africa and national China scaling inventories.

Similar to the total global emissions, changes between the two CEDS versions for the national-level and  $0.5^\circ \times 0.5^\circ$  gridded products will also result from updates to the energy consumption data, scaling inventories (Sects. 2.2–2.3), and spatial distribution proxies from EDGAR v4.3.2 (Sect. 2.1). Time series of differences between the CEDS<sub>Hoesly</sub> and CEDS<sub>GBD-MAPS</sub> inventories for 11 world regions are shown for each compound in Fig. S22. Fig. S22 shows that CEDS<sub>GBD-MAPS</sub> emissions are, in recent years, generally lower in each region, with the greatest differences in Africa, India, and China. The relative changes in Africa and India are discussed in Sect. 2. For China, the CEDS<sub>GBD-MAPS</sub> emissions are generally lower than the CEDS<sub>Hoesly</sub> estimates after the year 2010 as a result of the updated scaling inventory. Regional differences between inventories are also greater for OC and BC emissions relative to other compounds due to the added scaling procedure discussed in Sect. 2. Differences in spatial distributions are not discussed here as changes represent differences in the spatial proxies, which are largely from updates to the EDGAR inventory.

#### 4.1.2 Comparison to other global inventories (EDGAR and GAINS)

Figure 6 additionally provides a comparison of the CEDS<sub>GBD-MAPS</sub> global emissions to those from two widely used inventories: EDGAR v4.3.2 (Crippa et al., 2018; EC-JRC, 2018) and ECLIPSE v5a (GAINS) (IIASA, 2015; Klimont et al., 2017). For a comparison of global emissions across similar emission sectors, the EDGAR v4.3.2 inventory in Fig. 6 includes emissions from all reported sectors (including international shipping), except for those from agricultural waste burning and domestic and international aviation. Similarly, the GAINS ECLIPSE v5a baseline scenario inventory in Fig. 6 includes all reported emissions other than those from agricultural waste burning. These include contributions from aggregate residential and commercial combustion sources (“dom”), energy generation (“ene”), industrial combustion processes (“ind”), road and non-road transportation (“tra”), agricultural practices (“agr”), and waste disposal

(“wst”). GAINS ECLIPSE v5a baseline estimates for international shipping emissions are also included in Fig. 6. A table with sectoral mappings of the CEDS<sub>GBD-MAPS</sub>, EDGAR v4.3.2, and GAINS inventories is provided in Table S10.

The comparison in Fig. 6 shows that global emissions of all compounds in the CEDS<sub>GBD-MAPS</sub> inventory are consistently larger than in the EDGAR v4.3.2 inventory (Crippa et al., 2018). Global CEDS<sub>GBD-MAPS</sub> emissions of NO<sub>x</sub>, SO<sub>2</sub>, CO, and NMVOCs are at least 27 % larger, while global emissions of NH<sub>3</sub>, BC, and OC are within 52 %. Figure S23 indicates that differences in global BC and OC emissions are largely due to higher waste and residential and commercial emissions in the CEDS<sub>GBD-MAPS</sub> inventory. Figure 6, however, also shows that the trends in global emissions are similar between EDGAR v4.3.2 and CEDS<sub>GBD-MAPS</sub> for most compounds. For example, between 1970 and 2012, global emissions of SO<sub>2</sub>, NH<sub>3</sub>, NMVOCs, and BC peak in the same years. Global CO and NO<sub>x</sub> emissions both peak 1 year earlier in the CEDS<sub>GBD-MAPS</sub> inventory but otherwise follow similar historical trends. Trends in OC emissions are the most different between the two inventories, with a peak in emissions in 1988 in the EDGAR inventory compared to 2012 in the CEDS<sub>GBD-MAPS</sub> inventory. A comparison of relative sectoral contributions in Fig. S23 shows that these differences in OC emissions are largely due to the residential and commercial sectors, which may be underestimated in the EDGAR v4.3.2 inventory relative to GAINS (Crippa et al., 2018) and CEDS<sub>GBD-MAPS</sub>. Both inventories also show a net increase in global emissions of all compounds other than SO<sub>2</sub> between 1970 and 2012. Global SO<sub>2</sub> emissions follow a similar trend until 2007, after which the emissions in CEDS<sub>GBD-MAPS</sub> decrease at a faster rate than in EDGAR v4.3.2. These differences are largely due to the energy sector, which increases between 2006 and 2012 in EDGAR and decreases as a result of emission reductions in China in the CEDS<sub>GBD-MAPS</sub> inventory (Fig. S23). For all other compounds, the rate of increase in emissions between 1970 and 2012 is also slightly different between the two inventories. For example, NH<sub>3</sub> emissions in the CEDS<sub>GBD-MAPS</sub> inventory increase by 74 % compared to a 139 % increase in EDGAR. In contrast, BC and OC emissions increase at a faster rate in the CEDS<sub>GBD-MAPS</sub> inventory. Due to similar sources of uncertainty and the additional scaling of CEDS<sub>GBD-MAPS</sub> emissions to EDGAR (except for BC and OC), levels of uncertainty between the two inventories are expected to be similar, as discussed further in Sect. 4.2.

Similar to the comparison with EDGAR emissions, Fig. 6 also shows that global emissions in the CEDS<sub>GBD-MAPS</sub> inventory are generally larger than emission estimates from the GAINS model, published as part of the ECLIPSE v5a inventory (referred to here as GAINS) (Klimont et al., 2017). Two exceptions are for SO<sub>2</sub> emissions, which are up to 6 % lower than GAINS in select years, and BC emissions, which are consistently 5 %–15 % lower than GAINS for all years. While the sectoral definitions may slightly differ between

these inventories, Fig. S24 shows that these differences are largely due to different trends in energy and industry SO<sub>2</sub> emissions between 2005 and 2015 and consistently lower BC emissions from the residential and commercial sector in the CEDS<sub>GBD-MAPS</sub> inventory. For all years with overlapping data between 1990 and 2015, the absolute magnitude of global emissions is within  $\pm 15\%$  for NO<sub>x</sub>, SO<sub>2</sub>, NH<sub>3</sub>, and BC; within 22% for CO and OC; and within 50% for NMVOCs. Historical trends in each inventory are also similar for all compounds other than CO and NMVOCs (Fig. 6). Peak global emissions occur between 2010 and 2012 for NO<sub>x</sub>, BC, and OC, while both inventories show a net decrease in emissions in SO<sub>2</sub> and a net increase in emissions of NH<sub>3</sub>. In contrast, GAINS emissions of CO peak in 2010, while CEDS<sub>GBD-MAPS</sub> emissions peak in 1990. The largest differences in historical trends are for global NMVOC emissions, with GAINS showing a 3% decrease between 1990 and 2010, while CEDS<sub>GBD-MAPS</sub> NMVOC emissions increase by 13% over this same time period (Fig. 6). Sectoral contributions between the two inventories in Fig. S24 indicate that these differences are largely due differences in the energy, industry, and on-road transport emissions of NMVOCs. Uncertainties in the GAINS model have been previously estimated to fall between 10% and 30% in Europe for gas-phase species (Schöpp et al., 2005) and within the uncertainty estimates for BC and OC of other global bottom-up inventories (Klimont et al., 2017; Bond et al., 2004), as discussed in the following section.

## 4.2 Uncertainties

The level and sources of uncertainty in the CEDS<sub>GBD-MAPS</sub> inventory are similar to those in the CEDS<sub>Hoesly</sub> inventory, which are largely a function of uncertainty in the activity data, emission factors, and country-level inventories. As these uncertainties have been previously discussed in Hoesly et al. (2018), we have not performed a formal uncertainty analysis here but rather provide a brief summary of the sources of uncertainty associated with this work. We note plans for a robust uncertainty analysis in an upcoming release of the CEDS core system. While this section highlights many of the challenges associated with estimating comprehensive and accurate global bottom-up emission inventories, such inventories remain vital for their use in chemistry and climate models and for the development and evaluation of future control and mitigation strategies.

### 4.2.1 Uncertainties in activity data

As discussed in Sect. 2.1, CEDS default emissions from combustion sources are largely informed by fuel consumption data from the IEA 2019 World Energy Statistics Product (IEA, 2019). While this database provides energy consumption data as a function of detailed source sector and fuel type for most countries, the IEA data are uncertain and include

breaks in time series data that can lead to abrupt changes in the CEDS<sub>GBD-MAPS</sub> emissions for select sectors, fuels, and countries. For example, Fig. S7 shows an order of magnitude decrease (0.1 Tg C) in OC industrial emissions from North America between 1992 and 1993, which is driven by a break in IEA biofuel consumption data for the non-specified manufacturing industry sector (CEDS sector: 1A2g\_Ind-Comb-other) in the United States. While the magnitude of this particular change is negligible on the global scale, this is not the case for all sectors. For example, as noted in Sect. S4, a known issue in the IEA data in China in the energy sector causes peaks in the associated NO<sub>x</sub> and SO<sub>2</sub> CEDS<sub>GBD-MAPS</sub> emissions in 2004. These peak emissions may be overestimated by up to 4 and 10 Tg, respectively, which is large enough to impact historical trends in both regional (Fig. 8: NO<sub>x</sub> and SO<sub>2</sub>) and global (Figs. 6–7: SO<sub>2</sub>) emissions. These point to areas where improvements could be made to the underlying driver data in future work.

### 4.2.2 Uncertainties in global bottom-up inventories

Uncertainties in bottom-up emission inventories vary as a function of space, time, and compound, making total uncertainties difficult to quantify. Default emission estimates in the CEDS system are subject to uncertainties in underlying activity data, such as IEA energy consumption data, as well as activity drivers for process-level emissions. Knowledge of accurate emission factors also drives inventory uncertainty as EFs are not often available for all sectors in countries with emerging economies and are heavily dependent on the use, performance, and enforcement of control technologies within each sector and country (e.g., Zhang et al., 2009; Wang et al., 2015). While improvements in data collection and reporting standards may decrease the uncertainty in some underlying sources over time, the most recent years of CEDS<sub>GBD-MAPS</sub> emissions are still subject to considerable uncertainty. For instance, the degree of local and national compliance with control measures is often variable or unknown (e.g., Wang et al., 2015; Zheng et al., 2018); recent activity and regional emissions data are often updated as new information becomes available; and emissions in generally more uncertain regions, including India and Africa, are becoming an increasingly large fraction of global totals. Additionally, from a methodological standpoint, default CEDS emissions after 2010 also currently rely on the projection of emission factors from the GAINS EMF30 data release for sectors and countries where contemporary regional scaling inventories are not available.

As the CEDS system uses a “mosaic” approach and incorporates information from other global- and national-level inventories, the final CEDS<sub>GBD-MAPS</sub> emissions will also be subject to the same sources and levels of uncertainty as these external inventories. For example, as discussed in Sect. 2.1, default process-level emissions in CEDS<sub>GBD-MAPS</sub> are derived using emissions from the EDGAR v4.3.2 inventory,

with many countries additionally scaled to this inventory during Step 2. As reported and discussed in Crippa et al. (2018), EDGAR v4.3.2 emissions for 2012 at the regional level are estimated to have the smallest uncertainties for SO<sub>2</sub>, between 14.4 % and 47.6 %, with uncertainties in NO<sub>x</sub> between 17.2 % and 69.4 % (up to 124 % for Brazil), CO between 25.9 % and 123 % (lower for industrialized countries), and NMVOCs between 32.7 % and 148 % (lower for industrialized countries). Emissions of NH<sub>3</sub> are highly uncertain in all inventories (186 % to 294 % in EDGAR) due to uncertainties in the reporting of agricultural statistics and emission factors that will depend on individual farming practices, biological processes, and environmental conditions (e.g., Paulot et al., 2014). As noted in Crippa et al. (2018) and Klimont et al. (2017), EDGAR v4.3.2 and GAINS uncertainty estimates for BC and OC fall within the factor of 2 range that has been previously estimated by the seminal work of Bond et al. (2004). While CEDS<sub>GBD-MAPS</sub> emissions are not scaled to EDGAR v4.3.2 BC and OC emissions, estimates are derived from similar sources and are therefore expected to be consistent with uncertainties in both EDGAR and other global bottom-up inventories. It should also be noted that these reported uncertainty estimates from EDGAR only reflect the uncertainties associated with the emission estimation process and do not account for the potential of missing emissions sources or super-emitters within a given sector (Crippa et al., 2018).

To evaluate and improve the accuracy of these bottom-up emission estimates, inventories are increasingly using information from high-resolution satellite retrievals, particularly for major cities, large-area sources, natural sources, and large point sources (e.g., M. Li et al., 2017a; McLinden et al., 2016; Streets et al., 2013; van der Werf et al., 2017; Beirle et al., 2011; McLinden et al., 2012; Lamsal et al., 2011; Zheng et al., 2019; Elguindi et al., 2020). For example, both the CEDS<sub>Hoesly</sub> and CEDS<sub>GBD-MAPS</sub> inventories incorporate SO<sub>2</sub> emission estimates derived using satellite retrievals in McLinden et al. (2016) to account for previously missing SO<sub>2</sub> point sources in the CEDS 1B2\_Fugitive-petr-and-gas sector (described further in the supplement of Hoesly et al., 2018), with additional use of satellite data planned for a future CEDS core release. With the continued advancement of satellite retrievals, the development of source- and sector-specific inventories, such as CEDS<sub>GBD-MAPS</sub>, will continue to provide new opportunities for the application of new satellite-based inventories, which will aid in the quantification of spatial and temporal emissions from distinct sources associated with specific sectors and fuel types that may not be accurately estimated using conventional bottom-up approaches.

#### 4.2.3 Uncertainties in regional-level scaling inventories

Similar to the CEDS<sub>Hoesly</sub> inventory, the CEDS<sub>GBD-MAPS</sub> emissions will also reflect the uncertainties associated with

the inventories used for the scaling procedure. The inventories with the largest impact on the CEDS<sub>GBD-MAPS</sub> emission uncertainties relative to the CEDS<sub>Hoesly</sub> inventory will be those from China from Zheng et al. (2018), the DICE-Africa emission inventory from Marais and Wiedinmyer (2016), and the SMOG-India inventory from Venkataraman et al. (2018). While formal uncertainty analyses were not performed for all of these inventories, similar bottom-up methods used in these studies will result in similar sources of uncertainties (activity and emission factors) as the global inventories. For example, Zheng et al. (2018) state that the largest sources of uncertainty are the accuracy and availability of underlying data (reviewed in M. Li et al., 2017b) and that the levels of uncertainty for China emissions between 2010 and 2017 are expected to be similar to previous national-level bottom-up inventories derived using similar data sources and methodology, such as Zhao et al. (2011), Lu et al. (2011), and Zhang et al. (2009). Similar to global inventories, these previous regional studies estimate much lower levels of uncertainty for SO<sub>2</sub> and NO<sub>x</sub> ( $\pm 16\%$  and  $-13\%$  to  $+37\%$ , respectively) than for CO (70 %) and OC and BC emissions ( $-43\%$  to  $+258\%$  and  $-43\%$  to  $+208\%$ , respectively). Some sectors in China and other regions are particularly uncertain, as discussed further below.

Regional and national inventories, however, have the added benefit of using local knowledge to reduce potential uncertainties in emission factors and missing emission sources. For example, Marais and Wiedinmyer (2016) note that the DICE-Africa emissions are uncertain due to gaps in fuel consumption data. This inventory, however, also includes sources frequently missing in global inventories such as widespread diesel and petrol generator use, kerosene use, and ad hoc oil refining and have used emission factors for on-road car and natural-gas flaring that are more representative of the inefficient fuel combustion conditions in Africa (Marais and Wiedinmyer, 2016; Marais et al., 2019). As discussed in Sect. 2, the CEDS<sub>GBD-MAPS</sub> inventory may still underestimate total emissions from some of these sources (up to 11 % in 2013; Sect. 2.2.3) but otherwise will have uncertainties for total Africa emissions similar to the DICE-Africa inventory. For emissions in India, uncertainties also arise from missing fuel consumption data and the application of non-local or uncertain emission factors. Venkataraman et al. (2018), however, is one of the few studies to present a detailed uncertainty analysis of their inventory and use the propagation of source-specific activity data and emission factors to estimate that total emission uncertainties are smaller for SO<sub>2</sub> ( $-20\%$  to  $24\%$ ) than for NO<sub>x</sub> ( $-65\%$  to  $125\%$ ) and NMVOCs ( $-44\%$  to  $+66\%$ ). While uncertainties are not explicitly reported for OC and BC emissions, Fig. 1 in Venkataraman et al. (2018) indicates that uncertainties in these emissions are between  $-60\%$  and  $+95\%$ , consistent with BC and OC uncertainties reported in other bottom-up inventories. We also note the ongoing work to improve the accuracy of highly uncertain emission sectors in a

future release of the SMOG-India inventory through the Carbonaceous Aerosol Emissions, Source apportionment and Climate impacts (COALESCE) project (Venkataraman et al., 2020).

In addition to uncertainties in the scaling inventory emissions, uncertainties are also introduced by the CEDS<sub>GBD-MAPS</sub> scaling procedure. Uncertainties arise when mapping sectoral- and fuel-specific (when available) emissions between inventories (as discussed previously) as well as in the application of the calculated scaling factors outside the range of available scaling inventory years. For example, the implied CO EFs in Fig. S2 highlight one case in China where the EFs for oil and gas combustion in the on-road transport sector peak in 1999 at a value over 3 times larger than EFs in all other top-emitting countries. For China specifically, the calculated scaling factors for the year 2010 (earliest scaling inventory year) are applied to emissions from all years prior, which was calculated as a value of  $\sim 1.58$  for the on-road transport sector. The implied EF of  $\sim 1.8 \text{ g g}^{-1}$  for this sector in 2003 (Fig. S2) suggests that the SF from 2010 may not be representative of emissions during this earlier time period. We do note, however, that the 1999 peak in total CO emissions in China (Fig. S9) is driven by the IEA energy data and is consistent with the CEDS<sub>Hoesly</sub> inventory (Hoesly et al., 2018). In contrast, EFs from this sector in China after the year 2010 agree with the magnitude and trends found in other countries, further indicating that the scaling factors are most appropriate for years with overlapping inventory data. Other similar examples include coal energy emissions of SO<sub>2</sub> in Thailand (Fig. S2). In this case, the REAS scaling inventory spans the years 2000–2008. The default EFs for the energy sector, however, independently decrease between 1997 and 2001. As a result, when the implied EF of 3.3 for the year 2000 is applied to all historical energy emissions, the implied EFs prior to 1997 become an order of magnitude larger than those in nearly all other top-emitting countries (Fig. S2). Overall, the applicability of the scaling factors to emissions in years outside the available scaling inventory years remains uncertain due to real historical changes in activity, fuel-use, and emissions mitigation strategies. These uncertainties, however, vary by compound and sector as, for example, there are no similar peaks in on-road emissions for compounds other than CO in China.

Though the inclusion of these regional inventories can improve the accuracy of the global CEDS system (particularly during years with overlapping data), Hoesly et al. (2018) note that large uncertainties may still persist, even in developed countries with stringent reporting standards. In the US for example, it has been suggested that compared to the US National Emissions Inventory (US NEI), total NO<sub>x</sub> emissions from on-road and industrial sources in some regions may be overestimated by up to a factor of 2 (e.g., Travis et al., 2016). In addition, NH<sub>3</sub> emissions in agricultural regions in winter may be underestimated by a factor of 1.6 to 4.4 (Moravek et al., 2019), and national and regional emissions of NMVOCs

from oil and gas extraction regions, solvents, and the use of personal care products may also be underestimated by up to a factor of 2 (McDonald et al., 2018; Ahmadov et al., 2015).

#### 4.2.4 Uncertainties in sectoral and fuel contributions

Emissions reported as a function of individual source sectors are typically considered to have higher levels of uncertainty than those reported as country totals due to the cancellation of compounding errors (Schöpp et al., 2005). Source sectors with the largest levels of uncertainty in CEDS<sub>GBD-MAPS</sub> estimates are generally consistent with other inventories, which include waste burning, residential emissions, and agricultural processes (Hoesly et al., 2018). This higher level of sectoral uncertainty is reflected in the relatively larger uncertainties discussed above in global emissions of OC, BC, and NH<sub>3</sub> relative to other gas-phase species. In general, uncertainties from these sources are larger due to the difficulty in accurately tracking energy consumption statistics and uncertainties in the variability in source-specific emission factors, which will depend on local operational and environmental conditions. For example, residential emission factors from heating and cooking vary depending on technology used and operational conditions (e.g., Venkataraman et al., 2018; Carter et al., 2014; Jayarathne et al., 2018), while soil NO<sub>x</sub> emissions and NH<sub>3</sub> from wastewater and agriculture result from biological processes that depend on local practices and environmental conditions (e.g., Chen et al., 2012; Paulot et al., 2014). While uncertainties are not always reported at the sectoral level, Venkataraman et al. (2018) do report that industry emissions of NO<sub>x</sub> and NMVOCs in the SMOG-India inventory actually have larger uncertainties than those from the transportation, agriculture, and residential (NMVOCs only) sectors, while the relative uncertainties for SO<sub>2</sub> emissions follow the opposite trend. For emissions of total fine particulate matter, Venkataraman et al. (2018) estimate that the sectors with the largest uncertainties are the residential and industry emissions. Similarly, Lei et al. (2011) estimate that BC and OC emissions from the residential sector in China have the largest inventory uncertainties, while Zhang et al. (2009) and Zheng et al. (2018) also report relatively smaller uncertainties from power plants and heavy industry in China due to known activity data, local emission factors, pollution control technologies, and direct emissions monitoring. Overall, the mosaic scaling procedure in the CEDS system will result in similar levels of uncertainties as these regional scaling inventories.

With the release of fuel-specific information in the CEDS<sub>GBD-MAPS</sub> inventory, additional uncertainty in the allocation of fuel types is expected. In this work, activity data at the detailed sector and fuel level are taken from the IEA World Energy statistics (IEA, 2019) and are subject to the same sources of uncertainty. Emission factors for CEDS working sectors and fuels (Table S2) are derived from GAINS. In general, emissions from solid biofuel combus-

tion are considered to be less certain than fossil fuel consumption due to large uncertainties in both fuel consumption and EFs, particularly in the residential and commercial sectors. For example, by combining information from EDGAR v4.3.2 (Crippa et al., 2018) and a recent TNO-RWC (Netherlands Organization for Applied Scientific Research, Residential Wood Combustion) inventory from Denier van der Gon et al. (2015), Crippa et al. (2019) estimated that uncertainties in emissions from wood combustion in the residential sector in Europe are between 200 % and 300 % for OC, BC, and  $\text{NH}_3$ . Crippa et al. (2019) also report that these uncertainties are largely driven by uncertainties in regional emission factors as uncertainties in biofuel consumption are estimated to be between 38.9 % and 59.5 %. These uncertainties, however, are still larger than those estimated for fossil fuel consumption in many countries. As noted in Hoesly et al. (2018), increased levels of uncertainty in fossil fuel emissions are also expected in some countries, including the consumption and emission factors related to coal combustion in China (e.g., Liu et al., 2015; Guan et al., 2012; Hong et al., 2017), which will have the largest impacts on  $\text{CEDS}_{\text{GBD-MAPS}}$  emissions of  $\text{NO}_x$ ,  $\text{SO}_2$ , and BC. Specific to the  $\text{CEDS}_{\text{GBD-MAPS}}$  fuel inventory, additional uncertainties may arise from the potential underestimation of total coal, oil and gas, and biofuel emissions associated with fugitive emissions and gas flaring in the energy sector as well as waste incineration in the waste sector. As discussed above and in Hoesly et al. (2018), fugitive emissions are highly uncertain. The degree of underestimation in combustion fuel contributions will be dependent on the fractional contribution of process-level emissions in these sectors relative to those from coal, biofuel, and oil and gas combustion (Table S8). Additional uncertainties in the gridded fuel-specific products are discussed in the following section.

#### 4.2.5 Uncertainties and limitations in gridded emission fluxes

As noted in Sect. 2.1, global gridded  $\text{CEDS}_{\text{GBD-MAPS}}$  emission fluxes are provided to facilitate their use in earth system models. Relative to the reported country-total emission files, additional uncertainties are introduced in the  $0.5^\circ \times 0.5^\circ$  global gridded  $\text{CEDS}_{\text{GBD-MAPS}}$  emission fluxes through the use of source-specific spatial gridding proxies in CEDS Step 5. Historical spatial distributions within each country are largely based on normalized gridded emissions from the EDGAR v4.3.2 inventory. These spatial proxies are held constant after 2012, which serves to increase the uncertainties in spatial allocation in large countries in recent years. The magnitude of this uncertainty will depend on the specific compound and sector. For example, gridded emissions from the energy sector will not reflect the closure or fuel-switching of individual coal-fired power stations after 2012. Changes in total country-level emissions from this sector and fuel type, however, will be accurately reflected in the total country-

level emission files. This source of uncertainty is also present in the  $\text{CEDS}_{\text{Hoesly}}$  inventory. An additional source of uncertainty in the gridded emissions is that the same spatial allocations are applied uniformly across emissions of all fuel types within each source sector. This may lead to additional uncertainties if, for example, emissions from the use of coal, biofuel, oil and gas, and remaining sources within each sector are spatially distinct. These uncertainties, however, do not impact the final country-level  $\text{CEDS}_{\text{GBD-MAPS}}$  products because they are not gridded.

Lastly, while  $\text{CEDS}_{\text{GBD-MAPS}}$  emissions provide a global inventory of key atmospheric pollutants, this inventory does not include a complete set of sources or species required for GCM or CTM simulations of atmospheric chemical processes. As noted in Sect. 2, neither  $\text{CEDS}_{\text{Hoesly}}$  nor  $\text{CEDS}_{\text{GBD-MAPS}}$  estimates include emissions from large or small open fires, which must be supplemented with additional open-burning inventories, such as the Global Fire Emissions Database (GFED, 2019; van der Werf et al., 2017) or Fire INventory from NCAR (FINN, 2018; Wiedinmyer et al., 2011). In addition, simulations of atmospheric chemistry require emissions from biogenic sources, typically supplied from inventories, such as the Model of Emissions of Gases and Aerosols from Nature (MEGAN, 2019; Guenther et al., 2012). Other sources to consider in atmospheric simulations include volcanic emissions, sea spray, and windblown dust. In addition, the CEDS system does not include dust emissions from windblown and anthropogenic sources such as roads, combustion, or industrial process. Anthropogenic dust sources may contribute up to  $\sim 10\%$  of total fine-dust emissions in recent years and are important to consider when simulating concentrations of total atmospheric particulate matter (Philip et al., 2017). Lastly, the  $\text{CEDS}_{\text{GBD-MAPS}}$  inventory also excludes emissions of greenhouse gases such as methane and carbon dioxide ( $\text{CH}_4$ ,  $\text{CO}_2$ ). These compounds were previously included through 2014 in the  $\text{CEDS}_{\text{Hoesly}}$  inventory.

## 5 Data availability

The source code for the  $\text{CEDS}_{\text{GBD-MAPS}}$  system is available on GitHub ([https://github.com/emcduffie/CEDS/tree/CEDS\\_GBD-MAPS](https://github.com/emcduffie/CEDS/tree/CEDS_GBD-MAPS), last access: 1 December 2020, and <https://doi.org/10.5281/zenodo.3865670>; McDuffie et al., 2020a). To run the CEDS system, users are required to first purchase the proprietary energy consumption data from the IEA (World Energy Statistics; <https://www.iea.org/subscribe-to-data-services/world-energy-balances-and-statistics>, last access: 1 December 2020). The IEA is updated annually and provides the most comprehensive global energy statistics available to date. All additional input data are available in the CEDS GitHub repository.

Final products from the  $\text{CEDS}_{\text{GBD-MAPS}}$  system include total annual emissions for each country as well as

monthly global gridded ( $0.5^\circ \times 0.5^\circ$ ) emission fluxes for the years 1970–2017. Both products are available on Zenodo (<https://doi.org/10.5281/zenodo.3754964>; McDuffie et al., 2020c) and report total emissions and gridded fluxes as a function of 11 final source sectors and four fuel categories (total coal, solid biofuel, oil + gas, process). Time series of annual country-total emissions from 1970–2017 are provided in units of  $\text{kt yr}^{-1}$  and provide  $\text{NO}_x$  emissions as  $\text{NO}_2$ . These data do not speciate total NMVOCs into sub-VOC classes. In these .csv files, total anthropogenic emissions for each country are calculated as the sum of all sectors and fuel types within each country. For the global gridded products, emission fluxes of each compound as a function of 11 sectors and four fuel types are available for each year in individual netCDF files. These data are in units of  $\text{kg m}^{-2} \text{s}^{-1}$  and provide  $\text{NO}_x$  emissions as  $\text{NO}$ . Total NMVOCs are speciated into 25 sub-VOC classes as described in Sect. 2. For consistency with the CEDS data released for CMIP6 (CEDS, 2017a, b), gridded anthropogenic fluxes for 1970–2017 are additionally available in the CMIP6 format. Note that  $\text{NO}_x$  is in units of  $\text{NO}_2$  in this format. Additional file format details are in the README.txt file in the Zenodo repository (<https://doi.org/10.5281/zenodo.3754964>, McDuffie et al., 2020c).

To provide an example of the products and file formats available for download from the full CEDS<sub>GBD-MAPS</sub> repository, we have also prepared an additional data “snapshot” inventory that provides emissions in all three file formats described above for the 2014–2015 time period (McDuffie et al., 2020b). The gridded data are provided as monthly averages for the December 2014–February 2015 time period, while the annual data include total emissions from both 2014 and 2015. These data can be downloaded from <https://doi.org/10.5281/zenodo.3833935> (McDuffie et al., 2020b) and are further described in the associated README.txt file.

## 6 Summary and conclusions

We described the new CEDS<sub>GBD-MAPS</sub> global emission inventory for key atmospheric reactive gases and carbonaceous aerosol from 11 anthropogenic emission sectors and four fuel types (total coal, solid biofuel, liquid-fuel and natural-gas combustion, and remaining process-level emissions) over the time period from 1970–2017. The CEDS<sub>GBD-MAPS</sub> inventory was derived from an updated version of the Community Emissions Data System, which incorporates updated activity data for combustion- and process-level emission sources, updated scaling inventories, the added scaling of BC and OC emissions, and adjustments to the aggregation and gridding procedures to enable the extension of emission estimates to 2017 while retaining sectoral and fuel type information. We incorporated new regional scaling inventories for India and Africa; as a result default CEDS<sub>GBD-MAPS</sub> emissions

are now lower than previous CEDS<sub>Hoesly</sub> estimates for all compounds in these regions other than NMVOCs in Africa and BC in India. These updates improve the agreement of CEDS<sub>GBD-MAPS</sub> Africa emissions with those from EDGAR v4.3.2 as well as the agreement of all India emissions other than BC with both the EDGAR (2012) and GAINS (2010) inventories. Scaling default BC and OC estimates reduces these global emissions by up to 21 % and 28 %, respectively, relative to the CEDS<sub>Hoesly</sub> inventory. This reduction improves CEDS<sub>GBD-MAPS</sub> agreement with both GAINS and EDGAR global estimates of BC and OC, particularly in recent years. The resulting CEDS<sub>GBD-MAPS</sub> inventory provides the most contemporary global emission inventory to date for these key atmospheric pollutants and is the first to provide their global emissions as a function of both detailed source sector and fuel type.

Global 2017 emissions from the CEDS<sub>GBD-MAPS</sub> inventory suggest that coal and oil and gas combustion in both the energy and industry sectors are the largest global sources of  $\text{SO}_2$  emissions, while CO emissions are primarily from on-road transportation and biofuel combustion in the residential sector. Global emissions of both compounds peak by 1990 and decrease until 2017 as a result of continuous reductions in on-road transport emissions in Europe and North America as well as reductions in coal combustion emissions from the energy and industry sectors across these regions and in China. In contrast, global  $\text{NO}_x$ , BC, and OC emissions peak later, between 2010 and 2012, but also decrease until 2017 due to reductions in North America, Africa, and China. Dominant sources of  $\text{NO}_x$  in 2017 are from international shipping, energy, industry, and on-road transportation sectors. Major sources of BC emissions are from residential biofuel combustion and on-road transportation, while dominant OC sources are from the residential biofuel and the waste sector. Outside of international shipping, China is the largest regional source of global emissions of all compounds other than NMVOCs. As emissions in North America, Europe, and China continue to decrease, global emissions of  $\text{NO}_x$ , CO,  $\text{SO}_2$ , BC, and OC will increasingly reflect emissions in rapidly growing regions such as Africa, India, and countries throughout Asia, Latin America, and the Middle East. Lastly, in contrast to other compounds, global emissions of NMVOCs and  $\text{NH}_3$  continuously increase over the entire time period. These increases are predominantly due to increases in agricultural  $\text{NH}_3$  emissions in nearly all world regions as well as NMVOCs from increased waste, energy sector, and solvent use emissions. In 2017, global emissions of these compounds had the largest regional contributions from India, China, and countries throughout Africa, Asia, and the Pacific.

Historical global emission trends in the CEDS<sub>GBD-MAPS</sub> inventory are generally similar to those in three other global inventories: CEDS<sub>Hoesly</sub>, EDGAR v4.3.2, and ECLIPSE v5a (GAINS). Relative to the CEDS<sub>Hoesly</sub> inventory, however, CEDS<sub>GBD-MAPS</sub> emissions diverge in recent years, particu-



larly for  $\text{NO}_x$ , CO,  $\text{SO}_2$ , BC, and OC emissions. In addition to the use of updated underlying activity data in the CEDS<sub>GBD-MAPS</sub> inventory, emissions of these compounds were most impacted by the updated CEDS scaling inventories, including those for China, India, and Africa. These same updates also contribute to the different trends in global  $\text{NO}_x$ , CO, and  $\text{SO}_2$  emissions after 2010 between CEDS<sub>GBD-MAPS</sub> and the GAINS and EDGAR inventories. Global emissions between 1970 and 2017 from the CEDS<sub>GBD-MAPS</sub> inventory are generally smaller than the CEDS<sub>Hoesly</sub> emissions for all compounds other than NMVOCs and are consistently higher than all emissions from EDGAR v4.3.2. Global CEDS<sub>GBD-MAPS</sub> emissions are also larger than GAINS emissions, except for BC and select years of  $\text{SO}_2$  emissions.

Due to similar bottom-up methodologies and the use of EDGAR v4.3.2 data in the CEDS system, country-level CEDS<sub>GBD-MAPS</sub> emissions are expected to have similar sources and magnitudes of uncertainty as those in the CEDS<sub>Hoesly</sub>, EDGAR v4.3.2, GAINS, and scaling emission inventories. These inventories consistently predict the smallest uncertainties in emissions of  $\text{SO}_2$  and the largest for emissions of  $\text{NH}_3$ , OC, and BC. The latter three compounds largely depend on accurate knowledge of activity data and emission factors for small scattered sources that vary by location, combustion technologies used, and environmental conditions. Uncertainties in the sectoral and fuel allocations in CEDS<sub>GBD-MAPS</sub> emissions will also generally follow the uncertainties in the CEDS v2019-12-23 system and will largely depend on the accuracy of the fuel allocations for combustion sources in the underlying IEA activity data. Gridded CEDS<sub>GBD-MAPS</sub> emissions also have uncertainties associated with the accuracy of the normalized spatial emission distributions from EDGAR v4.3.2, which are equally applied to all four fuel categories and are held constant after 2012.

Contemporary global emission estimates with detailed sector- and fuel-specific information are vital for quantifying the anthropogenic sources of air pollution and mitigating the resulting impacts on human health, the environment, and society. While bottom-up methods can provide sector-specific emission estimates, previous global inventories of multiple compounds and sources have lagged in time and do not provide fuel-specific emissions for multiple compounds at the global scale. To address this community need, the CEDS<sub>GBD-MAPS</sub> inventory utilizes the CEDS system (v2019-12-23) to provide emissions of seven key atmospheric pollutants with detailed sectoral and fuel type information, extended to the year 2017. Due to the direct and secondary contribution of these reactive gases and carbonaceous aerosol to ambient air pollution, contemporary gridded and country-level emissions with both sector and fuel type information can provide new insights necessary to motivate and develop effective strategies for emission reductions and air pollution mitigation around the world. The CEDS<sub>GBD-MAPS</sub> source code is publicly available ([https://github.com/emcduffie/CEDS/tree/CEDS\\_GBD-MAPS](https://github.com/emcduffie/CEDS/tree/CEDS_GBD-MAPS) and

<https://doi.org/10.5281/zenodo.3865670>, McDuffie et al., 2020a), and both country-total and global gridded emissions from the 2020\_v1 version of this dataset are publicly available at Zenodo with the following DOI: <https://doi.org/10.5281/zenodo.3754964> (McDuffie et al., 2020c).

**Supplement.** The supplement for this article describes a list of known inventory issues at the time of submission as well as a number of additional CEDS<sub>GBD-MAPS</sub> details, tables and figures, and data sources, including the following: Boden et al. (2016, 2017), BP (2015), Doxsey-Whitfield et al. (2015), EC-JRC/PBL (2012, 2016), EIA (2019), IEA (2015), Klein Goldewijk et al. (2011), Sharma et al. (2019), Stohl et al. (2015), The World Bank (2016), UN (2014, 2015), Wiedinmyer et al. (2014), Commoner et al. (2000), Reyna-Bensusan et al. (2018), Nagpure et al. (2015), Meidiana and Gamse (2010), and US EPA, (2006). The supplement related to this article is available online at: <https://doi.org/10.5194/essd-12-3413-2020-supplement>.

**Author contributions.** EEM prepared the manuscript with contributions from all co-authors. RVM, MB, and SJS supervised the scientific content of this publication. EEM led the development of the CEDS<sub>GBD-MAPS</sub> source code and CEDS<sub>GBD-MAPS</sub> dataset, with significant contributions from SJS and PO as well as supplemental data from KT, CV, and EAM.

**Competing interests.** The authors declare that they have no conflict of interest.

**Acknowledgements.** We thank Christine Wiedinmyer and Qiang Zhang for their respective contributions to the DICE-Africa and updated China nation-level inventories, used here for scaling CEDS<sub>GBD-MAPS</sub> emissions. CEDS utilizes many sources of input data, and we are grateful for these contributions from a large number of research teams.

**Financial support.** This research has been supported by the Health Effects Institute (grant no. 4965/19-1).

**Review statement.** This paper was edited by David Carlson and reviewed by Hugo Denier van der Gon and one anonymous referee.

## References

- ADE: Australian Department of the Environment: National Pollution Inventory, 2017/2018, <http://www.npi.gov.au/npidata/action/load/advance-search> (lastaccess: 15 August 2019), 2019.
- Ahmadov, R., McKeen, S., Trainer, M., Banta, R., Brewer, A., Brown, S., Edwards, P. M., de Gouw, J. A., Frost, G. J., Gilman, J., Helmig, D., Johnson, B., Karion, A., Koss, A., Langford,

- A., Lerner, B., Olson, J., Oltmans, S., Peischl, J., Pétron, G., Pichugina, Y., Roberts, J. M., Ryerson, T., Schnell, R., Senff, C., Sweeney, C., Thompson, C., Veres, P. R., Warneke, C., Wild, R., Williams, E. J., Yuan, B., and Zamora, R.: Understanding high wintertime ozone pollution events in an oil- and natural gas-producing region of the western US, *Atmos. Chem. Phys.*, 15, 411–429, <https://doi.org/10.5194/acp-15-411-2015>, 2015.
- Ainsworth, E. A.: Understanding and improving global crop response to ozone pollution, *Plant J.*, 90, 886–897, <https://doi.org/10.1111/tpj.13298>, 2017.
- Amann, M., Bertok, I., Borken-Kleefeld, J., Cofala, J., Heyes, C., Höglund-Isaksson, L., Klimont, Z., Nguyen, B., Posch, M., Rafaj, P., Sandler, R., Schöpp, W., Wagner, F., and Winiwarter, W.: Cost-effective control of air quality and greenhouse gases in Europe: Modeling and policy applications, *Environ. Modell. Softw.*, 26, 1489–1501, <https://doi.org/10.1016/j.envsoft.2011.07.012>, 2011.
- Amann, M., Bertok, I., Borken-Kleefeld, J., Cofala, J., Heyes, C., Höglund-Isaksson, L., Kiesewetter, G., Klimont, Z., Schopp, W., Vellinga, N., and Winiwarter, W.: Adjusted historic emission data, projections, and optimized emission reduction targets for 2030 – a comparison with COM data 2013, IIASA, Laxenburg, Austria, available at: [http://ec.europa.eu/environment/air/pdf/review/TSAP\\_16a.pdf](http://ec.europa.eu/environment/air/pdf/review/TSAP_16a.pdf) (last access: 15 January 2018), 2015.
- Argentina UNFCCC Submission: Argentinian Inventory 1990–2012, submitted to UNFCCC, 2016.
- Avnery, S., Mauzerall, D. L., Liu, J., and Horowitz, L. W.: Global crop yield reductions due to surface ozone exposure: 1. Year 2000 crop production losses and economic damage, *Atmos. Environ.*, 45, 2284–2296, <https://doi.org/10.1016/j.atmosenv.2010.11.045>, 2011.
- Behera, S. N., Sharma, M., Aneja, V. P., and Balasubramanian, R.: Ammonia in the atmosphere: a review on emission sources, atmospheric chemistry and deposition on terrestrial bodies, *Environ. Sci. Pollut. R.*, 20, 8092–8131, <https://doi.org/10.1007/s11356-013-2051-9>, 2013.
- Beirle, S., Boersma, K. F., Platt, U., Lawrence, M. G., and Wagner, T.: Megacity Emissions and Lifetimes of Nitrogen Oxides Probed from Space, *Science*, 333, 1737, <https://doi.org/10.1126/science.1207824>, 2011.
- Boden, T. A., Marland, G., and Andres, R. J.: Global, Regional, and National Fossil-Fuel CO<sub>2</sub> Emissions, Carbon Dioxide Information Analysis Center, US Department of Energy, Oak Ridge, USA, 2016.
- Boden, T. A., Marland, G., and Andres, R. J.: Global, Regional, and National Fossil-Fuel CO<sub>2</sub> Emissions, Carbon Dioxide Information Analysis Center, US Department of Energy, Oak Ridge, USA, [https://doi.org/10.3334/CDIAC/00001\\_V2017](https://doi.org/10.3334/CDIAC/00001_V2017), 2017.
- Bond, T. C., Streets, D. G., Yarber, K. F., Nelson, S. M., Woo, J.-H., and Klimont, Z.: A technology-based global inventory of black and organic carbon emissions from combustion, *J. Geophys. Res.*, 109, D14203, <https://doi.org/10.1029/2003JD003697>, 2004.
- Dong, R., Jogani, R., Jung, S., Roden, C., Streets, D. G., and Trautmann, N. M.: Historical emissions of black and organic carbon aerosol from energy-related combustion, 1850–2000, *Global Biogeochem. Cycles*, 21, GB2018, <https://doi.org/10.1029/2006GB002840>, 2007.
- Bond, T. C., Doherty, S. J., Fahey, D. W., Forster, P. M., Berntsen, T., DeAngelo, B. J., Flanner, M. G., Ghan, S., Kärcher, B., Koch, D., Kinne, S., Kondo, Y., Quinn, P. K., Sarofim, M. C., Schultz, M. G., Schulz, M., Venkataraman, C., Zhang, H., Zhang, S., Bellouin, N., Guttikunda, S. K., Hopke, P. K., Jacobson, M. Z., Kaiser, J. W., Klimont, Z., Lohmann, U., Schwarz, J. P., Shindell, D., Storelvmo, T., Warren, S. G., and Zender, C. S.: Bounding the role of black carbon in the climate system: A scientific assessment, *J. Geophys. Res.-Atmos.*, 118, 5380–5552, <https://doi.org/10.1002/jgrd.50171>, 2013.
- BP: BP Statistical Review of World Energy, available at: <https://www.bp.com/statisticalreview> (last access: 15 January 2018), 2015.
- BP: Statistical Review of World Energy: 2019, available at: <https://www.bp.com/content/dam/bp/business-sites/en/global/corporate/pdfs/energy-economics/statistical-review/bp-stats-review-2019-full-report.pdf> (last access: 23 January 2020), 2019.
- Brock, C. A., Washenfelder, R. A., Trainer, M., Ryerson, T. B., Wilson, J. C., Reeves, J. M., Huey, L. G., Holloway, J. S., Parrish, D. D., Hübler, G., and Fehsenfeld, F. C.: Particle growth in the plumes of coal-fired power plants, *J. Geophys. Res.-Atmos.*, 107, D124155, <https://doi.org/10.1029/2001JD001062>, 2002.
- Carter, E. M., Shan, M., Yang, X., Li, J., and Baumgartner, J.: Pollutant Emissions and Energy Efficiency of Chinese Gasifier Cooking Stoves and Implications for Future Intervention Studies, *Environ. Sci. Technol.*, 48, 6461–6467, <https://doi.org/10.1021/es405723w>, 2014.
- Castellanos, P. and Boersma, K. F.: Reductions in nitrogen oxides over Europe driven by environmental policy and economic recession, *Sci. Rep.-UK*, 2, 265, <https://doi.org/10.1038/srep00265>, 2012.
- CEDS: v2017\_08\_30, available at: <https://esgf-node.llnl.gov/search/input4mips/> (last access: 7 January 2020), 2017a.
- CEDS: v2017\_10\_05, available at: <https://esgf-node.llnl.gov/search/input4mips/> (last access: 7 January 2020), 2017b.
- Chameides, W. L.: The photochemical role of tropospheric nitrogen oxides, *Geophys. Res. Lett.*, 5, 17–20, <https://doi.org/10.1029/GL005i001p00017>, 1978.
- Chen, Y., Roden, C. A., and Bond, T. C.: Characterizing Biofuel Combustion with Patterns of Real-Time Emission Data (PaRTED), *Environ. Sci. Technol.*, 46, 6110–6117, <https://doi.org/10.1021/es3003348>, 2012.
- Commoner, B., Bartlett, P. W., Eisl, H., and Couchot, K.: Air Transport of Dioxin from North American Sources to Ecologically Vulnerable Receptors in Nunavut, Arctic Canada: Final Report to the North American Commission for Environmental Cooperation, available at: <http://www3.cec.org/islandora/en/item/1596-long-range-air-transport-dioxin-from-north-american-sources-ecologically-vulnerable-en.pdf> (last access: 25 April 2020), 2000.
- Crippa, M., Guizzardi, D., Muntean, M., Schaaf, E., Dentener, F., van Aardenne, J. A., Monni, S., Doering, U., Olivier, J. G. J., Pagliari, V., and Janssens-Maenhout, G.: Gridded emissions of air pollutants for the period 1970–2012 within EDGAR v4.3.2, *Earth Syst. Sci. Data*, 10, 1987–2013, <https://doi.org/10.5194/essd-10-1987-2018>, 2018.
- Crippa, M., Janssens-Maenhout, G., Guizzardi, D., Van Dingenen, R., and Dentener, F.: Contribution and uncertainty

- of sectorial and regional emissions to regional and global PM<sub>2.5</sub> health impacts, *Atmos. Chem. Phys.*, 19, 5165–5186, <https://doi.org/10.5194/acp-19-5165-2019>, 2019.
- Crutzen, P. J.: The influence of nitrogen oxides on the atmospheric ozone content, *Q. J. Roy. Meteor. Soc.*, 96, 320–325, <https://doi.org/10.1002/qj.49709640815>, 1970.
- de Gouw, J. A., Parrish, D. D., Frost, G. J., and Trainer, M.: Reduced emissions of CO<sub>2</sub>, NO<sub>x</sub>, and SO<sub>2</sub> from US power plants owing to switch from coal to natural gas with combined cycle technology, *Earths Future*, 2, 75–82, <https://doi.org/10.1002/2013EF000196>, 2014.
- Denier van der Gon, H. A. C., Bergström, R., Fountoukis, C., Johansson, C., Pandis, S. N., Simpson, D., and Visschedijk, A. J. H.: Particulate emissions from residential wood combustion in Europe – revised estimates and an evaluation, *Atmos. Chem. Phys.*, 15, 6503–6519, <https://doi.org/10.5194/acp-15-6503-2015>, 2015.
- DICE-Africa: DICE-Africa User Manual, available at: <https://www2.acom.ucar.edu/modeling/dice-africa> (last access: 9 January 2020), 2016.
- Doxsey-Whitfield, E., MacManus, K., Adamo, S. B., Pistolesi, L., Squires, J., Borkovska, O., and Baptista, S. R.: Taking Advantage of the Improved Availability of Census Data: A First Look at the Gridded Population of the World, Version 4, *Papers in Applied Geography*, 1, 226–234, <https://doi.org/10.1080/23754931.2015.1014272>, 2015.
- Duncan, B. N., Yoshida, Y., de Foy, B., Lamsal, L. N., Streets, D. G., Lu, Z., Pickering, K. E., and Krotkov, N. A.: The observed response of Ozone Monitoring Instrument (OMI) NO<sub>2</sub> columns to NO<sub>x</sub> emission controls on power plants in the United States: 2005–2011, *Atmos. Environ.*, 81, 102–111, <https://doi.org/10.1016/j.atmosenv.2013.08.068>, 2013.
- ECCC: Environment and Climate Change Canada, EN\_APEI-Canada, Canada's 2019 Air Pollutant Emissions Inventory, available at: [http://data.ec.gc.ca/data/substances/monitor/canada-s-air-pollutant-emissions-inventory/APEI\\_Tables\\_Canada\\_Provinces\\_Territories/?lang](http://data.ec.gc.ca/data/substances/monitor/canada-s-air-pollutant-emissions-inventory/APEI_Tables_Canada_Provinces_Territories/?lang), last access: 13 August 2019.
- EC-JRC: Emissions Database for Global Atmospheric Research (EDGAR), release EDGARv4.3.2, available at: <https://edgar.jrc.ec.europa.eu/overview.php?v> (last access: 12 August 2019), 2018.
- EC-JRC/PBL: Emission Database for Global Atmospheric Research (EDGAR), release EDGAR v4.2 FT2012, available at: <http://edgar.jrc.ec.europa.eu> (last access: 15 January 2018), 2012.
- EC-JRC/PBL: Emission Database for Global Atmospheric Research (EDGAR), release version 4.3.1, available at: <http://edgar.jrc.ec.europa.eu/overview.php?v> (last access: 15 January 2018), 2016.
- EIA: US Energy Information Administration: Table 10.2a: Renewable Energy Consumption, Residential and Commercial Sectors, available at: <https://www.eia.gov/totalenergy/data/monthly/#renewable> (last access: 26 August 2019), 2019.
- EIA: US Energy Information Administration: Drilling Productivity Report, available at: <https://www.eia.gov/petroleum/drilling/>, last access: 7 April 2020.
- Elguindi, N., Granier, C., Stavrou, T., Darras, S., Bauwens, M., Cao, H., Chen, C., Denier van der Gon, H. A. C., Dubovik, O., Fu, T. M., Henze, D. K., Jiang, Z., Keita, S., Kuenen, J. J. P., Kurokawa, J., Liousse, C., Miyazaki, K., Müller, J. F., Qu, Z., Solmon, F., and Zheng, B.: Intercomparison of Magnitudes and Trends in Anthropogenic Surface Emissions From Bottom-Up Inventories, Top-Down Estimates, and Emission Scenarios, *Earths Future*, 8, e2020EF001520, <https://doi.org/10.1029/2020EF001520>, 2020.
- EMEP: Officially reported emission data to the European Monitoring and Evaluation Programme: EMEP\_NFR14\_LEVEL1 data, available at: [https://www.ceip.at/ms/ceip\\_home1/ceip\\_home/webdab\\_emepdatabase/reported\\_emissiondata/](https://www.ceip.at/ms/ceip_home1/ceip_home/webdab_emepdatabase/reported_emissiondata/), last access: 19 December 2019.
- FAOSTAT: FAOSTAT-Forestry database, available at: <http://www.fao.org/forestry/statistics/84922/en/> (last access: 15 January 2018), 2015.
- Feng, L., Smith, S. J., Braun, C., Crippa, M., Gidden, M. J., Hoesly, R., Klimont, Z., van Marle, M., van den Berg, M., and van der Werf, G. R.: The generation of gridded emissions data for CMIP6, *Geosci. Model Dev.*, 13, 461–482, <https://doi.org/10.5194/gmd-13-461-2020>, 2020.
- FINN: Fire INventory from NCAR, Version 1.5, available at: <http://bai.acom.ucar.edu/Data/fire/> (last access: 4 March 2020), 2018.
- GBD 2017 Risk Factor Collaborators: Global, regional, and national comparative risk assessment of 84 behavioural, environmental and occupational, and metabolic risks or clusters of risks for 195 countries and territories, 1990–2017: a systematic analysis for the Global Burden of Disease Study 2017, *The Lancet*, 392, 1923–1994, [https://doi.org/10.1016/S0140-6736\(18\)32225-6](https://doi.org/10.1016/S0140-6736(18)32225-6), 2018.
- GBD MAPS Working Group: Burden of Disease Attributable to Coal-Burning and Other Major Sources of Air Pollution in China, Special Report 20, Health Effects Institute, available at: <https://www.healtheffects.org/publication/burden-disease-attributable-coal-burning-and-other-air-pollution-sources-china> (last access: 1 December 2020), 2016.
- GBD MAPS Working Group: Burden of Disease Attributable to Major Air Pollution Sources in India, Special Report 21, Health Effects Institute available at: <https://www.healtheffects.org/publication/gbd-air-pollution-india>, (last access: 1 December 2020) 2018.
- GFED: Global Fire Emissions Database, available at: <http://globalfiredata.org/index.html> (last access: 15 March 2020), 2019.
- Gidden, M. J., Riahi, K., Smith, S. J., Fujimori, S., Luderer, G., Kriegler, E., van Vuuren, D. P., van den Berg, M., Feng, L., Klein, D., Calvin, K., Doelman, J. C., Frank, S., Fricko, O., Harmsen, M., Hasegawa, T., Havlik, P., Hilaire, J., Hoesly, R., Horing, J., Popp, A., Stehfest, E., and Takahashi, K.: Global emissions pathways under different socioeconomic scenarios for use in CMIP6: a dataset of harmonized emissions trajectories through the end of the century, *Geosci. Model Dev.*, 12, 1443–1475, <https://doi.org/10.5194/gmd-12-1443-2019>, 2019.
- Guan, D., Liu, Z., Geng, Y., Lindner, S., and Hubacek, K.: The gigatonne gap in China's carbon dioxide inventories, *Nat. Clim. Change*, 2, 672–675, <https://doi.org/10.1038/nclimate1560>, 2012.
- Guenther, A. B., Jiang, X., Heald, C. L., Sakulyanontvittaya, T., Duhl, T., Emmons, L. K., and Wang, X.: The Model of Emissions of Gases and Aerosols from Nature version 2.1

- (MEGAN2.1): an extended and updated framework for modeling biogenic emissions, *Geosci. Model Dev.*, 5, 1471–1492, <https://doi.org/10.5194/gmd-5-1471-2012>, 2012.
- Haywood, J. and Boucher, O.: Estimates of the direct and indirect radiative forcing due to tropospheric aerosols: A review, *Rev. Geophys.*, 38, 513–543, <https://doi.org/10.1029/1999RG000078>, 2000.
- Hoesly, R. M., Smith, S. J., Feng, L., Klimont, Z., Janssens-Maenhout, G., Pitkanen, T., Seibert, J. J., Vu, L., Andres, R. J., Bolt, R. M., Bond, T. C., Dawidowski, L., Kholod, N., Kurokawa, J.-I., Li, M., Liu, L., Lu, Z., Moura, M. C. P., O'Rourke, P. R., and Zhang, Q.: Historical (1750–2014) anthropogenic emissions of reactive gases and aerosols from the Community Emissions Data System (CEDS), *Geosci. Model Dev.*, 11, 369–408, <https://doi.org/10.5194/gmd-11-369-2018>, 2018.
- Hoesly, R., O'Rourke, P., Braun, C., Feng, L., Smith, S. J., Pitkanen, T., Seibert, J., Vu, L., Presley, M., Bolt, R., Goldstein, B., and Kholod, N.: CEDS: Community Emissions Data System (Version Dec-23-2019), Zenodo, <https://doi.org/10.5281/zenodo.3592073>, 2019.
- Hong, C., Zhang, Q., He, K., Guan, D., Li, M., Liu, F., and Zheng, B.: Variations of China's emission estimates: response to uncertainties in energy statistics, *Atmos. Chem. Phys.*, 17, 1227–1239, <https://doi.org/10.5194/acp-17-1227-2017>, 2017.
- HTAP2: RETRO NMVOC Ratio, available at: <http://iek8wikis.iek.fz-juelich.de/HTAPWiki/WP1.1?action> (last access: 7 January 2020), 2013.
- Huang, G., Brook, R., Crippa, M., Janssens-Maenhout, G., Schieberle, C., Dore, C., Guizzardi, D., Muntean, M., Schaaf, E., and Friedrich, R.: Speciation of anthropogenic emissions of non-methane volatile organic compounds: a global gridded data set for 1970–2012, *Atmos. Chem. Phys.*, 17, 7683–7701, <https://doi.org/10.5194/acp-17-7683-2017>, 2017.
- IEA: World Energy Statistics, available at: <http://www.iea.org/statistics/> (last access: 15 January 2018), 2015.
- IEA: World Energy Statistics 2019 Edition, Database Documentation, available at: [http://wds.iea.org/wds/pdf/WORLDBES\\_Documentation.pdf](http://wds.iea.org/wds/pdf/WORLDBES_Documentation.pdf), last access: 17 September 2019.
- IIASA: GAINS – Sulfur content of fuels, available at: <http://gains.iiasa.ac.at/models/index.html> (last access: 15 January 2018), 2014.
- IIASA: ECLIPSE v5a, available at: <https://www.iiasa.ac.at/web/home/research/researchPrograms/air/ECLIPSEv5a.html> (last access: 7 January 2020), 2015.
- IPCC: Summary for Policy Makers, in: *Climate Change 2013: The Physical Science Basis, Contribution of Working Group I to the Fifth Assessment Report of the Intergovernmental Panel on Climate Change*, edited by: Stocker, T. F., Qin, D., Plattner, G.-K., Tignor, M., Allen, S. K., Boschung, J., Nauels, Y., Xia, Y., Bex, V., and Midgley, P. M., Cambridge University Press, Cambridge, United Kingdom and New York, USA, 1–29, 2013.
- Janssens-Maenhout, G., Crippa, M., Guizzardi, D., Dentener, F., Muntean, M., Pouliot, G., Keating, T., Zhang, Q., Kurokawa, J., Wankmüller, R., Denier van der Gon, H., Kuenen, J. J. P., Klimont, Z., Frost, G., Darras, S., Koffi, B., and Li, M.: HTAP\_v2.2: a mosaic of regional and global emission grid maps for 2008 and 2010 to study hemispheric transport of air pollution, *Atmos. Chem. Phys.*, 15, 11411–11432, <https://doi.org/10.5194/acp-15-11411-2015>, 2015.
- Jayarathne, T., Stockwell, C. E., Bhave, P. V., Praveen, P. S., Rathnayake, C. M., Islam, Md. R., Panday, A. K., Adhikari, S., Maharjan, R., Goetz, J. D., DeCarlo, P. F., Saikawa, E., Yokelson, R. J., and Stone, E. A.: Nepal Ambient Monitoring and Source Testing Experiment (NAMASTE): emissions of particulate matter from wood- and dung-fueled cooking fires, garbage and crop residue burning, brick kilns, and other sources, *Atmos. Chem. Phys.*, 18, 2259–2286, <https://doi.org/10.5194/acp-18-2259-2018>, 2018.
- Jimenez, J. L., Canagaratna, M. R., Donahue, N. M., Prevot, A. S. H., Zhang, Q., Kroll, J. H., DeCarlo, P. F., Allan, J. D., Coe, H., Ng, N. L., Aiken, A. C., Docherty, K. S., Ulbrich, I. M., Grieshop, A. P., Robinson, A. L., Duplissy, J., Smith, J. D., Wilson, K. R., Lanz, V. A., Hueglin, C., Sun, Y. L., Tian, J., Laaksonen, A., Raatikainen, T., Rautiainen, J., Vaattovaara, P., Ehn, M., Kulmala, M., Tomlinson, J. M., Collins, D. R., Cubison, M. J., Dunlea, J., Huffman, J. A., Onasch, T. B., Alfarra, M. R., Williams, P. I., Bower, K., Kondo, Y., Schneider, J., Drewnick, F., Borrmann, S., Weimer, S., Demerjian, K., Salcedo, D., Cottrell, L., Griffin, R., Takami, A., Miyoshi, T., Hatakeyama, S., Shimono, A., Sun, J. Y., Zhang, Y. M., Dzepina, K., Kimmel, J. R., Sueper, D., Jayne, J. T., Herndon, S. C., Trimborn, A. M., Williams, L. R., Wood, E. C., Middlebrook, A. M., Kolb, C. E., Baltensperger, U., and Worsnop, D. R.: Evolution of Organic Aerosols in the Atmosphere, *Science*, 326, 1525, <https://doi.org/10.1126/science.1180353>, 2009.
- Klein Goldewijk, K., Beusen, A., van Drecht, G., and de Vos, M.: The HYDE 3.1 spatially explicit database of human-induced global land-use change over the past 12,000 years, *Global Ecol. Biogeogr.*, 20, 73–86, <https://doi.org/10.1111/j.1466-8238.2010.00587.x>, 2011.
- Klimont, Z., Kupiainen, K., Heyes, C., Purohit, P., Cofala, J., Rafaj, P., Borken-Kleefeld, J., and Schöpp, W.: Global anthropogenic emissions of particulate matter including black carbon, *Atmos. Chem. Phys.*, 17, 8681–8723, <https://doi.org/10.5194/acp-17-8681-2017>, 2017.
- Krotkov, N. A., McLinden, C. A., Li, C., Lamsal, L. N., Celarier, E. A., Marchenko, S. V., Swartz, W. H., Bucsela, E. J., Joiner, J., Duncan, B. N., Boersma, K. F., Veefkind, J. P., Levelt, P. F., Fioletov, V. E., Dickerson, R. R., He, H., Lu, Z., and Streets, D. G.: Aura OMI observations of regional SO<sub>2</sub> and NO<sub>2</sub> pollution changes from 2005 to 2015, *Atmos. Chem. Phys.*, 16, 4605–4629, <https://doi.org/10.5194/acp-16-4605-2016>, 2016.
- Kurokawa, J., Ohara, T., Morikawa, T., Hanayama, S., Janssens-Maenhout, G., Fukui, T., Kawashima, K., and Akimoto, H.: Emissions of air pollutants and greenhouse gases over Asian regions during 2000–2008: Regional Emission inventory in ASia (REAS) version 2, *Atmos. Chem. Phys.*, 13, 11019–11058, <https://doi.org/10.5194/acp-13-11019-2013>, 2013.
- Lacey, F. and Henze, D.: Global climate impacts of country-level primary carbonaceous aerosol from solid-fuel cookstove emissions, *Environ. Res. Lett.*, 10, 114003, <https://doi.org/10.1088/1748-9326/10/11/114003>, 2015.
- Lacey, F. G., Marais, E. A., Henze, D. K., Lee, C. J., van Donkelaar, A., Martin, R. V., Hannigan, M. P., and Wiedinmyer, C.: Improving present day and future estimates of anthropogenic sectoral emissions and the resulting air quality impacts in Africa, *Faraday Discuss.*, 200, 397–412, <https://doi.org/10.1039/C7FD00011A>, 2017.

- Lamsal, L. N., Martin, R. V., Padmanabhan, A., van Donkelaar, A., Zhang, Q., Sioris, C. E., Chance, K., Kurosu, T. P., and Newchurch, M. J.: Application of satellite observations for timely updates to global anthropogenic NO<sub>x</sub> emission inventories, *Geophys. Res. Lett.*, 38, L05810, <https://doi.org/10.1029/2010GL046476>, 2011.
- Lei, Y., Zhang, Q., He, K. B., and Streets, D. G.: Primary anthropogenic aerosol emission trends for China, 1990–2005, *Atmos. Chem. Phys.*, 11, 931–954, <https://doi.org/10.5194/acp-11-931-2011>, 2011.
- Lelieveld, J., Klingmüller, K., Pozzer, A., Burnett, R. T., Haines, A., and Ramanathan, V.: Effects of fossil fuel and total anthropogenic emission removal on public health and climate, *P. Natl. Acad. Sci. USA*, 116, 7192, <https://doi.org/10.1073/pnas.1819989116>, 2019.
- Li, C., McLinden, C., Fioletov, V., Krotkov, N., Carn, S., Joiner, J., Streets, D., He, H., Ren, X., Li, Z., and Dickerson, R. R.: India Is Overtaking China as the World's Largest Emitter of Anthropogenic Sulfur Dioxide, *Sci. Rep.-UK*, 7, 14304, <https://doi.org/10.1038/s41598-017-14639-8>, 2017.
- Li, M., Liu, H., Geng, G., Hong, C., Liu, F., Song, Y., Tong, D., Zheng, B., Cui, H., Man, H., Zhang, Q., and He, K.: Anthropogenic emission inventories in China: a review, *Natl. Sci. Rev.*, 4, 834–866, <https://doi.org/10.1093/nsr/nwx150>, 2017a.
- Li, M., Zhang, Q., Kurokawa, J.-I., Woo, J.-H., He, K., Lu, Z., Ohara, T., Song, Y., Streets, D. G., Carmichael, G. R., Cheng, Y., Hong, C., Huo, H., Jiang, X., Kang, S., Liu, F., Su, H., and Zheng, B.: MIX: a mosaic Asian anthropogenic emission inventory under the international collaboration framework of the MICS-Asia and HTAP, *Atmos. Chem. Phys.*, 17, 935–963, <https://doi.org/10.5194/acp-17-935-2017>, 2017b.
- Liang, C.-K., West, J. J., Silva, R. A., Bian, H., Chin, M., Davila, Y., Dentener, F. J., Emmons, L., Flemming, J., Folberth, G., Henze, D., Im, U., Jonson, J. E., Keating, T. J., Kucsera, T., Lenzen, A., Lin, M., Lund, M. T., Pan, X., Park, R. J., Pierce, R. B., Sekiya, T., Sudo, K., and Takemura, T.: HTAP2 multi-model estimates of premature human mortality due to intercontinental transport of air pollution and emission sectors, *Atmos. Chem. Phys.*, 18, 10497–10520, <https://doi.org/10.5194/acp-18-10497-2018>, 2018.
- Liu, Z., Guan, D., Wei, W., Davis, S. J., Ciais, P., Bai, J., Peng, S., Zhang, Q., Hubacek, K., Marland, G., Andres, R. J., Crawford-Brown, D., Lin, J., Zhao, H., Hong, C., Boden, T. A., Feng, K., Peters, G. P., Xi, F., Liu, J., Li, Y., Zhao, Y., Zeng, N., and He, K.: Reduced carbon emission estimates from fossil fuel combustion and cement production in China, *Nature*, 524, 335–338, <https://doi.org/10.1038/nature14677>, 2015.
- Lu, Z., Zhang, Q., and Streets, D. G.: Sulfur dioxide and primary carbonaceous aerosol emissions in China and India, 1996–2010, *Atmos. Chem. Phys.*, 11, 9839–9864, <https://doi.org/10.5194/acp-11-9839-2011>, 2011.
- Marais, E. A. and Wiedinmyer, C.: Air Quality Impact of Diffuse and Inefficient Combustion Emissions in Africa (DICE-Africa), *Environ. Sci. Technol.*, 50, 10739–10745, <https://doi.org/10.1021/acs.est.6b02602>, 2016.
- Marais, E. A., Silvern, R. F., Vodonos, A., Dupin, E., Bockarie, A. S., Mickley, L. J., and Schwartz, J.: Air Quality and Health Impact of Future Fossil Fuel Use for Electricity Generation and Transport in Africa, *Environ. Sci. Technol.*, 53, 13524–13534, <https://doi.org/10.1021/acs.est.9b04958>, 2019.
- Mauzerall, D. L., Sultan, B., Kim, N., and Bradford, D. F.: NO<sub>x</sub> emissions from large point sources: variability in ozone production, resulting health damages and economic costs, *Atmos. Environ.*, 39, 2851–2866, <https://doi.org/10.1016/j.atmosenv.2004.12.041>, 2005.
- McDonald, B. C., de Gouw, J. A., Gilman, J. B., Jathar, S. H., Akherati, A., Cappa, C. D., Jimenez, J. L., Lee-Taylor, J., Hayes, P. L., McKeen, S. A., Cui, Y. Y., Kim, S.-W., Gentner, D. R., Isaacman-VanWertz, G., Goldstein, A. H., Harley, R. A., Frost, G. J., Roberts, J. M., Ryerson, T. B., and Trainer, M.: Volatile chemical products emerging as largest petrochemical source of urban organic emissions, *Science*, 359, 760, <https://doi.org/10.1126/science.aag0524>, 2018.
- McDuffie, E. E., Hoesly, R., O'Rourke, P., Braun, C., Feng, L., Smith, S. J., Pitkanen, T., Seibert, J. J., Vu, L., Presley, M., Bolt, R., Goldstein, B., and Kholod, N.: CEDS\_GBD-MAPS\_SourceCode\_2020\_v1.0, Zenodo, <https://doi.org/10.5281/zenodo.3865670>, 2020a.
- McDuffie, E. E., Smith, S. J., O'Rourke, P., Tibrewal, K., Venkataraman, C., Marais, E. A., Zheng, B., Crippa, M., Brauer, M., and Martin, R. V.: CEDS\_GBD-MAPS: Data Snapshot (2014–2015), Zenodo, <https://doi.org/10.5281/zenodo.3833935>, 2020b.
- McDuffie, E. E., Smith, S. J., O'Rourke, P., Tibrewal, K., Venkataraman, C., Marais, E. A., Zheng, B., Crippa, M., Brauer, M., and Martin, R. V.: CEDS\_GBD-MAPS: Global Anthropogenic Emission Inventory of NO<sub>x</sub>, SO<sub>2</sub>, CO, NH<sub>3</sub>, NMVOCs, BC, and OC from 1970–2017 (Version 2020\_v1.0), Zenodo, <https://doi.org/10.5281/zenodo.3754964>, 2020c.
- McLinden, C. A., Fioletov, V., Boersma, K. F., Krotkov, N., Sioris, C. E., Veefkind, J. P., and Yang, K.: Air quality over the Canadian oil sands: A first assessment using satellite observations, *Geophys. Res. Lett.*, 39, L04804, <https://doi.org/10.1029/2011GL050273>, 2012.
- McLinden, C. A., Fioletov, V., Shephard, M. W., Krotkov, N., Li, C., Martin, R. V., Moran, M. D., and Joiner, J.: Space-based detection of missing sulfur dioxide sources of global air pollution, *Nat. Geosci.*, 9, 496, <https://doi.org/10.1038/ngeo2724>, 2016.
- MEGAN: The Model of Emissions of Gases and Aerosols from Nature, Version 3.1, available at: <https://sites.google.com/uci.edu/bai/megan/data-and-code> (last access: 4 March 2020), 2019.
- Meidiana, C. and Gamse, T.: Development of Waste Management Practices in Indonesia, *European Journal of Scientific Research*, 40, 199–210, 2010.
- Mickley, L. J., Jacob, D. J., Field, B. D., and Rind, D.: Effects of future climate change on regional air pollution episodes in the United States, *Geophys. Res. Lett.*, 31, L24103, <https://doi.org/10.1029/2004GL021216>, 2004.
- Moravek, A., Murphy, J. G., Hrdina, A., Lin, J. C., Pennell, C., Franchin, A., Middlebrook, A. M., Fibiger, D. L., Womack, C. C., McDuffie, E. E., Martin, R., Moore, K., Baasandorj, M., and Brown, S. S.: Wintertime spatial distribution of ammonia and its emission sources in the Great Salt Lake region, *Atmos. Chem. Phys.*, 19, 15691–15709, <https://doi.org/10.5194/acp-19-15691-2019>, 2019.
- Mozurkewich, M.: The dissociation constant of ammonium nitrate and its dependence on temperature, relative hu-

- midity and particle size, *Atmos. Environ.*, 27, 261–270, [https://doi.org/10.1016/0960-1686\(93\)90356-4](https://doi.org/10.1016/0960-1686(93)90356-4), 1993.
- Nagpure, A. S., Ramaswami, A., and Russell, A.: Characterizing the Spatial and Temporal Patterns of Open Burning of Municipal Solid Waste (MSW) in Indian Cities, *Environ. Sci. Technol.*, 49, 12904–12912, <https://doi.org/10.1021/acs.est.5b03243>, 2015.
- NEI: 2011 National Emissions Inventory (NEI) Data, available at: <https://www.epa.gov/air-emissions-inventories/2011-national-emissions-inventory-nei-data> (last access: 12 December 2020), 2013.
- Paulot, F., Jacob, D. J., Pinder, R. W., Bash, J. O., Travis, K., and Henze, D. K.: Ammonia emissions in the United States, European Union, and China derived by high-resolution inversion of ammonium wet deposition data: Interpretation with a new agricultural emissions inventory (MASAGE\_NH3), *J. Geophys. Res.-Atmos.*, 119, 4343–4364, <https://doi.org/10.1002/2013JD021130>, 2014.
- Philip, S., Martin, R. V., Snider, G., Weagle, C. L., van Donkelaar, A., Brauer, M., Henze, D. K., Klimont, Z., Venkataraman, C., Guttikunda, S. K., and Zhang, Q.: Anthropogenic fugitive, combustion and industrial dust is a significant, underrepresented fine particulate matter source in global atmospheric models, *Environ. Res. Lett.*, 12, 044018, <https://doi.org/10.1088/1748-9326/aa65a4>, 2017.
- RAQC: Regional Air Quality Council: Summary of State Implementation Plans, available at: [https://raqc.egnyte.com/dl/KZXQmQtFaQ2019\\_SIP\\_Summaries\\_Update.pdf](https://raqc.egnyte.com/dl/KZXQmQtFaQ2019_SIP_Summaries_Update.pdf) (last access: 23 January 2020), 2019.
- Reyna-Bensusan, N., Wilson, D. C., and Smith, S. R.: Uncontrolled burning of solid waste by households in Mexico is a significant contributor to climate change in the country, *Environ. Res.*, 163, 280–288, <https://doi.org/10.1016/j.envres.2018.01.042>, 2018.
- Sadavarte, P. and Venkataraman, C.: Trends in multi-pollutant emissions from a technology-linked inventory for India: I. Industry and transport sectors, *Atmos. Environ.*, 99, 353–364, <https://doi.org/10.1016/j.atmosenv.2014.09.081>, 2014.
- Saxena, P. and Seigneur, C.: On the oxidation of SO<sub>2</sub> to sulfate in atmospheric aerosols, *Atmos. Environ.*, 21, 807–812, [https://doi.org/10.1016/0004-6981\(87\)90077-1](https://doi.org/10.1016/0004-6981(87)90077-1), 1987.
- Schöpp, W., Klimont, Z., Suutari, R., and Cofala, J.: Uncertainty analysis of emission estimates in the RAINS integrated assessment model, *Environ. Sci. Policy*, 8, 601–613, <https://doi.org/10.1016/j.envsci.2005.06.008>, 2005.
- Sharma, G., Sinha, B., Pallavi, Hakkim, H., Chandra, B. P., Kumar, A., and Sinha, V.: Gridded Emissions of CO, NO<sub>x</sub>, SO<sub>2</sub>, CO<sub>2</sub>, NH<sub>3</sub>, HC<sub>1</sub>, CH<sub>4</sub>, PM<sub>2.5</sub>, PM<sub>10</sub>, BC, and NMVOC from Open Municipal Waste Burning in India, *Environ. Sci. Technol.*, 53, 4765–4774, <https://doi.org/10.1021/acs.est.8b07076>, 2019.
- Shindell, D. and Smith, C. J.: Climate and air-quality benefits of a realistic phase-out of fossil fuels, *Nature*, 573, 408–411, <https://doi.org/10.1038/s41586-019-1554-z>, 2019.
- SMoG-India: Speciated Multi-pollutant Generator, available at: <https://sites.google.com/view/smogindia> (last access: 28 February 2020), 2019.
- South Korea National Institute of Environmental Research: National air pollutants emission service, available at: <http://airemiss.nier.go.kr/> (last access: 15 January 2018), 2016.
- Stevens, C. J., Dise, N. B., Mountford, J. O., and Gowing, D. J.: Impact of Nitrogen Deposition on the Species Richness of Grasslands, *Science*, 303, 1876, <https://doi.org/10.1126/science.1094678>, 2004.
- Stohl, A., Aamaas, B., Amann, M., Baker, L. H., Bellouin, N., Berntsen, T. K., Boucher, O., Cherian, R., Collins, W., Daskalakis, N., Dusinska, M., Eckhardt, S., Fuglestedt, J. S., Harju, M., Heyes, C., Hodnebrog, Ø., Hao, J., Im, U., Kanakidou, M., Klimont, Z., Kupiainen, K., Law, K. S., Lund, M. T., Maas, R., MacIntosh, C. R., Myhre, G., Myriokefalitakis, S., Orlivié, D., Quaas, J., Quennehen, B., Raut, J.-C., Rumbold, S. T., Samset, B. H., Schulz, M., Seland, Ø., Shine, K. P., Skeie, R. B., Wang, S., Yttri, K. E., and Zhu, T.: Evaluating the climate and air quality impacts of short-lived pollutants, *Atmos. Chem. Phys.*, 15, 10529–10566, <https://doi.org/10.5194/acp-15-10529-2015>, 2015.
- Streets, D. G., Canty, T., Carmichael, G. R., de Foy, B., Dickerson, R. R., Duncan, B. N., Edwards, D. P., Haynes, J. A., Henze, D. K., Houyoux, M. R., Jacob, D. J., Krotkov, N. A., Lamsal, L. N., Liu, Y., Lu, Z., Martin, R. V., Pfister, G. G., Pinder, R. W., Salawitch, R. J., and Wecht, K. J.: Emissions estimation from satellite retrievals: A review of current capability, *Atmos. Environ.*, 77, 1011–1042, <https://doi.org/10.1016/j.atmosenv.2013.05.051>, 2013.
- TEPA: Taiwan Emission Data System, available at: <https://erdb.epa.gov.tw/eng/DataRepository/EnvMonitor/ReportInspectAirTEDS.aspx?topic1> (last access: 15 January 2018), 2016.
- The World Bank: World Development Indicators, available at: [http://databank.worldbank.org/data/download/WDI\\_excel.zip](http://databank.worldbank.org/data/download/WDI_excel.zip) (last access: 15 January 2018), 2016.
- Travis, K. R., Jacob, D. J., Fisher, J. A., Kim, P. S., Marais, E. A., Zhu, L., Yu, K., Miller, C. C., Yantosca, R. M., Sulprizio, M. P., Thompson, A. M., Wennberg, P. O., Crouse, J. D., St. Clair, J. M., Cohen, R. C., Laughner, J. L., Dibb, J. E., Hall, S. R., Ullmann, K., Wolfe, G. M., Pollack, I. B., Peischl, J., Neuman, J. A., and Zhou, X.: Why do models overestimate surface ozone in the Southeast United States?, *Atmos. Chem. Phys.*, 16, 13561–13577, <https://doi.org/10.5194/acp-16-13561-2016>, 2016.
- UN: World Urbanization Prospects: The 2014 Revision, available at: [https://esa.un.org/unpd/wup/CD-ROM/WUP2014\\_XLS\\_CD\\_FILES/WUP2014-F01-Total\\_Urban\\_Rural.xls](https://esa.un.org/unpd/wup/CD-ROM/WUP2014_XLS_CD_FILES/WUP2014-F01-Total_Urban_Rural.xls) (last access: 15 January 2018), 2014.
- UN: UN World Population Prospects: The 2015 Revision, available at: <http://esa.un.org/unpd/wpp/DVD/> (last access: 15 January 2018), 2015.
- UN: World urbanization prospects: The 2018 revision, annual percentage of population at mid-year residing in urban areas by region, subregion, country and area, 1950–2050, available at: <https://population.un.org/wup/Download/> (last access: 24 July 2019), 2018.
- UN: World Population Prospects 2019: Total population (both sexes combined) by region, subregion and country, annually for 1950 to 2100, available at: <https://esa.un.org/unpd/wpp/Download/Standard/Population/> (last access: 24 July 2019), 2019.
- UNFCCC: National Inventory Submissions of Annex I Parties to the UNFCCC, available at: <https://di.unfccc.int/> (last access: 12 August 2019), 2019.
- US EPA: An inventory of sources and environmental releases of dioxin-like compounds in the US for the years 1987, 1995, and

- 2000, US Environmental Protection Agency, Washington DC, USA, EPA/600/P-03/002F, 667 pp., 2006.
- US EPA: Criteria Air Pollutants, available at: <https://www.epa.gov/criteria-air-pollutants> (last access: 23 January 2020), 2018.
- US EPA: National Annual Emissions Trend: 1970–2018, available at: <https://www.epa.gov/air-emissions-inventories/air-pollutant-emissions-trends-data>, last access: 26 August 2019.
- van der Werf, G. R., Randerson, J. T., Giglio, L., van Leeuwen, T. T., Chen, Y., Rogers, B. M., Mu, M., van Marle, M. J. E., Morton, D. C., Collatz, G. J., Yokelson, R. J., and Kasibhatla, P. S.: Global fire emissions estimates during 1997–2016, *Earth Syst. Sci. Data*, 9, 697–720, <https://doi.org/10.5194/essd-9-697-2017>, 2017.
- Venkataraman, C., Brauer, M., Tibrewal, K., Sadavarte, P., Ma, Q., Cohen, A., Chaliyakunnel, S., Frostad, J., Klimont, Z., Martin, R. V., Millet, D. B., Philip, S., Walker, K., and Wang, S.: Source influence on emission pathways and ambient PM<sub>2.5</sub> pollution over India (2015–2050), *Atmos. Chem. Phys.*, 18, 8017–8039, <https://doi.org/10.5194/acp-18-8017-2018>, 2018.
- Venkataraman, C., Bhushan, M., Dey, S., Ganguly, D., Gupta, T., Habib, G., Kesarkar, A., Phuleria, H., and Raman, R. S.: Indian Network Project on Carbonaceous Aerosol Emissions, Source Apportionment and Climate Impacts (COALESCE), *B. Am. Meteorol. Soc.*, 101, E1052–E1068, 2020.
- Wang, S., Zhang, Q., Martin, R. V., Philip, S., Liu, F., Li, M., Jiang, X., and He, K.: Satellite measurements oversee China's sulfur dioxide emission reductions from coal-fired power plants, *Environ. Res. Lett.*, 10, 114015, <https://doi.org/10.1088/1748-9326/10/11/114015>, 2015.
- Wiedinmyer, C., Akagi, S. K., Yokelson, R. J., Emmons, L. K., Al-Saadi, J. A., Orlando, J. J., and Soja, A. J.: The Fire INventory from NCAR (FINN): a high resolution global model to estimate the emissions from open burning, *Geosci. Model Dev.*, 4, 625–641, <https://doi.org/10.5194/gmd-4-625-2011>, 2011.
- Wiedinmyer, C., Yokelson, R. J., and Gullett, B. K.: Global Emissions of Trace Gases, Particulate Matter, and Hazardous Air Pollutants from Open Burning of Domestic Waste, *Environ. Sci. Technol.*, 48, 9523–9530, <https://doi.org/10.1021/es502250z>, 2014.
- Zhang, Q., Streets, D. G., Carmichael, G. R., He, K. B., Huo, H., Kannari, A., Klimont, Z., Park, I. S., Reddy, S., Fu, J. S., Chen, D., Duan, L., Lei, Y., Wang, L. T., and Yao, Z. L.: Asian emissions in 2006 for the NASA INTEX-B mission, *Atmos. Chem. Phys.*, 9, 5131–5153, <https://doi.org/10.5194/acp-9-5131-2009>, 2009.
- Zhao, Y., Nielsen, C. P., Lei, Y., McElroy, M. B., and Hao, J.: Quantifying the uncertainties of a bottom-up emission inventory of anthropogenic atmospheric pollutants in China, *Atmos. Chem. Phys.*, 11, 2295–2308, <https://doi.org/10.5194/acp-11-2295-2011>, 2011.
- Zheng, B., Tong, D., Li, M., Liu, F., Hong, C., Geng, G., Li, H., Li, X., Peng, L., Qi, J., Yan, L., Zhang, Y., Zhao, H., Zheng, Y., He, K., and Zhang, Q.: Trends in China's anthropogenic emissions since 2010 as the consequence of clean air actions, *Atmos. Chem. Phys.*, 18, 14095–14111, <https://doi.org/10.5194/acp-18-14095-2018>, 2018.
- Zheng, B., Chevallier, F., Yin, Y., Ciais, P., Fortems-Cheiney, A., Deeter, M. N., Parker, R. J., Wang, Y., Worden, H. M., and Zhao, Y.: Global atmospheric carbon monoxide budget 2000–2017 inferred from multi-species atmospheric inversions, *Earth Syst. Sci. Data*, 11, 1411–1436, <https://doi.org/10.5194/essd-11-1411-2019>, 2019.

Supplement of Earth Syst. Sci. Data, 12, 3413–3442, 2020  
<https://doi.org/10.5194/essd-12-3413-2020-supplement>  
© Author(s) 2020. This work is distributed under  
the Creative Commons Attribution 4.0 License.



*Supplement of*

**A global anthropogenic emission inventory of atmospheric pollutants from sector- and fuel-specific sources (1970–2017): an application of the Community Emissions Data System (CEDs)**

**Erin E. McDuffie et al.**

*Correspondence to:* Erin E. McDuffie ([erin.mcduffie@wustl.edu](mailto:erin.mcduffie@wustl.edu))

The copyright of individual parts of the supplement might differ from the CC BY 4.0 License.



## **Section S1. CEDS Update Details: CEDSv2019-12-23 relative to CEDSv2016-07-26**

CEDSv2019-12-23 (Hoesly et al., 2019) was the first full public CEDS release (<https://github.com/JGCRI/CEDS>) and is used as the core system version in this work. An earlier version, CEDSv2016-07-26 was used to produce the CEDS<sub>Hoesly</sub> inventory, as described in detail in Hoesly et al. (2018) and its supplement. Changes to the CEDS code between versions v2016-07-26 and v2019-12-23 are described in the CEDS System Release Notes on GitHub (<https://github.com/JGCRI/CEDS/wiki/Release-Notes>). These updates include structural changes as well as improvements in the emissions data. The most significant improvements, which are also carried through to the CEDS<sub>GBD-MAPS</sub> inventory include:

- Updated residential waste burning estimates
- Fixed an error in 1960s USA SO<sub>2</sub> emissions and several other issues.

These updates are described in further detail in the following sections. A graphical summary of the differences between versions v2016-07-26 (CEDS<sub>Hoesly</sub>) and v2019-12-23 is available at the CEDS repository (<https://github.com/JGCRI/CEDS/> at the link “Graphs of emission differences”). Additional updates are described in the CEDS System Release Notes (<https://github.com/JGCRI/CEDS/wiki/Release-Notes>) and the git log of the CEDS<sub>GBD-MAPS</sub> system, available for download at [https://github.com/emcduffie/CEDS/tree/CEDS\\_GBD-MAPS](https://github.com/emcduffie/CEDS/tree/CEDS_GBD-MAPS).

### **S1.1 Residential waste burning**

Updates to emissions from residential open waste burning reduces emissions of all air pollutant species, particularly BC and OC emissions in lower income countries. The major change is a reduction in the assumed amount of uncollected waste that is burnt. The previous CEDS estimate was based on the 2010 value from Wiedinmyer et al. (2014) who assumed that 60% of uncollected solid waste was combusted. We conducted a literature survey, summarized below, to provide more insight into this value. We note that, for the purpose of emission estimation, the parameter we wish to know is the fraction of waste by weight that is combusted. This will be smaller than the fraction of waste that is disposed of through burning, since a significant portion of waste can be inert (e.g., ash, glass, and metals).

Reyna-Bensusan et al. (2018) examined waste disposal by surveying a “representative community” in Mexico about waste generation rates and disposal practices (Huejutla de Reyes Municipality). The Municipality has areas ranging from rural to urban and peri-urban in character. They found that in rural areas with limited access to municipal waste collection (69% had access only to a once-a-month service), 36% of household waste by weight was combusted. Commoner et al. (2000) additionally found in a survey in the Mexico state of Morelos that 14% of household waste was combusted in backyard burning, which corresponded to 52% of uncollected household waste, although only waste practices were surveyed, and waste generation rates were taken from national statistics. This is likely to overestimate the total amount of waste burnt since rural households generate half the waste per capita as compared to urban households (Reyna-Bensusan et al., 2018).

Nagpure et al. (2015) examined waste disposal using a more direct field methodology in three neighborhoods in Delhi India. The neighborhood with the lowest socio-economic status, where “field observation showed very sparse waste management facilities” had the highest rate of waste burning of ~24% of the total generated.

For Indonesia, Meidiana and Gamse (2010) report on government statistics that imply that only 15% of uncollected waste was burnt in 2006, while 70% was burnt in 2001. It is not clear if this difference is a true difference in burning rate, or different statistical methodologies.

Data is not necessary more available in higher income countries. In the United States residential waste has long been disposed by burning in barrels (“barrel burning”), particularly in rural areas. However, “The amount of refuse that is combusted annually in the United States in residential backyard burn barrels is largely unknown (US EPA, 2006).” This same report identified seven literature sources of survey data largely developed “to estimate the barrel-burning activity in a specific state, county, or region.” The “prevalence of barrel burning within the rural population [was found] to range from 12 to 40%”. The EPA ultimately assumed that from 40% (1995 and 1987) to 28% (2000) of the rural population burned household refuse, the decrease reflecting a larger number of jurisdictions banning refuse burning in 2000 as compared to earlier years. EPA further assumed that 63% of the household refuse (not including yard waste) was combusted. The confidence of these estimates is rated as low. Multiplying burning prevalence by the fraction of waste burnt results in overall waste burnt fractions of 25% (1995 and 1987) and 18% (2000) for rural populations.

Overall, the fraction of residential waste that is combusted is uncertain and is likely to vary spatially and over time. For the current estimate, informed by the literature discussed above, we assume that 30% of uncollected waste is burnt, which is half the value assumed by Wiedinmyer et al. (2014), with a correspondingly lower emissions level.

With one exception the per-capita waste generation rates from Wiedinmyer et al. (2014) have been retained. For India, however, we use the value from Sharma et al. (2019), which is twice the value in Wiedinmyer et al. (2014), leaving estimates from India largely unchanged.

## **S1.2 Other Changes**

An error in US SO<sub>2</sub> emissions over the 1960s caused an incorrect step-increase in emissions in 1960 in CEDSv2016-07-26. This update will not be carried through to CEDS<sub>GBD-MAPS</sub> as these emissions are reported from 1970 onward. An error that caused a spike in BC emissions in the Netherlands was also corrected and the consistency of Korea BC and OC emissions with the Korea national inventory was improved. These issues and their fixes are further described in the *issues* section of the CEDS GitHub repository. There are also small differences in the CEDSv2016-07-26 and CEDSv2019-12-23 emissions in the US after 2011, particularly NH<sub>3</sub>, due to scaling to more recent EPA Trends data. Note also that the monthly seasonality profile for the gridded industrial sector emissions was removed in CEDSv2019-12-23. While there is likely some seasonality in emissions in this sector, seasonality in the CEDSv2016-07-26 data was judged to be too large.

## **Section S2. CEDS Update Details: CEDS<sub>GBD-MAPS</sub> relative to CEDSv2019-12-23**

Section 2 in the Main Text describes updates to the CEDSv2019-12-23 code that are used to derive the new 1970 – 2017 CEDS<sub>GBD-MAPS</sub> inventory. Sections S2.1 – S2.5 below provide additional details regarding these updates. The CEDS<sub>GBD-MAPS</sub> source code is available at: [https://github.com/emcduffie/CEDS/tree/CEDS\\_GBD-MAPS](https://github.com/emcduffie/CEDS/tree/CEDS_GBD-MAPS).

### **S2.1 Activity Data Updates – Additional Details**

For the CEDS<sub>GBD-MAPS</sub> system, we have updated the inputs for activity data for both types of CEDS source categories (combustion and process) in order to enable the extension of the CEDS<sub>GBD-MAPS</sub> inventory out to the year 2017. We note that the distinction between CEDS combustion and process category sources is reflective of both the emission sector definition and CEDS methodology. For example, the 1A1bc\_Other\_transformation sector includes emissions from fuel combustion, but is treated as a process sector in CEDS due to the complexity of its processes, which include emissions from coal coke production, oil refining, and charcoal production (Hoesly et al., 2018). Other similar process sectors include emissions from the 5C\_waste-incineration and 1B1\_Fugitive-petr-and-gas sectors. Unlike CEDS combustion source categories, emissions from all process sectors are assigned to a single ‘process’ fuel-type, which may misallocate total emissions from biofuel, coal, and liquid oil and gas combustion to the process source category in the final fuel-specific CEDS<sub>GBD-MAPS</sub> products, as discussed in Sect. 4.2.

#### **S2.1.1 Combustion Sources**

For CEDS<sub>GBD-MAPS</sub> combustion category sources, activity data are primarily from energy consumption data, which have been updated to use the 2019 release of the World Energy Statistics from the International Energy Agency (IEA, 2019) for 40 OECD and 114 non-OECD countries and regions. For a small number of countries in Africa, Asia, and the Americas, data are only reported by the IEA at an aggregate region-level and are further disaggregated into their individual countries using historical CO<sub>2</sub> emissions data, as described in Hoesly et al. (2018). Historical national-level CO<sub>2</sub> emissions have been updated here to the most recent release from the Carbon Dioxide Information Analysis Center (CDIAC), which includes data from 1750 to 2014 (Boden et al., 2017). As IEA energy consumption data are provided at finer sectoral and fuel-type resolution than CEDS working sectors and fuels, CEDS Step 1 maps the IEA data to 52 working CEDS sectors and nine working fuel-types. Table S1 provides an example of the mapping between IEA fuels and CEDS working fuel types. Following the CEDSv2019-12-23 procedures, IEA data for residential biofuel consumption from the U.S. are replaced with renewable energy consumption data from the U.S. Energy Information Administration (EIA, 2019), which have been updated here to include the period from 1970 – 2017. In addition, CEDS<sub>GBD-MAPS</sub> no longer applies corrections to the IEA data for coal consumption from China, which were previously used in the CEDSv2019-12-23 system. There is, however, a known issue in the updated IEA data from China that is listed in Sect. S4 below. As described in Hoesly et al. (2018), the CEDSv2019-12-23 system additionally used coal, oil, and gas consumption data from the BP Energy Statistics product (BP, 2015) to extend available IEA data (IEA, 2015) out to the year 2014. Complete IEA data for the year 2017 are available in this work (IEA, 2019), therefore BP energy statistics are no longer used to extend emission estimates, but have been updated (BP, 2019) here as they are also used to estimate emissions from fossil fuel flaring.

**Table S1. CEDS fuel-type definitions. CEDS<sub>GBD-MAPS</sub> fuel types, CEDS working fuel-type definitions, and IEA fuel-types**

<b>CEDS Fuels</b>	
<b>Coal</b>	<b>Liquid Fuel + Natural Gas</b>
<i>Brown coal</i>	<i>Heavy Oil</i>
Brown coal (if no detail)	Oil shale and oil sands
Lignite	Crude/NGL/feedstocks
Peat	Crude oil
Peat products	Fuel oil
<i>Coal Coke</i>	Bitumen
Coke oven coke	Paraffin waxes
<i>Hard coal</i>	Petroleum coke
Hard coal (if no detail)	Other oil products
Anthracite	<i>Diesel Oil</i>
Coking coal	Gas/diesel oil excl. biofuels
Other bituminous coal	Lubricants
Sub-bituminous coal	Biodiesels
Patent fuel	<i>Light Oil</i>
Gas coke	Refinery stocks
Coal tar	Additives/blending components
BKB	Other hydrocarbons
<b>Biofuel</b>	Ethane
<i>Biofuel</i>	Liquefied petroleum gases (LPG)
Industrial waste	Motor gasoline excl. biofuels
Municipal waste (renewable)	Aviation gasoline
Municipal waste (non-renewable)	Gasoline type jet fuel
Primary solid biofuels	Kerosene type jet fuel excl. biofuels
Non-specified primary biofuels/waste	Other kerosene
Charcoal	Naptha
<b>Process</b>	White spirit & SBP
<i>Process</i>	Biogasoline
	Other liquid biofuels
	Bio jet kerosene
	<i>Natural Gas</i>
	Natural gas liquids
	Gas works gas
	Coke oven gas
	Blast furnace gas
	Other recovered gases
	Natural gas
	Refinery gas
	Biogases

### S2.1.2 Process Sources

For CEDS<sub>GDD-MAPS</sub> process category sources, activity drivers are primarily from the UN World Population and World Urbanization Prospects, which are updated here to extend to 2017 (UN, 2019, 2018). These data are used as activity drivers for all CEDS process sources except for 5C\_waste-incineration, 1B2\_Fugitive-pert-and-gas, and 1B2d\_Fugitive-other-energy. As described in Hoesly et al. (2018), pulp and paper consumption data (FAOSTAT, 2015) are used for default emission estimates of waste incineration (held constant here after 2014), while the latter two sectors now use a composite product that is derived from updated 2019 IEA energy statistics. World Bank data were not updated in this work (last year 2014) relative to CEDSv2019-12-23 since these data are only used to supplement population data for Kosovo. Table S2 summarizes the activity driver dataset updates that are used in CEDS<sub>GDD-MAPS</sub> relative to CEDSv2019-12-23. The Supplemental Information of Hoesly et al. (2018) provides a complete list of all additional CEDS input datasets, which have not been updated in this work.

**Table S2. Comparison of activity driver datasets that are updated between CEDSv2019-12-23 and CEDS<sub>GDD-MAPS</sub> systems. For a complete list of CEDS activity drivers, see Hoesly et al. (2018).**

CEDS Emission Source Category	Hoesly et al. (2018)	CEDS <sub>GDD-MAPS</sub>
Fuel combustion	(IEA, 2015) (BP, 2015) EIA, 2(The World Bank, 2016;UN, 2014, 2015;Wiedinmyer et al., 2014)015 (biofuel from US) (Boden et al., 2016)	(IEA, 2019) (BP, 2019) (flaring estimates only) (EIA, 2019) (biofuel from US) (Boden et al., 2017)
Process	(UN, 2014, 2015) (The World Bank, 2016) (FAOSTAT, 2015)	(UN, 2019, 2018) (The World Bank, 2016) (FAOSTAT, 2015)

## S2.2. Emission Factors & Inventory Input Updates – Additional Details

### S2.2.1 Combustion Sources

The datasets used to calculate default emission factors (EF) for combustion sources in the CEDS<sub>GDD-MAPS</sub> system are largely unchanged relative to those in CEDSv2019-12-23 (see Table 2 in Hoesly et al. (2018) for a complete list). For reactive gases, combustion EFs are primarily estimated using information from the GAINS model (as released for the Energy Modeling Forum 30 (EMF30) project (Klimont et al., 2017;Stohl et al., 2015)), SPEW for BC and OC (Bond et al., 2007), and the U.S. 2011 NEI for NH<sub>3</sub>. As described in Hoesly et al. (2018), EF calculations take into account historical changes in emission abatement strategies, while some EFs for SO<sub>2</sub> are also calculated explicitly using fuel sulfur content, ash retention, and country-specific percent controls (NEI, 2013). EF and emission calculations do not include information about the vertical distribution of emissions. For countries with missing contemporary sectoral or fuel-type information, EFs are extended forward to 2017 using trends from GAINS projections. The minimum allowable EFs for road transportation have also been extended to 2017, which ensures the use of realistic EFs from this sector in recent years for countries with missing data.

### S2.2.2 Process Sources

For non-combustion sectors, EFs in CEDS<sub>GBD-MAPS</sub> Step 1 are estimated using existing emission inventories and calculated activity drivers, as described previously in Sect. 2.1. These emission estimates are primarily from the global EDGAR inventory, which has been updated in this work to use a more recent release of EDGAR (v4.3.2; EC-JRC, 2018; Crippa et al., 2018). For emissions of waste combustion, all versions of the CEDS system use country-specific EFs for 2010 from Wiedinmyer et al. (2014), along with estimates of the total mass. As described in Sect. S1.1 above, relative to CEDSv2016-07-26, assumptions for the fraction of waste burnt have been updated in both CEDSv2019-12-23 and CEDS<sub>GBD-MAPS</sub>, along with estimates for the amount of waste generated per-capita in India (Sharma et al., 2019). Additional details on these updates can be found in the core CEDS system release notes (<https://github.com/JGCRI/CEDS/wiki/Release-Notes>). Similar to combustion sources, missing EFs are also extended forward and backwards in time to produce a complete time series for 1970 - 2017. Table 2 in Hoesly et al. (2018) provides a complete list of all input datasets used to estimate default process source emissions. Other than those described here, all remaining datasets are unchanged in this work relative to CEDSv2019-12-23. Despite uncertainties in contemporary EFs and default emission estimates for both source categories, many of these values are later scaled to match contemporary regional and national-level inventories (see Sect. 2.2).

## **S2.3 Default CEDS Emissions Scaling Procedure Updates – Additional Details**

### **S2.3.1 Scaling Mapping Files & Misc. Details**

The first step of the scaling procedure is to aggregate emissions from common sectors and fuel-types into “scaling sectors” and “scaling fuel” groups (when fuel-specific emissions are available) for each scaling inventory. This is necessary as there are often differences in the availability and definitions of emission from source sectors and fuel-types between CEDS and the scaling inventories. Total default CEDS emissions within these aggregate groups are then scaled to the corresponding emissions in each scaling inventory, using the scaling factors calculated from Eq. (2) in the main text. All mapping files can be found at: [https://github.com/emcduffie/CEDS/tree/CEDS\\_GBD-MAPS/input/mappings/scaling](https://github.com/emcduffie/CEDS/tree/CEDS_GBD-MAPS/input/mappings/scaling), with specific examples described below.

The first column in each mapping file provides the sectoral names from the scaling inventory. When emissions are reported as a function of fuel type, the second column lists the fuel-types reported for each emission sector in the scaling inventory. When applicable, column three defines the aggregate scaling fuel groups. Column four defines the aggregate scaling sector groups. Columns five and six list the CEDS working sectors and working fuels that correspond to these aggregate scaling groups. Table S3 provides an example scaling mapping file for the DICE-Africa scaling inventory. Table S3 shows that the DICE-Africa inventory reports combined emissions from gas (petrol) and diesel use in cars and motorcycles. The CEDS system does not differentiate between different types of on-road sources and therefore, DICE-Africa emissions from both cars and motorcycles are mapped to the common ‘road\_transport’ scaling sector, which corresponds to the CEDS 1A3b\_Road sector. Similarly, the DICE-Africa inventory does not distinguish between emissions from gas and diesel fuel, therefore total CEDS road emissions from light\_oil and diesel\_oil combustion in the road sector are scaled to the total DICE-Africa emissions reported for cars and motorcycles. Example scaling factors for select years and countries in Africa, as a function of scaling sector are provided in Table S4. Data are included for illustrative purposes only. Following original CEDS protocols, scaling

factors are limited to values between 0.01 and 100, with select inventories and sectors expanded to a range of 0.001 and 1000, as described below in Section S2.3.2. As discussed in Hoesly et al. (2018), particularly small or large scaling factors may result for multiple reasons, including default CEDS estimates that are drastically different than regional emissions or imprecise mapping between CEDS and regional emission sectors.

**Table S3. Example scaling mapping file for DICE-Africa in CEDS<sub>GBD-MAPS</sub> system.**

DICE-Africa sector	DICE-Africa fuel	Scaling Fuel	Scaling Sector	CEDS Sector	CEDS Fuel
cars	gas_diesel	gas_diesel	road_transport	1A3b_Road	light_oil
		gas_diesel	road_transport	1A3b_Road	diesel_oil
motorcycles	gas_diesel	gas_diesel	road_transport		
charcoal-use	biomass	biomass	residential	1A4b_Residential	biomass
household-crop-residue-use	biomass	biomass	residential		
household-fuelwood-use	biomass	biomass	residential		
kerosene-use	light_oil	light_oil	residential	1A4b_Residential	light_oil
other-fuelwood-use <sup>a</sup>	biomass	n/a	n/a	n/a	n/a
adhoc-oil-refining <sup>a</sup>	process	n/a	n/a	n/a	n/a
generator-use <sup>a</sup>	gas_diesel	n/a	n/a	n/a	n/a
charcoal-production <sup>a</sup>	biomass	n/a	n/a	n/a	n/a
gas-flares <sup>a</sup>	process	n/a	n/a	n/a	n/a

<sup>a</sup>Suggested additions, not replacements, see Sect. S2.3.2

**Table S4. Example BC scaling factors for select DICE-Africa countries and years.**

Country (ISO)	Scaling Sector	Scaling Fuel	2006	2007	2008	2009	2010	2011	2012	2013	2014	2015
ago	residential	biomass	0.332	0.338	0.344	0.350	0.355	0.361	0.367	0.373	0.373	0.373
ago	residential	light oil	0.340	0.311	0.282	0.252	0.223	0.194	0.165	0.136	0.136	0.136
ago	road_transport	gas_diesel	0.307	0.293	0.278	0.264	0.250	0.235	0.221	0.207	0.207	0.207
nam	residential	biomass	0.297	0.320	0.342	0.364	0.386	0.409	0.431	0.453	0.453	0.453
nam	residential	light oil	44.71	44.72	44.72	44.72	44.73	44.73	44.73	44.74	44.74	44.74
nam	road_transport	gas_diesel	0.274	0.260	0.247	0.234	0.220	0.207	0.194	0.180	0.180	0.180

Relative to CEDS v2019-12-23, minor adjustments have been made to other inventory scaling mapping files in order to better reflect the overlap between CEDS<sub>GBD-MAPS</sub> working sectors and the updated scaling inventories. One example is the adjustment of scaling factors for agricultural NO<sub>x</sub> emissions for the U.S. NEI and Canadian APEI inventories. In these national inventories, NO<sub>x</sub> emissions from soils are not reported (report NH<sub>3</sub> emissions only). In CEDSv2019-12-23, NO<sub>x</sub> emissions from the sum of all agricultural working sectors (3B+3D+3E+3I; including soil emissions) are scaled to the total agricultural NO<sub>x</sub> emissions reported in these scaling inventories, resulting in scaled CEDS agricultural NO<sub>x</sub> emissions that are erroneously low. In this work, CEDS<sub>GBD-MAPS</sub> 3D\_Soil-emissions from the US and Canada are no longer scaled to these inventories and default emission estimates are used for this working sector. These updated scaling mapping files can be found at: [https://github.com/emcduffie/CEDS/tree/CEDS\\_GBD-MAPS/input/mappings/scaling](https://github.com/emcduffie/CEDS/tree/CEDS_GBD-MAPS/input/mappings/scaling).

After the scaling procedure, CEDS<sub>GBD-MAPS</sub> emissions are then disaggregated back into the original 52 CEDS working sectors and 9 working fuel-types (Table 2, combustion source only) using the initial fractional contributions from each sector and fuel-type. This method allows CEDS to maintain detailed fuel and sectoral information while simultaneously scaling total country-level emissions to authoritative inventories. This process, however, often results in total CEDS<sub>GBD-MAPS</sub> emissions that are higher than the individual scaling inventories, depending on the amount of

overlap with each inventory. For example, Fig. (S1) shows that in China, total  $\text{CEDS}_{\text{GBD-MAPS}}$  emissions for OC after 2010 are larger than those in the national scaling inventory, reported by Zheng et al. (2018). This difference is largely due to the inclusion of the waste sector in  $\text{CEDS}_{\text{GBD-MAPS}}$ , which is not reported in the Zheng et al. (2018) inventory. In contrast, other inventories report emissions from sources that are not included in CEDS, such as open burning on agricultural fields or road dust emissions. In these cases, these sectors are not included in the CEDS scaling procedure and are not included in the final  $\text{CEDS}_{\text{GBD-MAPS}}$  inventory. In addition, sectors such as domestic shipping are not scaled and are always set to default CEDS estimates due to large uncertainties and differences in the definitions of these sectors in individual scaling inventories. To illustrate the outcome of the scaling procedure, implied emission factors for the top 15 emitting countries are additionally shown in Figure S2 for the select fuel-types and sectors that dominantly contribute to global emission of each compound. Various anomalies in the implied EFs can arise from multiple sources of uncertainty, including the underlying activity data or application of scaling factors outside the available scaling inventory years, as is the case with the on-road CO emission factor for China in 1999. These uncertainties are discussed further in Section 4.2 in the main text.

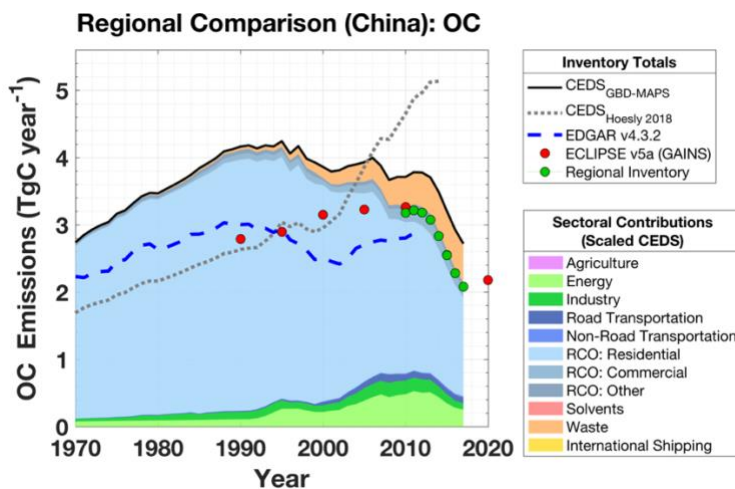


**Figure S1.** Inventory comparison of annual OC emissions from China. Black line) total  $\text{CEDS}_{\text{GBD-MAPS}}$  emissions, colored by sectoral contributions, dashed gray line)  $\text{CEDS}_{\text{Hoesly}}$  emissions, dashed blue line) EDGAR v4.3.2 emissions, red dots) ECLIPSE v5a (GAINS) inventory with 2015 and 2020 projections, green dots) scaling inventory from Zheng et al. (2018). This comparison does not include contributions from agricultural waste burning, shipping, or aviation emissions.



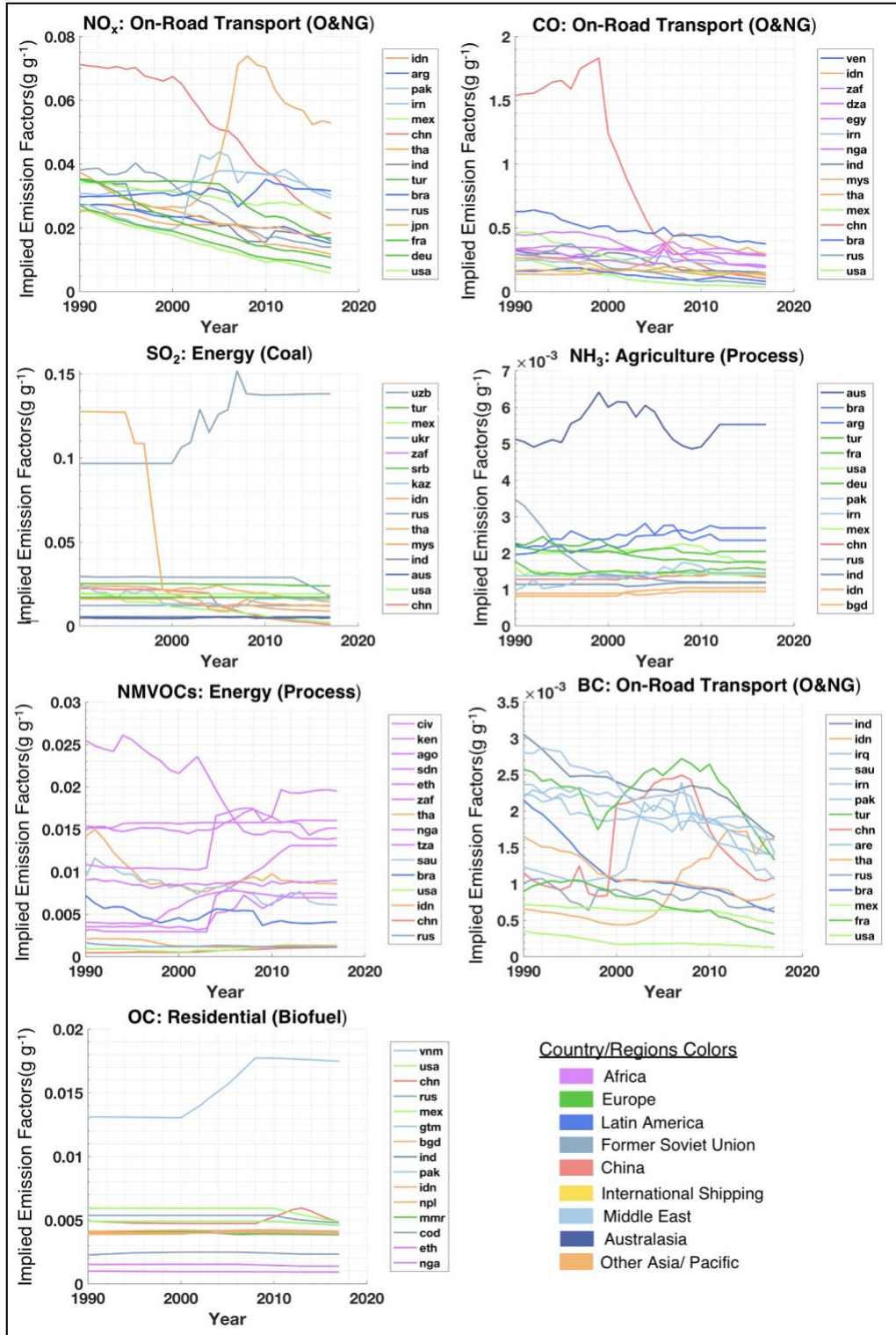


Figure S2. Time-series of implied (post-scaling) emission factors for select fuel and sector combinations that dominantly contribute to global emissions of each compounds. NO<sub>x</sub>, CO, and BC: oil & natural gas combustion in the on-road transport sector, SO<sub>2</sub>: coal combustion in the energy sector, NH<sub>3</sub>: agricultural emissions, NMVOCs: process-level energy sources, and OC: residential biofuel combustion. Time series are shown for the top 15 emitting countries, listed by their ISO codes to the right of each panel. Time series are colored by the region of each country.

### S2.3.2 Africa Emissions Scaling

As discussed in the main text, new scaling inventories are included in this work for emissions from India and Africa. For African countries, default CEDS<sub>GBD-MAPS</sub> emissions for residential and road sectors are scaled to the respective values in the DICE-Africa inventory (Marais and Wiedinmyer, 2016) for 2006 and 2013, as a function of diesel, light oil (Table S1), and biofuel use. For years between 2006 and 2013, scaling factors (SFs) from Eq. (2) in the main text are linearly interpolated within the CEDS system. These SFs are held constant before 2006 and after 2013. DICE-Africa OC emissions from cars are additionally scaled by 0.14 prior to the CEDS scaling procedure in order to correct for a previous error in the DICE-Africa OC EFs ([http://wiki.seas.harvard.edu/geos-chem/index.php/DICE-Africa\\_anthropogenic\\_emissions\\_inventory#Scale\\_DICE-Africa\\_emissions\\_to\\_address\\_errors\\_in\\_inventory](http://wiki.seas.harvard.edu/geos-chem/index.php/DICE-Africa_anthropogenic_emissions_inventory#Scale_DICE-Africa_emissions_to_address_errors_in_inventory)).

Upper and lower bounds of scaling factor are additionally relaxed here to limits of 1000 and 0.001 (100 and 0.01 in CEDS<sub>v2019-12-23</sub>) to ensure better agreement between DICE-Africa and CEDS<sub>GBD-MAPS</sub> sectoral totals. In a small number of instances, calculated scaling factors are outside this range, which may reflect differences in sectoral definitions between the two inventories or real uncertainties in the magnitude of sectoral-level emissions in Africa.

As also noted in the main text, DICE-Africa emission estimates from gas flares across Africa and ad-hoc oil refining in the Niger Delta are not included in the CEDS<sub>GBD-MAPS</sub> scaling procedure (Table S2). Total default CEDS<sub>GBD-MAPS</sub> emissions in Africa for each compound in 2013 from the 1B2\_fugitive\_petr\_gas (gas flaring) sector are almost always larger than the respective DICE-Africa gas-flaring emissions, suggesting that emissions from this source sector may be accurately represented in default CEDS<sub>GBD-MAPS</sub> estimates. However, in the event that gas-flaring emissions from the DICE-Africa inventory are not accounted for in the CEDS<sub>GBD-MAPS</sub> default emissions, the CEDS<sub>GBD-MAPS</sub> 1B2\_fugitive\_petr\_gas emissions across Africa may be underestimated by up to 28% (or up to < 0.01 Tg) for each compound in 2013 (Table S3).

In addition, DICE-Africa emissions from petrol/diesel use in residential generators, as well as fuelwood use for charcoal production and other commercial activities are not included in the CEDS<sub>GBD-MAPS</sub> scaling procedure. These sectors are not explicitly represented by the CEDS<sub>GBD-MAPS</sub> working sectors and are only expected to be represented in the CEDS<sub>GBD-MAPS</sub> default estimates to the extent that these sources are included in the IEA energy consumption data. Emissions from charcoal production will be allocated to the 1A1bc\_Other-Transformation sector, while commercial fuelwood use would be allocated to the 1A4a\_Commercial-institutional sector. In the event that these sources are not included in default CEDS<sub>GBD-MAPS</sub> emissions, the emissions from biofuel use in the CEDS other transformation and commercial sectors in 2013 may be underestimated by up to 100% (or up to 6 Tg) for each compound (Table S5). Similarly, residential generator use may be allocated to the 1A4b\_Residential (RCO-R) and/or 1A4c\_Agriculture-forestry-fishing (RCO-Other) sectors. In the event that generators are not accounted for in default estimates, CEDS emissions from light oil/diesel use in the residential sectors may be underestimated by up to 84% (or up to 0.25 Tg) for each compound (Table S5). While these maximum possible under-predictions represent large fractions of emissions from individual fuels and sectors, the sum of these potential missing emissions correspond to maximum under-predictions in total 2013 CEDS<sub>GBD-MAPS</sub> emissions in Africa of less than 11% (or < 10.5 Tg) for each compound (Table S3). Possible under-predictions of <11% are within typical uncertainties of bottom-up emission

inventories (Sect. 4.2.3). Table S5, however, does indicate that some emissions from commercial and residential sectors in Africa may be underpredicted in CEDS<sub>GBD-MAPS</sub> inventory.

**Table S5. Maximum possible under-predictions in sectoral CEDS<sub>GBD-MAPS</sub> Africa emissions relative to DICE-Africa**

DICE Sectors (Fuels)	CEDS Sectors (Fuels)	NO <sub>x</sub>		SO <sub>2</sub>		CO		NMVOC		NH <sub>3</sub>		BC		OC	
		Tg <sup>a</sup>	% <sup>b</sup>	Tg <sup>a</sup>	% <sup>b</sup>	Tg <sup>a</sup>	% <sup>b</sup>	TgC <sup>a</sup>	% <sup>b</sup>	Tg <sup>a</sup>	% <sup>b</sup>	TgC <sup>a</sup>	% <sup>b</sup>	TgC <sup>a</sup>	% <sup>b</sup>
Gas Flares	1B2_fugitive_petr_gas	0.03	<0.1	-	-	<0.01	<0.1	<0.01	<0.1	-	-	<0.01	14	<0.01	28
Residential Generators (gas/diesel)	1A4b_Residential + 1A4c_Agriculture-forestry-fishing (light oil + diesel oil)	0.25	84	0.01	26	0.05	48	<0.01	2	-	-	<0.01	<0.01	<0.01	0.1
Charcoal production (fuelwood)	1A1bc_Other-transformation (process)	<0.01	16	-	-	6.0	99	2.5	99	0.03	99	<0.01	16	0.02	81
Com. Activity (fuelwood)	1A4a_Commercial-institutional (biomass)	0.09	100	0.03	88	4.5	98	2.0	99	<0.01	68	0.05	68	0.2	68
Sum of above sectors	All CEDS <sub>GBD-MAPS</sub> Africa Emissions	0.37	6	0.04	0.7	10.5	11	4.5	9	0.03	0.5	0.05	6.5	0.22	8

<sup>a</sup>Sum DICE-Africa 2013 emissions from each country within the given sector

<sup>b</sup>Potential underprediction in CEDS<sub>GBD-MAPS</sub> sectoral emissions, assuming DICE-Africa emissions are not accounted for in default CEDS estimates (i.e., 100\* (CEDS<sub>GBD-MAPS</sub> Em. + DICE-Africa Em.) / CEDS<sub>GBD-MAPS</sub> Em.)

As discussed in the main text, Fig. 3 compares the scaled CEDS<sub>GBD-MAPS</sub> emissions of all compounds in Africa to those from the CEDS<sub>Hoesly</sub> inventory. Large differences include the reductions of NO<sub>x</sub> and BC emissions from the on-road transport sector in CEDS<sub>GBD-MAPS</sub> relative to the CEDS<sub>Hoesly</sub> inventory. As discussed in Sect. 2.2, these reductions are largely driven by a difference in EFs used for emissions from diesel vehicles. For the on-road transport sector, the DICE-Africa inventory uses activity data from the UN energy database for total petrol/diesel use in the transport sector, which is then divided into usage for motorcycles and vehicles as described in Marais and Wiedinmyer (2016). Vehicle activity data are not split further, and a single EF is applied to total vehicle activity data to calculate DICE-Africa emissions from all on-road cars. This DICE-Africa EFs for cars are consistent with the default CEDS EFs for on-road gasoline emissions and will be more representative of light vehicles than larger diesel trucks, which have default EFs in CEDS roughly twice as large.

### S2.3.2 India Emissions Scaling

We also scale emissions from India to a new 2015 emissions inventory described in Venkataraman et al. (2018) (SMoG-India). Similar scaling sector and fuel definitions are defined as described above. As described in the main text, emissions for NO<sub>x</sub>, SO<sub>2</sub>, CO, NMVOCs, OC, and BC are available for 17 sectors and nine fuel types. Scaling mapping files can be found at: [https://github.com/emcduffie/CEDS/tree/CEDS\\_GBD-MAPS/input/mappings/scaling](https://github.com/emcduffie/CEDS/tree/CEDS_GBD-MAPS/input/mappings/scaling). Scaling factors were calculated for the year 2015 and applied forward and back to the entire 1970 – 2017 timeseries. Due to uncertainties in the sectoral mapping and applicability of 2015 scaling factors over the entire time period, we note the potential misallocation of the SMoG-India ‘Informal Industry’ sector to the CEDS<sub>GBD-MAPS</sub> 1A2c\_ind-Comb-Food-tobacco sector (rather than the 1A2g-Comb-Ind-other sector). This misallocation results in CEDS<sub>GBD-MAPS</sub> NO<sub>x</sub> emissions in India possibly overpredicted by up to ~1 Tg between 1987-2014 (see also Sect. S4). While sectoral

misallocations impact the magnitude of sub-sector emissions, total  $\text{CEDS}_{\text{GBD-MAPS}}$  industry emissions in 2015 are equivalent to total industry emissions (information + light + heavy industry) from the SMOG-India inventory.

In addition, there are cases where default CEDS emissions for a specific sector/fuel-type combination equal 0, resulting in emissions of 0 after the scaling process. To avoid missing emissions in these instances, CEDS working fuel types are aggregated into “scaling fuels” (total coal, total liquid fuel, natural gas, and process emissions) in a similar manor to the scaling sectors (as described above in Sect. S2.3), and are later re-allocated to the CEDS working fuel types according to distributions prior to scaling. While this process may result in a slightly different fuel distribution at the most detailed level, final  $\text{CEDS}_{\text{GBD-MAPS}}$  emissions (both gridded and country-level products) are aggregated into contributions from total coal, biofuel, oil and gas, and process emissions.

#### **S2.4 Default BC and OC Emission Scaling Procedure Updates – Additional Details**

Relative to CEDS v2019-12-23, BC and OC emissions are now scaled to available regional- and national-level inventories.  $\text{CEDS}_{\text{GBD-MAPS}}$  emissions for OC and BC from countries within each scaling inventory are shown in Fig. S3 and S4. These figures additionally compare these emissions to those from the  $\text{CEDS}_{\text{Hoesly}}$ , GAINS (ECLIPSE v5a) (Klimont et al., 2017), EDGAR v4.3.2 (Crippa et al., 2018), and scaling inventories. As described above and in the main text, regional inventories and final  $\text{CEDS}_{\text{GBD-MAPS}}$  emissions may not agree depending on the level of overlap between the sectoral emissions included in each scaled inventory. For example, the national emissions from China (Zheng et al., 2018) are lower than the  $\text{CEDS}_{\text{GBD-MAPS}}$  estimates due to waste emissions that are not included in the national-inventory.

It should also be noted that emissions from the metal and chemical industrial sectors in Japan are underestimated in both  $\text{CEDS}_{\text{Hoesly}}$  and  $\text{CEDS}_{\text{GBD-MAPS}}$  relative to the country level inventory (preliminary update from Kurokawa et al., 2013). Default CEDS emissions for these sectors are estimated to be zero in CEDS Step 1 and are therefore not scaled to the available inventory emissions. This underprediction is largest for years prior to 1995 (see Fig. S4) and is reduced in recent years due to a decreasing fractional contribution of these sectors to total OC and BC emissions in the Kurokawa et al., 2013 inventory (40% to 28% for OC, 2% to 1.6% for BC between 1990 and 2010). In addition,  $\text{CEDS}_{\text{GBD-MAPS}}$  emissions are not scaled to EMEP emissions (EMEP, 2019) prior to 2000 due to changes in inventory reporting (Fig. S3).

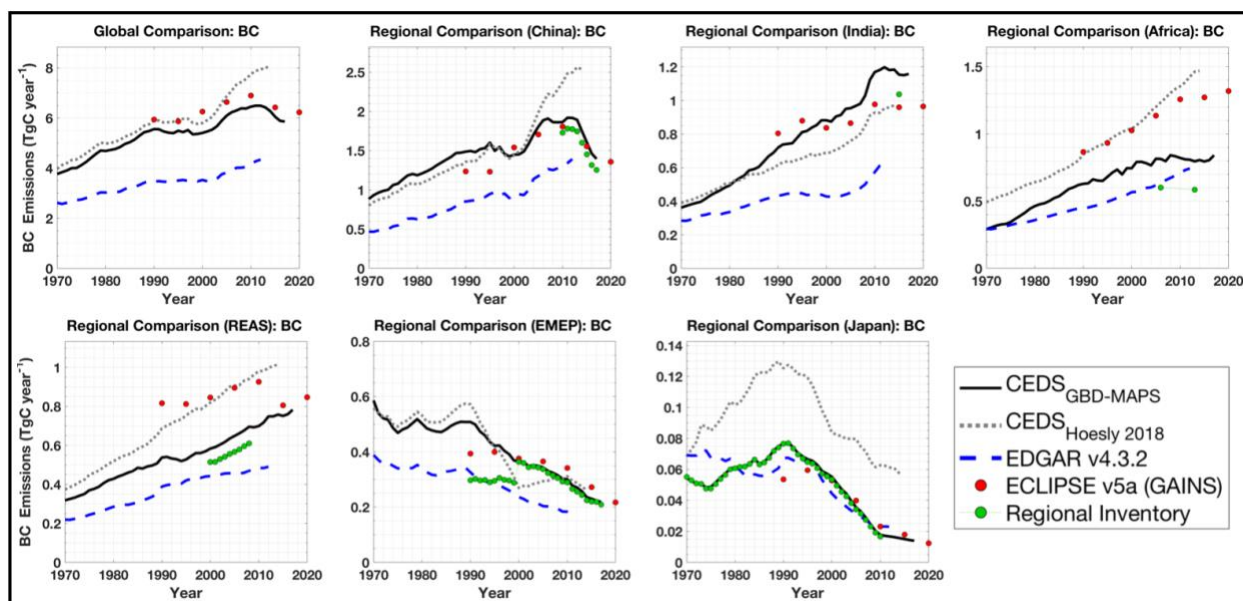


Figure S3. Time series of BC emissions from CEDS<sub>GBD-MAPS</sub> (black line), CEDS<sub>Hoesly</sub> (gray dashed line), EDGAR v4.3.2 (blue dashed line), and ECLIPSE v5a baseline current legislation (CLE) inventory from the GAINS model (red dots). Each panel shows total annual emissions from each designated country/region. GAINS values for 2015 and 2020 are emission projections. Global inventories show reported emissions from all sectors excluding open burning, shipping, and aviation. Respective regional inventories are shown by green dots/lines and include all reported emissions that are also included in regional CEDS<sub>GBD-MAPS</sub> emissions (e.g., do not include open burning, road dust, shipping, aviation, etc). Note: in the regional comparisons, CEDS<sub>GBD-MAPS</sub>, CEDS<sub>Hoesly</sub>, and EDGAR v4.3.2 emissions also include inland navigation, while GAINS v5a CLE do not include any shipping emissions. In the global comparison, all available shipping emissions (inland navigation and international shipping) are included in each inventory. REAS and EMEP member countries listed in Table S6.

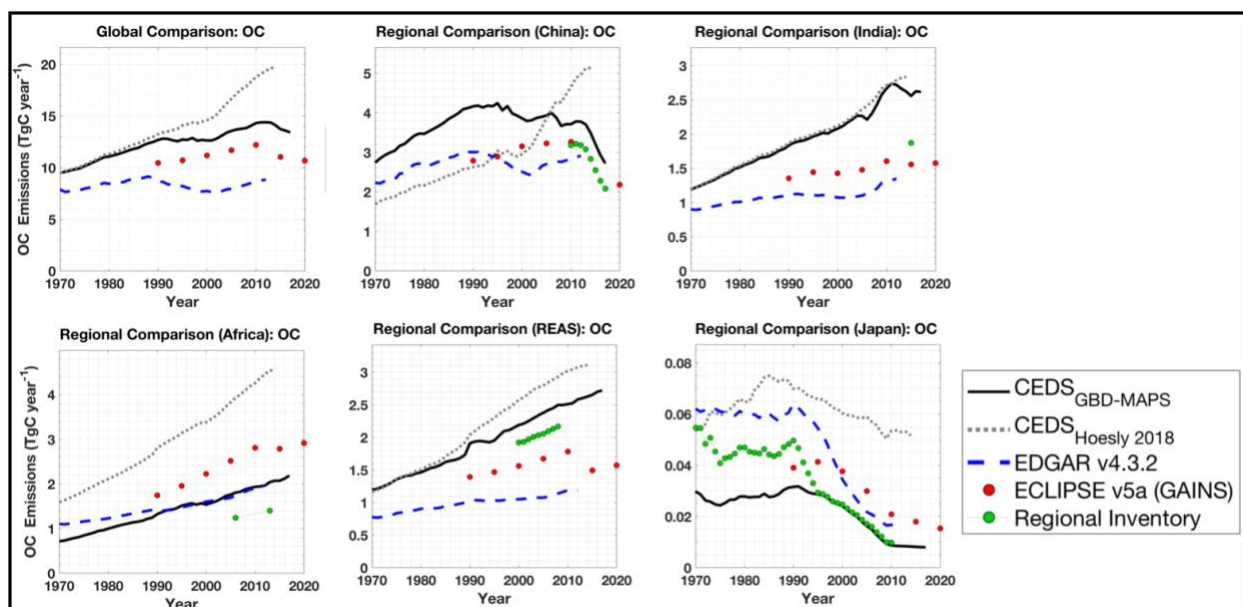


Figure S4. Same as Fig. S3, but for OC emissions.

**Table S6. Countries included in REAS and EMEP regions**

REAS	Afghanistan Bangladesh Indonesia Laos Malaysia Tajikistan Taiwan	Bhutan Maldives Myanmar Sri Lanka Turkmenistan Vietnam	Brunei Darussalam DPR Korea Kazakhstan Nepal Pakistan Philippines	Cambodia Kyrgyzstan Mongolia Singapore Thailand Uzbekistan
EMEP	Albania Belarus Bulgaria Denmark Georgia Iceland Luxembourg Norway Sweden United Kingdom	Armenia Austria Croatia Finland Greece Ireland Macedonia Poland Slovakia	Belgium Cyprus France Italy Malta Montenegro Portugal Slovenia Spain	Czech Republic Estonia Germany Hungary Kyrgyzstan Latvia Netherlands Romania Switzerland

### S2.5 Spatial Gridding & Aggregation Updates – Additional Details

Relative to CEDSv2019-12-23, CEDS emissions prior to gridding are now aggregated into 17 intermediate sectors as a function of four fuel categories: total coal (hard coal + brown coal + coal coke), solid biofuel, the sum of liquid fuel (heavy oil + light oil + diesel oil) and natural gas, and all remaining ‘process’ emissions.

CEDS Step 5 then spatially allocates total country-level emission estimates on to a  $0.5^{\circ} \times 0.5^{\circ}$  global grid to facilitate their use in earth system models. The procedure for spatially allocating CEDS total country-level emissions is largely unchanged between CEDSv2019-12-23 and CEDS<sub>GBD-MAPS</sub>. This process uses normalized spatial distribution proxies that are compound- and sector-specific. In CEDSv2019-12-23, proxy distribution data are primarily from gridded EDGAR emissions (v4.2 and v4.3) (EC-JRC/PBL, 2012, 2016) and HYDE population (Klein Goldewijk et al., 2011) (primarily for historical extension prior to 1970 and waste emissions). In CEDSv2019-12-23, gridding proxies are then held constant after 2008 or 2010 (ROAD transportation only). For the CEDS<sub>GBD-MAPS</sub> inventory, we have updated the compound- and sector-specific normalized spatial proxies for 1970 – 2012 to use the most recent release of the EDGAR inventory (v4.3.2) (Table S7). Spatial proxies are then held constant for all years after 2012. These updates extend many of the latest spatial proxies from 2008 to 2012 but may still introduce uncertainty in the gridded CEDS<sub>GBD-MAPS</sub> products between 2013 and 2017 for sectoral emissions that have experienced large changes in their normalized spatial distributions within large countries (Sect. 4.2.5). The same sector-specific gridding proxy is also applied to emissions from each fuel group within each sector. This process may introduce additional uncertainties into the gridded CEDS<sub>GBD-MAPS</sub> products as discussed in Sect. 4.2. These uncertainties do not impact the final country-level CEDS<sub>GBD-MAPS</sub> products because they are not gridded.

As further described in Hoesly et al. (2018), sectors that do not have congruent emissions between CEDS and EDGAR v4.3.2 inventories use population data from HYDE (Klein Goldewijk et al., 2011) and Gridded Population of the World (GPW) (Doxsey-Whitfield et al., 2015) products as backup spatial proxies. Supplemental Table S7 provides a complete list of gridding proxies as a function of sector. All sectors that do not use EDGAR data use the same spatial proxies as in CEDSv2019-12-23. For example, emissions from the waste sector are gridded using

yearly estimates of population, which have not been updated relative to CEDSv2019-12-23 and are therefore held constant after the year 2015.

**Table S7. Gridding proxies used for spatial allocation, listed by sector.**

<b>CEDS final sectors</b>	<b>CEDS intermediate gridding sectors</b>	<b>Spatial Proxy<sup>a</sup></b>	<b>Years<sup>b</sup></b>
Agriculture (AGR)	Agriculture	EDGAR v4.3.2 AGR	1970 – 2012
International Shipping (SHP)	International Shipping	ECLIPSE and additional data <sup>c</sup>	1990, 1995, 2000, 2005, 2010, 2015
	International Shipping (tanker loading)	ECLIPSE and additional data <sup>c</sup>	1996
On-Road Transportation (ROAD)	On-Road Transportation	EDGARv4.3.2 ROAD	2010
Non-Road Transportation (NRTR)	Non-Road Transportation	EDGAR v4.3.2 NRTR	1970 - 2012
Residential, Commercial, Other - Residential (RCOR)	Residential, Commercial, Other - Residential	EDGAR v4.3.2 RCO	1970 – 2012
Residential, Commercial, Other - Commercial (RCOC)	Residential, Commercial, Other - Commercial	EDGAR v4.3.2 RCO	1970 – 2012
Residential, Commercial, Other - Other (RCOO)	Residential, Commercial, Other - Other	EDGAR v4.3.2 RCO	1970 – 2012
Energy (ENE)	Oil and gas fugitive/flaring	ECLIPSE FLR <sup>c</sup>	1970 – 2015
	Electricity and heat production	EDGAR v4.3.2 ELEC	1970 – 2012
	Fuel production and transformation	EDGAR v4.3.2 ETRN	1970 – 2012
	Fossil Fuel Fires	EDGAR v4.3.2 FFFI	1970 - 2012
Waste (WST)	Waste	HYDE population, GPW v4 (modified rural population) <sup>c</sup>	1970 – 2015
Industry (IND)	Industrial Combustion	EDGAR v4.3.2 INDC	1970 – 2012
	Industrial process and product use	EDGAR v4.3.2 INPU	1970 – 2012
Solvent production and application (SLV)	Solvent production and application (SLV)	EDGAR v4.3.2 SLV	1970 - 2012

<sup>a</sup>All species and sectors use population as a backup proxy.

<sup>b</sup>Spatial proxies held constant for years not listed. For example, EDGAR v4.3.2 proxies from 2012 are used for years 2012-2017. All sectors use population as a backup proxy (2016-2017 use 2015 population).

<sup>c</sup>Not updated relative CEDS<sub>Hoesly</sub> inventory.

After the gridding procedure, the 17 intermediate sectors are then aggregated into 11 final sectors, by effectively splitting the original CEDSv2019-12-23 emissions from the TRA sector into ‘On-Road’ and ‘Non-Road/Other’ contributions and splitting the original RCO sector into individual contributions from the Residential, Commercial, and Other sectors. Table 2 contains a complete breakdown of the definitions of CEDS working, intermediate gridding, and final sectors. Figure S5 illustrates the level of detail available in this new CEDS<sub>GBD-MAPS</sub> inventory by illustrating global BC emissions in 2017 from 1) all source sectors, 2) the residential sector only, 3) residential biofuel-use only, and 4) residential coal-use only.

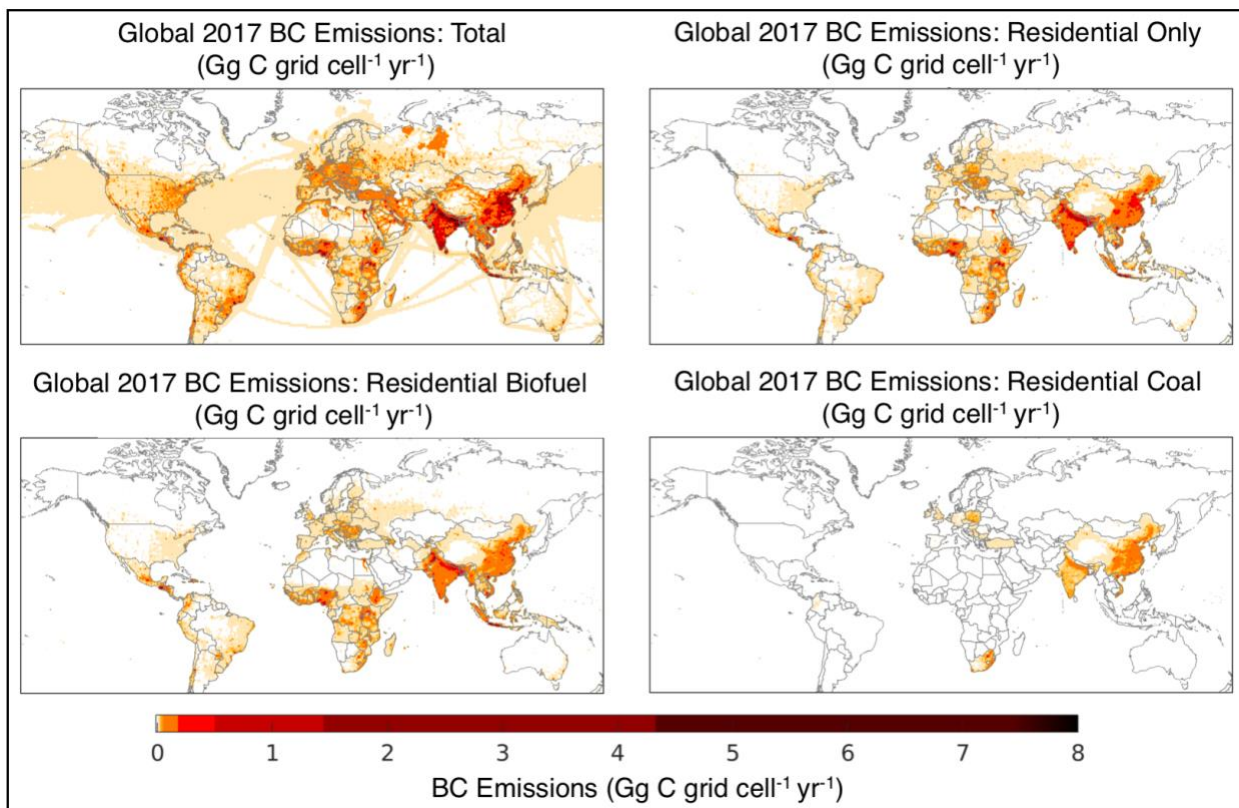


Figure S5. Map of global BC emissions for 2017 from (top left) all sectors, (top right) residential emissions only, (bottom left) residential biofuel only, and (bottom right) residential coal only.



### Section S3. Supplemental Results

**Table S8. Fractional sectoral and fuel-type contributions to 2017 global emissions of each compound. Sectoral contributions in bold sum to 100% for each compound (i.e., AGR + ENE + ... SHP =100%). Fractional contributions of fuel-types within each sector sum to 100% for each compound (i.e., ENE coal + ENE biofuel + ENE Oil+Gas + ENE Process =100%).**

Sector	Fuel-Type	NO <sub>x</sub>	CO	SO <sub>2</sub>	NH <sub>3</sub>	NMVOC	BC	OC
<b>AGR</b>	<b>Total</b>	<b>5%</b>	-	-	<b>75%</b>	-	-	-
AGR	Coal	-	-	-	-	-	-	-
AGR	Biofuel	-	-	-	-	-	-	-
AGR	Oil + Gas	-	-	-	-	-	-	-
AGR	Process	100	-	-	100	-	-	-
<b>ENE</b>	<b>Total</b>	<b>22%</b>	<b>11%</b>	<b>42%</b>	<b>2%</b>	<b>36%</b>	<b>10%</b>	<b>8%</b>
ENE	Coal	46	10	63	4	<1	3	7
ENE	Biofuel	3	2	<1	3	<1	15	53
ENE	Oil + Gas	35	8	18	6	<1	2	<1
ENE	Process	16	80	19	87	99	80	40
<b>IND</b>	<b>Total</b>	<b>15%</b>	<b>14%</b>	<b>36%</b>	<b>2%</b>	<b>6%</b>	<b>12%</b>	<b>10%</b>
IND	Coal	49	36	38	5	25	47	17
IND	Biofuel	10	11	1	39	25	24	78
IND	Oil + Gas	36	5	25	11	9	29	5
IND	Process	5	48	36	45	41	-	-
<b>ROAD</b>	<b>Total</b>	<b>23%</b>	<b>32%</b>	<b>2%</b>	<b>1%</b>	<b>17%</b>	<b>20%</b>	<b>7%</b>
ROAD	Coal	-	-	-	-	-	-	-
ROAD	Biofuel	-	-	-	-	-	-	-
ROAD	Oil + Gas	100	100	100	100	100	100	100
ROAD	Process	-	-	-	-	-	-	-
<b>NRTR</b>	<b>Total</b>	<b>6%</b>	<b>1%</b>	<b>1%</b>	<b>&lt;1%</b>	<b>1%</b>	<b>1%</b>	<b>&lt;1%</b>
NRTR	Coal	<1	<1	<1	<1	<1	<1	<1
NRTR	Biofuel	-	-	-	-	-	-	-
NRTR	Oil + Gas	100	100	100	100	100	100	100
NRTR	Process	<1	<1	<1	<1	<1	<1	<1
<b>RCOR</b>	<b>Total</b>	<b>3%</b>	<b>35%</b>	<b>4%</b>	<b>6%</b>	<b>18%</b>	<b>38%</b>	<b>54%</b>
RCOR	Coal	9	13	68	<1	2	13	8
RCOR	Biofuel	57	86	22	96	97	70	92
RCOR	Oil + Gas	34	1	10	3	1	17	<1
RCOR	Process	-	-	-	-	-	-	-
<b>RCOC</b>	<b>Total</b>	<b>1%</b>	<b>&lt;1%</b>	<b>2%</b>	<b>&lt;1%</b>	<b>&lt;1%</b>	<b>5%</b>	<b>4%</b>
RCOC	Coal	-	47	68	23	16	45	38
RCOC	Biofuel	-	12	1	28	29	28	54
RCOC	Oil + Gas	100	41	31	49	55	27	8
RCOC	Process	-	-	-	-	-	-	-
<b>RCOO</b>	<b>Total</b>	<b>3%</b>	<b>3%</b>	<b>1%</b>	<b>&lt;1%</b>	<b>1%</b>	<b>6%</b>	<b>2%</b>
RCOO	Coal	2	10	36	12	4	13	22
RCOO	Biofuel	1	21	1	11	23	10	48
RCOO	Oil + Gas	97	69	63	77	73	77	30
RCOO	Process	-	-	-	-	-	-	-
<b>SLV</b>	<b>Total</b>	-	-	-	<b>&lt;1%</b>	<b>17%</b>	-	-
SLV	Coal	-	-	-	-	-	-	-
SLV	Biofuel	-	-	-	-	-	-	-
SLV	Oil + Gas	-	-	-	-	-	-	-
SLV	Process	-	-	-	100	100	-	-
<b>WST</b>	<b>Total</b>	<b>2%</b>	<b>3%</b>	<b>&lt;1%</b>	<b>14%</b>	<b>2%</b>	<b>5%</b>	<b>13%</b>
WST	Coal	-	-	-	-	-	-	-
WST	Biofuel	-	-	-	-	-	-	-
WST	Oil + Gas	-	-	-	-	-	-	-
WST	Process	100	100	100	100	100	100	100
<b>SHP</b>	<b>Total</b>	<b>20%</b>	<b>&lt;1%</b>	<b>12%</b>	<b>&lt;1%</b>	<b>2%</b>	<b>3%</b>	<b>1%</b>
SHP	Coal	-	-	-	-	-	-	-
SHP	Biofuel	-	-	-	-	-	-	-
SHP	Oil + Gas	100	100	100	100	27	100	100
SHP	Process	-	-	-	-	73	-	-

**Table S9. Region/Country definitions for main text Fig. 8 and supplemental Fig. S7-S20 (grouped by geographical location)**

Region/Country	Member Countries			
Africa	Algeria Burkina Faso Cameroon Cape Verde Eritrea Guinea Kenya Madagascar Mauritius Niger Sao Tome and Principe Somalia Tunisia Zimbabwe	Angola Botswana Chad DR Congo Ethiopia Gambia Liberia Malawi Morocco Nigeria Senegal South Africa Swaziland Uganda	Burundi Central African Republic Congo Djibouti Gabon Guinea-Bissau Libya Mali Mozambique Reunion Seychelles South Sudan Tanzania Western Sahara	Benin Cote d'Ivoire Comoros Egypt Ghana Equatorial Guinea Lesotho Mauritania Namibia Rwanda Sierra Leone Sudan Togo Zambia
China	China			
Europe	Albania Bulgaria Denmark Gibraltar Iceland Luxembourg Netherlands Romania Spain United Kingdom	Austria Croatia Finland Greece Ireland Macedonia Norway Serbia and Montenegro Sweden	Belgium Cyprus France Greenland Italy Malta Poland Slovakia Switzerland	Bosnia Czech Republic Germany Hungary Liechtenstein Montenegro Portugal Slovenia Turkey
Former Soviet Union	Armenia Georgia Lithuania Russia	Azerbaijan Kazakhstan Moldova Ukraine	Belarus Kyrgyzstan Tajikistan Uzbekistan	Estonia Latvia Turkmenistan
India	India			
Latin America/Oceania	Antigua and Barbuda Barbados Brazil Colombia Dominica Faeroe Islands Guadeloupe Honduras Mexico Panama Saint Lucia Trinidad and Tobago Venezuela	Argentina Belize British Virgin Islands Costa Rica Dominican Republic Falkland Islands Guatemala Haiti Montserrat Paraguay St Pierre and Miquelon Turks and Caicos Islands	Aruba Bermuda Cayman Islands Cuba Ecuador French Guiana Jamaica Netherland Antilles Peru Sint Maarten St Vincent and Grenadines US Virgin Islands	Bahamas Bolivia Chile Curacao El Salvador Grenada Guyana Martinique Nicaragua Saint Kitts and Nevis Suriname Uruguay
North America	United States	Canada	Puerto Rico	
Other Asia/Pacific	American Samoa Cambodia Fiji Indonesia Macao Mongolia Niue Republic of Korea Sri Lanka Tokelau Wallis and Futuna Islands	Bangladesh Cook Islands French Polynesia Japan Malaysia Myanmar Palau Samoa Taiwan Tongo	Bhutan DPR Korea Guam Kiribati Maldives Nepal Papua New Guinea Singapore Thailand Vanuatu	Brunei Darussalam FS of Micronesia Hong Kong Laos Marshall Islands New Caledonia Philippines Soloman Islands Timor-Leste Vietnam
Australasia	Australia	New Zealand		
Middle East	Afghanistan Israel Pakistan Saudi Arabia	Bahrain Jordan Palestine Syria	Iraq Kuwait Oman United Arab Emirates	Islamic Republic of Iran Lebanon Qatar Yemen

To supplement the results presented in Sect. 3, Fig. S6 provides time series of the contributions of each source sector to global emissions, for each compound. Figures S7-S12 additionally show time series of sectoral emissions of each compound in dominant source regions, including North America, Europe, China, India, Africa, and the Other Asia/Pacific region (Table S9). To highlight the fuel-type information in the CEDS<sub>GBD-MAPS</sub> inventory, Fig. S13 also illustrates global emissions of each compound as a function of fuel-group and sector, while Fig. S13-S20 illustrate the fuel-type contributions to emissions from the 11 world regions listed above. Figures S21 and S22 compare CEDS<sub>GBD-MAPS</sub> and CEDS<sub>Hoesly</sub> emissions. Figures S23 and S24 provide an additional comparison of CEDS<sub>GBD-MAPS</sub> global sectoral emissions to sectoral emissions reported from the EDGAR v4.3.2 and GAINS (ECLIPSE v5a) inventories.

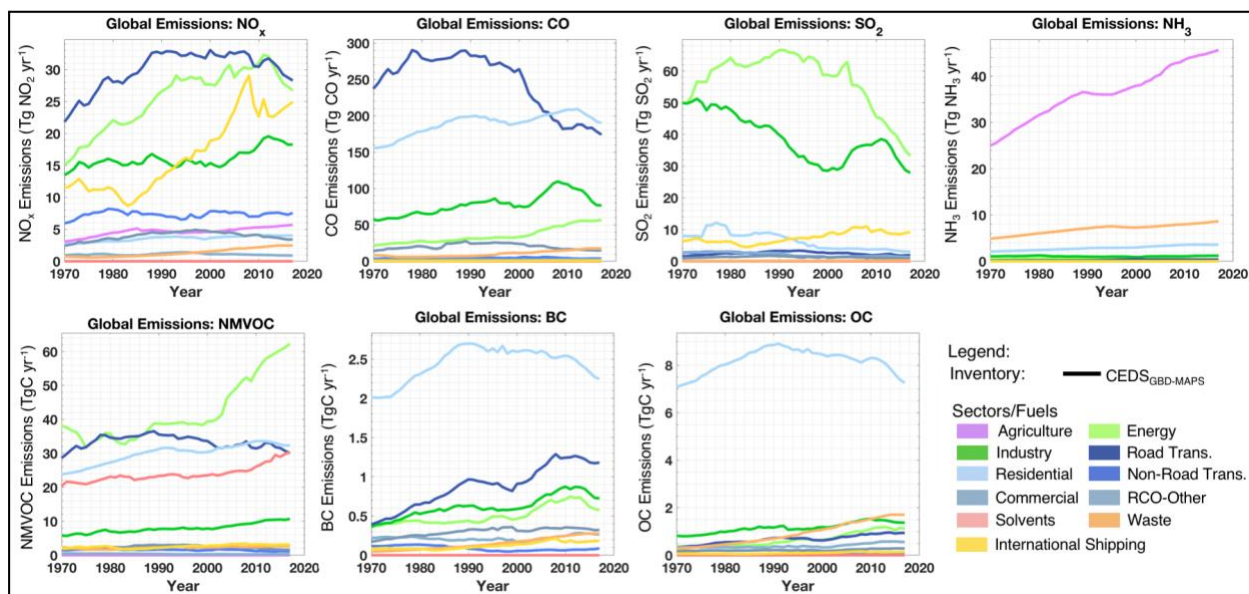


Figure S6. Time series of global emissions for each compound as a function of emission sector (all fuel types shown).

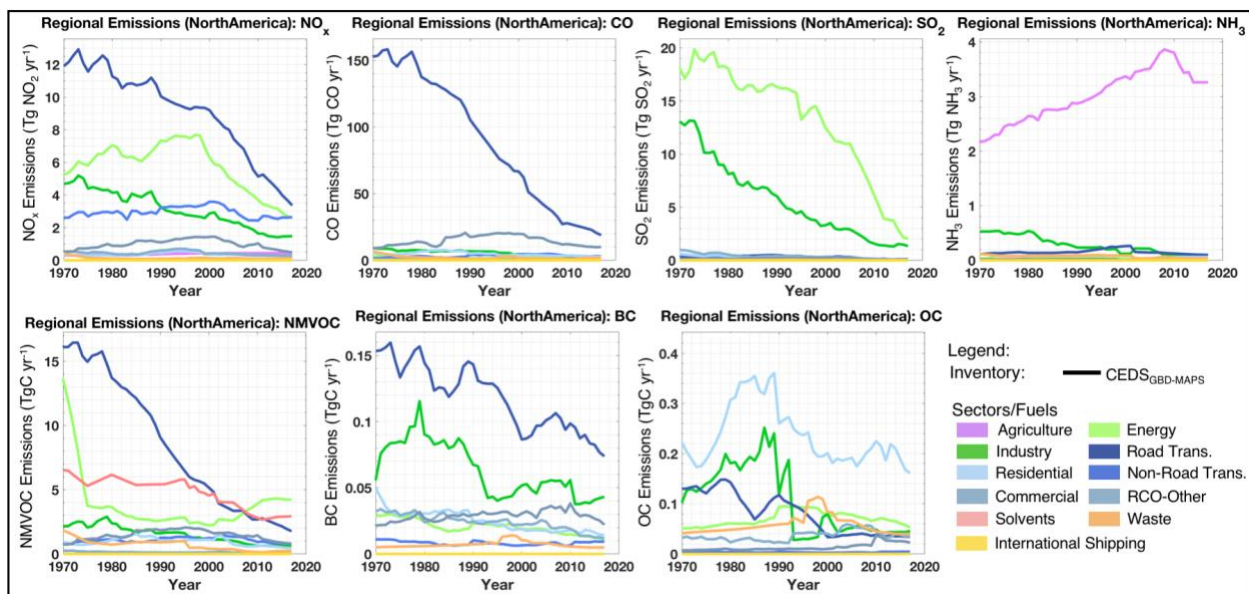


Figure S7. Time series of emissions in North America, as a function of emission sector (all fuel types shown).

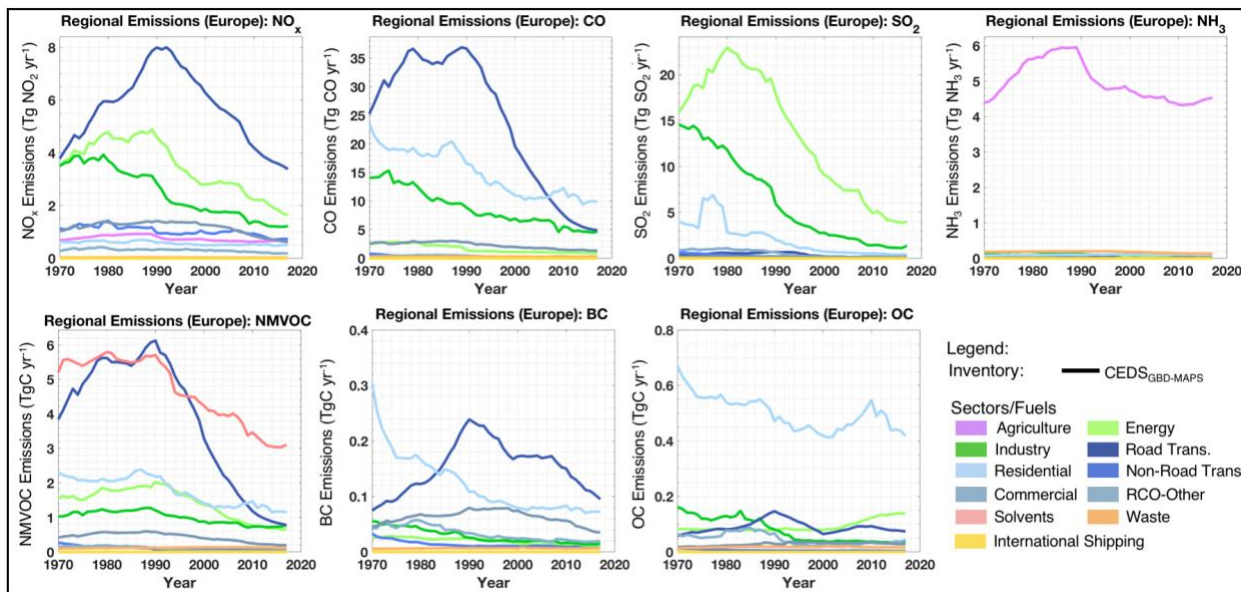


Figure S8. Time series of emissions in Europe, as a function of emission sector (all fuel types shown).

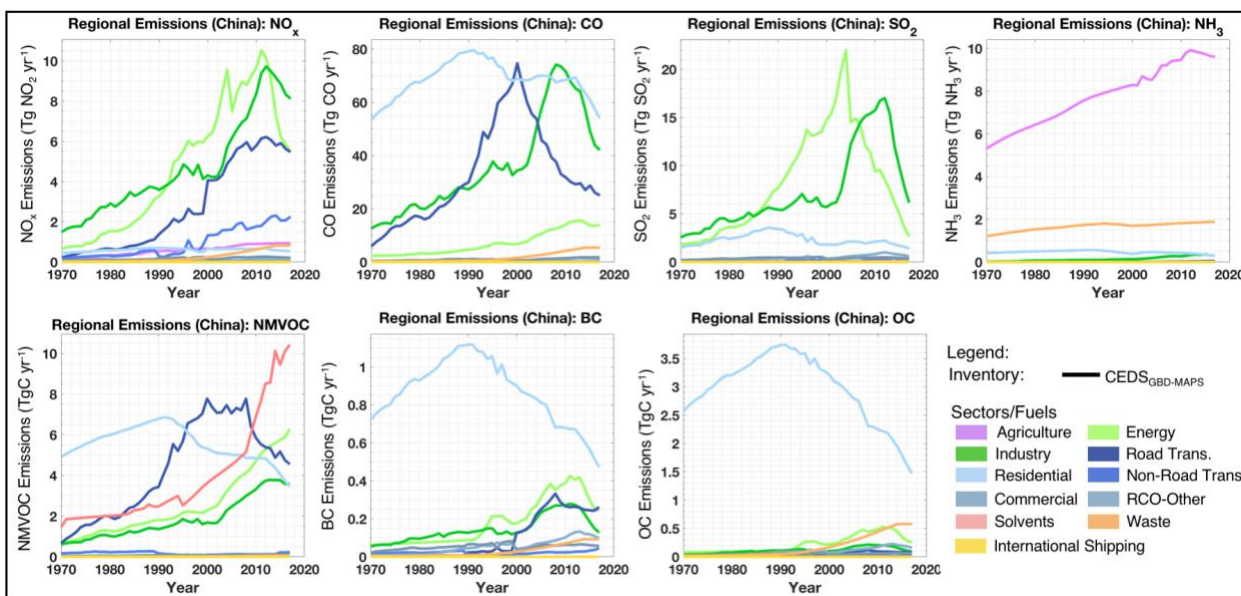


Figure S9. Time series of emissions in China, as a function of emission sector (all fuel types shown).

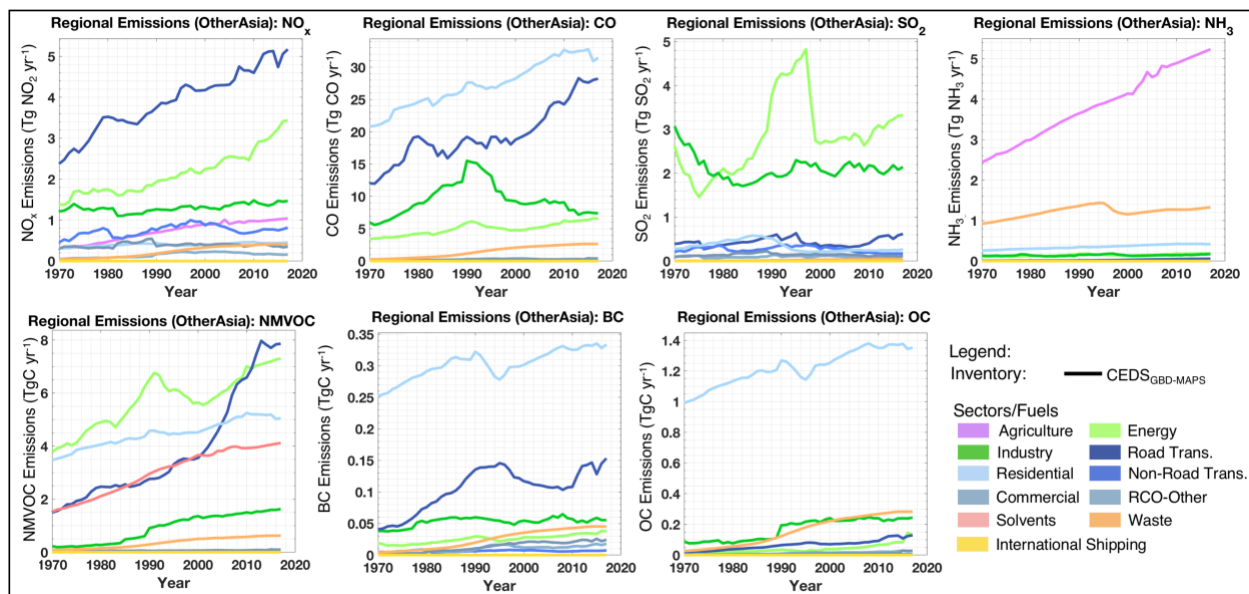


Figure S10. Time series of emissions in the Other Asia/Pacific region (Table S9), as a function of emission sector (all fuel types shown).

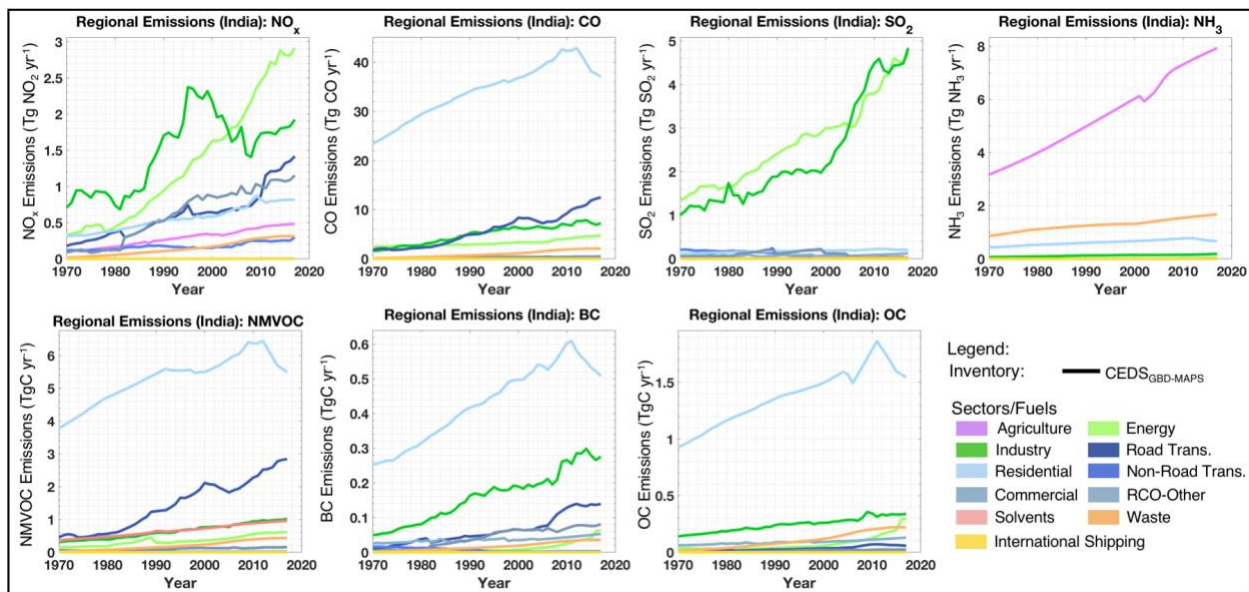


Figure S11. Time series of emissions in India, as a function of emission sector (all fuel types shown).

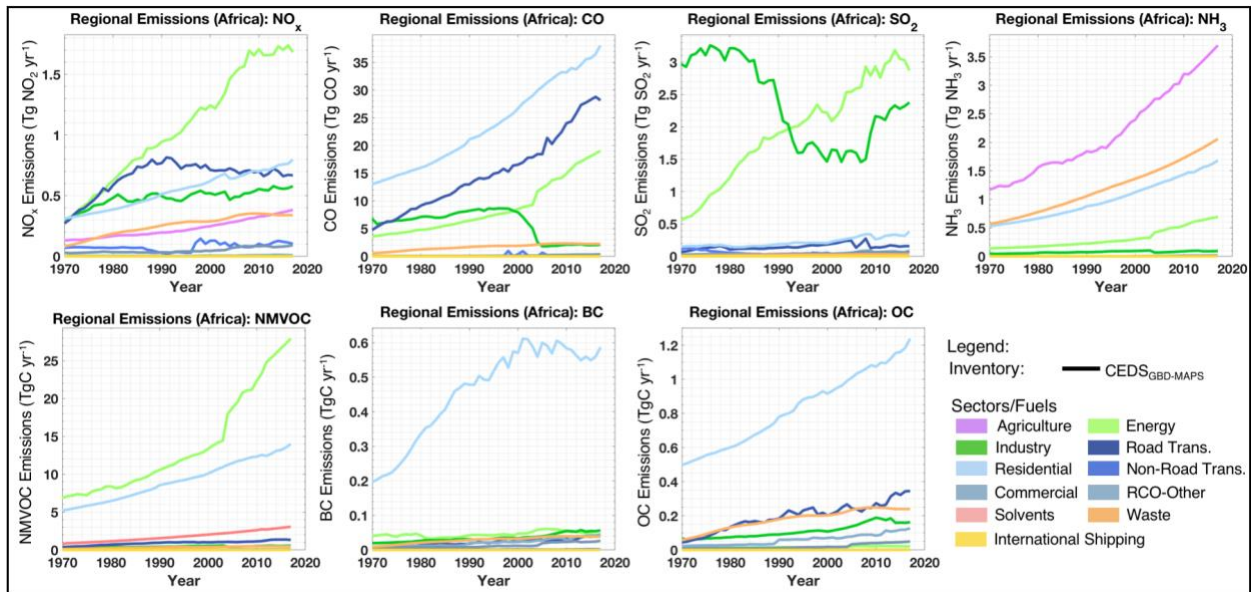


Figure S12. Time series of emissions in Africa, as a function of emission sector (all fuel types shown).

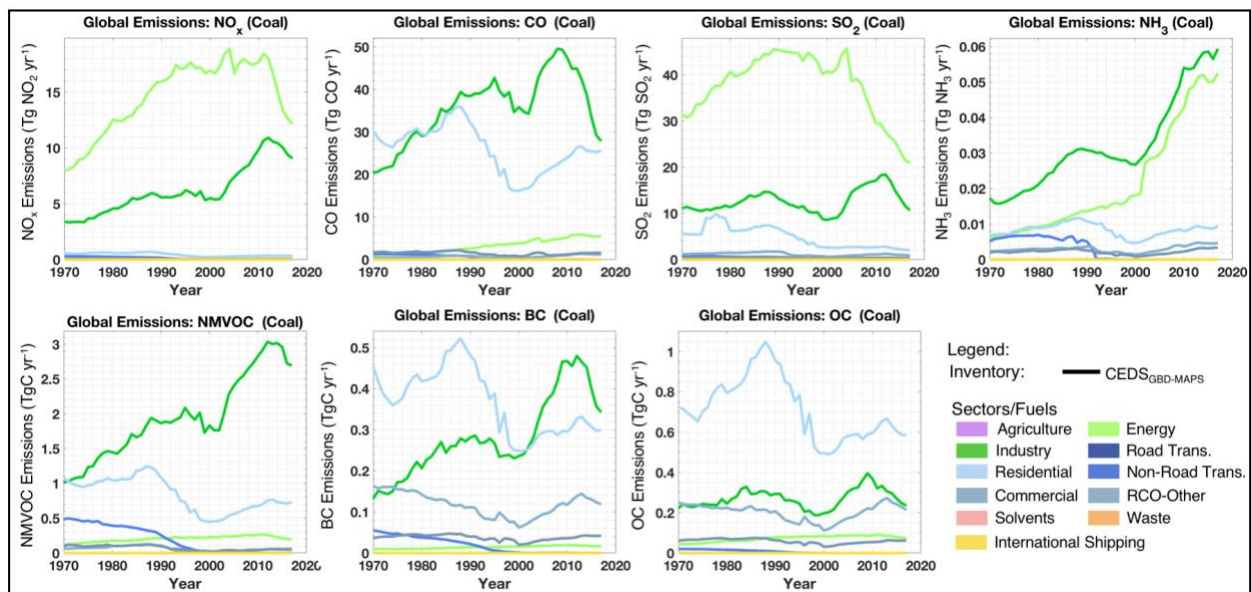


Figure S13. Time series of global sectoral emissions associated with coal combustion.

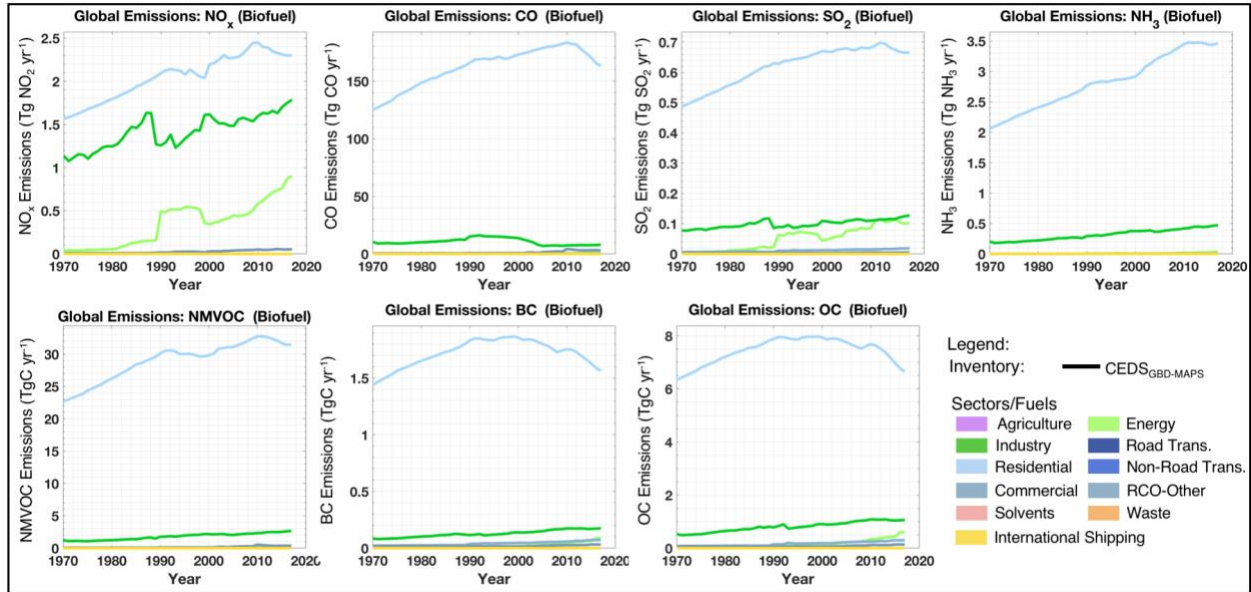


Figure S14. Time series of global sectoral emissions associated with solid biofuel combustion.

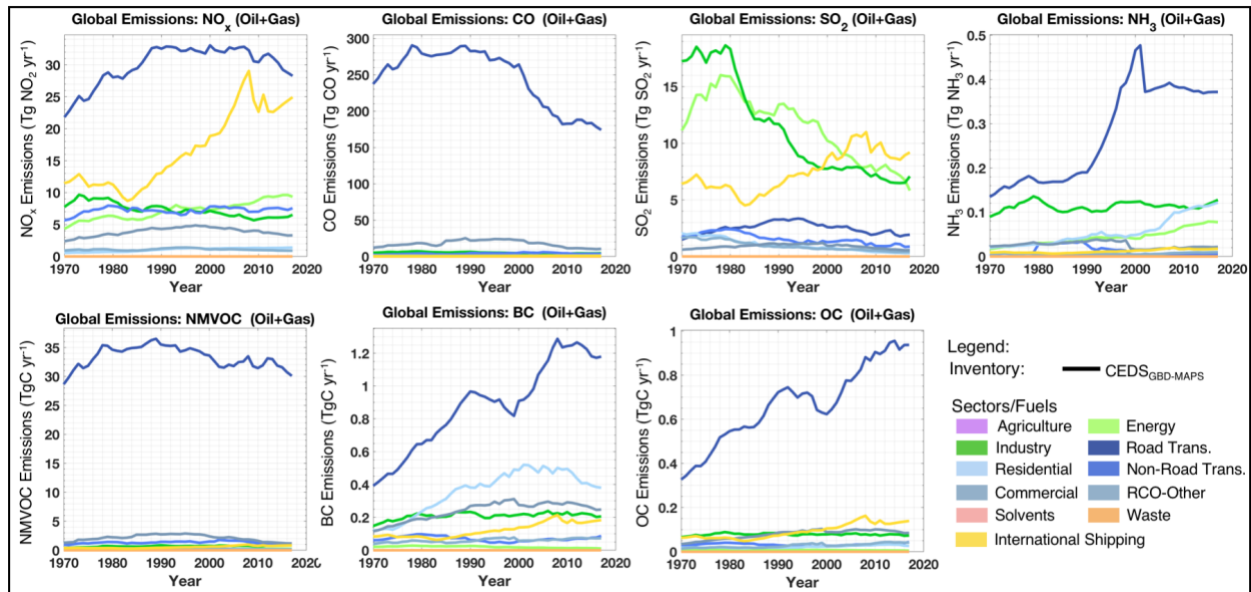


Figure S15. Timeseries of global sectoral emissions associated with the combustion of liquid oil and natural gas.

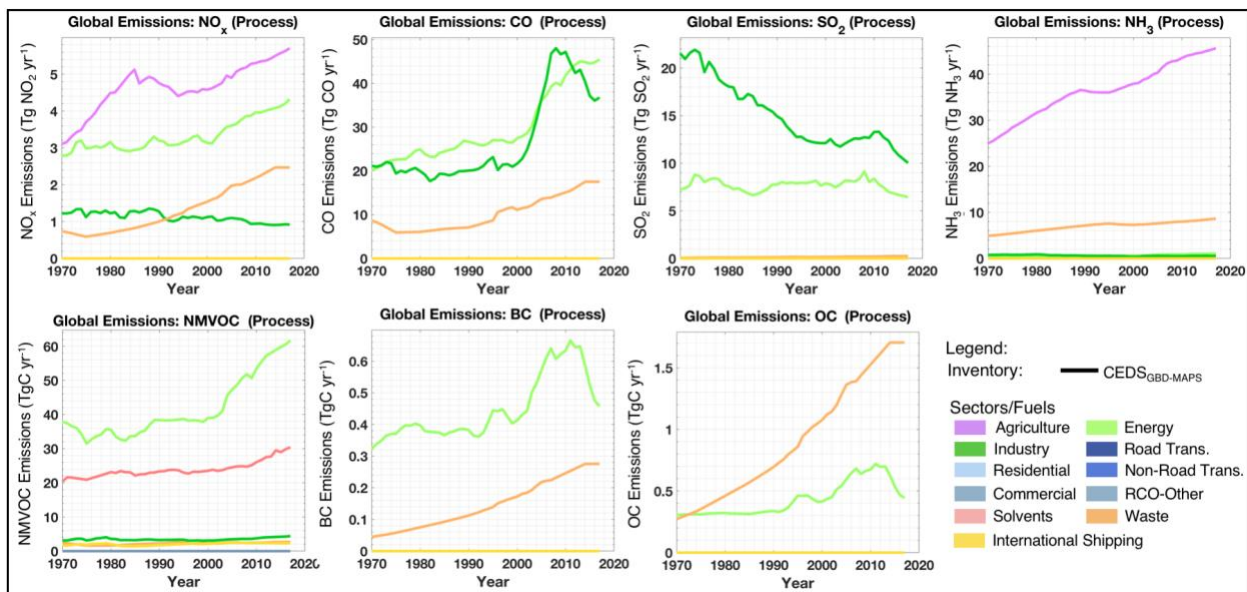


Figure S16. Timeseries of global sectoral emissions associated with CEDS process-level emission sources (Table 2)

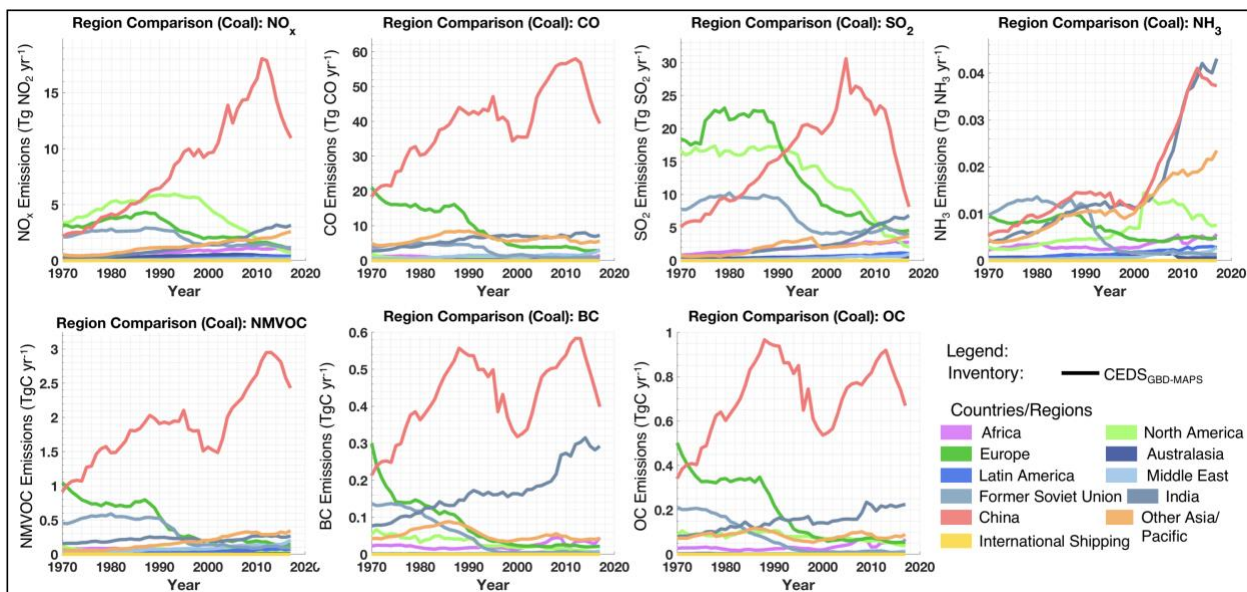


Figure S17. Timeseries of emissions associated with coal combustion, split into contributions from 11 world countries/regions (from coal combustion in all sectors).



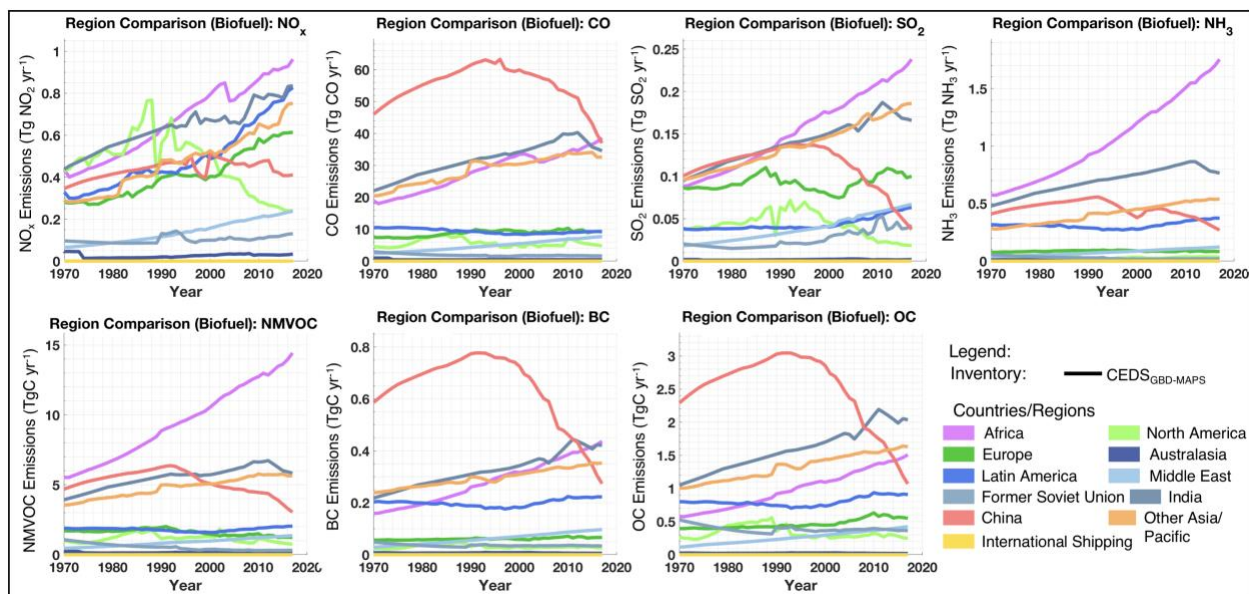


Figure S18. Timeseries of emissions associated with solid biofuel combustion, split into contributions from 11 world countries/regions (from biofuel combustion in all sectors).

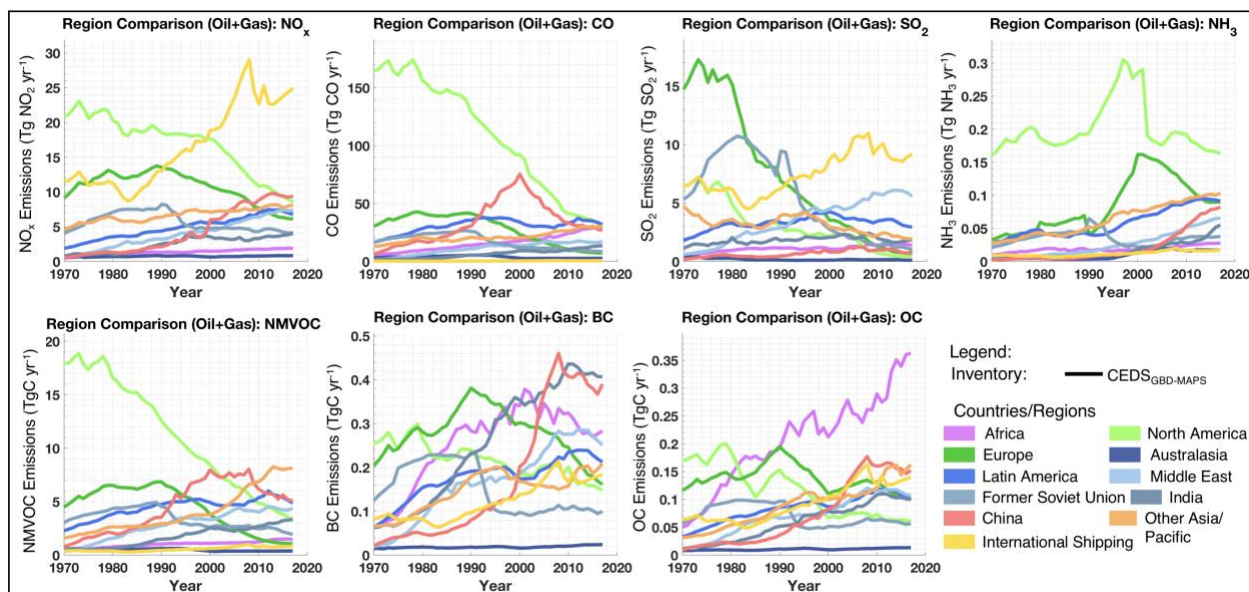


Figure S19. Timeseries of emissions associated with the combustion of liquid oil and natural gas, split into contributions from 11 world countries/regions.

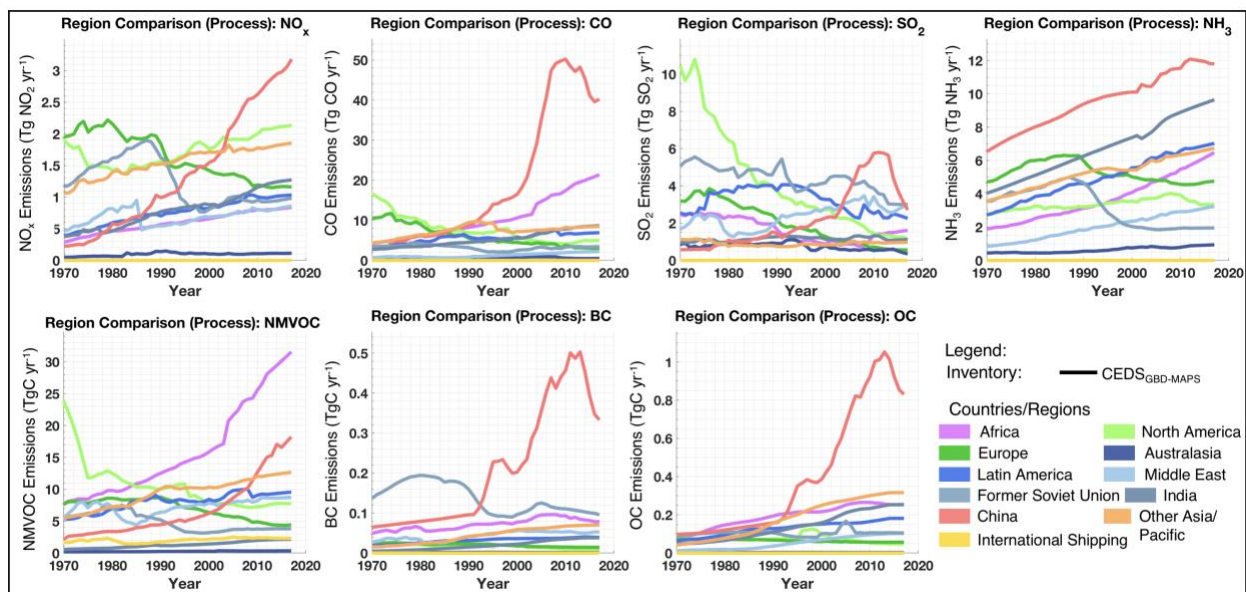


Figure S20. Timeseries of emissions from CEDS process-level sources (Table 2), split into contributions from 11 world countries/regions.

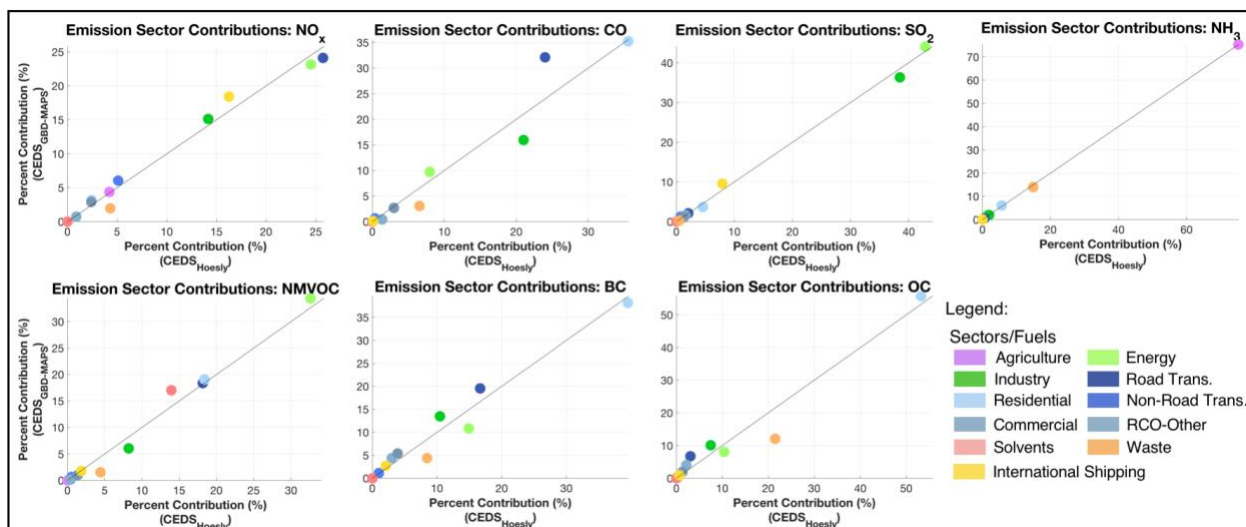


Figure S21. Comparison of CEDS sectoral fractional contributions in the CEDS<sub>GBD-MAPS</sub> (y-axis) and CEDS<sub>Hoesly</sub> (x-axis) inventories. Fractional contributions are calculated from global total emissions from all fuel types (= Sector X/ Total global emissions). Black line in the 1:1 line. Points are colored by sector.

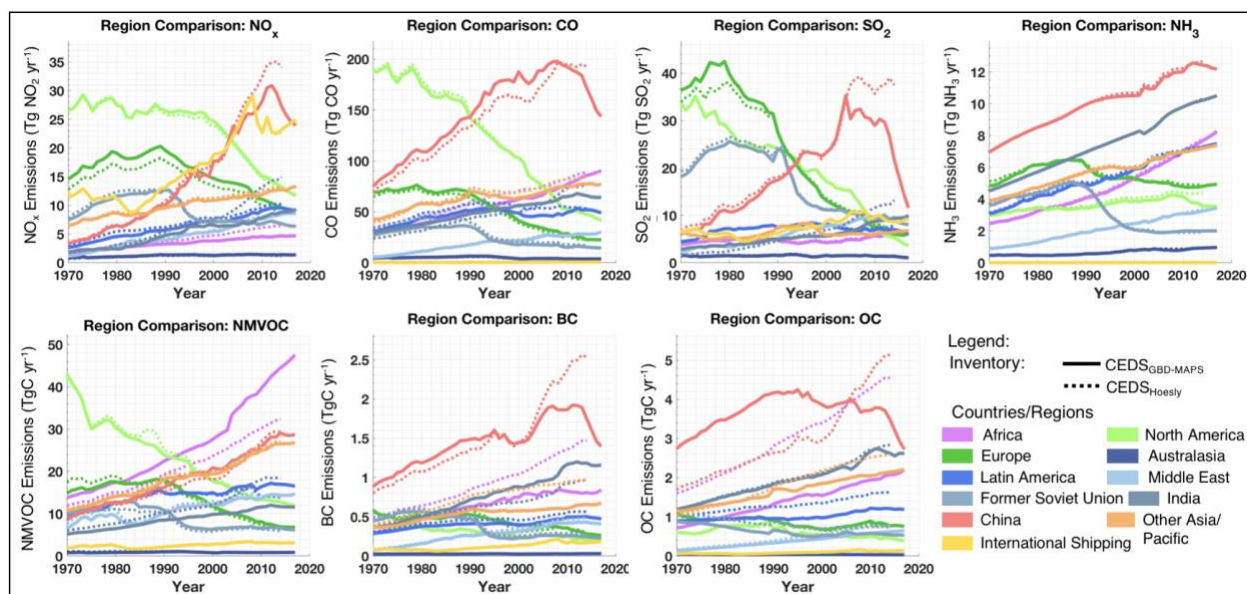


Figure S22. Comparison of CEDS<sub>Hoesly</sub> and CEDS<sub>GBD-MAPS</sub> emissions as a function of 11 world regions.

Table S10. Mapping between EDGAR v4.3.2, ECLIPSE v5a (GAINS), and CEDS<sub>GBD-MAPS</sub> sectors for Fig. S23-S24

Aggregate Figure Sectors	CEDS <sub>GBD-MAPS</sub> Final Sectors	EDGAR v4.3.2 Reported Sectors	ECLIPSE v5a (gridded data) sectors
Agriculture	AGR	4A – Enteric fermentation 4B – Manure management 4C – Rice cultivation 4D1/4D2/4D4 – Direct soil emissions	Agriculture – livestock and arable land operations (AGR)
Energy	ENE	1A1a – Public electricity and heat production 1A1bc/1A5 – Other energy industries 1B1 – Fugitive solid fuels 1B2 – Fugitive oil and gas 7A – Fossil fuel fires	Energy – power plants, energy production/ conversion, fossil fuel distribution (ENE)
Industry	IND	1A2 – Manufacturing and Construction 2A1 – Cement Production 2A2 – Lime Production 2A4 – Soda Ash Production 2A7 – Other mineral production 2B – Other Chemical Production 2C – Metal Production 2D – Pulp/paper/food/drink Production	Industrial combustion (IND)
On-road + Non-Road Transportation	ROAD NRTR	1A3b – Road transportation 1A3c – Rail transportation 1A3d – Inland navigation 1A3e – Other transportation	Transport – on-road and non-road (TRA)
Residential + Commercial + Other	RCOR RCOC RCOO	1A4 – Residential and other sectors	Residential and commercial combustion (DOM)
Solvent Use	SLV	3A – Solvent and other product use: paint 3B – Solvent and other product use: degrease 3C – Solvent and other product use: chemicals 3D – Solvent and other product use: other	Solvent use (SLV)
Waste	WST	6A – Solid waste disposal on land 6B – Wastewater handling 6C – Waste incineration 6D – Other waste handling	Waste disposal, including burning (WST)
International Shipping	SHP	1C2 – International shipping	International shipping (SHP)

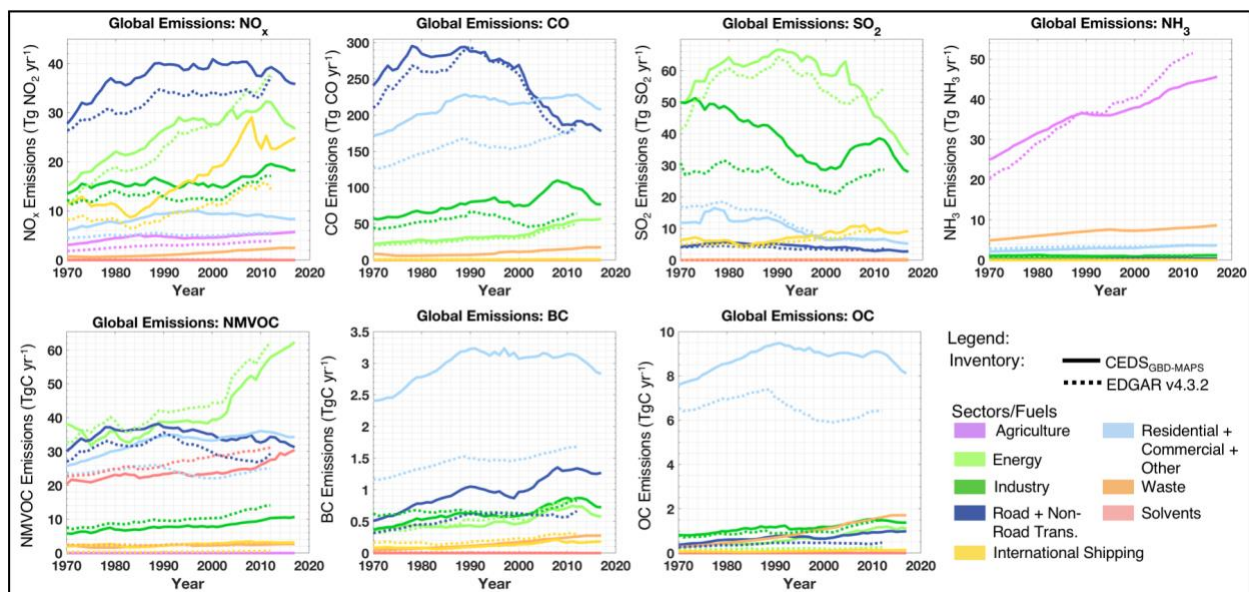


Figure S23. Comparison of sectoral global emissions in CEDS<sub>GBD-MAPS</sub> and EDGARv4.3.2 inventories. CEDS<sub>GBD-MAPS</sub> emissions are shown by solid lines, EDGARv4.3.2 data are shown by dashed lines. Sectoral mappings are in Table S10.

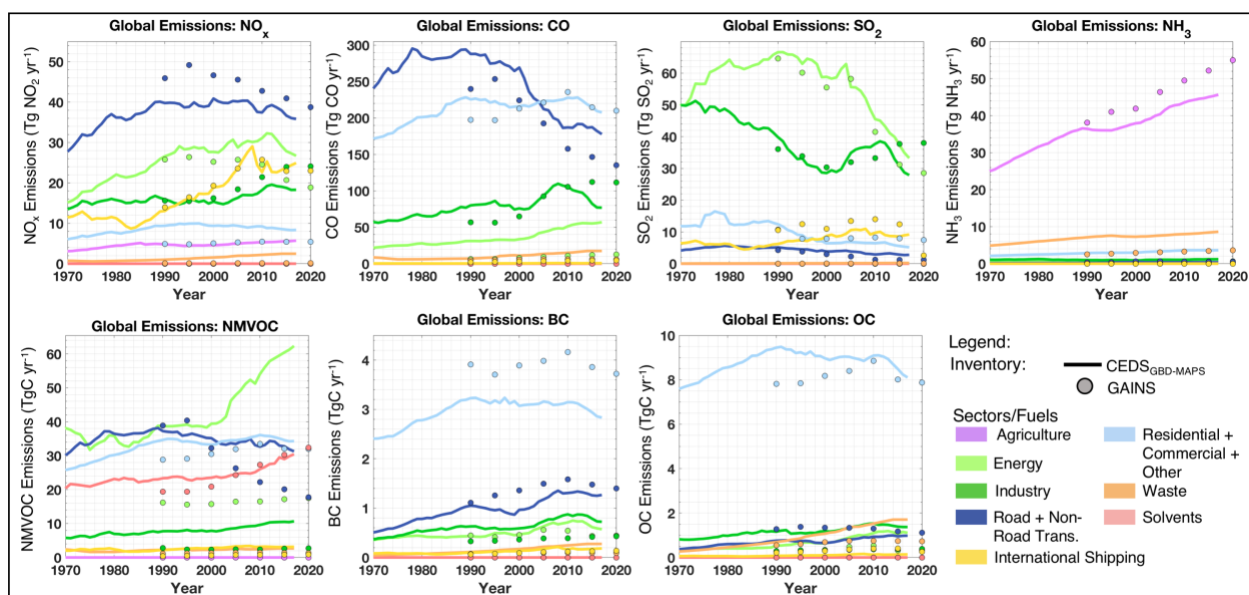


Figure S24. Comparison of sectoral global emissions in CEDS<sub>GBD-MAPS</sub> and GAINS inventories. CEDS<sub>GBD-MAPS</sub> emissions are shown by solid lines, GAINS data are shown by dashed lines. Sectoral mappings are in Table S10.

#### Section S4. Known Inventory Issues

This list is up to date as the submission of the ESSD discussion paper describing the CEDS<sub>GBD-MAPS</sub> system and the associated data. These issues are in addition to known issues already recognized from the core CEDSv2019-12-23 system (<https://github.com/JGCRI/CEDS/issues>). New issues after this point will be listed using the issues tracking system on the GitHub repository for both the core CEDS and CEDS<sub>GBD-MAPS</sub> systems at: <https://github.com/JGCRI/CEDS/issues> and <https://github.com/emcduffie/CEDS/issues>.

- SO<sub>2</sub> and NO<sub>x</sub> emissions from the energy sector in China are too large between 1978 and 2004. This issue results from an issue in the underlying IEA energy data, which manifests in the spikes in SO<sub>2</sub> and NO<sub>x</sub> energy emissions in 2004 that are visible in Fig. S9. This issue may result in up to a 10 Tg overprediction in SO<sub>2</sub> emissions from the energy sector in 2004, which decrease to a maximum possible overprediction of 0.3 Tg by 1978. For NO<sub>x</sub> emissions, the maximum overprediction is 4 Tg in 2004, which decreases to 0.1 Tg by 1978.
- As discussed in Sect. S2.3, industrial emissions of NO<sub>x</sub> in India may be overpredicted by up to 1 Tg between 1987 and 2014. This results from the potential misallocation of the SMOG-India ‘Informal Industry’ sector to the CEDS<sub>GBD-MAPS</sub> 1A2c\_ind-Comb-Food-tobacco sector, rather than the 1A2g-Comb-Ind-other sector.
- Industry emissions of NO<sub>x</sub> and SO<sub>2</sub> in China may not account for emissions from metal smelting due to uncertainties in the MEIC sectoral scaling mapping files for industry sector emissions.
- Residential emissions of SO<sub>2</sub> from the combustion of coal may be over-predicted by up to 4 Tg between 1972 – 1980 (Fig. S13). This sudden increase in emissions from this sector is associated with the CEDS<sub>GBD-MAPS</sub> procedures and not the underlying IEA energy data.

## References

- Boden, T. A., Marland, G., and Andres, R. J.: Global, Regional, and National Fossil-Fuel CO<sub>2</sub> Emissions, Carbon Dioxide Information Analysis Center, U.S. Department of Energy, Oak Ridge, Tenn., U.S.A., 2016.
- Boden, T. A., Marland, G., and Andres, R. J.: Global, Regional, and National Fossil-Fuel CO<sub>2</sub> Emissions, Carbon Dioxide Information Analysis Center, U.S. Department of Energy, Oak Ridge, Tenn., U.S.A., doi: 10.3334/CDIAC/00001\_V2017, 2017.
- Bond, T. C., Bhardwaj, E., Dong, R., Jogani, R., Jung, S., Roden, C., Streets, D. G., and Trautmann, N. M.: Historical emissions of black and organic carbon aerosol from energy-related combustion, 1850–2000, *Global Biogeochemical Cycles*, 21, 10.1029/2006GB002840, 2007.
- BP: BP Statistical Review of World Energy, [bp.com/statisticalreview](http://bp.com/statisticalreview) (last access: 15 January 2018), 2015.
- BP: Statistical Review of World Energy: 2019, <https://www.bp.com/content/dam/bp/business-sites/en/global/corporate/pdfs/energy-economics/statistical-review/bp-stats-review-2019-full-report.pdf> (last access: January 23, 2020), 2019.
- Commoner, B., Bartlett, P. W., Eisl, H., and Couchot, K.: Air Transport of Dioxin from North American Sources to Ecologically Vulnerable Receptors in Nunavut, Arctic Canada: Final Report to the North American Commission for Environmental Cooperation., <http://www3.cec.org/islandora/en/item/1596-long-range-air-transport-dioxin-from-north-american-sources-ecologically-vulnerable-en.pdf> (last access: 25 April, 2020), 2000.
- Crippa, M., Guizzardi, D., Muntean, M., Schaaf, E., Dentener, F., van Aardenne, J. A., Monni, S., Doering, U., Olivier, J. G. J., Pagliari, V., and Janssens-Maenhout, G.: Gridded emissions of air pollutants for the period 1970–2012 within EDGAR v4.3.2, *Earth Syst. Sci. Data*, 10, 1987-2013, 10.5194/essd-10-1987-2018, 2018.
- Doxsey-Whitfield, E., MacManus, K., Adamo, S. B., Pistolesi, L., Squires, J., Borkovska, O., and Baptista, S. R.: Taking Advantage of the Improved Availability of Census Data: A First Look at the Gridded Population of the World, Version 4, *Papers in Applied Geography*, 1, 226-234, 10.1080/23754931.2015.1014272, 2015.

EC-JRC: Emissions Database for Global Atmospheric Research (EDGAR), release EDGARv4.3.2  
[https://edgar.jrc.ec.europa.eu/overview.php?v=432\\_AP](https://edgar.jrc.ec.europa.eu/overview.php?v=432_AP),  
[https://data.europa.eu/doi/10.2904/JRC\\_DATASET\\_EDGAR](https://data.europa.eu/doi/10.2904/JRC_DATASET_EDGAR), (last access: 12 August 2019), 2018.

EC-JRC/PBL: Emission Database for Global Atmospheric Research (EDGAR), release EDGAR v4.2 FT2012,  
<http://edgar.jrc.ec.europa.eu> (last access: 15 January 2018), 2012.

EC-JRC/PBL: Emission Database for Global Atmospheric Research (EDGAR), release version 4.3.1,  
<http://edgar.jrc.ec.europa.eu/overview.php?v=431> (last access: 15 January 2018), 2016.

EIA: U.S. Energy Information Administration: Table 10.2a: Renewable Energy Consumption, Residential and Commercial Sectors, <https://www.eia.gov/totalenergy/data/monthly/#renewable> (last access: 26 August 2019), 2019.

EMEP: Officially reported emission data to the European Monitoring and Evaluation Programme: EMEP\_NFR14\_LEVEL1 data,  
[https://www.ceip.at/ms/ceip\\_home1/ceip\\_home/webdab\\_emepdatabase/reported\\_emissiondata/](https://www.ceip.at/ms/ceip_home1/ceip_home/webdab_emepdatabase/reported_emissiondata/) (last access: 19 December 2019), 2019.

FAOSTAT: FAOSTAT-Forestry database, <http://www.fao.org/forestry/statistics/84922/en/> (last access: 15 January 2018), 2015.

Hoesly, R., O'Rourke, P., Braun, C., Feng, L., Smith, S. J., Pitkanen, T., Siebert, J., Vu, L., Presley, M., Bolt, R., Goldstein, B., and Kholod, N.: CEDS: Community Emissions Data System (Version Dec-23-2019), <http://doi.org/10.5281/zenodo.3592073> (last access: March 15, 2020), 2019.

Hoesly, R. M., Smith, S. J., Feng, L., Klimont, Z., Janssens-Maenhout, G., Pitkanen, T., Siebert, J. J., Vu, L., Andres, R. J., Bolt, R. M., Bond, T. C., Dawidowski, L., Kholod, N., Kurokawa, J. I., Li, M., Liu, L., Lu, Z., Moura, M. C. P., O'Rourke, P. R., and Zhang, Q.: Historical (1750–2014) anthropogenic emissions of reactive gases and aerosols from the Community Emissions Data System (CEDS), *Geosci. Model Dev.*, 11, 369-408, 10.5194/gmd-11-369-2018, 2018.

IEA: World Energy Statistics, <http://www.iea.org/statistics/> (last access: 15 January 2018), 2015.

IEA: World Energy Statistics 2019 Edition, Database Documentation, [http://wds.iea.org/wds/pdf/WORLDBES\\_Documentation.pdf](http://wds.iea.org/wds/pdf/WORLDBES_Documentation.pdf) (last access: 17 September 2019), 2019.

Klein Goldewijk, K., Beusen, A., van Drecht, G., and de Vos, M.: The HYDE 3.1 spatially explicit database of human-induced global land-use change over the past 12,000 years, *Global Ecology and Biogeography*, 20, 73-86, 10.1111/j.1466-8238.2010.00587.x, 2011.

Klimont, Z., Kupiainen, K., Heyes, C., Purohit, P., Cofala, J., Rafaj, P., Borken-Kleefeld, J., and Schöpp, W.: Global anthropogenic emissions of particulate matter including black carbon, *Atmos. Chem. Phys.*, 17, 8681-8723, 10.5194/acp-17-8681-2017, 2017.

Kurokawa, J., Ohara, T., Morikawa, T., Hanayama, S., Janssens-Maenhout, G., Fukui, T., Kawashima, K., and Akimoto, H.: Emissions of air pollutants and greenhouse gases over Asian regions during 2000–2008: Regional Emission inventory in ASia (REAS) version 2, *Atmos. Chem. Phys.*, 13, 11019-11058, 10.5194/acp-13-11019-2013, 2013.

Marais, E. A., and Wiedinmyer, C.: Air Quality Impact of Diffuse and Inefficient Combustion Emissions in Africa (DICE-Africa), *Environ. Sci. Technol.*, 50, 10739-10745, 10.1021/acs.est.6b02602, 2016.

Meidiana, C., and Gamse, T.: Development of Waste Management Practices in Indonesia, *European Journal of Scientific Research*, 40, 199-210, 2010.

Nagpure, A. S., Ramaswami, A., and Russell, A.: Characterizing the Spatial and Temporal Patterns of Open Burning of Municipal Solid Waste (MSW) in Indian Cities, *Environ. Sci. Technol.*, 49, 12904-12912, 10.1021/acs.est.5b03243, 2015.

NEI: 2011 National Emissions Inventory (NEI) Data, [https://www.epa.gov/air-emissions-inventories/2011-national-emissions-inventory-nei-data\(last\)](https://www.epa.gov/air-emissions-inventories/2011-national-emissions-inventory-nei-data(last)), 2013.

Reyna-Bensusan, N., Wilson, D. C., and Smith, S. R.: Uncontrolled burning of solid waste by households in Mexico is a significant contributor to climate change in the country, *Environmental Research*, 163, 280-288, <https://doi.org/10.1016/j.envres.2018.01.042>, 2018.

Sharma, G., Sinha, B., Pallavi, Hakkim, H., Chandra, B. P., Kumar, A., and Sinha, V.: Gridded Emissions of CO, NO<sub>x</sub>, SO<sub>2</sub>, CO<sub>2</sub>, NH<sub>3</sub>, HCl, CH<sub>4</sub>, PM<sub>2.5</sub>, PM<sub>10</sub>, BC, and NMVOC from Open Municipal Waste Burning in India, *Environ. Sci. Technol.*, 53, 4765-4774, 10.1021/acs.est.8b07076, 2019.

Stohl, A., Aamaas, B., Amann, M., Baker, L. H., Bellouin, N., Berntsen, T. K., Boucher, O., Cherian, R., Collins, W., Daskalakis, N., Dusinska, M., Eckhardt, S., Fuglestedt, J. S., Harju, M., Heyes, C., Hodnebrog, Ø., Hao, J., Im, U., Kanakidou, M., Klimont, Z., Kupiainen, K., Law, K. S., Lund, M. T., Maas, R., MacIntosh, C. R., Myhre, G., Myriokefalitakis, S., Olivie, D., Quaas, J., Quennehen, B., Raut, J. C., Rumbold, S. T., Samset, B. H., Schulz, M., Seland, Ø., Shine, K. P., Skeie, R. B., Wang, S., Yttri, K. E., and Zhu, T.: Evaluating the climate and air quality impacts of short-lived pollutants, *Atmos. Chem. Phys.*, 15, 10529-10566, 10.5194/acp-15-10529-2015, 2015.

The World Bank: World Development Indicators, [databank.worldbank.org/data/download/WDI\\_excel.zip](http://databank.worldbank.org/data/download/WDI_excel.zip) (last access: 15 January 2018), 2016.

UN: World Urbanization Prospects: The 2014 Revision, [https://esa.un.org/unpd/wup/CD-ROM/WUP2014\\_XLS\\_CD\\_FILES/WUP2014-F01-Total\\_Urban\\_Rural.xls](https://esa.un.org/unpd/wup/CD-ROM/WUP2014_XLS_CD_FILES/WUP2014-F01-Total_Urban_Rural.xls) (last access: 15 January 2018), 2014.

UN: UN World Population Prospects: The 2015 Revision, <http://esa.un.org/unpd/wpp/DVD/> (last access: 15 January 2018), 2015.

UN: World urbanization prospects: The 2018 revision, annual percentage of population at mid-year residing in urban areas by region, subregion, country and area, 1950-2050, [https://population.un.org/wup/Download/\(last\)](https://population.un.org/wup/Download/(last)) (last access: 24 July 2019), 2018.

UN: World Population Prospects 2019: Total population (both sexes combined) by region, subregion and country, annually for 1950 to 2100, [https://esa.un.org/unpd/wpp/Download/Standard/Population/\(last\)](https://esa.un.org/unpd/wpp/Download/Standard/Population/(last)), 2019.

US EPA: An inventory of sources and environmental releases of dioxin-like compounds in the U.S. for the years 1987, 1995, and 2000, U.S. Environmental Protection Agency, Washington DC, EPA/600/P-03/002F, 2006.

Venkataraman, C., Brauer, M., Tibrewal, K., Sadavarte, P., Ma, Q., Cohen, A., Chaliyakunnel, S., Frostad, J., Klimont, Z., Martin, R. V., Millet, D. B., Philip, S., Walker, K., and Wang, S.: Source influence on emission pathways and ambient PM<sub>2.5</sub> pollution over India (2015–2050), *Atmos. Chem. Phys.*, 18, 8017-8039, 10.5194/acp-18-8017-2018, 2018.

Wiedinmyer, C., Yokelson, R. J., and Gullett, B. K.: Global Emissions of Trace Gases, Particulate Matter, and Hazardous Air Pollutants from Open Burning of Domestic Waste, *Environ. Sci. Technol.*, 48, 9523-9530, 10.1021/es502250z, 2014.

Zheng, B., Tong, D., Li, M., Liu, F., Hong, C., Geng, G., Li, H., Li, X., Peng, L., Qi, J., Yan, L., Zhang, Y., Zhao, H., Zheng, Y., He, K., and Zhang, Q.: Trends in China's anthropogenic emissions since 2010 as the consequence of clean air actions, *Atmos. Chem. Phys.*, 18, 14095-14111, 10.5194/acp-18-14095-2018, 2018.



**ADDITIONAL MATERIALS AVAILABLE ON THE HEI WEBSITE**

**Research Report 210**

**Global Burden of Disease from Major Air Pollution Sources**

**(GBD MAPS): A Global Approach**

**Erin McDuffie et al.**

**Additional Materials 2: McDuffie EE, Martin RV, Spadaro J, Burnett R, Smith SJ, O'Rourke P, et al. 2021. Source sector and fuel contributions to ambient PM2.5 and attributable mortality across multiple spatial scales. Nat Commun 12:3594; doi:10.1038/s41467-021-23853-y.**

Additional Materials 2 was not formatted or edited by HEI. It is distributed under the Creative Commons Attribution 4.0 License. This document was part of the HEI Special Review Panel's review process.








---

Correspondence concerning the Investigators' Report may be addressed to Dr. Michael Brauer, The University of British Columbia, School of Population and Public Health, 366A – 2206 East Mall, Vancouver, BC V6T1Z3, Canada; e-mail: [michael.brauer@ubc.ca](mailto:michael.brauer@ubc.ca), [guxens@isglobal.org](mailto:guxens@isglobal.org).

© 2021 Health Effects Institute, 75 Federal Street, Suite 1400, Boston, MA 02110



# Source sector and fuel contributions to ambient PM<sub>2.5</sub> and attributable mortality across multiple spatial scales

Erin E. McDuffie <sup>1,2</sup>✉, Randall V. Martin <sup>1,2</sup>, Joseph V. Spadaro<sup>3</sup>, Richard Burnett<sup>4</sup>, Steven J. Smith <sup>5</sup>, Patrick O'Rourke<sup>5</sup>, Melanie S. Hammer<sup>1,2</sup>, Aaron van Donkelaar<sup>2,1</sup>, Liam Bindle <sup>1,2</sup>, Viral Shah<sup>6,10</sup>, Lyatt Jaeglé<sup>6</sup>, Gan Luo<sup>7</sup>, Fangqun Yu <sup>7</sup>, Jamiu A. Adeniran<sup>8</sup>, Jintai Lin <sup>8</sup> & Michael Brauer <sup>4,9</sup>

Ambient fine particulate matter (PM<sub>2.5</sub>) is the world's leading environmental health risk factor. Reducing the PM<sub>2.5</sub> disease burden requires specific strategies that target dominant sources across multiple spatial scales. We provide a contemporary and comprehensive evaluation of sector- and fuel-specific contributions to this disease burden across 21 regions, 204 countries, and 200 sub-national areas by integrating 24 global atmospheric chemistry-transport model sensitivity simulations, high-resolution satellite-derived PM<sub>2.5</sub> exposure estimates, and disease-specific concentration response relationships. Globally, 1.05 (95% Confidence Interval: 0.74–1.36) million deaths were avoidable in 2017 by eliminating fossil-fuel combustion (27.3% of the total PM<sub>2.5</sub> burden), with coal contributing to over half. Other dominant global sources included residential (0.74 [0.52–0.95] million deaths; 19.2%), industrial (0.45 [0.32–0.58] million deaths; 11.7%), and energy (0.39 [0.28–0.51] million deaths; 10.2%) sectors. Our results show that regions with large anthropogenic contributions generally had the highest attributable deaths, suggesting substantial health benefits from replacing traditional energy sources.

<sup>1</sup>Department of Energy, Environmental, and Chemical Engineering, Washington University in St. Louis, St. Louis, MO, USA. <sup>2</sup>Department of Physics and Atmospheric Science, Dalhousie University, Halifax, NS, Canada. <sup>3</sup>Spadaro Environmental Research Consultants (SERC), Philadelphia, PA, USA. <sup>4</sup>Institute for Health Metrics and Evaluation, University of Washington, Seattle, WA, USA. <sup>5</sup>Joint Global Change Research Institute, Pacific Northwest National Laboratory, College Park, MD, USA. <sup>6</sup>Department of Atmospheric Sciences, University of Washington, Seattle, WA, USA. <sup>7</sup>Atmospheric Sciences Research Center, University at Albany, Albany, NY, USA. <sup>8</sup>Department of Atmospheric and Oceanic Sciences, School of Physics, Peking University, Beijing, China. <sup>9</sup>School of Population and Public Health, University of British Columbia, Vancouver, BC, Canada. <sup>10</sup>Present address: Harvard John A. Paulson School of Engineering and Applied Sciences, Harvard University, Cambridge, MA, USA. ✉email: [erin.mcduffie@wustl.edu](mailto:erin.mcduffie@wustl.edu)

Long-term exposure to ambient (outdoor) fine particulate matter less than  $2.5\ \mu\text{m}$  in diameter ( $\text{PM}_{2.5}$ ) is the largest environmental risk factor for human health, with an estimated 4.1 million attributable deaths worldwide (7.3% of the total number of global deaths) in 2019<sup>1</sup>. Outdoor  $\text{PM}_{2.5}$  mass is primarily composed of inorganic ions, carbonaceous compounds (black and organic carbon, including secondary organic aerosol), and mineral dust. Sources include direct emissions such as forest fires and agricultural waste burning<sup>2,3</sup>, windblown mineral dust from arid regions<sup>4</sup>, and inefficient fuel combustion<sup>5</sup>, as well as secondary emissions from atmospheric chemical reactions between primary gas-phase pollutant precursors. These precursors are emitted from both combustion and non-combustion processes that include residential energy use, on- and off-road vehicles, energy generation, solvent use, industrial processes, and agricultural fertilizer application<sup>6</sup>. Once emitted, the chemical production of  $\text{PM}_{2.5}$  mass in the atmosphere is highly non-linear<sup>7,8</sup>. Due to its myriad of sources and complex formation chemistry, both the total mass and chemical constituents of  $\text{PM}_{2.5}$  depend on local environmental conditions, dominant sources, and the magnitude of those source-specific emissions. In addition, as air pollution and atmospheric chemistry do not adhere to political boundaries<sup>9–11</sup>, mitigation efforts require consideration of transboundary effects across multiple locations, informed by studies of  $\text{PM}_{2.5}$  source contributions and the attributable disease burden across a range of sub-national to global scales.

Source contribution studies across multiple spatial scales help to inform specific mitigation strategies and prioritize limited resources for effective action<sup>12</sup>. A large number of previous studies have used chemical observations or dispersion-based models to quantify sources of  $\text{PM}_{2.5}$  mass, but have largely focused on specific locations or short-term events<sup>13–15</sup>. In comparison, comprehensive assessments of the sources and impacts of  $\text{PM}_{2.5}$  across large spatial scales have been relatively limited by available long-term  $\text{PM}_{2.5}$  surface measurements. A recent study, for example, found that most countries between 2010 and 2016 had fewer than 10 long-term ground-based  $\text{PM}_{2.5}$  monitors per million people, while 60% of all countries had no long-term monitors<sup>16</sup>. Therefore, to assess the global and regional  $\text{PM}_{2.5}$  disease burden and its source contributions, recent studies have employed 3D chemical transport models as a means to relate changes in surface emissions to atmospheric  $\text{PM}_{2.5}$  concentrations. These studies typically use adjoint models, tagged-tracer, or zero-out (brute-force) approaches to assess the influence of individual surface sources on  $\text{PM}_{2.5}$  mass and attributable mortality and morbidity. These previous studies, however, have largely focused on individual cities, countries, regions<sup>11,17–24</sup>, or source sectors<sup>3,25–35</sup>, often with relatively coarse spatial resolution and emissions that may not reflect current conditions. In contrast, global-scale studies that account for transboundary effects using both consistent methodologies and sectoral definitions across all world regions help to place air pollution in a global context and allow for comparability of the disease burden and its source contributions across multiple locations. Relatively few of these previous global studies, however, have provided an assessment of the contributions from more than one source sector or aggregate fuel category in recent years<sup>36–40</sup>, thereby limiting their ability to inform or prioritize specific air quality management policies under current global conditions.

In today's rapidly changing society, the accuracy and policy relevance of such global studies is contingent on (1) the availability of contemporary and detailed emission inventories, (2) scientifically rigorous chemical transport models, (3) global fine resolution  $\text{PM}_{2.5}$  exposure estimates, and (4) disease-specific concentration-response functions (CRFs) derived from contemporary air pollution epidemiologic studies. First, emission

datasets that capture recent trends are particularly important in highly polluted regions, such as China, India, and Africa, that have experienced large and rapid changes in  $\text{PM}_{2.5}$  precursor emissions in the last decade<sup>6,41,42</sup>. Disaggregation of these emissions across multiple sectors, fuel types, and regions also increases their policy relevance, as detailed source contribution studies can quantify the health benefits from specific and achievable strategies such as transitions away from coal use for energy generation or solid biofuel for residential cooking and heating. Second, to accurately reflect current  $\text{PM}_{2.5}$  chemical production regimes under various emission scenarios, 3D atmospheric-chemical transport models require state-of-the-science chemical and physical mechanisms, evaluated against surface observations of  $\text{PM}_{2.5}$  mass and composition. Third, to capture and compare national and sub-national impacts across all world regions, these studies additionally require high-resolution  $\text{PM}_{2.5}$  exposure estimates, such as those that utilize recent advances in satellite retrievals, chemical transport models, and ground-based monitoring<sup>43</sup>. Lastly, integration of these source simulations and exposure estimates with updated disease-specific CRFs can motivate policy action by refining previous  $\text{PM}_{2.5}$  disease burden estimates<sup>37,38,44,45</sup>, incorporating spatial variation in the underlying health status and cause of death composition, and by comparably quantifying the dominant sources of this burden across global, national, and sub-national scales.

In this study, we integrate the emissions, modeling,  $\text{PM}_{2.5}$  exposure, and CRF components described above to provide a globally comprehensive and contemporary source categorization of  $\text{PM}_{2.5}$  mass and the attributable disease burden. In this work, we identify residential energy use, industrial processes, and energy generation as dominant sectors contributing to global  $\text{PM}_{2.5}$  exposure and its attributable mortality. We also find that eliminating fossil fuel combustion emissions would substantially reduce (>25%) the global disease burden attributable to annual  $\text{PM}_{2.5}$  exposure, with over half of this contribution from the combustion of coal. While the relative contributions from individual sectors and fuels vary across national and sub-national scales, the comprehensive nature of this work provides detailed source information relevant to developing  $\text{PM}_{2.5}$  mitigation strategies and predicts a large potential health benefit from replacing traditional energy sources.

## Results

In this work, we couple emission sensitivity simulations using the GEOS-Chem 3D global chemical transport model with newly available high-resolution ( $1\ \text{km} \times 1\ \text{km}$ ) satellite-derived  $\text{PM}_{2.5}$  exposure estimates<sup>43</sup>, national-level baseline burden data, and updated CRFs from the 2019 Global Burden of Disease (GBD)<sup>1</sup>. We use these data and methods to quantify the relative contributions from 24 individual emission sectors and fuel categories to annual population-weighted mean (PWM)  $\text{PM}_{2.5}$  mass concentrations and the attributable disease burden across 21 world regions, 204 countries (defined in Supplementary Table 1), and 200 sub-national areas.

**$\text{PM}_{2.5}$  exposure and attributable disease burden.** In 2017, the global PWM  $\text{PM}_{2.5}$  mass concentration was  $41.7\ \mu\text{g}\ \text{m}^{-3}$ , with 91% of the world's population experiencing annual average concentrations higher than the World Health Organization (WHO) annual average guideline of  $10\ \mu\text{g}\ \text{m}^{-3}$ . As shown in Fig. 1a and b, exposures were highest in countries throughout Asia, the Middle East, and Africa. To maintain consistency with the GBD<sup>1</sup>, we use the same gridded ( $\sim 10 \times 10\ \text{km}$ ) outdoor  $\text{PM}_{2.5}$  concentration estimates<sup>43,47,48</sup>, further downscaled to a spatial resolution of  $0.01^\circ \times 0.01^\circ$  ( $\sim 1 \times 1\ \text{km}$ ) using a newly and publicly

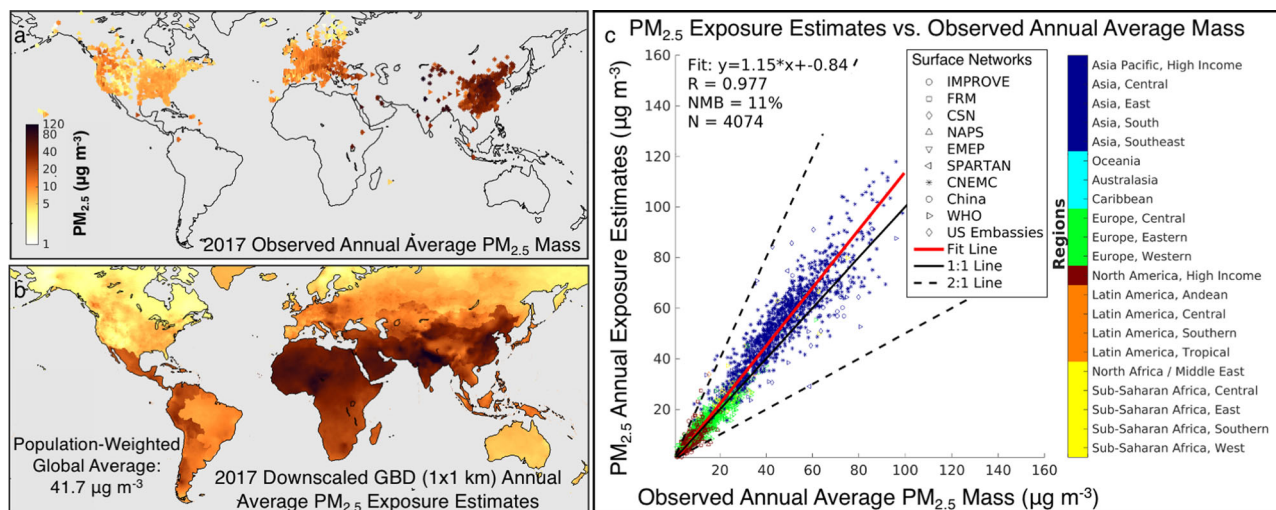


**Fig. 1** Evaluation of  $\text{PM}_{2.5}$  exposure estimates relative to surface observations. **a** Annual average observations of total  $\text{PM}_{2.5}$  mass in the year 2017; symbol shapes correspond to monitor network. **b** Annual  $\text{PM}_{2.5}$  exposure estimates for 2017, downscaled to  $0.01^\circ \times 0.01^\circ$  resolution. **c** Correlation between the 2017 exposure estimates and observed annual average concentrations, colored by Global Burden of Disease (GBD) region (Supplementary Table 1); symbol shape corresponds to the observation network; correlation slope, intercept, coefficient, normalized mean bias (NMB), and number of observation points are provided. ( $\text{NMB} = 100 \cdot \Sigma (\text{exposure estimate} - \text{observations}) / \Sigma \text{ observations}$ ).

available high-resolution satellite-derived product<sup>43</sup> (Methods). Figure 1c compares the resulting downscaled ( $\sim 1 \times 1$  km)  $\text{PM}_{2.5}$  concentrations to all readily available 2017 annual surface observations ( $N = 4074$ ) of total  $\text{PM}_{2.5}$  mass. Though annual surface observations are largely limited to regions in North America, Europe, and Asia, the downscaled estimates in Fig. 1c are consistent with co-located annual average observations, with a correlation coefficient ( $r$ ) of 0.977 and a normalized mean bias of +11% or  $4.6 \mu\text{g m}^{-3}$ .

The global ambient  $\text{PM}_{2.5}$  disease burden was estimated by integrating national-level annual PWM  $\text{PM}_{2.5}$  concentrations with CRFs<sup>49</sup> and national baseline data consistent with the 2019 GBD<sup>1</sup> (GBD2019 CRF). These updated CRFs better reflect the uncertainty of health effects at high  $\text{PM}_{2.5}$  concentrations. Globally, we estimate that 3.83 million deaths (95% Confidence Interval: 2.72–4.97 million) were attributable to annual ambient  $\text{PM}_{2.5}$  exposure in the year 2017 (Fig. 2: top left panel). Attributable deaths were primarily from ischemic heart disease (IHD) and Stroke (63%; Fig. 2: top left, right pie chart), followed by chronic obstructive pulmonary disease (COPD), lung cancer (LC), lower respiratory infections (LRI), and type II diabetes (DM). In addition, there were a total of 2.07 (95% CI: 0.02–5.02) million attributable incidences of neonatal disorders (low birth weight (LBW) and pre-term births (PTB)) worldwide (Supplementary Data 1). National-level results for 204 countries are provided in the center map of Fig. 2 (and Supplementary Data 1). The largest numbers of attributable deaths occurred in China ( $\sim 1.4$  [95% CI: 1.05–1.70] million) and India (0.87 [95% CI: 0.68–1.04] million), together accounting for 58% of the global total ambient  $\text{PM}_{2.5}$  mortality burden. The larger burden in China, despite a lower national  $\text{PM}_{2.5}$  exposure level reflects differences in population age distribution and the relative baselines associated with each disease in each country (Supplementary Fig. 1). Figure 2 also shows a large  $\text{PM}_{2.5}$  disease burden in countries such as the U.S. where country-level PWM  $\text{PM}_{2.5}$  exposure levels are below the WHO guideline, highlighting the risks associated with  $\text{PM}_{2.5}$  exposures below  $10 \mu\text{g m}^{-3}$  but above the GBD counterfactual<sup>50</sup> (Supplementary Fig. 2; Methods). Supplementary Data 1 provides all national exposure and disease burden estimates, as well as fractional disease contributions.

As an additional sensitivity test, exposure and burden estimates for the year 2019 were additionally calculated with publicly available 2019 exposure estimates and national-level baseline burden data (Supplementary Text 1). No change was found in the global PWM  $\text{PM}_{2.5}$  concentration (Supplementary Data 3), however due to changes in population characteristics (i.e., size and age decomposition in a particular country), the attributable deaths increased from 3.8 (95% CI: 2.72–4.97) million to 4.1 (95% CI: 2.9–5.3) million in 2019 (consistent with GBD2019<sup>1</sup>) (Supplementary Text 1; Supplementary Data 3). Disease burden estimates were also calculated using CRFs from an updated version of the Global Exposure Mortality Model (GEMM)<sup>44</sup> (Supplementary Text 2; Supplementary Fig. 2). While the fractional disease contributions predicted by the updated GEMM were similar to those from the GBD2019 CRFs (Supplementary Fig. 3), the absolute number of attributable deaths in each country/region were nearly always larger when the GEMM was applied.

#### Global and national sector and fuel-type contributions.

Figure 2 also provides the relative (fractional) contributions of emission sectors and fuel types to annual  $\text{PM}_{2.5}$  exposure levels and the attributable disease burden. As described in the Methods, fractional contributions are quantified using a recently updated version of the 3D GEOS-Chem chemical transport model<sup>46</sup> (Supplementary Text 3), evaluated against available surface observations (Supplementary Text 4; Supplementary Figs. 4, 5) in a series of 24 sensitivity simulations (Supplementary Table 2) with a newly released global anthropogenic emissions dataset (CEDSGBD-MAPS<sup>6</sup>) that includes sector- and fuel-specific emissions for the year 2017 (Supplementary Text 5; Supplementary Fig. 6).

Results in Fig. 2 (and Supplementary Data 1) show that on the global scale, roughly 40% of the  $\text{PM}_{2.5}$  disease burden was attributable to residential (19.2%; 0.74 [95% CI: 0.52–0.95] million deaths), industrial (11.7%; 0.45 [0.32–0.58] million deaths), and energy (10.2%; 0.39 [0.28–0.51] million deaths) sector emissions, which are typically associated with fuel combustion<sup>6</sup>. To investigate combustion contributions across all sectors, the middle pie chart in Fig. 2 (and Supplementary Data 2) illustrates the potential health benefits from eliminating specific

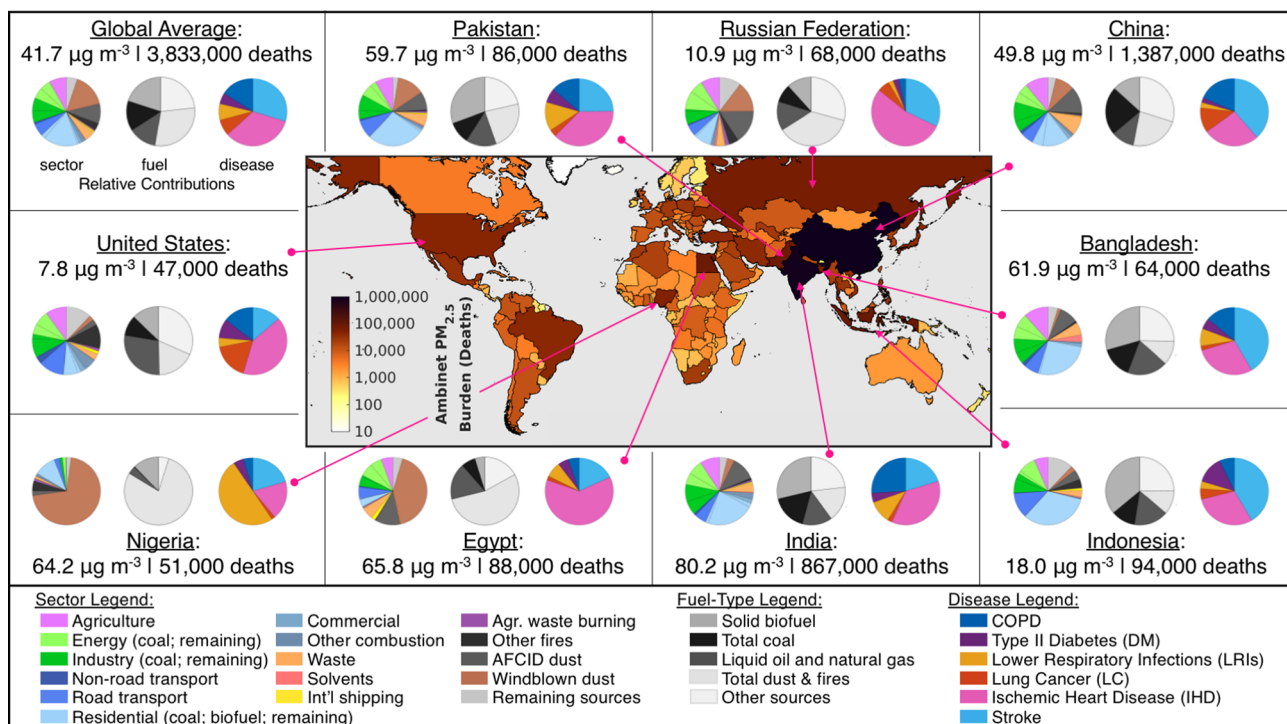


**Fig. 2 Absolute ambient  $PM_{2.5}$  burden and fractional sector, fuel, and disease contributions for the global average and top nine countries.** Map: National-level outdoor  $PM_{2.5}$  disease burden in 2017 (from the 2019 Global Burden of Disease concentration-response relationships). Panels: Annual average population-weighted  $PM_{2.5}$  exposure levels and attributable mortality (rounded to the nearest 1000). (Left pie charts) fractional sectoral source contributions. ‘Other fires’ include deforestation, boreal forest, peat, savannah, and temperate forest fires. ‘Remaining sources’ include volcanic  $SO_2$ , lightning  $NO_x$ , biogenic soil  $NO$ , aircraft emissions, and oceanic and biogenic sources (Supplementary Table 2). Energy and industry sectors also include separate contributions from coal use (first wedge, counterclockwise). The residential sector separates the contributions from coal (first wedge) and solid biofuel (second wedge). (middle pie charts) fuel-type contributions. The ‘total dust & fires’ category is the sum of windblown and AFCID (anthropogenic fugitive, combustion, and industrial) dust, agricultural waste burning, and other fires. Other sources are primarily from non-combustion or uncategorized combustion sources (agriculture, solvents, biogenic SOA, waste incineration, etc.). (Right pie charts) Relative disease contributions (not including pre-term birth and low birth weight). Supplementary Data 1 and 2 provide all data in this figure, including the number of neonatal incidences.

types of combustible fuels. For example, Fig. 2 shows that nearly 1.05 (95% CI: 0.74–1.36) million or 27.3% of total  $PM_{2.5}$  attributable deaths could be avoided by eliminating emissions from fossil-fuel combustion (coal = 14.1%, O&NG = 13.2%), with an additional 20% or nearly 0.77 (95% CI: 0.54–0.99) million deaths avoidable by eliminating solid biofuel combustion, primarily used for residential heating and cooking. The remaining sources in the middle pie charts largely correspond to non-combustion and natural sources, such as windblown dust, which was the second single largest sectoral source of  $PM_{2.5}$  exposure at the global scale (16.1%) (Fig. 2). This source was estimated to lead to 0.62 (95% CI: 0.44–0.80) million attributable deaths worldwide under the assumption of equal toxicity of all  $PM_{2.5}$  sources and components (Discussion). Other  $PM_{2.5}$  sources such as on-road transportation, non-combustion agriculture emissions, and anthropogenic dust each had relatively smaller global contributions ranging between 6.0 and 9.3% (0.23 [95% CI: 0.16–0.30] to 0.36 [0.25–0.46] million deaths). Additional global source sectors, including solvents, shipping, and natural sources such as fires, biogenic, and soil emissions each contributed to less than 5.2% of the annual global PWM  $PM_{2.5}$  mass. Supplementary Data 1 and 2 provide a complete data set of the global fractional sector and fuel contributions.

While global contributions provide a snapshot of globally important sectors and fuel-types, regional and country-level contributions provide information more relevant to local sources of ambient  $PM_{2.5}$  mass. Therefore, Fig. 2 additionally shows the relative contributions for nine countries with the largest number

of attributable deaths associated with long-term ambient  $PM_{2.5}$  exposure (from the GBD2019 CRFs). These top countries differ from those with the highest PWM  $PM_{2.5}$  concentrations (Supplementary Data 1), highlighting the importance of demographic factors and disease-specific baseline estimates in calculating the total burden of disease. The majority of attributable deaths in these countries were from Stroke and IHD, except for Nigeria, where childhood LRIs were the largest cause of mortality attributable to ambient  $PM_{2.5}$  exposure. Sectoral pie charts in Fig. 2 show that source contributions varied between countries, with residential contributions ranging from 4.0% in Egypt to 33.1% in Indonesia, while the sum of energy and industry emissions ranged from 3.2% in Nigeria to 27.3% in India. Windblown dust was the most variable sector within these countries, ranging from 1.5% in Bangladesh to 70.6% in Nigeria. Of the three anthropogenic fuel categories (coal, oil & natural gas, and solid biofuel), coal was the largest source of  $PM_{2.5}$  attributable mortality in China (22.7%; 315,000 [95% CI: 239,000–385,000] deaths), O&NG was the largest contributor in Egypt, Russia, and the United States (13.7–27.9%; 9000 [4000–16,000] to 13,000 [4500–24,000] deaths), and solid biofuel combustion was largest in the remaining five countries (12.3–36.0%; 6000 [4500–8000] to 250,000 [196,500–300,000] deaths). Results further show that use of these fuels in China and India alone each contribute to roughly 10% of the global ambient  $PM_{2.5}$  disease burden (Supplementary Data 2).

For a more holistic world view, bar charts in Fig. 3 show the relative sector and fuel contributions for all 21 world regions and

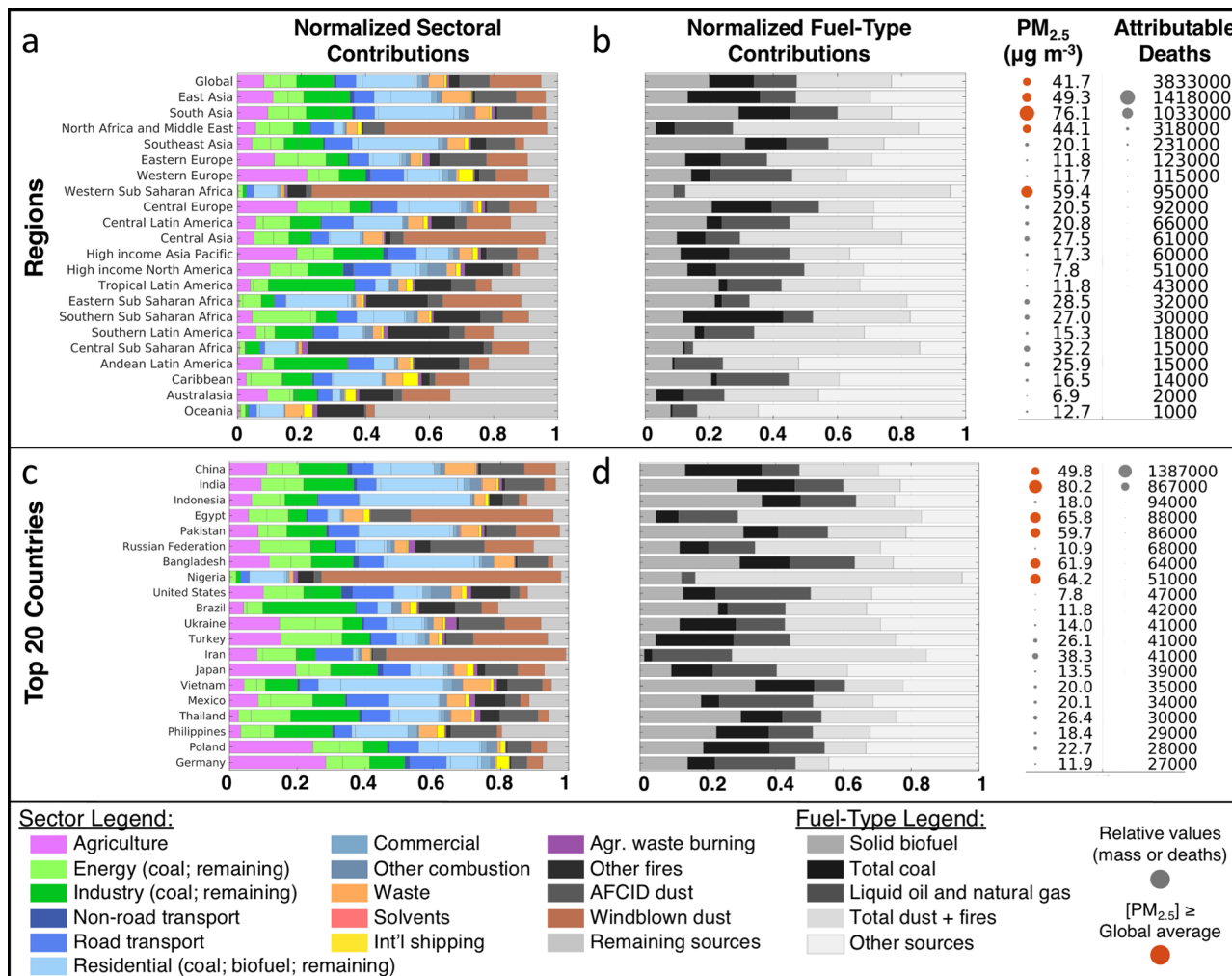


**Fig. 3 Relative (fractional) source and fuel contributions to annual population-weighted mean PM<sub>2.5</sub> mass and attributable deaths in 2017.** **a, c** Normalized sectoral source contributions for 21 world regions and the global average (**a**) and top 20 countries (**c**). Sorted by decreasing number of ambient PM<sub>2.5</sub>-attributable deaths (rounded to the nearest 1000). **b, d** Normalized contributions from the combustion of three fuel categories and remaining PM<sub>2.5</sub> sources. To the right of **b** and **d**, annual population-weighted mean PM<sub>2.5</sub> concentrations and associated attributable deaths are provided for each region/country. Relative amounts are illustrated by relative dot sizes. Concentrations above or equal to the global average are colored red.

the top 20 countries with the largest number of PM<sub>2.5</sub>-attributable deaths. The relative contributions of PM<sub>2.5</sub>-disease pairs for these same regions and countries are shown in Supplementary Fig. 3. The color scheme to the right of panels b and d in Fig. 3 shows that four of the 21 regions and six of the top 20 countries each had PWM PM<sub>2.5</sub> concentrations higher than the global average. Similar to the pie charts in Fig. 2, Fig. 3 panels a and c show that residential energy use was the largest contributing sector in South, East, and Southeast Asia, largely driven by trends in India, Indonesia, Pakistan, Bangladesh, and Vietnam. Other notable features include the dominant contribution from windblown dust throughout North Africa, the Middle East, Central Asia, and Western Sub-Saharan Africa, as well as dominant fire contributions in Southern Latin America, Central Sub-Saharan Africa, Oceania, and North America. Large agricultural contributions were found in Western and Central Europe and Pacific Asia, along with dominant contributions from industrial processes in Andean and Tropical Latin America. Comparing all world regions, Fig. 3a shows that areas with the lowest number of PM<sub>2.5</sub> attributable deaths generally had the smallest relative contributions from non-natural PM<sub>2.5</sub> sources. Similarly, Fig. 3b shows that regions with greater attributable deaths had relatively larger contributions from anthropogenic fuel combustion emissions. Exceptions include

Western and Central Sub-Saharan Africa, where combined contributions from windblown dust and fires were greatest (81.0 and 68.4%).

Figure 4a provides a map of the dominant contributing fuel type in each country to further highlight the national-level variability in relative fuel contributions. For example, Fig. 4a shows that despite a recent decline in global coal emissions<sup>6</sup>, coal was the dominant combustible fuel type contributing to the PM<sub>2.5</sub> disease burden in 20 countries, including China, Eswatini, South Africa, and countries throughout Central and Eastern Europe. At the national level, South Africa and neighboring Eswatini both had the largest relative coal contributions of all countries at more than 36.5% each (~9000 [95% CI: 6000–12,500] attributable deaths in total). Countries with the lowest relative coal contributions (<0.1%) included those in other regions of Africa, as well as small island nations. O&NG combustion typically dominated in more developed countries throughout North America, Australasia, and Western Europe, as well as parts of North Africa, the Middle East, Central Asia, and Eastern Europe. Of all world regions, North America and Western Europe had the largest relative O&NG contributions at ~25% each (43,000 [95% CI: 19,500–72,500] deaths total), while the lowest was in Central Sub-Saharan Africa at 2.5% (<1000 deaths total). Third, regional

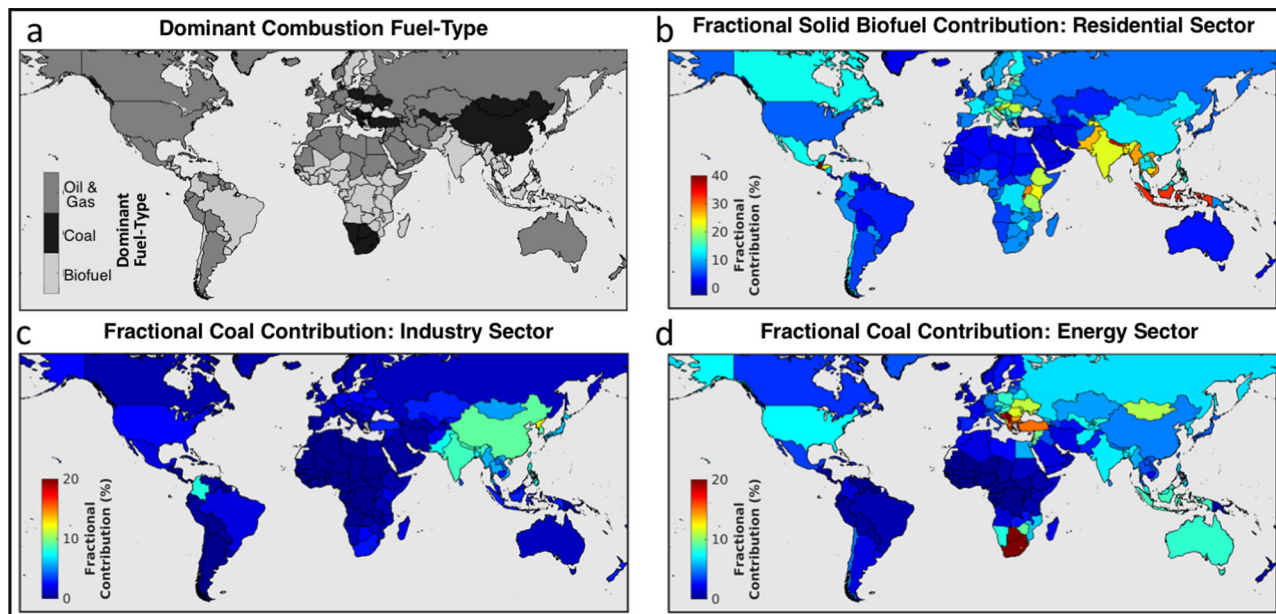


**Fig. 4 Fractional contributions from select combustion fuel types and sectors.** **a** The combustion fuel-type with the largest relative contribution to  $PM_{2.5}$  mass and mortality in each country. **b–d** The fractional contributions from solid biofuel combustion in the residential sector (**b**), coal combustion in the industry sector (**c**), and coal combustion in the energy sector (**d**). Note the color scale change between (**b**) and (**c, d**).

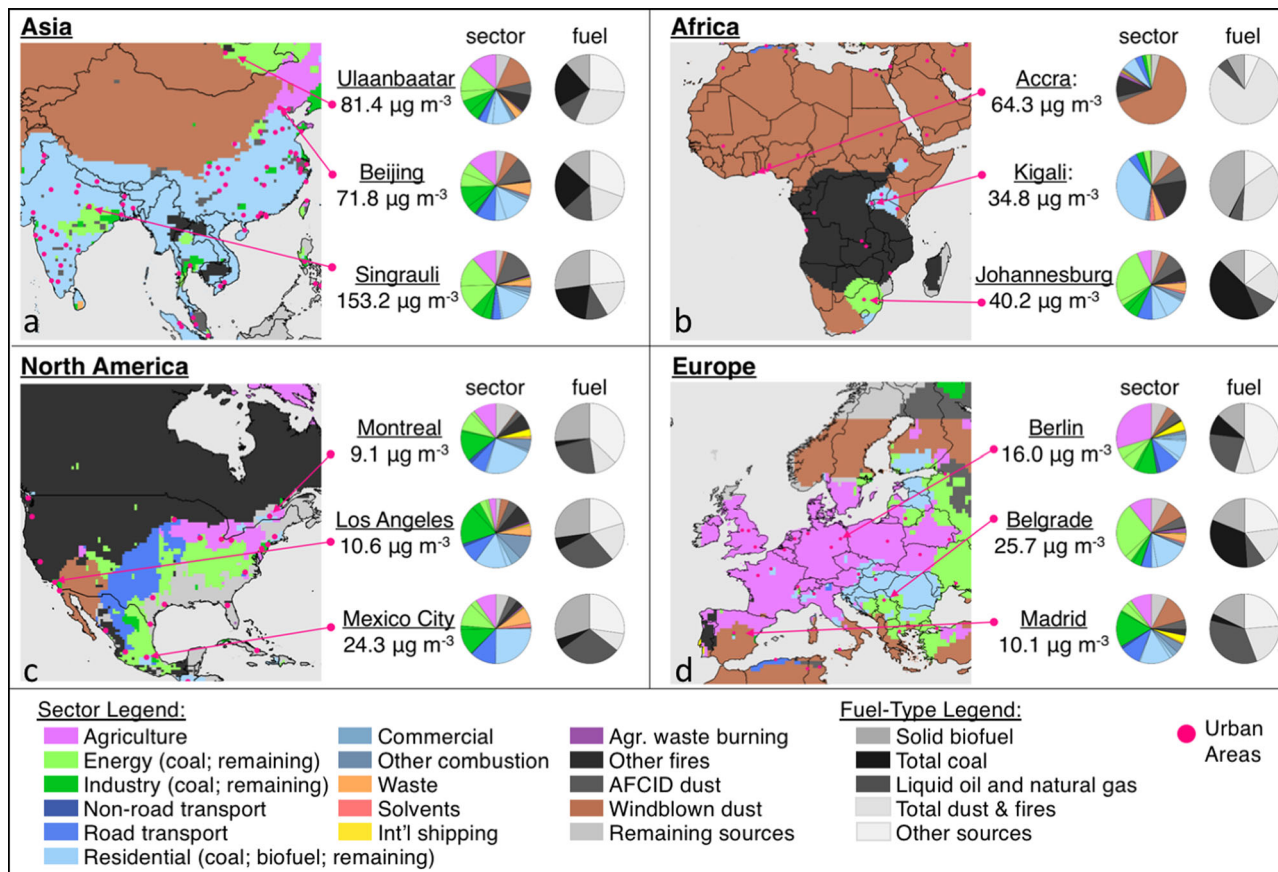
solid biofuel contributions (largely from the residential sector) were largest in South and Southeast Asia at between 29.2 and 31.2% each (373,500 [95% CI: 279,500–465,000] deaths total). Solid biofuel was the dominant contributing combustible fuel in 76 countries including throughout Central, Eastern, and Sub-Saharan Africa, parts of Central and Western Europe, Asia, and Tropical Latin America. National-level fractional contributions ranged from 0.2% in small island nations to at least 40% in Guatemala, Nepal, and Rwanda (8500 [95% CI: 6500–11,000] total deaths).

Figure 4b–d additionally provides an assessment of three detailed emission reduction strategies that test policy-relevant scenarios of select fuel and sector combinations. These panels show the fractional contributions of  $PM_{2.5}$  mass and attributable mortality avoidable by eliminating the use of (b) residential biofuel, (c) industrial sector coal combustion, and (d) coal combustion for energy generation. Figure 4a reveals that while coal is the dominant fuel type in both China and South Africa, coal from the energy sector contributes to a greater fraction of attributable deaths (20.5%) in South Africa than does the industry sector (2.7%), while the opposite is true for China (4.7% energy coal, 9.1% industry coal). Similarly, in countries throughout Central and Eastern Europe where coal is the dominant contributing fuel, the targeted reduction of coal use in the energy sector may lead to immediately larger air quality benefits than targeting coal use in the industrial sector (Fig. 4c and d). For residential biofuel use, the relative contributions are generally largest in regions where residential emissions are the dominant source sector (Fig. 3a). At the national scale, the combustion of solid biofuel for home heating and cooking contributed up to 46.1% of the total  $PM_{2.5}$  mass and attributable deaths in Guatemala (Supplementary Data 1). These examples highlight the potential air quality benefits from specific and achievable reduction strategies. Detailed comparisons across countries in Fig. 4 and Supplementary Data 1 can further identify opportunities with the greatest potential health gains and identify countries who have successfully managed reductions from these select sources.

**Sub-national source contributions.** To investigate sub-national variability in  $PM_{2.5}$  mass and its sources, we leverage the high-resolution downscaled exposure estimates ( $0.01^\circ \times 0.01^\circ$ ) to estimate PWM  $PM_{2.5}$  mass for 200 sub-national areas. We additionally apply gridded model sensitivity simulation results ( $0.5^\circ \times 0.625^\circ$  in North America, Europe, and East Asia,  $2^\circ \times 2.5^\circ$  elsewhere) to the sub-national exposure levels to estimate the relative source contributions in these same areas. Sub-national area boundaries are identified by the nearest dominant city and are defined using T3 urban extent data from the Atlas of Urban Expansion<sup>51</sup>. This dataset provides urban boundaries for 200 metropolitan areas that had more than 100,000 inhabitants in 2010.

$PM_{2.5}$  exposure estimates reveal a large public health benefit from reducing  $PM_{2.5}$  exposure in urban areas. For example, Supplementary Data 1 shows that more than 65% of the select 200 areas experienced higher PWM  $PM_{2.5}$  concentrations than their corresponding national averages. In a few extreme cases in India, for example, average PWM  $PM_{2.5}$  concentrations exceeded  $150 \mu g m^{-3}$ , nearly twice that of the national average and over 15 times larger than the WHO guideline.

Figure 5 shows that both PWM  $PM_{2.5}$  mass and dominant  $PM_{2.5}$  surface sources vary at the sub-national scale, highlighting the importance of developing region-specific air quality strategies. For example, while residential emissions are the largest source of average  $PM_{2.5}$  exposure and attributable mortality in China and India, areas surrounding Beijing and Singrauli (Madhya Pradesh, India) have relatively larger contributions from the energy and industry sectors. Similarly, while the transportation sector was the largest PWM  $PM_{2.5}$  source in the U.S., Fig. 5c illustrates regionally varying sources, with dominant contributions from forest fires in the west, windblown dust in the arid southwest, agricultural, on-road transportation, and energy throughout the midwest and east coast, and highly uncertain sources such as secondary organic aerosol (SOA) in the southeast. In Europe, the non-combustion agriculture sector is a dominant source of PWM  $PM_{2.5}$  mass and mortality across large portions of the region, however pie charts in Fig. 5d also illustrate areas with relatively



**Fig. 5 Sub-national sources of PM<sub>2.5</sub> mass and attributable mortality.** Results are shown for (a) Asia, (b) Africa, (c) North America, and (d) Europe. Maps illustrate the single source with the largest contribution in each model grid cell (0.5° × 0.625°). Population-weighted mean PM<sub>2.5</sub> concentrations (calculated from 0.01° × 0.01° PM<sub>2.5</sub> exposure estimates) and regional fractional source contributions are also shown for a select sub-set of sub-national regions, identified by the name of the nearest major city.

large contributions from the energy, industry, and residential sectors. For Africa, energy generation from coal combustion was the largest source of PM<sub>2.5</sub> attributable deaths in South Africa (Supplementary Data 1), though Fig. 5b shows that this influence was centered around Johannesburg (26.1%), while the area around Port Elizabeth was dominantly influenced by windblown dust and other non-combustion sources (Supplementary Data 1). Pie charts in all panels of Fig. 5 highlight that in all regions, a large number of sources collectively contribute to sub-national PM<sub>2.5</sub> mass formation, not only the largest sources illustrated in the map panels.

While annual PM<sub>2.5</sub> exposure estimates in Fig. 5 were derived from urban-relevant spatial scales (i.e., 0.01° × 0.01°), we note that the source contributions here are limited by the resolution of the GEOS-Chem model (above) and of the emissions dataset (0.5° × 0.5°). As a result, source contributions maps in Fig. 5 are effective at highlighting sub-national source contributions, but urban-level contributions would be improved with more spatially resolved simulations and emissions. Sub-national and urban scale PM<sub>2.5</sub> exposure estimates and fractional source contributions are vital for identifying reduction strategies with the greatest public health benefit, which will become increasingly important as ~65% of the world’s population is projected to live in urban areas by 2050<sup>52</sup>.

**Discussion**

We provide a comprehensive and quantitative evaluation of the individual sector and fuel contributions to annual PWM PM<sub>2.5</sub> mass and its disease burden, relevant to the development and

prioritization of effective mitigation strategies. We find that over 1 million (27.3%) attributable deaths were avoidable by eliminating PM<sub>2.5</sub> mass associated with emissions from fossil-fuel combustion (total coal + O&NG). These results add to the growing evidence of the public health benefit achievable from global decarbonization strategies<sup>53</sup>. While global total coal contributions (14.1%) were slightly larger than those from O&NG (13.2%), the relative balance between these two fuel categories varied at the regional, country (Figs. 2 and 3), and sub-national levels (Fig. 5). As the largest number of PM<sub>2.5</sub> attributable deaths occurred in China and India, complete elimination of coal and O&NG combustion in these two countries could reduce the global PM<sub>2.5</sub> disease burden by nearly 20% (Supplementary Data 2).

Comparisons here with prior analyses are limited by differences in estimation years as well as differences in spatial resolution and input data, including chemical transport models, CRFs, and emissions, population, exposure, and burden datasets. Fractional fossil-fuel contributions to the PM<sub>2.5</sub> disease burden (27.3%) for the year 2017 were lower than the only previous global fractional estimate of 41% for the year 2015<sup>36</sup>. Observed differences are largely driven by countries that have experienced recent reductions in fossil-fuel emissions<sup>6</sup>, such as China, the U. S., and Western European countries, including Germany and Italy. Absolute contributions in this work were also lower than recent fossil fuel attributable mortality estimates derived using different CRFs<sup>54</sup>. Compared to two previous national-level studies, fractional coal contributions in 2017 were also 17% smaller than a 2013 estimate for China<sup>17</sup>, but generally consistent to

within 1% for a 2015 estimate for India<sup>18</sup> (Supplementary Text 6). Emission inputs suggest that PM<sub>2.5</sub> precursor emissions from coal combustion (e.g., SO<sub>2</sub>) have decreased by up to 60% between 2013 and 2017 in China, while these same emission sources in India have increased by up to 7% between 2015 and 2017<sup>6</sup>. Fossil-fuel contributions in our analysis may also be lower limits as some sub-sectoral emission categories such as flaring and fossil-fuel fires were not assigned to a fuel category in the emissions dataset<sup>6</sup>, but rather were included in the ‘other sources’ category in this analysis (Supplementary Text 5).

The use of solid biofuel across all sectors in 2017 contributed to an additional 767,000 (95% CI: 543,000–994,500) attributable deaths worldwide (20%), with this source in India and China again responsible for roughly 11% of the global PM<sub>2.5</sub> disease burden. Solid biofuel emissions in countries throughout South and Southeast Asia, as well as Central and Western Sub-Saharan Africa were largely associated with residential solid biofuel use for household heating and cooking (Fig. 5b). Large fractional contributions of this source were consistent to within 4% of the only previous global estimate<sup>25</sup>. Results in 2017 were also consistent to within 3% of two previous national-level estimates of fractional PM<sub>2.5</sub> disease burden contributions from residential heating and cooking in China in 2013<sup>17</sup> and in India in 2015<sup>18</sup> (Supplementary Text 6). While emissions from biofuel combustion have recently decreased in China, other world regions are experiencing a simultaneous increase<sup>6</sup>, highlighting the continued importance of considering residential solid biofuel emissions for future air quality improvement strategies. Considerations of net air quality benefits will also be important in regions where a transition from residential solid biofuel use to fossil fuel energy sources may lead to immediate indoor and outdoor air quality improvements and health benefits<sup>55</sup>, while at the same time increasing the relative fossil fuel contributions.

For major contributing global source sectors (Fig. 2), relative contributions were generally consistent with previous global studies, though differences again may arise due to real temporal changes or differences in input datasets, chemical transport models, or sectoral definitions used. Comparisons with previous national-level studies are more variable, with summaries provided in Supplementary Text 6. At the global scale, the residential energy sector was the single largest contributing source to the 2017 global PM<sub>2.5</sub> disease burden and had a relative contribution (~20%) similar to previous global estimates of 8–31% in 2000–2014<sup>37–39,56</sup>. In addition, the global 2017 contribution from the combined energy (10.2%) and industry (11.7%) sectors was consistent with two previous global combined estimates of 21 and 33% in 2010–2014<sup>37,39</sup>. Different reported relative contributions between the energy and industry sectors may be driven by differences in sectoral definitions. Global estimates for fractional contributions from dust and the transport sector were also generally consistent with previous global estimates. The total 2017 dust contribution (windblown and anthropogenic) of 25% was similar to two previous global studies of 18–24%<sup>37,39</sup>. Similarly, previous estimates for the transportation sector of between 5–12% in 2005–2015<sup>32,37–39</sup> encompass the 2017 value of 7.6%. In contrast, contributions from the agriculture sector (8%) were slightly lower than previous global estimates of 9–25% in 2010–2015<sup>37,39,57</sup>, even when 2017 contributions from agricultural waste burning (+1%) were included.

Smaller global sectors include waste, fires, solvent use, and international shipping, which each contributed to <5% of the 2017 global PM<sub>2.5</sub> disease burden. These sources however may be important to consider for national and sub-national control strategies (Fig. 5; Supplementary Text 6). The number of global attributable deaths from the waste sector (184,000; 95% CI: 130,500–238,500 deaths) in 2017 was 30% lower than the only

previous estimate of domestic waste burning<sup>29</sup>. Global contributions from solvent use have not been previously reported. For international shipping, global mortality estimates (27,000; 95% CI: 19,000–35,000 deaths) fell within the range of a previous 2002 estimate<sup>33</sup>, but were 75–95% lower than a more recent study, largely due to differences in the CRFs<sup>58</sup>. In contrast to anthropogenic sources, annual open fire contributions are expected to vary strongly with annual fire activity<sup>3</sup>, and may increase in regions where the number and severity of wildfires is projected to increase<sup>59</sup>. The global 2017 total fire contribution was 4.1%, consistent with two previous estimates of ~5% in 2010 and 2014<sup>37,39</sup>. Figure 5, however, shows that fires were the single largest contributor to the PM<sub>2.5</sub> disease burden in select regions throughout North America, Southeast Asia, and Africa. These relative contributions are generally consistent with a previous global-scale estimate<sup>3</sup>, though mixed agreement with previous national-level estimates likely highlights the interannual variability of this source. For example, 2017 contributions in India and China (~1%) were lower than previous estimates of 1–8% for 2013–2015<sup>17,18,28,37</sup>, contributions in the U.S. (~13%) were more than double a previous 2010 estimate<sup>37</sup>, and contributions in Canada (18.9%) were consistent with a previous 2013 study<sup>11</sup>. All remaining PM<sub>2.5</sub> sources (Supplementary Table 2) contributed to 5.2% or less at the global scale.

Similar to previous studies, fractional and absolute source contributions to PWM PM<sub>2.5</sub> mass and the attributable disease burden are subject to uncertainties in the emissions dataset, PM<sub>2.5</sub> exposure estimates, 3D chemical-transport model, national-level baseline mortality estimates, and the disease-specific GBD2019 CRFs. Following methods from previous similar studies<sup>36,37,60</sup>, the 95% CI of the 2017 PM<sub>2.5</sub> disease burden is derived from uncertainties in the GBD2019 CRFs, resulting in a range of 2.72 million–4.97 million global attributable deaths. An additional sensitivity study is presented in Supplementary Text 7 to test the impact of uncertainties associated with the baseline mortality data, which for the majority of world regions results in smaller uncertainty bounds than those associated with CRF uncertainties (Supplementary Fig. 7). As described in the Methods, the GEOS-Chem model is evaluated against available surface observations and uncertainties in the emissions dataset are discussed elsewhere<sup>6</sup>. In addition, sub-national fractional source contributions (Fig. 5) are limited to the resolution of the model and emissions, while the urban exposure estimates are further subject to greater uncertainties in the satellite-derived products for small spatial scales<sup>43,47</sup>. Future developments of global high-resolution simulations, as well as increasing the accuracy and precision of satellite-derived PM<sub>2.5</sub> estimates will serve to reduce these uncertainties in PM<sub>2.5</sub> mass and source contributions at both the national and sub-national scales.

In addition to uncertainties in the general methodology, this work also assumes equitoxicity of aerosol mass and its sources, including from windblown mineral dust<sup>61</sup>. This assumption is necessary for use with the GBD2019 and GEMM CRFs and is consistent with US EPA<sup>62</sup> and WHO<sup>63</sup> assessments. This assumption may under- or over-estimate the relative PM<sub>2.5</sub> burden contributions from select sectors provided they contribute to more or less toxic components of total PM<sub>2.5</sub> mass. We additionally note that by simultaneously reducing emissions across all geographic regions, this study did not explicitly investigate national contributions from long-range or regional transport<sup>11,64</sup>. As the implementation of mitigation policies is typically constrained to political borders, specific policies may need to consider the regional influence on local pollution levels. We lastly note that results from the sensitivity simulations (Methods) largely reflect changes in PM<sub>2.5</sub> mass associated with the complete elimination of each individual emission source. Therefore, the



same relative contributions may not be expected from studies that test more moderate reduction strategies or simultaneous reductions of multiple sources (Supplementary Text 8).

The comprehensive nature of our analysis provides detailed source information to inform PM<sub>2.5</sub> mitigation strategies and provides potential health benefit estimates to further motivate action. Results show that residential, energy, industry, and total dust sources are among the largest contributing sectors to the global PM<sub>2.5</sub> disease burden, while the relative contributions from individual sources and fuels vary at the national and sub-national levels. Roughly 1 million deaths could be avoided by the global elimination of fossil-fuel combustion, with 20% of this burden associated with fossil-fuel use in China and India alone (Fig. 2). Despite recent global reductions in air pollutant emissions from coal, this fuel was still the dominant contributing combustible fuel type to the PM<sub>2.5</sub> disease burden in 20 countries, including China and countries throughout Southern Sub-Saharan Africa and Central Europe (Fig. 4). The use of solid biofuel was a primary source of emissions from the residential sector and was the dominant contributing combustible fuel in 78 countries, especially throughout the tropics (Fig. 4). While natural sources of PM<sub>2.5</sub> mass dominantly contributed in more arid regions (Fig. 3), countries with the greatest PM<sub>2.5</sub> disease burden generally had the largest relative contributions from anthropogenic sources, demonstrating a clear path towards attaining global air quality improvements.

## Methods

This study integrates newly available high-resolution satellite-derived PM<sub>2.5</sub> exposure estimates, CRFs from the 2019 GBD, and fractional source contribution results from 24 emission sensitivity simulations to provide the most comprehensive global source contribution results to-date. This work also provides global estimates of PM<sub>2.5</sub>-attributable deaths from the use of coal, O&NG, and solid biofuel. The following sections describe the details of the high-resolution PM<sub>2.5</sub> exposure estimates, attributable disease burden calculations, set-up and evaluation of the chemical transport model, sector- and fuel-specific emissions dataset, and fractional simulated source contribution calculations. A schematic of this overall process is provided in Supplementary Text 9 and Supplementary Fig. 8.

**High-resolution PM<sub>2.5</sub> exposure estimates.** To maintain consistency with the GBD project, while also improving the accuracy of the population-exposure estimates, we downscale the 2019 GBD exposure estimates<sup>1,47,48</sup> to a 0.01° × 0.01° (~1 km × 1 km) grid using a newly available high-resolution PM<sub>2.5</sub> dataset from Hammer et al.<sup>43</sup>. Supplementary Text 10 (Supplementary Fig. 9) describes this process of spatial downscaling by incorporating the spatial information from the Hammer et al.<sup>43</sup> product. This downscaling process is independent of the modeled fractional source contribution results and maintains the average PM<sub>2.5</sub> mass concentration (area average only) from the original GBD product. The sensitivity of the PM<sub>2.5</sub> exposure estimates to the downscaling process are evaluated in Supplementary Text 10 and Supplementary Fig. 10. Exposure estimates for the year 2019 were derived using these same methods with both GBD and Hammer et al.<sup>43</sup> data for the year 2019.

**National-level PM<sub>2.5</sub> disease burden.** The total disease burden from six mortality endpoints and two neonatal disorders associated with exposure to annual average outdoor PM<sub>2.5</sub> mass (from the downscaled GBD-product) was calculated following a similar methodology as the 2019 GBD project<sup>1</sup>. First, Eq. (1) was used to derive cause-specific population attributable fractions (PAFs) for each endpoint using national-level PM<sub>2.5</sub> concentrations (population-weighted) from the downscaled GBD exposure estimates and recently updated relative risk curves (RR\*), derived using a Meta Regression-Bayesian, Regularized, Trimmed (MR-BRT) spline from the 2019 GBD (Supplementary Fig. 2)<sup>1</sup>. MR-BRT curves use splines with Bayesian priors, which avoids using relative risk estimates for active smoking, previously necessary to avoid over-estimation of risks at high exposure levels. These meta-regressions were applied to the latest observational cohort and case-control studies of mortality or disease incidence from outdoor PM<sub>2.5</sub> pollution cohort and case-control studies; cohort, case-control, and randomized-controlled trials of household use of solid fuel for cooking; as well as cohort and case-control studies of secondhand smoke.

$$\text{PAF}_{\text{age, disease, country}} = 1 - \frac{1}{\text{RR}^*_{\text{age, disease, [PWM PM}_{2.5}]_{\text{country}}}} \quad (1)$$

Consistent with the 2019 GBD, the resulting RR\* (or CRF) values from the MR-BRT splines in Eq. (1) are gender-independent and describe the excess risk of

non-accidental mortality from adult (25 years and older) IHD, Stroke, COPD, LC, DM, and childhood and adult (under 5 years and 25 years and older) acute LRIs. Consistent with the 2019 GBD, RR\*s for each disease in Eq. (1) are also a function of annual PWM PM<sub>2.5</sub> mass exposure in each country and the difference between this exposure level and the Theoretical Minimum Risk Exposure Level (TMREL). The TMREL in this work, as in the GBD2019, is assumed to have a uniform distribution ranging between 2.4 and 5.9 μg m<sup>-3</sup>. Thus, RR\* = RR(age, PWM PM<sub>2.5</sub>)/RR(age, TMREL). RR\* values were also stratified by quinquennial age group (25–29, ..., 95+), with age-specific RR\* values applied to IHD and stroke outcomes. In contrast, age-independent RR\*s were applied to the other health outcomes (age group 25 and over for COPD, LC, and type II DM, and the combined age groups under 5 and 25 and over for LRI). Supplementary Fig. 2 provides an illustration of select RR\* (or CRF) values for these diseases as a function of annual PM<sub>2.5</sub> mass exposure, as well as the CRFs for two neonatal disorders, which include the number of preterm (PTB; gestational age less than 37 weeks) and low birth weight (LBW; below 2.5 kg) incidences. The 95% CI for the CRF values was determined from the distribution of 2000 randomly selected values of the TMREL.

As shown in Eq. (2), the PAFs for each age group, disease, and country were then multiplied by the age- and country-specific baseline mortality data for each disease and summed over all relevant age groups (*m*) and diseases (*n*) to obtain the total national-level PM<sub>2.5</sub> burden associated with exposure to both outdoor and household (indoor) PM<sub>2.5</sub> mass. National cause- and age-specific baseline mortality data for the years 2017 and 2019 were extracted from the GHDx database<sup>65</sup>. The national-level baselines for PTB and LBW were calculated from the 2019 GBD statistics of the number of annual live births and the percentage of LBW and PTB cases at the national and regional levels<sup>66,67</sup>.

$$\text{PM}_{2.5} \text{ Attributable Mortality}_{\text{country}} = \sum_{\text{disease}} \sum_{\text{age}} \text{PAF}_{\text{age, disease, country}} \times \text{Baseline Mortality}_{\text{age, disease, country}} \quad (2)$$

Finally, to separate the contributions from outdoor and indoor household co-exposure, the national-level total PM<sub>2.5</sub> attributable mortality values from Eq. (2) were scaled using Eq. (3) to account for the risk of co-exposure to household air pollution included in the CRFs. Country-specific adjustment factors were derived from a comparison of national-level burdens in Eq. (2) to those derived for outdoor exposure only in the 2019 GBD study. As a result of these adjustments, the PM<sub>2.5</sub> attributable mortality and source contribution results presented in this analysis reflect contributions from indoor sources of air pollution (e.g., biomass combustion for residential heating and cooking) to the extent that they impact ambient PM<sub>2.5</sub> concentrations.

$$\text{Outdoor PM}_{2.5} \text{ Attributable Mortality}_{\text{country}} = \text{PM}_{2.5} \text{ Attributable Mortality}_{\text{country}} \times \text{Adjustment Factor}_{\text{country}} \quad (3)$$

The overall approach described here generally follows that of the 2019 GBD, but deviates in part by calculating national-level PAFs rather than PAFs for each grid cell, and by using publicly available national baseline data from the IHME<sup>65</sup>, rather than both national and sub-national baseline estimates. We find that the aggregate-country level method used in this work is consistent to within 5% of the grid-cell methodology used in the GBD.

As discussed in Supplementary Text 2, we also calculate the PAFs for each PM<sub>2.5</sub>-disease pair (plus two neonatal disorders) using an updated version of the GEMM<sup>44</sup>. To aid in the comparison with GBD2019 CRF estimates, the original GEMM was updated to include CR curves for Type-II Diabetes, PTBs, and LBWs as well as newly available observational studies (described in Supplementary Text 2). For the neonatal outcomes, only the number of PTB and LBW cases were estimated, whereas the 2019 GBD estimated neonatal death mediated by the impact of PM<sub>2.5</sub> on birthweight and short gestation. As the GEMM is exclusively developed from studies of outdoor PM<sub>2.5</sub> exposure, total outdoor PM<sub>2.5</sub> attributable deaths in Supplementary Data 1 and 2 were taken directly from Eq. (2) and did not require scaling factors to remove the risk associated with indoor PM<sub>2.5</sub> exposure.

**Simulated fractional sector and fuel-type contributions.** Fractional sector and fuel-specific contributions were derived from a series of emission sensitivity simulations, using the 3D GEOS-Chem chemical transport model<sup>46</sup>. As described in Supplementary Text 3, we used the GEOS-Chem v12.1.0 source code, updated to account for scientific updates to physical deposition, reactive nitrogen chemistry, and surface emissions ([https://github.com/emcduffie/GC\\_v12.1.0\\_EEM](https://github.com/emcduffie/GC_v12.1.0_EEM)). Model simulations were run from December 2016 to January 2018 to allow for one month of spin-up. The model was run globally at a resolution of 2° × 2.5° and was supplemented with three nested simulations with resolutions of 0.5° × 0.625° over North America, Europe, and Asia.

Gridded emission datasets are the backbone of any modeling source contribution study. In this work, we leverage a newly developed emissions dataset developed from the Community Emissions Data System that has been updated for the GBD-MAPS project (<https://sites.wustl.edu/acag/datasets/gbd-maps/>)<sup>6</sup>. This dataset provides global gridded (0.5° × 0.5°) emissions of key PM<sub>2.5</sub> components (black and organic carbon) and gas-phase precursors from 11 individual

anthropogenic source sectors and multiple fuel types for the year 2017. Supplementary Fig. 6 illustrates these global emissions as a function of source sector and chemical compound. Additional emission inputs used for model sensitivity simulations largely include those from fires (forest fires and agricultural waste burning)<sup>68</sup>, biogenic sources, and anthropogenic<sup>69</sup> and windblown dust. Supplementary Text 5 provides further emission details.

In source sensitivity simulations, it remains vital to evaluate the model's ability to predict total PM<sub>2.5</sub> concentrations as well as regional chemical production regimes. Comparisons to total PM<sub>2.5</sub> mass provide confidence in the model's ability to accurately simulate total mass production. Additional comparisons to PM<sub>2.5</sub> chemical components imply accuracy in the model's ability to capture PM<sub>2.5</sub> formation chemistry and provide confidence in the model's ability to accurately predict chemical changes in response to specific emission scenarios. In this work, we evaluated the base GEOS-Chem simulation (including all emission sources) against all available long-term surface observations of both PM<sub>2.5</sub> mass and its chemical composition. As described in Supplementary Text 4, the observational dataset was compiled from more than 10 long-term observation networks and over 4000 individual sites (Supplementary Figs. 4 and 5a).

The comparisons in Supplementary Fig. 5 indicate that individual components in the base GEOS-Chem simulation agree to within  $-0.3$  to  $0.6 \mu\text{g m}^{-3}$  of the observed annual average concentrations for all PM<sub>2.5</sub> chemical components. These observations ( $N < 230$ ) were largely limited to North America, Europe, and China, however, Supplementary Fig. 5 also demonstrates the large improvement in the long-standing bias of aerosol nitrate in our updated version of the GEOS-Chem model<sup>70</sup> relative to the default version. Supplementary Fig. 5 also demonstrates relative improvements in the updated model in concentrations of sulfate, ammonium, and dust. In terms of total PM<sub>2.5</sub> mass, Supplementary Fig. 10a shows that the base model predictions were consistent with the 2017 observations (NMB of +5%, and correlation ( $r$ ) of 0.89).

For the 24 individual emission sensitivity simulation sets (1 global +3 nested per set), we employed a zeroing out (brute force) method<sup>20,36–38</sup>, where fractional PM<sub>2.5</sub> mass contributions from each source were calculated from simulations that systematically remove individual source sectors or fuel-specific emissions. Supplementary Table 2 provides a detailed list of the 24 individual sensitivity tests. Resulting simulated spatially resolved PM<sub>2.5</sub> mass contributions from each source category were calculated following Eq. (4) and Eq. (5), where simulated gridded total PM<sub>2.5</sub> mass concentrations from each sensitivity study were first compared to the total gridded PM<sub>2.5</sub> mass in the base simulation (4), and then were compared to the sum of PM<sub>2.5</sub> mass from all  $j$  simulations (5) to calculate the gridded fractional contributions.

$$[\text{PM}_{2.5}]_{\text{source}} = [\text{PM}_{2.5}]_{\text{base simulation}} - [\text{PM}_{2.5}]_{\text{source sensitivity simulation}} \quad (4)$$

$$(\% \text{PM}_{2.5})_{\text{source}} = \frac{[\text{PM}_{2.5}]_{\text{source}}}{\sum_{j=1}^{24} [\text{PM}_{2.5}]_j} \quad (5)$$

Lastly, Eq. (6) was used to calculate the fractional source contributions to PWM PM<sub>2.5</sub> mass in 200 sub-national areas, 204 countries, 21 world regions, and for the global average. First, absolute contributions from each source were calculated from the product of the spatially resolved fractional PM<sub>2.5</sub> source contributions from Eq. (5) and the spatially resolved downscaled GBD exposure estimates from Fig. 1, averaged over  $i$  grid boxes and weighted by the total population in a given region or country. Fractional contributions were then calculated by dividing these absolute source contributions by the total PWM PM<sub>2.5</sub> concentration in a given region, country, or area. In Eq. (6), variable  $i$  represents individual grid boxes to distinguish the use of spatially resolved vs. spatially averaged products. Population-weighted fractional source contributions were calculated at the spatial resolution of the GEOS-Chem model. Supplementary Data 1 and 2 provide the resulting population-weighted fractional source contributions from Eq. (6).

$$(\% \text{Contribution})_{\text{source}} = \frac{\sum_{i=1}^n (\% \text{PM}_{2.5})_{\text{source},i} \times [\text{GBD PM}_{2.5}]_i \times \text{population}_i}{\sum_{i=1}^n \text{population}_i} \bigg/ \frac{\sum_{i=1}^n [\text{GBD PM}_{2.5}]_i \times \text{population}_i}{\sum_{i=1}^n \text{population}_i} \quad (6)$$

Following the approach of previous studies<sup>20,37</sup>, fractional contributions from Eq. (6) are then applied to national-level PM<sub>2.5</sub> exposure levels (population-weighted) and total disease burden estimates (provided in Supplementary Data 1 and 2) to calculate the absolute contributions from each source (reported in the Main Text). This method eliminates the sensitivity of the burden calculation to the order in which emission sectors are removed in model sensitivity simulations.

## Data availability

Supplementary Data files 1 and 2 provide the global, regional, national, and sub-national fractional sector and fuel contributions to PM<sub>2.5</sub> mass and disease burden for the year 2017. Supplementary Data files 1 and 2 also provide the total disease burden estimates determined by the GBD2019 and GEMM CRFs and the fractional disease-specific contributions to each (Supplementary Data 1 only). Supplementary Data 3 provides the 2019 PM<sub>2.5</sub> exposure estimates. A data visualization tool for all Supplementary Data is

available at: <https://gbdmaps.med.ubc.ca/>. Gridded model fractional source contribution results are available at: <https://zenodo.org/record/4739100>. CEDS<sub>GBD-MAPS</sub> emissions data are available at: <https://zenodo.org/record/3754964>. Input datasets required for this analysis (including high-resolution exposure estimates and GBD baseline burden data and CRFs) are available at: <https://zenodo.org/record/4642700>.

## Code availability

The GEOS-Chem model source code used for sensitivity simulations is available at: [https://github.com/emcduffie/GC\\_v12.1.0\\_EEM](https://github.com/emcduffie/GC_v12.1.0_EEM) and <https://zenodo.org/record/4718622>. The CEDS source code used to develop the global emissions dataset is available at: <https://github.com/emcduffie/CEDS> and <https://doi.org/10.5281/zenodo.3865670>. The analysis scripts used in here are available at: <https://github.com/emcduffie/GBD-MAPS-Global> and <https://zenodo.org/record/4718618>.

Received: 20 January 2021; Accepted: 17 May 2021;

Published online: 14 June 2021

## References

- GBD 2019 Risk Factor Collaborators. Global burden of 87 risk factors in 204 countries and territories, 1990–2019: a systematic analysis for the Global Burden of Disease Study 2019. *Lancet* **396**, 1223–1249 (2020).
- Yokelson, R. J. et al. Emissions from biomass burning in the Yucatan. *Atmos. Chem. Phys.* **9**, 5785–5812 (2009).
- Johnston, F. H. et al. Estimated global mortality attributable to smoke from landscape fires. *Environ. Health Perspect.* **120**, 695–701 (2012).
- Reid, J. S. et al. Comparison of size and morphological measurements of coarse mode dust particles from Africa. *J. Geophys. Res. Atmos.* <https://doi.org/10.1029/2002JD002485> (2003).
- Bond, T. C. et al. Historical emissions of black and organic carbon aerosol from energy-related combustion, 1850–2000. *Global Biogeochem. Cycles* <https://doi.org/10.1029/2006GB002840> (2007).
- McDuffie, E. E. et al. A global anthropogenic emission inventory of atmospheric pollutants from sector- and fuel-specific sources (1970–2017): an application of the Community Emissions Data System (CEDS). *Earth Syst. Sci. Data* **12**, 3413–3442 (2020).
- Womack, C. C. et al. An odd oxygen framework for wintertime ammonium nitrate aerosol pollution in urban areas: NOx and VOC control as mitigation strategies. *Geophys. Res. Lett.* **46**, 4971–4979 (2019).
- Lu, K. et al. Fast photochemistry in wintertime haze: consequences for pollution mitigation strategies. *Environ. Sci. Technol.* **53**, 10676–10684 (2019).
- Liang, C. K. et al. HTAP2 multi-model estimates of premature human mortality due to intercontinental transport of air pollution and emission sectors. *Atmos. Chem. Phys.* **18**, 10497–10520 (2018).
- Zhang, Q. et al. Transboundary health impacts of transported global air pollution and international trade. *Nature* **543**, 705–709 (2017).
- Meng, J. et al. Source contributions to ambient fine particulate matter for Canada. *Environ. Sci. Technol.* **53**, 10269–10278 (2019).
- West, J. J. et al. What we breathe impacts our health: improving understanding of the link between air pollution and health. *Environ. Sci. Technol.* **50**, 4895–4904 (2016).
- Watson, J. G., Antony Chen, L. W., Chow, J. C., Doraiswamy, P. & Lowenthal, D. H. Source apportionment: findings from the U.S. supersites program. *J. Air Waste Manag. Assoc.* **58**, 265–288 (2008).
- Pui, D. Y. H., Chen, S.-C. & Zuo, Z. PM<sub>2.5</sub> in China: measurements, sources, visibility and health effects, and mitigation. *Particuology* **13**, 1–26 (2014).
- Karagulian, F. et al. Contributions to cities' ambient particulate matter (PM): a systematic review of local source contributions at global level. *Atmos. Environ.* **120**, 475–483 (2015).
- Martin, R. V. et al. No one knows which city has the highest concentration of fine particulate matter. *Atmos. Environ.: X* **3**, 100040 (2019).
- GBD MAPS Working Group. Burden of Disease Attributable to Coal-Burning and Other Major Sources of Air Pollution in China. Special Report 20. (Health Effects Institute. <https://www.healtheffects.org/publication/burden-disease-attributable-coal-burning-and-other-air-pollution-sources-china> (2016).
- GBD MAPS Working Group. Burden of Disease Attributable to Major Air Pollution Sources in India. Special Report 21., Health Effects Institute. <https://www.healtheffects.org/publication/gbd-air-pollution-india> (2018).
- Caiazzo, F., Ashok, A., Waitz, I. A., Yim, S. H. L. & Barrett, S. R. H. Air pollution and early deaths in the United States. Part I: Quantifying the impact of major sectors in 2005. *Atmos. Environ.* **79**, 198–208 (2013).
- Gu, Y. et al. Impacts of sectoral emissions in China and the implications: air quality, public health, crop production, and economic costs. *Environ. Res. Lett.* **13**, 084008 (2018).

21. Liu, J. et al. Air pollutant emissions from Chinese households: a major and underappreciated ambient pollution source. *Proc. Natl Acad. Sci. USA* **113**, 7756 (2016).
22. Lacey, F. G. et al. Improving present day and future estimates of anthropogenic sectoral emissions and the resulting air quality impacts in Africa. *Faraday Discuss.* **200**, 397–412 (2017).
23. Kheirbek, I., Haney, J., Douglas, S., Ito, K. & Matte, T. The contribution of motor vehicle emissions to ambient fine particulate matter public health impacts in New York City: a health burden assessment. *Environ. Health* **15**, 89 (2016).
24. Thakrar, S. K. et al. Reducing mortality from air pollution in the United States by targeting specific emission sources. *Environ. Sci. Tech. Lett.* <https://doi.org/10.1021/acs.estlett.0c00424> (2020).
25. Chafe, Z. A. et al. Household cooking with solid fuels contributes to ambient PM2.5 air pollution and the burden of disease. *Environ. Health Perspect.* **122**, 1314–1320 (2014).
26. Chambliss, S. E., Silva, R., West, J. J., Zeinali, M. & Minjares, R. Estimating source-attributable health impacts of ambient fine particulate matter exposure: global premature mortality from surface transportation emissions in 2005. *Environ. Res. Lett.* **9**, 104009 (2014).
27. Gao, M. et al. The impact of power generation emissions on ambient PM2.5 pollution and human health in China and India. *Environ. Int.* **121**, 250–259 (2018).
28. Hu, J. et al. Premature mortality attributable to particulate matter in China: source contributions and responses to reductions. *Environ. Sci. Technol.* **51**, 9950–9959 (2017).
29. Kodros, J. K. et al. Global burden of mortalities due to chronic exposure to ambient PM 2.5 from open combustion of domestic waste. *Environ. Res. Lett.* **11**, 124022 (2016).
30. Saikawa, E. et al. The impact of China's vehicle emissions on regional air quality in 2000 and 2020: a scenario analysis. *Atmos. Chem. Phys.* **11**, 9465–9484 (2011).
31. Wu, R. et al. Air quality and health benefits of China's emission control policies on coal-fired power plants during 2005–2020. *Environ. Res. Lett.* **14**, 094016 (2019).
32. Anenberg, S., Miller, J., Henze, D. & Minjares, R. A global snapshot of the air pollution-related health impacts of transportation sector emissions in 2010 and 2015. The International Council on Clean Transportation (ICCT). <https://theicct.org/publications/health-impacts-transport-emissions-2010-2015> (2019).
33. Corbett, J. J. et al. Mortality from ship emissions: a global assessment. *Environ. Sci. Technol.* **41**, 8512–8518 (2007).
34. Marais, E. A. et al. Air quality and health impact of future fossil fuel use for electricity generation and transport in Africa. *Environ. Sci. Technol.* **53**, 13524–13534 (2019).
35. Lacey, F. G., Henze, D. K., Lee, C. J., van Donkelaar, A. & Martin, R. V. Transient climate and ambient health impacts due to national solid fuel cookstove emissions. *Proc. Natl Acad. Sci. USA* **114**, 1269 (2017).
36. Lelieveld, J. et al. Effects of fossil fuel and total anthropogenic emission removal on public health and climate. *Proc. Natl Acad. Sci. USA* **116**, 7192 (2019).
37. Lelieveld, J., Evans, J. S., Fnais, M., Giannadaki, D. & Pozzer, A. The contribution of outdoor air pollution sources to premature mortality on a global scale. *Nature* **525**, 367 (2015).
38. Silva Raquel, A., Adelman, Z., Fry Meridith, M. & West, J. J. The impact of individual anthropogenic emissions sectors on the global burden of human mortality due to ambient air pollution. *Environ. Health Perspect.* **124**, 1776–1784 (2016).
39. Weagle, C. L. et al. Global sources of fine particulate matter: interpretation of PM2.5 chemical composition observed by SPARTAN using a global chemical transport model. *Environ. Sci. Technol.* **52**, 11670–11681 (2018).
40. Lee, C. J. et al. Response of global particulate-matter-related mortality to changes in local precursor emissions. *Environ. Sci. Technol.* **49**, 4335–4344 (2015).
41. Marais, E. A. & Wiedinmyer, C. Air quality impact of diffuse and inefficient combustion emissions in Africa (DICE-Africa). *Environ. Sci. Technol.* **50**, 10739–10745 (2016).
42. Zheng, B. et al. Trends in China's anthropogenic emissions since 2010 as the consequence of clean air actions. *Atmos. Chem. Phys.* **18**, 14095–14111 (2018).
43. Hammer, M. S. et al. Global estimates and long-term trends of fine particulate matter concentrations (1998–2018). *Environ. Sci. Technol.* <https://doi.org/10.1021/acs.est.0c01764> (2020).
44. Burnett, R. et al. Global estimates of mortality associated with long-term exposure to outdoor fine particulate matter. *Proc. Natl Acad. Sci. USA* **115**, 9592 (2018).
45. GBD 2017 Risk Factor Collaborators. Global, regional, and national comparative risk assessment of 84 behavioural, environmental and occupational, and metabolic risks or clusters of risks for 195 countries and territories, 1990–2017: a systematic analysis for the Global Burden of Disease Study 2017. *Lancet* **392**, 1923–1994 (2018).
46. Bey, I. et al. Global modeling of tropospheric chemistry with assimilated meteorology: model description and evaluation. *J. Geophys. Res. Atmos.* **106**, 23073–23095 (2001).
47. Shaddick, G. et al. Data integration for the assessment of population exposure to ambient air pollution for global burden of disease assessment. *Environ. Sci. Technol.* **52**, 9069–9078 (2018).
48. Shaddick, G. et al. Data integration model for air quality: a hierarchical approach to the global estimation of exposures to ambient air pollution. *J. R. Stat. Soc. C-Appl.* **67**, 231–253 (2018).
49. Global Burden of Disease Collaborative Network. Global Burden of Disease Study 2019 (GBD 2019) Particulate Matter Risk Curves. (Seattle, United States of America: Institute for Health Metrics and Evaluation (IHME)), <https://doi.org/10.6069/KHWH-2703> (2021).
50. Pappin Amanda, J. et al. Examining the shape of the association between low levels of fine particulate matter and mortality across three cycles of the Canadian census health and environment cohort. *Environ. Health Perspectives* <https://doi.org/10.1289/EHP5204> (2019).
51. Angel, S. et al. (New York: New York University, Nairobi: UN-Habitat, and Cambridge, MA: Lincoln Institute of Land Policy, 2016).
52. United Nations. 2018 Revision of the World Urbanization Prospects. <https://population.un.org/wup/>
53. Shindell, D. & Smith, C. J. Climate and air-quality benefits of a realistic phase-out of fossil fuels. *Nature* **573**, 408–411 (2019).
54. Vohra, K. et al. Global mortality from outdoor fine particle pollution generated by fossil fuel combustion: results from GEOS-Chem. *Environ. Res.* **195**, 110754 (2021).
55. Grieshop, A. P., Marshall, J. D. & Kandlikar, M. Health and climate benefits of cookstove replacement options. *Energy Policy* **39**, 7530–7542 (2011).
56. Butt, E. W. et al. The impact of residential combustion emissions on atmospheric aerosol, human health, and climate. *Atmos. Chem. Phys.* **16**, 873–905 (2016).
57. Pozzer, A., Tsimpidi, A. P., Karydis, V. A., de Meij, A. & Lelieveld, J. Impact of agricultural emission reductions on fine-particulate matter and public health. *Atmos. Chem. Phys.* **17**, 12813–12826 (2017).
58. Sofiev, M. et al. Cleaner fuels for ships provide public health benefits with climate tradeoffs. *Nat. Commun.* **9**, 406 (2018).
59. Jolly, W. M. et al. Climate-induced variations in global wildfire danger from 1979 to 2013. *Nat. Commun.* **6**, 7537 (2015).
60. Achakulwisut, P., Brauer, M., Hystad, P. & Anenberg, S. C. Global, national, and urban burdens of paediatric asthma incidence attributable to ambient NO<sub>2</sub> pollution: estimates from global datasets. *Lancet Planet. Health* **3**, e166–e178 (2019).
61. Querol, X. et al. Monitoring the impact of desert dust outbreaks for air quality for health studies. *Environ. Int.* **130**, 104867 (2019).
62. U.S. EPA. (U.S. Environmental Protection Agency, Washington, DC, EPA/60/R-19/188, 2019).
63. WHO. Review of evidence on health aspects of air pollution - REVIHAAP. <https://www.euro.who.int/en/health-topics/environment-and-health/air-quality/publications/2013/review-of-evidence-on-health-aspects-of-air-pollution-revihaap-project-final-technical-report> (2013).
64. Lin, J. et al. Carbon and health implications of trade restrictions. *Nat. Commun.* **10**, 4947 (2019).
65. IHME. <http://ghdx.healthdata.org/gbd-results-tool> (2020).
66. Blencowe, H. et al. National, regional, and worldwide estimates of low birthweight in 2015, with trends from 2000: a systematic analysis. *Lancet Glob. Health* **7**, e849–e860 (2019).
67. Chawanpaiboon, S. et al. Global, regional, and national estimates of levels of preterm birth in 2014: a systematic review and modelling analysis. *Lancet Glob. Health* **7**, e37–e46 (2019).
68. van der Werf, G. R. et al. Global fire emissions estimates during 1997–2016. *Earth Syst. Sci. Data* **9**, 697–720 (2017).
69. Philip, S. et al. Anthropogenic fugitive, combustion and industrial dust is a significant, underrepresented fine particulate matter source in global atmospheric models. *Environ. Res. Lett.* **12**, 044018 (2017).
70. Heald, C. L. et al. Atmospheric ammonia and particulate inorganic nitrogen over the United States. *Atmos. Chem. Phys.* **12**, 10295–10312 (2012).

## Acknowledgements

The research described in the article was conducted under contract (Grant Agreement: #4965/19-1) to the Health Effects Institute (HEI), an organization jointly funded by the U.S. Environmental Protection Agency (EPA; Assistance Award No. R-82811201) and certain motor vehicle engine manufacturers. The contents of this article do not

necessarily reflect the views of the HEI or its sponsors, nor do they necessarily reflect the views and policies of the EPA or motor vehicle and engine manufacturers. We would like to thank Chi Li, Jun Meng, Crystal Weagle, Brian Boys, and Colin Lee for support during the development of the GEOS-Chem simulations and analysis scripts.

### Author contributions

M.B., R.V.M., and E.E.M. conceived the project. E.E.M. developed and conducted the model simulations and model analysis scripts, with computing support from L.B.. E.E.M. conducted the disease burden analysis, as directed by M.B. and J.V.S., with contributions from R.B., M.S.H. and A.v.D. provided high-resolution satellite-derived PM<sub>2.5</sub> exposure estimates. J.L. and J.A.A. provided compiled observations of PM<sub>2.5</sub> chemical components from China. E.E.M., S.J.S., and P.O. contributed to the development of the CEDS<sub>GBD-MAPS</sub> dataset. V.S., L.J., G.L., and F.Y. supported the update of the GEOS-Chem model. E.E.M., M.B., and R.V.M. wrote the manuscript with contributions from all co-authors.

### Competing interests

The authors declare no competing interests.

### Additional information

**Supplementary information** The online version contains supplementary material available at <https://doi.org/10.1038/s41467-021-23853-y>.

**Correspondence** and requests for materials should be addressed to E.E.M.

**Peer review information** *Nature Communications* thanks Hao Guo, Stefan Reis, and the other, anonymous, reviewer(s) for their contribution to the peer review of this work. Peer reviewer reports are available.

**Reprints and permission information** is available at <http://www.nature.com/reprints>

**Publisher's note** Springer Nature remains neutral with regard to jurisdictional claims in published maps and institutional affiliations.



**Open Access** This article is licensed under a Creative Commons Attribution 4.0 International License, which permits use, sharing, adaptation, distribution and reproduction in any medium or format, as long as you give appropriate credit to the original author(s) and the source, provide a link to the Creative Commons license, and indicate if changes were made. The images or other third party material in this article are included in the article's Creative Commons license, unless indicated otherwise in a credit line to the material. If material is not included in the article's Creative Commons license and your intended use is not permitted by statutory regulation or exceeds the permitted use, you will need to obtain permission directly from the copyright holder. To view a copy of this license, visit <http://creativecommons.org/licenses/by/4.0/>.

© The Author(s) 2021

## Supplementary Information for

### Source Sector and Fuel Contributions to Ambient PM<sub>2.5</sub> and Attributable Mortality Across Multiple Spatial Scales

Erin E. McDuffie<sup>1,2\*</sup>, Randall V. Martin<sup>1,2</sup>, Joseph V. Spadaro<sup>3</sup>, Richard Burnett<sup>4</sup>, Steven J. Smith<sup>5</sup>, Patrick O'Rourke<sup>5</sup>, Melanie Hammer<sup>1,2</sup>, Aaron van Donkelaar<sup>2,1</sup>, Liam Bindle<sup>1,2</sup>, Viral Shah<sup>6†</sup>, Lyatt Jaeglé<sup>6</sup>, Gan Luo<sup>7</sup>, Fangqun Yu<sup>7</sup>, Jamiu Adeniran<sup>8</sup>, Jintai Lin<sup>8</sup>, Michael Brauer<sup>9,4</sup>

<sup>1</sup>Department of Energy, Environmental, and Chemical Engineering, Washington University in St. Louis, St. Louis, MO, USA

<sup>2</sup>Department of Physics and Atmospheric Science, Dalhousie University, Halifax, NS, Canada

<sup>3</sup>Spadaro Environmental Research Consultants (SERC)

<sup>4</sup>Institute for Health Metrics and Evaluation, University of Washington, Seattle, WA, USA

<sup>5</sup>Joint Global Change Research Institute, Pacific Northwest National Laboratory, College Park, MD, USA

<sup>6</sup>Department of Atmospheric Sciences, University of Washington, Seattle, WA, USA

<sup>7</sup>Atmospheric Sciences Research Center, University at Albany, Albany, New York, USA

<sup>8</sup>Laboratory for Climate and Ocean-Atmosphere Studies, School of Physics, Peking University, Beijing, China

<sup>9</sup>School of Population and Public Health, University of British Columbia, Vancouver, BC, Canada

<sup>†</sup>Now at: Harvard John A. Paulson School of Engineering and Applied Sciences, Harvard University, Cambridge, MA, USA

Corresponding Author: Erin E. McDuffie

Email: [erin.mcduffie@wustl.edu](mailto:erin.mcduffie@wustl.edu)

#### **This file includes:**

Supplementary Text 1 to 10

Supplementary Figures 1 to 10

Supplementary Tables 1 to 2

#### **Other Supplementary Information for this manuscript include:**

Supplementary Data 1-3

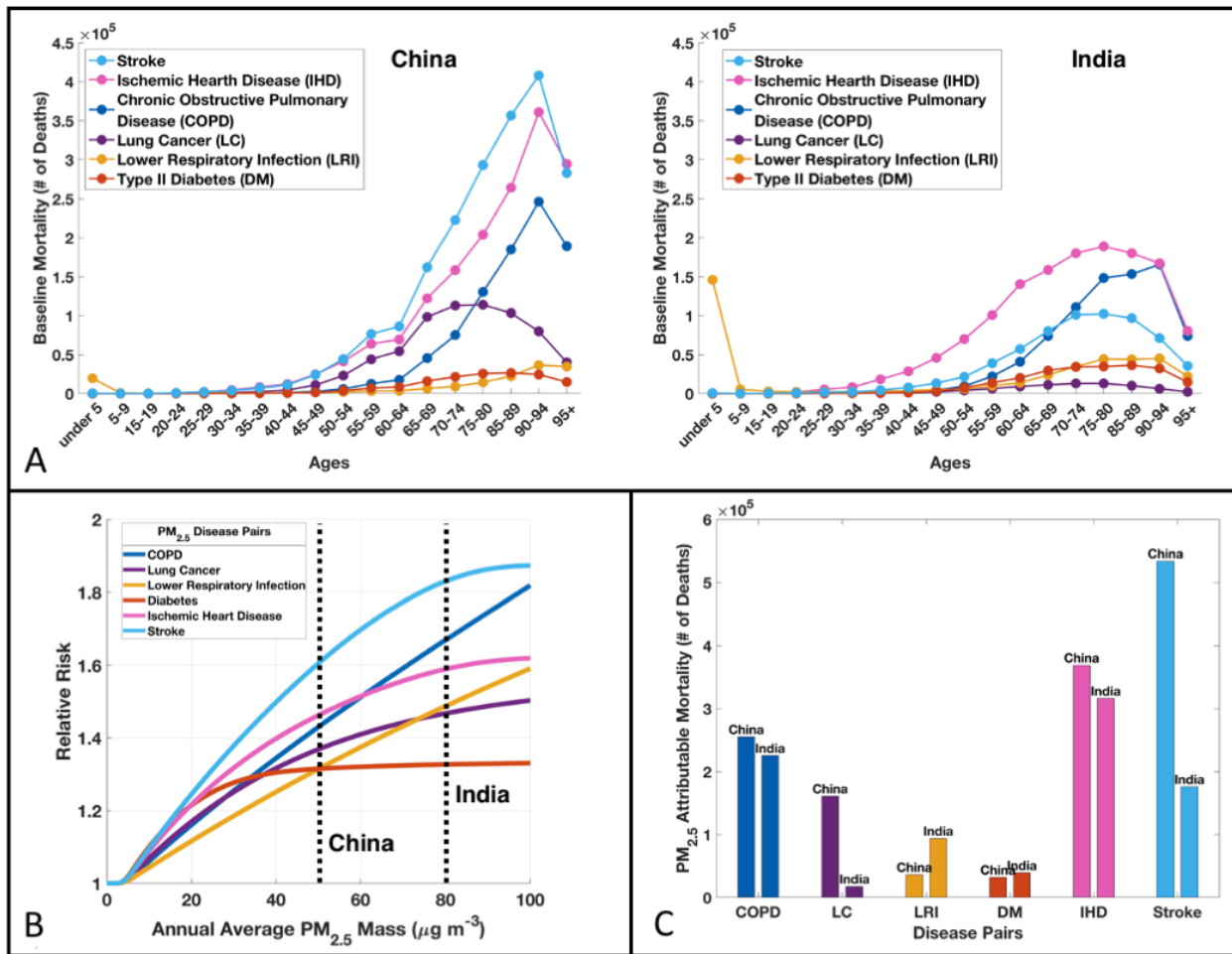
## Additional Supporting Tables and Figures

This supplementary information file describes the details of the analysis configuration. A key objective of including these details is to promote transparency and reproducibility. In this work, world countries and regions follow those used in the Global Burden of Disease (GBD) Project, as shown in Supplementary Table 1.

**Supplementary Table 1. Member countries and territories of the 21 GBD world regions.**

GBD Region	Member Countries			
<b>Asia Pacific, High Income</b>	Brunei Darussalam	Japan	South Korea	Singapore
<b>Asia, Central</b>	Armenia	Azerbaijan	Georgia	Kazakhstan
	Kyrgyzstan	Mongolia	Tajikistan	Turkmenistan
	Uzbekistan			
<b>Asia, East</b>	China	Taiwan (Province of China)		
	North Korea (Democratic People's Republic of Korea)			
<b>Asia, South</b>	Bangladesh	Bhutan	India	Nepal
	Pakistan			
<b>Asia, Southeast</b>	Cambodia	Indonesia	Malaysia	Maldives
	Mauritius	Myanmar	Philippines	Sri Lanka
	Seychelles	Thailand	Timor-Leste	Vietnam
	Laos (Loa People's Democratic Republic)			
<b>Oceania</b>	American Samoa	Cook Islands	Fiji	Guam
	Kiribati	Marshall Islands	Nauru	Niue
	Palau	Papua New Guinea	Samoa	Solomon Islands
	Tokelau	Tonga	Tuvalu	Vanuatu
	Federated States of Micronesia		Northern Mariana Islands	
<b>Australasia</b>	Australia	New Zealand		
<b>Caribbean</b>	The Bahamas	Barbados	Belize	Bermuda
	Cuba	Dominica	Dominican Republic	Grenada
	Guyana	Haiti	Jamaica	Puerto Rico
	Saint Lucia	Suriname	Antigua and Barbuda	Saint Kitts and Nevis
	Trinidad and Tobago	US Virgin Islands	Saint Vincent and the Grenadines	
<b>Europe, Central</b>	Albania	Bulgaria	Croatia	Czech Republic (Czechia)
	Hungary	North Macedonia	Montenegro	Poland
	Romania	Serbia	Slovakia	Slovenia
	Bosnia and Herzegovina			
<b>Europe, Eastern</b>	Belarus	Estonia	Latvia	Lithuania
	Republic of Moldova	Russian Federation	Ukraine	
<b>Europe, Western</b>	Andorra	Austria	Belgium	Cyprus
	Denmark	Finland	France	Germany
	Greece	Iceland	Ireland	Israel
	Italy	Luxembourg	Malta	Monaco
	Netherlands	Norway	Portugal	San Marino
	Spain	Sweden	Switzerland	United Kingdom
<b>North America, High Income</b>	Canada	Greenland	United States	
<b>Latin America, Andean</b>	Bolivia (Plurinational State of)		Ecuador	Peru
<b>Latin America, Central</b>	Colombia	Costa Rica	El Salvador	Guatemala
	Honduras	Mexico	Nicaragua	Panama
	Venezuela (Bolivarian Republic of)			
<b>Latin America, Southern</b>	Argentina	Chile	Uruguay	
<b>Latin America, Tropical</b>	Brazil	Paraguay		
<b>North Africa / Middle East</b>	Afghanistan	Algeria	Bahrain	Egypt
	Iraq	Jordan	Kuwait	Lebanon
	Libya	Morocco	Palestine	Oman
	Qatar	Saudi Arabia	Sudan	Syrian Arab Republic
	Tunisia	Turkey	Yemen	United Arab Emirates
	Iran (Islamic Republic of)			

<b>Sub-Saharan Africa, Central</b>	Angola Central African Republic	Congo Democratic Republic of the Congo	Equatorial Guinea	Gabon
<b>Sub-Saharan Africa, Eastern</b>	Burundi Ethiopia Mozambique Uganda	Comoros Kenya Rwanda Zambia	Djibouti Madagascar Somalia United Republic of Tanzania	Eritrea Malawi South Sudan
<b>Sub-Saharan Africa, South</b>	Botswana Eswatini	Lesotho Zimbabwe	Namibia	South Africa
<b>Sub-Saharan Africa, Western</b>	Benin Chad Guinea Mauritania Sierra Leone	Burkina Faso Cote d'Ivoire Guinea-Bissau Niger Togo	Cameroon The Gambia Liberia Nigeria Sao Tome and Principe	Cape Verde Ghana Mali Senegal



**Supplementary Figure 1. PM<sub>2.5</sub> Disease Burden Comparison for India and China.** (A) GBD2019 background baseline mortality data as a function of population age and disease. (B) GBD2019 concentration response functions (same as Supplementary Figure 2), with dashed lines showing population weighted mean PM<sub>2.5</sub> concentrations for China and India. (C) Total PM<sub>2.5</sub> attributable deaths in China and India as a function of disease.

### **Supplementary Text 1. 2019 Exposure Estimates – Additional Details**

Following the downscaling procedure described in the Methods (and Supplementary Text 9), we apply high-resolution (gridded at  $\sim 1 \text{ km} \times \sim 1 \text{ km}$ ) exposure estimates for the year 2019 (weighted by 2019 gridded population<sup>1</sup>) to the GBD2019 CRFs with 2019 baseline mortality data to assess changes in the estimated disease burden between 2017 and 2019. Disease burden estimates are independent from model emission sensitivity simulations and do not require changes or projections in emissions. In both years, the same nine countries were estimated to have largest number of PM<sub>2.5</sub> attributable deaths, though the annual number of deaths in each country was larger in 2019 than 2017, except for in Russia. Similarly, annual population-weighted mean (PWM) PM<sub>2.5</sub> concentrations also increased in each of these top nine countries, except for in China and the United States. The complex relationship between annual national PM<sub>2.5</sub> concentrations and resulting attributable deaths highlights the importance of multiple factors in disease burden estimations. For neonatal disorders, the incidence associated with outdoor PM<sub>2.5</sub> exposure totaled to 2.07 (95% CI: 0.02-5.02) million worldwide, which increased marginally to 2.09 (95% CI: 0.02-5.06) million in 2019. At the sub-national level, the top four of the 200 select areas with the highest PM<sub>2.5</sub> concentrations (Singrauli, Kanpur, Sitapur, and Ahmedabad, India) all experienced increases in PWM PM<sub>2.5</sub> mass, persisting at levels between 14 and 16 times greater than the WHO annual average guidelines. Of the 200 sub-national areas, 45% experienced no change or an increase in PWM PM<sub>2.5</sub> concentration between 2017 and 2019. The area surrounding Pune, India had the largest absolute increase from 57 to 63.2  $\mu\text{g m}^{-3}$ , while the area surrounding Xingping, China had the largest absolute decrease from 68.4 to 60.1  $\mu\text{g m}^{-3}$ . These changes serve to identify potential locations with effective mitigation strategies or those locations with the most to gain from pollution reductions. Supplementary Data 3 provides the PWM values for the global area, each of the 21 world regions, 204 countries, and 200 sub-national areas.

### **Supplementary Text 2. GEMM Sensitivity Study – Additional Details**

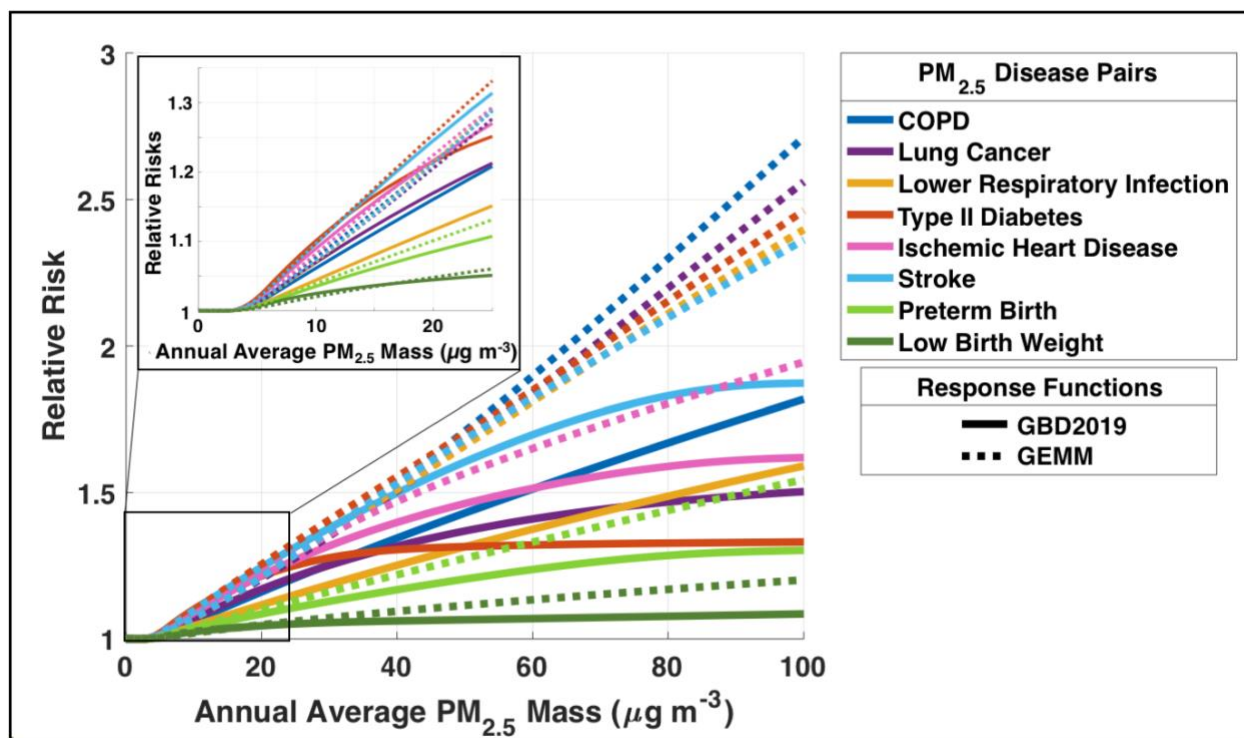
As an alternative to the GBD estimates, previous global studies have used the GEMM. The GEMM exclusively incorporates risk information from cohort studies of outdoor air pollution (41 cohorts from 16 countries)<sup>2</sup> on non-accidental mortality and was highly sensitive to one particular cohort of Chinese men<sup>3</sup> in the original version. Another feature of the GEMM is that



its non-accidental mortality estimate suggests a larger impact of PM<sub>2.5</sub> exposure on mortality than the sum of cause-specific attributable mortality estimates. As new evidence on links between PM<sub>2.5</sub> and other (e.g., chronic kidney disease, dementia) causes of death emerge, this difference between cause-specific and all-cause (non-accidental) attributable mortality will decrease.

Application of the GEMM-based disease-specific estimates to the disease burden, however, should also be employed with caution. As further discussed in Hystad, et al.<sup>4</sup> the GEMM is based on analyses of non-accidental mortality primarily derived from epidemiologic studies conducted in high-income countries. When applied to disease burden estimates, this assumes similar distributions of causes of death, including the relative proportion of the specific diseases linked to air pollution and the population age distribution in high-income countries as in low and middle-income countries. This leads to uncertainty since the relative frequencies of the various causes of deaths differ markedly between countries of the world. In particular, application to Africa and South Asia is likely to lead to substantial uncertainty. As the GBD2019 CRFs are derived directly from studies of specific diseases, they can be more reliably applied to disease-specific mortality rates across countries. Other sources of uncertainty such as the assumptions of equitoxicity, variation in e.g., healthcare access and quality and population characteristics, and extrapolation to concentrations beyond those included in epidemiologic studies are common to the application of both the GBD2019 CRFs and the GEMM.

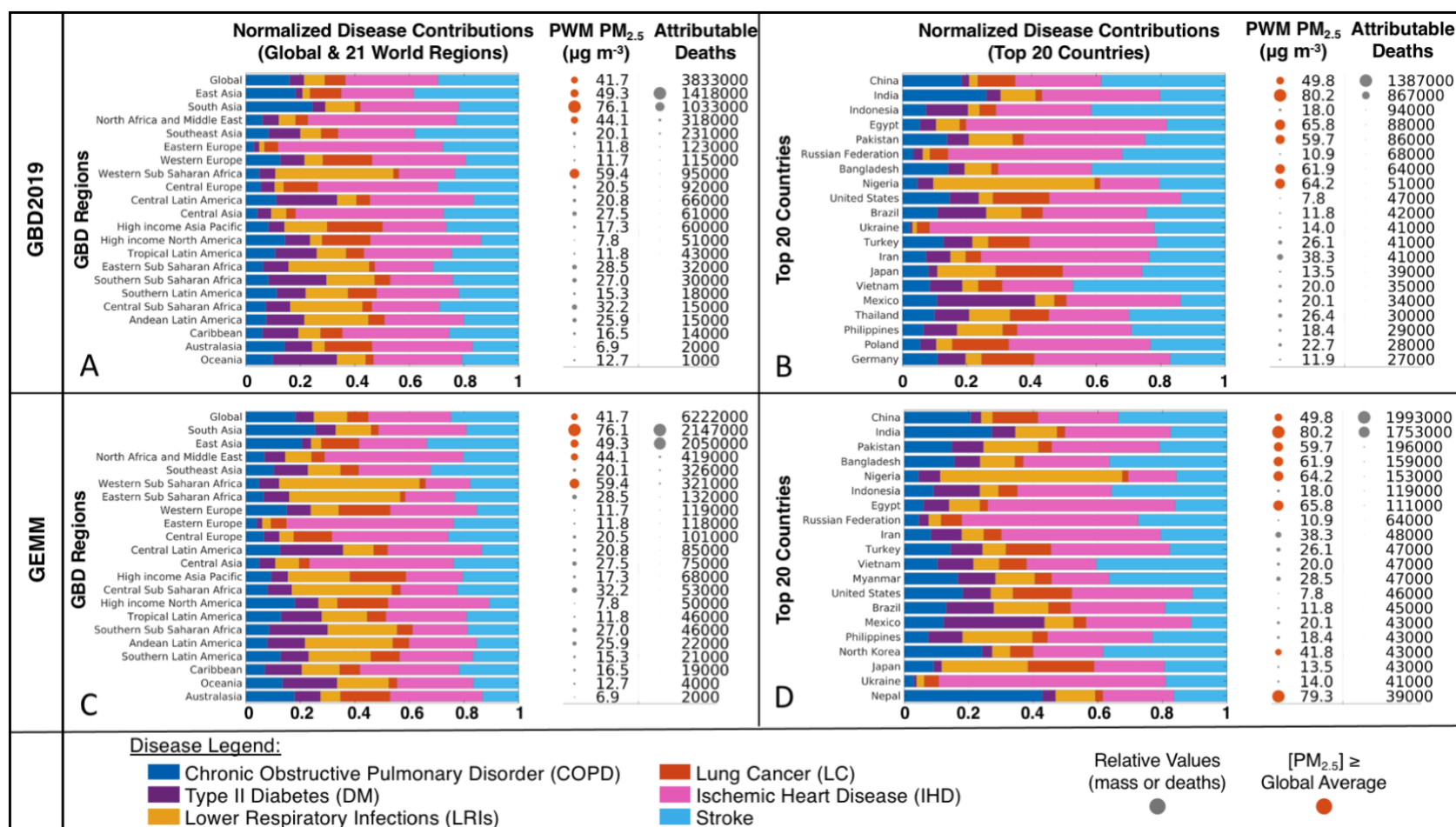
To address some of these uncertainties, the GEMM CRFs in this work were updated as described in the Methods to include the same ambient PM cohort studies that are inputs to the GBD2019 CRFs and to add functions for diabetes and reproductive outcomes. Supplementary Figure 2 compares the disease-specific CRFs for the GBD2019 and updated GEMM. With these updates, and when restricted to the five NCDs +LRI that are included in the GBD2019 CRFs, 2017 global GEMM attributable mortality estimates were lower than previous GEMM estimates for 2015 when only the four NCDs +LRI were included (6.2 million vs 6.9 million)<sup>2</sup>. Globally, the updated GEMM CRFs estimated a PM<sub>2.5</sub> attributable burden of 6.2 (95% CI: 4.4 to 7.8) million deaths in 2017. While satellite-based estimates have shown a recent decreasing trend in PWM PM<sub>2.5</sub> mass across East Asia, Europe, and the Eastern U.S.<sup>5</sup>, a detailed analysis of differences (temporal trends vs. methodological differences) between the original and updated GEMM estimates is outside the scope of this work.



**Supplementary Figure 2. Concentration response functions for the GBD2019 and updated GEMM. Solid Lines:** GBD2019 CRFs, **Dashed Lines:** updated GEMM. Line colors correspond to the central values of eight disease-response pairs. For illustrative purposes, response curves for IHD and Stroke correspond to the 60-64 age group, COPD, LC, and DM responses are for all ages over 25 years, and LRIs are for ages under 5 years and greater than 25 years. Preterm births are at a gestational age less than 37 weeks (PTB) and weights below 2.5 kg (LBW). For illustrative purposes, the insert highlights the relative risks at exposure levels less than  $25 \mu\text{g m}^{-3}$ .

Supplementary Figure 3 shows the relative disease-specific contributions from both the updated GEMM and GBD2019 CFRs for 21 world regions (A, C), and the top 20 countries with the largest number of attributable deaths (B, D). S1-Fig. 2 shows that the relative disease contributions predicted by the updated GEMM were similar to those from the GBD2019 CRFs. For example, both predict that the largest number of attributable deaths at the global scale were from IHD, and then in decreasing order from Stroke, COPD, LRI, LC, and DM. The absolute number of attributable deaths, however, were nearly always larger from the GEMM (Supplementary Data 1). Two exceptions were for North America and Australasia. These regions had the lowest PWM  $\text{PM}_{2.5}$  concentrations and the difference in relative predictions reflect the lower relative risks for IHD, Stroke, and Diabetes in the updated GEMM at  $\text{PM}_{2.5}$  concentrations below  $10 \mu\text{g m}^{-3}$  (Supplementary Figure 2). As a result of these and other differences in the CRFs, the GEMM and GBD2019 CRFs also predicted different relative

rankings of the top 20 countries. Supplementary Figure 3b and d show that both the GBD2019 CRFs and GEMM predicted the same top two countries (China and India), but that the relative rankings for the next 18 countries differ. In addition to ranking differences, the GBD2019 CRFs also included Thailand (16<sup>th</sup>), Poland (19<sup>th</sup>), and Germany (20<sup>th</sup>) in the top 20 countries, while the GEMM alternatively predicted that Myanmar (12<sup>th</sup>), North Korea (17<sup>th</sup>), and Nepal (20<sup>th</sup>) ranked in the top 20. This comparison closes a portion of the gap between previous GEMM and GBD disease burden results, however, the accuracy of both estimates are dependent on the availability of robust and high-resolution exposure data, particularly in high exposure areas.



**Supplementary Figure 3: Normalized disease contributions to total attributable mortality in 2017 for 21 world regions (A, C) and 20 countries (B, D) with the highest outdoor PM<sub>2.5</sub> disease burden.** Panels show results estimated using the GBD2019 CRFs (A, B) and the updated GEMM (C, D). Bar charts show the relative contributions of six PM<sub>2.5</sub>-disease pairs to regional and national-level outdoor PM<sub>2.5</sub> attributable deaths, sorted by decreasing number of deaths. The number of LBW and PTB incidences are included in Supplementary Data 1. PWM PM<sub>2.5</sub> concentrations and number of attributable deaths are additionally provided for each region/country. Relative amounts are illustrated by relative dot sizes (except for the global total disease burden). Red dots indicate regions/countries with PM<sub>2.5</sub> exposure levels equivalent or larger than the global average.

### Supplementary Text 3. Global Model Details

PM<sub>2.5</sub> source sensitivity simulations for the year 2017 are shown in Supplementary Table 2 and are conducted with the GEOS-Chem 3D atmospheric chemical transport model<sup>6</sup>. The GEOS-Chem model solves for the evolution of atmospheric aerosols and gases using meteorological data, global and regional emission inventories, and algorithms that represent the physics and chemistry of atmospheric processes. Global simulations are conducted from December 2016 to January 2018 (1-month spin-up) at 2°×2.5° horizontal resolution and 47 vertical layers. Global simulations are supplemented with three additional one-way nested simulations at 0.5°×0.625° horizontal resolution that cover North America (10° N – 70° N, 140° W – 40° W), Europe (30° N – 70° N, 30° W – 50° E), and China and Southeast Asia (11° S – 55° N, 60° E – 150° E)<sup>7</sup>. Each simulation is driven by assimilated meteorological data from the Goddard Earth Observing System from the NASA Global Modeling and Assimilation Office (GMAO). We use the MERRA-2 historical reanalysis product, archived at a 3-hour temporal resolution for 3D fields and 1-hour for 2D fields. The transport and chemistry timesteps are set to 10 and 20 minutes respectively, to optimize simulation accuracy and computational efficiency<sup>8</sup>.

In this work, we use the GEOS-Chem ‘tropchem’ chemical mechanism that includes coupled aerosol-oxidant chemistry in the troposphere and stratosphere. The gas-phase mechanism includes detailed HO<sub>x</sub>-NO<sub>x</sub>-VOC-ozone chemistry<sup>6</sup>, coupled to aerosol chemistry for inorganic sulfate-nitrate-ammonium aerosol<sup>9,10</sup>, as well as carbonaceous (black and organic carbon) aerosol<sup>10,11</sup>, sea salt<sup>12</sup>, and dust<sup>13,14</sup>. Relative humidity dependent aerosol size distributions and optical properties are based on the Global Aerosol Data Set<sup>15,16</sup>, with updates for organics and secondary inorganics from observations<sup>17,18</sup>, mineral dust<sup>14,19,20</sup>, and absorbing brown carbon<sup>21</sup>. Aerosol thermodynamic partitioning between sulfate-nitrate-ammonium is computed with the ISORORPIA II thermodynamic model<sup>22</sup>, while the BC mechanism is described by Wang, et al. <sup>10</sup>. We use the simple, irreversible, direct yield scheme for secondary organic aerosol (SOA) from Kim, et al. <sup>11</sup>, as this mechanism has been shown to better reproduce available observations of global organic aerosol mass relative to the more complex scheme<sup>23</sup>. For physical processes, GEOS-Chem uses the TPCORE advection algorithm<sup>24</sup> and computes convective transport from the convective mass fluxes in the meteorological data, as described by Wu, et al. <sup>25</sup>. In this work, boundary layer mixing uses the non-local mixing scheme as implemented by Lin and McElroy <sup>26</sup>.

The core source code for this work is GEOS-Chem v12.1.0<sup>27</sup>, released Nov. 2018. To correct a long-standing bias in nitrate aerosol concentrations<sup>28,29</sup>, the v12.1.0 source code has been updated here as part of the Global Burden of Disease – Major Air Pollution Sources project (<https://sites.wustl.edu/acag/datasets/gbd-maps/>). The code is available on GitHub: [https://github.com/emcduffie/GC\\_v12.1.0\\_EEM](https://github.com/emcduffie/GC_v12.1.0_EEM). Major updates follow literature recommendations and include an updated parameterization for the heterogeneous uptake of N<sub>2</sub>O<sub>5</sub> from McDuffie, et al.<sup>30</sup>, the added heterogeneous production of ClNO<sub>2</sub> following Shah, et al.<sup>31</sup> and recommended ClNO<sub>2</sub> yield reductions from McDuffie, et al.<sup>32</sup>, a reduction in the deposition of HNO<sub>3</sub> under cold conditions following Shah, et al.<sup>31</sup>, as well as an update to the wet deposition scheme following recommendations in Luo, et al.<sup>29</sup>. In addition to the updates described in Luo, et al.<sup>29</sup>, the rate of SO<sub>2</sub> removal in clouds is also reduced, and the rainout efficiencies for hydrophilic OC and BC species are reduced by 50% following recent recommendations<sup>33</sup>. These and additional minor code updates are described in the GitHub README file.

To evaluate the impact of these model updates, Supplementary Figure 5b shows a bar chart of the normalized mean bias (NMB) in the simulated global annual averages of aerosol nitrate, sulfate, ammonium, total organic carbon, black carbon, fine dust, and sea salt in the default v12.1.0 GEOS-Chem source code and the updated model, compared to annual average observations (described in Supplementary Text 4). As shown in Supplementary Figure 5b, the mechanistic model updates described above reduce the NMB in the updated GEOS-Chem simulated concentrations of aerosol nitrate from 2 µg/m<sup>3</sup> to 0.5 µg/m<sup>3</sup> relative to observed values. Model updates additionally improve the model-observation agreement of ammonium, black carbon, and dust compared to the default model. In contrast, the negative bias in sea salt is enhanced in the updated base simulation relative to the default source code. The annual PWM mass concentrations of each observed compound are additionally provided in Supplementary Figure 5b (gridded population from the Gridded Population of the World Database<sup>1</sup>). These indicate that the smallest model NMB's are found for the compounds that contribute to the largest fraction of total PM<sub>2.5</sub> mass. As further shown in the right panel of Supplementary Figure 5b, there is general agreement in the fractional contributions of each chemical compound to total PM<sub>2.5</sub> mass, providing confidence in the model's ability to accurately predict changes in the chemical production of PM<sub>2.5</sub> under various emission sensitivity simulations.

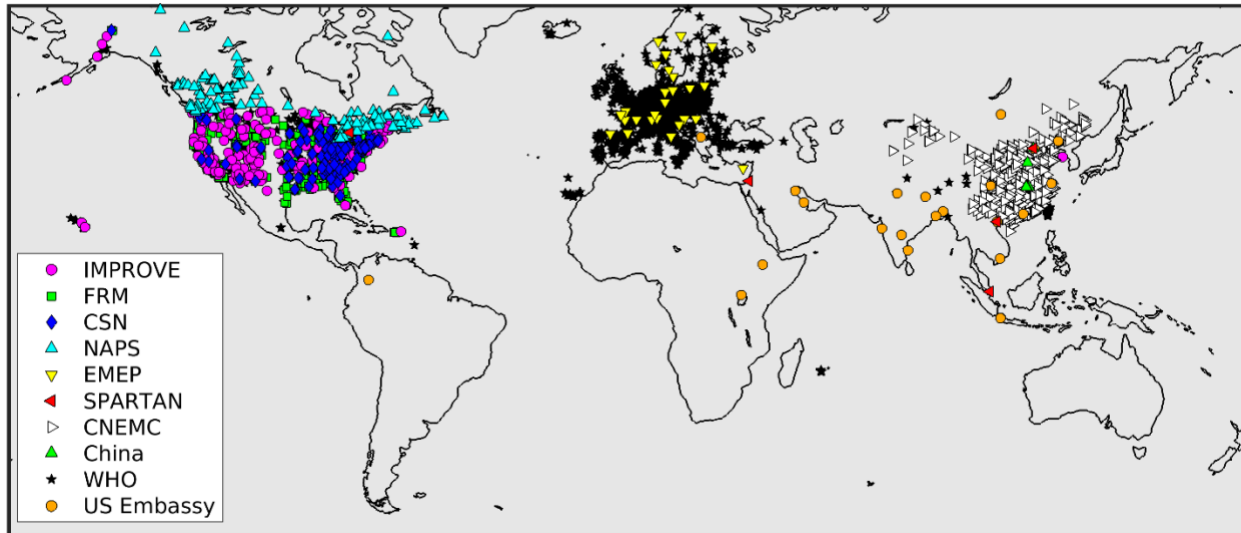
Lastly, total PM<sub>2.5</sub> mass concentrations are calculated using modeled output mass concentrations of aerosol nitrate (NO<sub>3</sub><sup>-</sup>), sulfate (SO<sub>4</sub><sup>2-</sup>), ammonium (NH<sub>4</sub><sup>+</sup>), sea salt, dust, organic mass, and black carbon, as described in the analysis scripts package (<https://github.com/emcduffie/GBD-MAPS-Global>). In this work, spatially gridded annual total PM<sub>2.5</sub> mass concentrations are calculated by averaging monthly PM<sub>2.5</sub> concentrations. National-level PM<sub>2.5</sub> concentrations are averaged over the grid cells within each country's geographical borders.

#### **Supplementary Text 4. Observational PM<sub>2.5</sub> Dataset for Model Evaluation**

Evaluation of base model performance is a vital component of any analyses that derives results from modeled emission sensitivity simulations. In this work, the base 2017 GEOS-Chem PM<sub>2.5</sub> simulation and downscaled PM<sub>2.5</sub> exposure estimates (Fig. 1) are evaluated against a dataset of annual-average surface observations of total PM<sub>2.5</sub> mass and PM<sub>2.5</sub> chemical composition (where available). This section describes methods used to develop this observational dataset.

Supplementary Figure 4 provides a map of the individual measurement sites in this dataset, colored by their measurement networks. More extensive sampling and analysis details are reported from the North American networks than those from other regions, which have larger uncertainties due to a lack of consistent reporting on sampling and analysis protocols (particularly for EMEP and WHO datasets). Based on available reported metadata, some networks also provide mass concentrations derived from multiple sampling and analysis methods. Here we attempt to reduce sampling differences by selecting for consistent analysis methods between sites and networks when this information is available (described in detail below). Observational data also include uncertainties in the amount of aerosol water assumed in the gravimetric analysis of PM<sub>2.5</sub> and degree of volatilization of PM<sub>2.5</sub> and its chemical components (particularly ammonium nitrate and organics) during sampling and/or filter transport. Uncertainties in these observational datasets should be considered when comparing to modeled results.

## 2017 PM<sub>2.5</sub> Surface Observation Network Sites

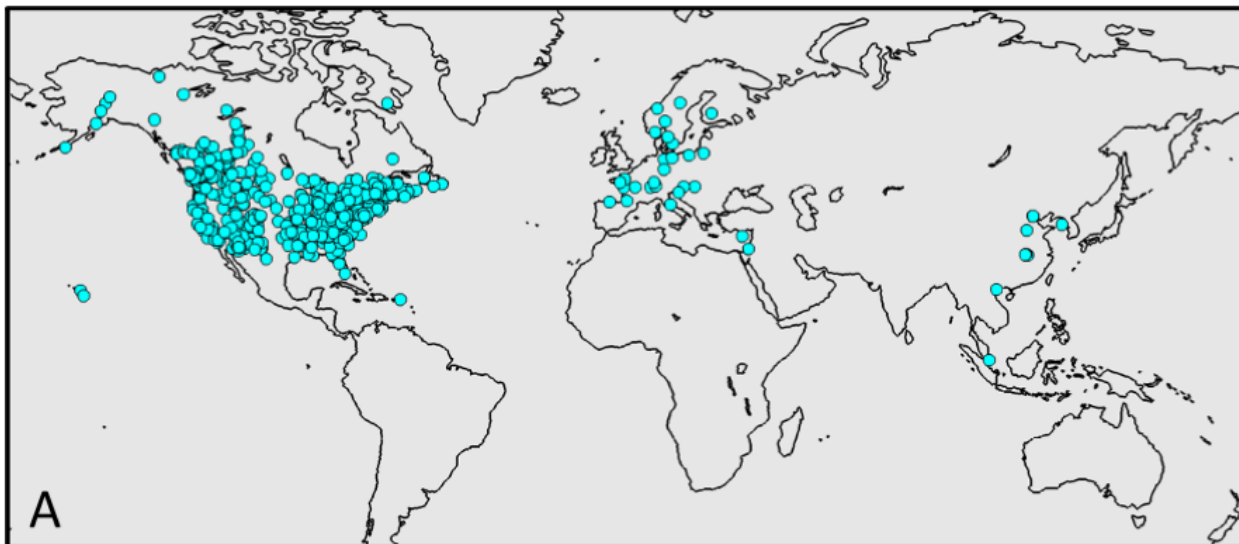


**Supplementary Figure 4: Map of 2017 long-term PM<sub>2.5</sub> sampling stations.** Symbol colors and shapes reflect individual monitoring networks. This figure includes sites that are used both for the total PM<sub>2.5</sub> mass and speciated PM<sub>2.5</sub> mass model evaluations.

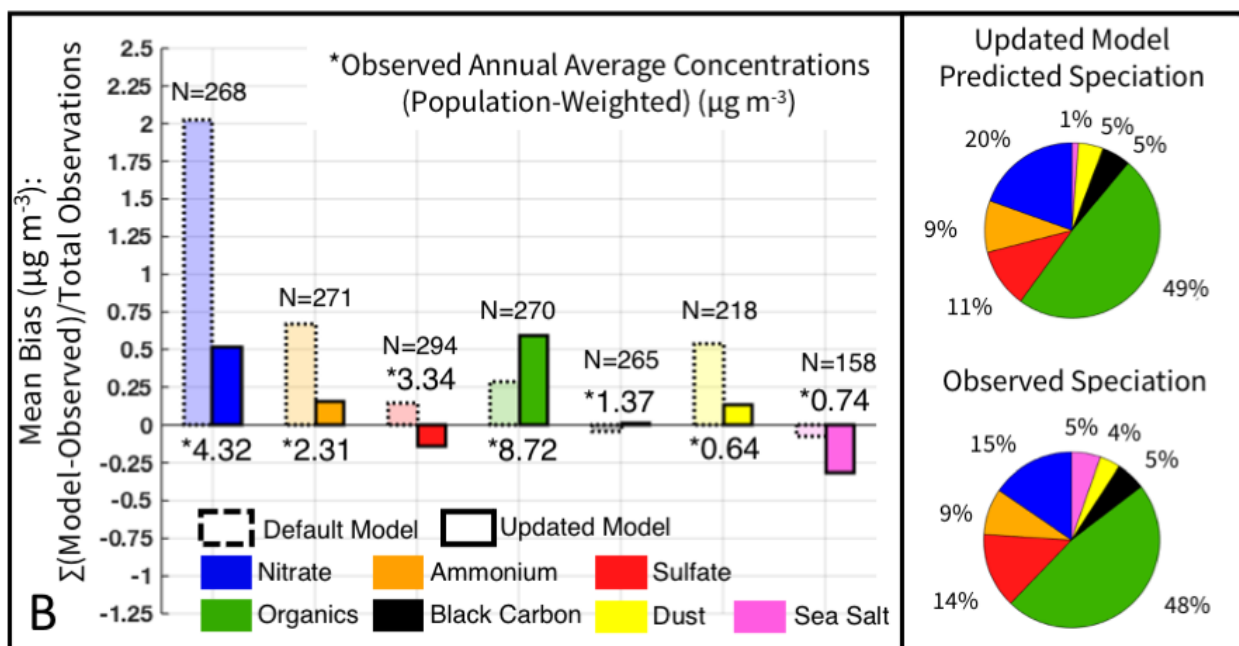
The following sub-sections describe the individual networks that provide long-term measurements of PM<sub>2.5</sub> total mass and/or PM<sub>2.5</sub> chemical components. Estimates of PM<sub>2.5</sub> chemical composition in 2017 are available for a more select number of sites than total PM<sub>2.5</sub> mass, as shown in Supplementary Figure 5a. These sites are primarily in populated regions throughout North America, Europe, select sites in China, and 5 international sites through the SPARTAN network<sup>34,35</sup>. Data from the SPARTAN network and the compiled speciated inventory for China are used for the speciated comparison in Supplementary Figure 5b and are not used in Fig. 1. Annual average values from each site are calculated from the calculated monthly averages. Dataset development details can be found in the analysis scripts package at: <https://github.com/emceduffie/GBD-MAPS-Global>.



## 2017 Long-Term PM<sub>2.5</sub> Composition Observation Sites



## 2017 Annual Simulated vs. Observed PM<sub>2.5</sub> Speciation



**Supplementary Figure 5: Evaluation of default and updated base model simulation of PM<sub>2.5</sub> chemical components.** (A) map of available long-term surface observations of PM<sub>2.5</sub> chemical components. (B) Bar plot of the normalized mean bias between the simulated and observed concentrations of individual PM<sub>2.5</sub> components (nitrate, ammonium, sulfate, organic aerosol, black carbon, dust, and sea salt). Light bars represent the values from the default v12.1.0 GEOS-Chem model. Darker bars show results from the updated model source code used here. Population-weighted average observed concentrations of each component are also provided. Pie charts illustrate the fractional distribution of PM<sub>2.5</sub> components from the updated model (top) and the observations (bottom).

### ***WHO (World Health Organization) Compilation – Global***

The World Health Organization has compiled an extensive database of annual-average surface-level PM<sub>2.5</sub> concentrations from around the world. In this work, these data are downloaded from <https://www.who.int/airpollution/data/cities/en/>. Only direct PM<sub>2.5</sub> measurements are used here, not those calculated from PM<sub>10</sub> measurements (as in the GBD exposure calibration procedure), due to uncertainties in this conversion. This dataset is filtered to only include annual average measurements from 2017 for sites that report at least 75% measurement coverage. Data sources are available in the downloaded dataset, but measurement methods and analysis techniques are not readily available for the reported observations. We assume that data are reported at 35% RH and at local temperature and pressure. Observations from other regional networks may also be included in this compiled dataset, especially over North America and Europe. To ensure that these sites are not double counted in the model evaluation, we remove sites from the WHO dataset that are within 0.1° of other network sites.

### ***US Embassy Measurements – Global***

The U.S. Department of State collects air quality monitoring data from U.S. embassies and consulates around the world and has partnered with the U.S. Environmental Protection Agency to report data at AirNow.gov. Hourly observations from Beta-Attenuation Monitors (BAMs) are available for 28 sites in 2017 (55 sites by 2020). Hourly data for each site are downloaded from: <https://www.airnow.gov/international/us-embassies-and-consulates>. In this work, hourly raw concentrations are averaged into annual values and filtered to remove sites with <75% temporal data coverage. We assume that data are reported for local conditions (ambient pressure and temperature) and 35% RH.

### ***CNEMC (China National Environmental Monitoring Centre) – China***

The government of China has facilitated the deployment of nearly 2000 sites that measure PM<sub>2.5</sub> mass and its chemical composition. At the time of this study, only total PM<sub>2.5</sub> mass concentrations were publicly available. Data can be downloaded from: <http://www.cnemc.cn/en/> and are available from May 2014 onward. Both Thermo Fisher Tapered Element Oscillating Microbalance (TEOM) 1405F analyzers and BAMs are used for continuous sampling of PM<sub>2.5</sub> mass, reported at each site at hourly time resolution. As

described in Wu, et al.<sup>36</sup>, both methods use heaters to reduce the humidity in sampled air. This heating, however, can lead to mass loss due to the volatilization of PM<sub>2.5</sub> components. As a result, previous studies have reported lower total PM<sub>2.5</sub> mass measurements from TEOM instruments relative to US Federal Reference Methods (FRM)<sup>37</sup>, largely as a result of the loss of semi-volatile compounds<sup>38</sup> and particularly in cold ambient temperatures<sup>39</sup>. To minimize this potential under-reporting, the 1405F monitoring system additionally measures concentrations in the volatilized portion of air, while a smart heater is used with the BAMs to minimize heating while also controlling the RH of the sample at 35%<sup>36</sup>. In this work, we assume that all CNEMC mass concentrations are reported at 35% RH and at local temperature and pressure, consistent with other networks. Monthly averages for January-December 2017 are then calculated for each site that reports a complete number of 24 measurements each day, for at least 20 days each month (~75% temporal coverage each month).

#### ***FRM Sites (Federal Reference Method) – United States***

FRM sites follow protocols specified in Appendix L to Part 50 of Title 40 in the United States Code of Federal Regulations (CFR) – *Reference Method for the Detection of Fine Particulate Matter as PM<sub>2.5</sub> in the Atmosphere*. These sites measure total PM<sub>2.5</sub> mass by gravimetric analysis of a Teflon collection filter. Samples are collected on a filter for a 24-hour period every 3<sup>rd</sup> day, then transported to an analysis facility where filters are allowed to equilibrate for a minimum of 24 hours prior to weighing. The temperature and RH must be controlled between 20-23°C and 30-40%, respectively during the analysis. All data are reported at local ambient conditions (pressure and temperature). For this work, FRM data were downloaded from: <http://views.cira.colostate.edu/fed/QueryWizard/>, with additional details in the analysis scripts package. Data are saved as monthly averages for all sites with at least 10 measurements during the month (8 for February).

#### ***IMPROVE (Interagency Monitoring of Protected Visual Environments) – United States***

Details about the IMPROVE network are reported elsewhere<sup>40</sup> and at <http://vista.cira.colostate.edu/Improve/>. IMPROVE sites are generally focused on rural areas and follow the same sampling procedures at each site. Briefly, each site has four measurement modules:

- 1) Teflon filter for gravimetric mass and X-ray fluorescence (XRF) analysis of trace elements
- 2) denuder + Nylon filter for anions by ion chromatography

3) Quartz filter for organic carbon by thermal optical reflectance (TOR) and calculation of elemental carbon using HIPS (Hybrid Integrating Plate and Sphere system).

4) Coarse mode sampler

Samples are collected for 24 hours, every 3<sup>rd</sup> day, after which they are transported to laboratories for analysis (without controlling for temperature or pressure). Samples are allowed to equilibrate for a few minutes prior to sampling. Data are reported at local, ambient conditions (pressure and temperature). For this work, IMPROVE data were downloaded from: <http://views.cira.colostate.edu/fed/QueryWizard/>, with additional file formatting details listed in the analysis scripts package. Data for each compound are saved as monthly averages for all sites with at least 10 daily measurements during the month (8 for February). In this work, spatially and seasonally varying OM:OC ratios are used to convert total monthly organic carbon measurements to total organic mass. Ammonium is re-constructed from sulfate and nitrate ion measurements, assuming pure ammonium nitrate and ammonium sulfate in the aerosol phase. Dust is reconstructed from trace elements assuming normal oxides in typically occurring soil dust following Supplementary Eq. 1. Sea salt is calculated as 1.8\*chloride following White <sup>41</sup>. Black carbon is taken as elemental carbon.

$$\text{Dust} = 2.2 \times \text{Al} + 2.49 \times \text{Si} + 1.63 \times \text{Ca} + 2.42 \times \text{Fe} + 1.94 \times \text{Ti} \quad (\text{S-Eq. 1})$$

#### ***CSN (Chemical Speciation Network) – United States***

Details about the CSN network are reported elsewhere<sup>42</sup>. In contrast to IMPROVE, CSN sites focus primarily on urban areas and do not use the same sampling instrumentation/methods at each site. In general, collection and analysis methods are similar to those listed for the IMPROVE network, with the analysis of some species (i.e., organic and elemental carbon) following IMPROVE protocols. Similar to IMPROVE, samples are collected for 24 hours, every 3<sup>rd</sup> day. Samples are transported overnight, held at a temperature of  $\leq 4^{\circ}\text{C}$  to minimize sample volatilization. Gravimetric analysis of PM<sub>2.5</sub> follows the FRM protocol where the samples are allowed to equilibrate for 24 hours prior to analysis and measured in a controlled clean room between 20-23°C and 30-40% RH. All data are reported at local, ambient conditions (pressure and temperature). For this work, CSN data were downloaded from: <http://views.cira.colostate.edu/fed/QueryWizard/>, with additional details in the analysis scripts package. Data for each compound are saved as monthly averages for all sites with at least 10 daily measurements during the month (8 for February). The final calculation of

organic mass, black carbon, sea salt, and dust follow the procedures used for IMPROVE data, described above.

### ***NAPS (National Air Pollution Surveillance Program) – Canada***

The NAPS network was designed to provide long-term air quality data across populated regions in Canada. The NAPS network includes sites with 24-hour integrated measurements of PM<sub>2.5</sub> mass and its components every 3-6 days, as well as sites with continuous, hourly PM<sub>2.5</sub> measurements. Data are available at: <http://data.ec.gc.ca/data/air/monitor/national-air-pollution-surveillance-naps-program/Data-Donnees/2017/?lang=en>. In 2017, hourly measurements were reported from a variety of instruments including the TEOM, Scientific Synchronized Hybrid Ambient Real-time Particulate (SHARP) model 5030, and Met-One BAM. Additional integrated PM<sub>2.5</sub> zip files contain Excel files for each monitoring site across Canada. Integrated daily filters are collected for 24 hours every 3-6 days and are allowed to equilibrate in the laboratory prior to sampling. The temperature and humidity are controlled during weighing between 20-26°C and 37-47% RH, respectively. Some sites have a dual Teflon-nylon filter collection system to collect nitrate loss during sampling. Due to known losses of ammonium nitrate on Teflon filters, only nitrate data from sites with a dual filter cartridge are used in this analysis. For these sites, total nitrate is calculated as the sum of nitrate measured by IC from the Teflon filter and nitrate and nitrite collected from the Nylon filter and analyzed by IC. Data for each compound are saved as monthly averages for all sites with at least 5 daily measurements during the month (4 for February). For continuous PM<sub>2.5</sub> data, hourly data are also averaged for months with at least 5 sampling days and 24 hours of valid measurements each day. All data are reported at local, ambient conditions (pressure and temperature). In this work, concentrations of organic mass, dust, sea salt, nitrate, ammonium, and sulfate are calculated as for the IMPROVE and CSN data, described above. Black carbon is calculated from the difference between total carbon and organic carbon.

### ***EMEP (European Evaluation and Monitoring Program) – Europe***

Measurements collected by partner organizations across Europe are reported to the EMEP database. Despite standard metadata protocols, lack of consistent compliance has resulted in largely unknown sampling methods and analysis protocols for the data available from this network. For this work, the EMEP dataset was downloaded from <http://ebas.nilu.no>, with

additional details in the analysis script package. Due to limited measurements of silicon, dust is not calculated from this dataset. Reported sampling frequencies range from 1 hour to 1-month. Where metadata is available, measurements have been filtered for data greater than reported detection limits. Due to a lack of consistent reporting of meta-data, there are a large number of uncertainties in the data from this network including measurement methods, sample filter types, or whether data have been corrected to standard or local conditions. Here, we assume data are reported in local conditions for consistency in units with national ambient air quality standards and do not apply any other filters. Data for each compound are then standardized to a time series of daily averages and saved as monthly averages for all sites with at least 4 daily measurements during the month<sup>43</sup>. In this work, concentrations of organic mass, sea salt, nitrate, ammonium, and sulfate are calculated as for the IMPROVE, CSN, and NAPS data, described above. Black carbon is taken as elemental carbon.

#### ***Compiled PM<sub>2.5</sub> Mass and Chemical Components - China***

Additional total PM<sub>2.5</sub> mass and chemical composition data for select sites in 2017 in China have been compiled from literature sources. The data used in this work include measurements from<sup>44-48</sup>, which report data from 14 measurement locations throughout Beijing, Hebei, Zhejiang, Jiangsu, Shaanxi, and Inner Mongolia provinces, collected at various times during the period between August 2016 and February 2018. Measurement techniques for OC and BC include DRI- Thermal/optical carbon analyzers, while sulfate, nitrate, and ammonium measurement methods include IC. Additional sampling and analysis details for each study are provided in the above references. Available reported data were compiled into annual averages for each measurement site for comparison with model results.

#### ***SPARTAN (Surface Particulate Matter Network) – Global***

An overview of the SPARTAN network is available in Snider, et al.<sup>34</sup>, Weagle, et al.<sup>35</sup>, and McNeill, et al.<sup>49</sup>. The SPARTAN network provides publicly available data for PM<sub>2.5</sub> total mass, chemical composition, and optical characteristics in populated regions of the world where air quality monitoring has been historically limited. SPARTAN reported complete yearly data from 5 sites in 2017 and has since grown to report data from 21 sites worldwide. SPARTAN monitors sample ambient air on a Teflon filter, intermittently for a total of 24 hours over a 9-day period, following protocols described in Snider, et al.<sup>34</sup>. Filters are then shipped in sealed containers at ambient temperature to analysis labs in North America where

they undergo analysis for total gravimetric PM<sub>2.5</sub> mass and concentrations of ions, equivalent black carbon, and trace elements. Particle bound water is calculated and residual mass (i.e., total PM<sub>2.5</sub> – inorganic mass + particle bound water) is considered to be organic mass. Total PM<sub>2.5</sub> mass is measured gravimetrically following EPA protocols under laboratory conditions where temperature and RH are controlled to between 20-23°C and 30-40%, respectively. Equivalent black carbon is measured by light absorbance with a smoke stain reflectometer, calibrated to co-located TOR measurements on a quartz filter. More recent analysis techniques for SPARTAN filters include XRF, HIPS, UV-Vis<sup>49,50</sup>, the measurement of organics through FT-IR<sup>51</sup>, and ongoing research activities to measure organic spectra through Aerosol Mass Spectroscopy<sup>52</sup>. For this work, SPARTAN data have been downloaded from: <https://www.spartan-network.org/data>, with additional details in the analysis scripts package. Due to known loss of ammonium and nitrate on Teflon filters, these compounds are not used from SPARTAN. Data for each compound are saved as monthly averages for all sites with at least two reported measurements. Dust is reconstructed as  $10 * ([Al] + [Mg] + [Fe])$  following Weagle, et al. <sup>35</sup>. Sea salt is calculated as  $2.54 * [Na] - 0.1 [Al]$  following Weagle, et al. <sup>35</sup>. Black carbon is taken as equivalent black carbon.

### **Supplementary Text 5. Model Input Emission Details**

Global input emissions for the GEOS-Chem model are primarily for the year 2017 from the Community Emissions Data System<sup>53</sup>, updated for the GBD-MAPS project: CEDS<sub>GBD-MAPS</sub><sup>54,55</sup>. The CEDS<sub>GBD-MAPS</sub> emissions dataset is available on Zenodo<sup>56</sup> and uses contemporary energy consumption data from the International Energy Agency, source and fuel-specific emission factors, as well as a mosaic scaling approach to incorporate global emission estimates (such as the EDGAR v4.3.2<sup>57</sup> inventory and ECLIPSEv5a inventory from the GAINS model<sup>58,59</sup>) with regional inventories to calculate monthly emission fluxes ( $\text{kg m}^{-2} \text{ s}^{-1}$ ) of key atmospheric pollutants ( $\text{NO}_x$ ,  $\text{SO}_2$ , CO, speciated NMVOCs,  $\text{NH}_3$ , BC, and OC). Emissions are disaggregated into contributions from 11 anthropogenic source sectors and 4 fuel categories (solid biofuel, total coal, the sum of liquid fuel and natural gas, and all other non-combustion sources). CEDS emissions are gridded at a  $0.5^\circ \times 0.5^\circ$  spatial resolution and do not include vertical distribution information. Further details about this dataset are described in McDuffie, et al. <sup>54</sup> and Hoesly, et al. <sup>53</sup>. CEDS<sub>GBD-MAPS</sub> emissions for 2017 are incorporated into the GEOS-Chem model using the

HEMCO emissions module<sup>60</sup> and are systematically removed in sensitivity simulations by zeroing out individual sources. Monthly CEDS<sub>GBD-MAPS</sub> emissions are additionally distributed over a 24-hr period using sector-specific diel scaling factors, calculated from the U.S. NEI 2011v1 dataset, implemented in HEMCO by Travis, et al. <sup>61</sup>.

Supplementary Table 2 provides details about the CEDS and non-CEDS emission sources used for model emission sensitivity simulations in the main text. Non-CEDS emission sources include dust emissions from windblown, fugitive, combustion, and industrial sources (AFCID), as well as emissions from aircraft, open fires, volcanoes, lightning, the ocean, and biogenic sources. If emissions from 2017 are not available from a given source, the latest available year is used. Supplementary Figure 6 shows the total global annual emissions of NO<sub>x</sub>, SO<sub>2</sub>, CO, NH<sub>3</sub>, OC, BC, total NMVOCs, and fine dust used in the base 2017 GEOS-Chem simulation. The categories shown in Supplementary Figure 6 correspond to the emission sensitivity simulation categories in Supplementary Table 2.

We also note that the fuel-specific contributions in this work may be lower estimates as some sub-sectoral emission categories were not assigned to a particular combustion fuel-type in the emissions dataset, as shown in Table 2 in McDuffie, et al. <sup>54</sup>. For example, contributions from fuel production, flaring, transformation, and fossil-fuel fires in the energy sector were not assigned to a combustion fuel-type. As a result, PM<sub>2.5</sub> contributions from these sources were included in the ‘other sources’ fuel category in Figs. 2-5 rather than the O&NG category. These contributions, however, were included in the total energy sector fractional results in these same figures. In addition, the emissions dataset does not include primary emissions of PM<sub>2.5</sub> associated with road, tire, and brake wear or ash from coal combustion. While the former source has been shown to have relatively small global PM<sub>2.5</sub> contributions <sup>59</sup>, both sources may be important in regions with large fractional contributions from transportation and coal use.



**Supplementary Table 2. Model emission sensitivity simulation descriptions.** Includes emissions dataset references and descriptions. Note: “calculated” emissions depend on meteorological variables and are computed at the time of simulation.

#	Sector Sensitivity Simulation	Dataset	Year	Reference	Notes
1	<b>Agriculture (AGR)</b> includes manure management, soil fertilizer emissions, rice cultivation, enteric fermentation, and other agriculture	CEDS <sub>GBD-MAPS</sub>	2017	54,56	-
2	<b>Energy Production (ENE)</b> Includes electricity and heat production, fuel production and transformation, oil and gas fugitive/flaring, and fossil fuel fires	CEDS <sub>GBD-MAPS</sub>	2017	54,56	-
3	<b>Industry (IND)</b> Includes Industrial combustion (iron and steel, non-ferrous metals, chemicals, pulp and paper, food and tobacco, non-metallic minerals, construction, transportation equipment, machinery, mining and quarrying, wood products, textile and leather, and other industry combustion) and non-combustion industrial processes and product use (cement production, lime production, other minerals, chemical industry, metal production, food, beverage, wood, pulp, and paper, and other non-combustion industrial emissions)	CEDS <sub>GBD-MAPS</sub>	2017	54,56	-
4	<b>Road Transportation (ROAD)</b> includes cars, motorcycles, heavy and light duty trucks and buses	CEDS <sub>GBD-MAPS</sub>	2017	54,56	-
5	<b>Non-Road/Off-Road Transportation (NRTR)</b> Includes Rail, Domestic navigation, Other transportation	CEDS <sub>GBD-MAPS</sub>	2017	54,56	-
6	<b>Residential Combustion (RCO-R)</b> includes residential heating and cooking	CEDS <sub>GBD-MAPS</sub>	2017	54,56	-
7	<b>Commercial Combustion (RCO-C)</b> Includes commercial and institutional combustion	CEDS <sub>GBD-MAPS</sub>	2017	54,56	
8	<b>Other Combustion (RCO-O)</b> Includes combustion from agriculture, forestry, and fishing	CEDS <sub>GBD-MAPS</sub>	2017	54,56	-
9	<b>Solvents (SLV)</b> Includes solvents production and application (degreasing and cleaning, paint application, chemical products manufacturing and processing, and other product use)	CEDS <sub>GBD-MAPS</sub>	2017	54,56	-
10	<b>Waste (WST)</b> Includes solid waste disposal, waste incineration, waste-water handling, and other waste handling	CEDS <sub>GBD-MAPS</sub>	2017	54,56	-
11	<b>International Shipping (SHP)</b> Includes international shipping and tanker loading	CEDS <sub>GBD-MAPS</sub>	2017	54,56,62,63	A
12	<b>Agricultural Waste Burning (AGBURN)</b> Includes open fires from agricultural waste burning	GFED4.1s	2017	64,65	B
13	<b>Other Open Fires (OBURN)</b> Includes deforestation, boreal forest, peat, savannah, and temperate forest fires	GFED4.1s	2017	64,65	B
14	<b>Fugitive, Combustion, Industrial dust (AFCID)</b>	AFCID	2012, 2013, 2015	66	C
15	<b>Windblown Dust (WDUST)</b>	DEAD model	calculated	67,68	D
16	<b>Remaining Emission Sources (OTHER)</b> Includes all remaining emission sources:				
	volcanic SO <sub>2</sub>	AeroCom	2017		E
	aircraft	AEIC	2005	69	
	lightning NO <sub>x</sub>	LightNOx	calculated	70	F
	biogenic Soil NO	Soil NO <sub>x</sub>	calculated	71	G
	ocean	SeaFlux, GEIA, SeaSalt, Inorg Iodine	calculated	12,72-77	H
	biogenic emissions	MEGANv2.1	calculated	78	I
	very short-lived iodine and bromine species	LIANG_BROMOCARB ORDONEZ_IODOCARB	2000	79,80	
	decaying plants	DECAYING PLANTS		73	
	<b>Fuel Sensitivity Simulations</b>	<b>Dataset</b>	<b>Year</b>	<b>Reference</b>	<b>Notes</b>
17	<b>Total Coal</b> Includes hard coal, brown coal, coal coke	CEDS <sub>GBD-MAPS</sub>	2017	54,56	-
18	<b>Solid Biofuel</b>	CEDS <sub>GBD-MAPS</sub>	2017	54,56	-

	Includes solid biofuel				
19	<b>Liquid Oil and Natural Gas</b> Includes light and heavy oil, diesel oil, and natural gas	CEDS <sub>GBD-MAPS</sub>	2017	54,56	-
20	<b>Process</b> Includes non-combustion CEDS 'process' source emissions.	CEDS <sub>GBD-MAPS</sub>	2017	54,56	-
	<b>Sector &amp; Fuel Sensitivity Simulations</b>	<b>Dataset</b>	<b>Year</b>	<b>Reference</b>	<b>Notes</b>
21	<b>Total Coal from Energy Production</b> Includes hard coal, brown coal, coal coke; Includes electricity and heat production.	CEDS <sub>GBD-MAPS</sub>	2017	54,56	J
22	<b>Total Coal from Industrial Processes</b> Includes hard coal, brown coal, coal coke; Includes Industrial combustion (iron and steel, non-ferrous metals, chemicals, pulp and paper, food and tobacco, non-metallic minerals, construction, transportation equipment, machinery, mining and quarrying, wood products, textile and leather, and other industry combustion)	CEDS <sub>GBD-MAPS</sub>	2017	54,56	K
23	<b>Total Coal from Residential Combustion (RCO-R)</b> Includes hard coal, brown coal, coal coke; Includes residential heating and cooking	CEDS <sub>GBD-MAPS</sub>	2017	54,56	-
24	<b>Solid Biofuel from Residential Combustion (RCO-R)</b> Includes solid biofuel; Includes residential heating and cooking	CEDS <sub>GBD-MAPS</sub>	2017	54,56	-

<sup>A</sup>CEDS International shipping emissions run with the PARANOX ship plume module, which calculates co-emitted concentrations of O<sub>3</sub> and HNO<sub>3</sub> in aged shipping plumes.

<sup>B</sup>Official GFED4 emissions have been released through 2016. 2017 and 2018 emissions are available through a beta release (<https://www.geo.vu.nl/~gwerf/GFED/GFED4/>) that provides updates to estimated monthly emissions of dry matter (DM) and carbon (C) based on the relationship between MODIS active fire detections and the GFED4s inventory for the years 2013-2016. To distribute monthly emissions, these files also include daily variability based on active fire distributions and diurnal cycles based on climatological data following the approach of Mu, et al. <sup>65</sup>. Emission factors for individual species (kg or kg C/ kg DM) are from the original GFED4s release.

<sup>C</sup>The AFCID (Anthropogenic Fugitive, Combustion, and Industrial Dust) inventory is based on 2015 global monthly average primary particulate matter emissions from the ECLIPSEv5a inventory and regional monthly mean inventories for 2013 over India and 2012 over China.

<sup>D</sup>Global windblown mineral dust emissions are calculated for the year 2017 using the dust entrainment and deposition (DEAD) model.

<sup>E</sup>Emissions obtained from NASA/GMAO and include contributions from eruptive and degassing volcanic emissions in 2017, details are here: <http://ftp.as.harvard.edu/gcgrid/data/ExtData/HEMCO/VOLCANO/v2019-08/README>

<sup>F</sup>Lightning emissions of NO match OTD/LIS climatological observations of lightning flashes from May 1995 – December 2013, as described by Murray et al., 2012.

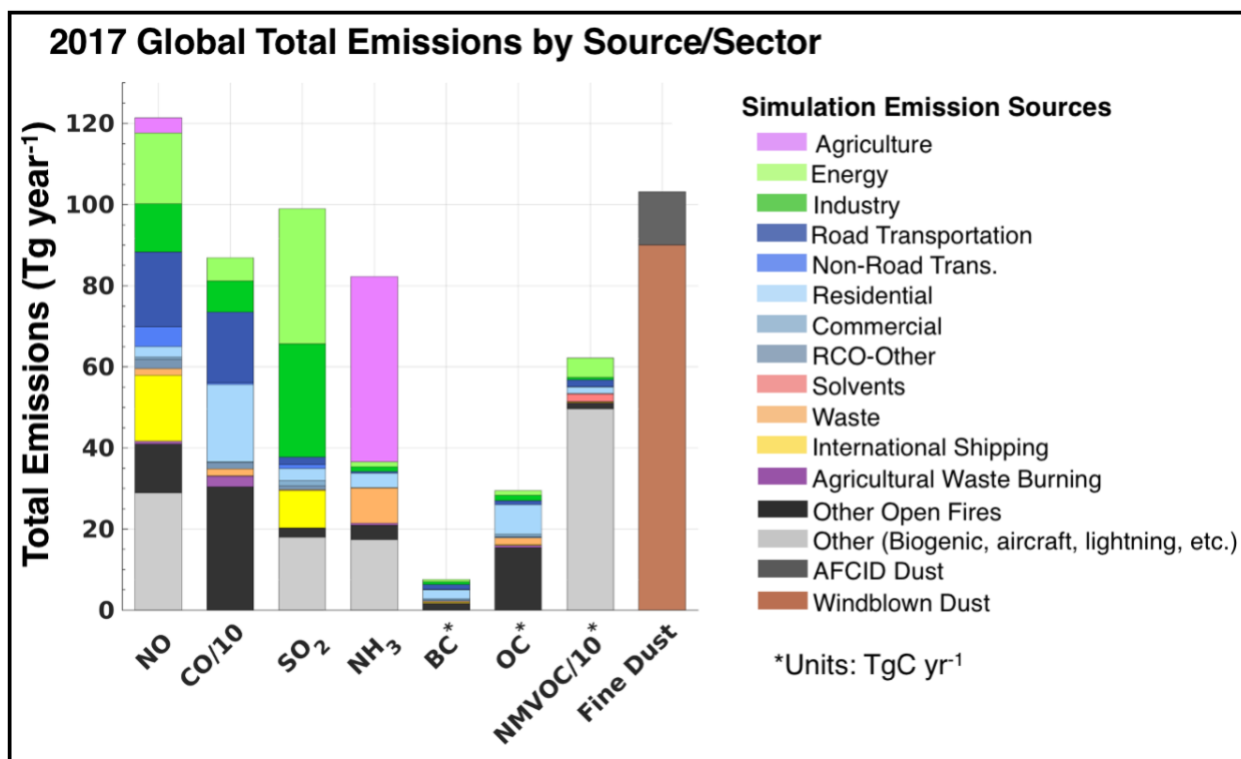
<sup>G</sup>Soil NO<sub>x</sub> emissions are calculated as a function of surface vegetation type, temperature, precipitation history, and a canopy reduction factor, following the parameterization described in Hudman, et al. <sup>71</sup>. Note that fertilizer emissions are not included in this calculation as fertilized soil emissions are included in the CEDS<sub>GBD-MAPS</sub> inventory.

<sup>H</sup>Ocean-air exchange fluxes for DMS, acetone, acetaldehyde, and inorganic iodine are from <sup>74</sup>, <sup>72</sup>, <sup>73</sup>, and <sup>77</sup>, respectively. Ocean emissions of NH<sub>3</sub> from natural sources are set to 1990 levels from GEIA and NH<sub>3</sub> emissions from arctic seabirds are from <sup>76</sup> and <sup>75</sup>. Sea salt emissions are calculated following <sup>12</sup>.

<sup>I</sup>Biogenic emissions are calculated using the Model of Emissions of Gases and Aerosols from Nature (MEGAN) v2.1.

<sup>J</sup>Energy emissions from fuel production and transformation, oil and gas fugitive/flaring, and fossil fuel fire emissions are not assigned to specific fuel types

<sup>K</sup>Industry emissions from non-combustion industrial processes and product use (cement production, lime production, other minerals, chemical industry, metal production, food, beverage, wood, pulp, and paper, and other non-combustion industrial emissions) are not assigned to specific fuel types.



**Supplementary Figure 6: Global total 2017 base simulation emissions.** Emissions are colored by source sector category. BC, OC, and total NMVOCs are provided in units of Tg carbon yr<sup>-1</sup>. Emissions of CO and NMVOCs are divided by 10 for illustration purposes only. Note: OC emissions do not include the GEOS-Chem chemical compound SOAP (secondary organic aerosol precursor), which is emitted from biogenic sources and co-emitted with CO. Emissions of this compound, however, are included in each model simulation.

### Supplementary Text 6. Fractional Fuel and Sector Contributions – Additional Comparisons to Previous Nation-Level Studies

To provide further context for our results, this section provides further comparisons to previous national-level studies that have also used 3D chemical transport models to quantify PM<sub>2.5</sub> source contributions and/or the associated ambient PM<sub>2.5</sub> disease burden. Where available, we primarily compare the reported fractional contributions to minimize methodological and input data differences. As described in the main text, differences in sectoral definitions (e.g., including fires in the agricultural sector or waste in the residential sector) highlight the importance of clearly defining emission sector definitions in source contribution studies (e.g., Supplementary Table 2). This text is not an exhaustive review of previous studies.

## *Fuel Types*

Previous studies using similar methodologies have typically combined all anthropogenic sources for global or regional scale analyses<sup>81-83</sup> or reported contributions from single or aggregate fuel-types<sup>84</sup>, typically for select countries such as China and India<sup>85-87</sup>. Previous studies also provide estimates of years prior to 2017, which may not capture recent trends in PM<sub>2.5</sub> chemical precursor emissions, such as recent reductions in China<sup>88</sup>.

Previous national-level studies have only investigated the contribution from coal combustion emissions for select countries and sectors. For example, previous studies have discussed the importance of residential, energy, and industrial coal use on local and regional PM<sub>2.5</sub> pollution in India<sup>87</sup> and China<sup>86</sup>, particularly during winter<sup>89,90</sup>. Emission reduction policies in China have also recently targeted coal use in these sectors. Fractional coal contributions in the residential, energy, and industry sectors in this study in 2017 were estimated to account for 5.3%, 4.7%, and 9.1% of total PM<sub>2.5</sub> sources in China and 1.4%, 7.0%, and 8.2% in India. These are generally smaller than the corresponding contributions of 4%, 9%, and 17% in 2013 for China<sup>86</sup>, but generally agree well with the 8% contributions from both energy and industrial coal use in India in 2015<sup>87</sup>. When considering total coal use across all sectors, these previous studies have estimated contributions of 40% in China and 16% in India<sup>86,87</sup>. In 2017, total coal contributions were lower in China (22.7%) and slightly larger in India (17.1%), which may be a result of different methodologies, but is also consistent with recent emission trends in these respective countries.

For solid biofuel, Chafe, et al.<sup>84</sup> previously investigated the contribution of residential cooking with biofuel to the PM<sub>2.5</sub> mass and associated burden at both global and regional scales for the year 2010. Both studies predict large relative contributions in South and Southeast Asia, though Chafe, et al.<sup>84</sup> also predict fractional contributions from biofuel cooking in Southern Sub-Saharan Africa and Southern Latin America that were more than twice as large as those in this work. Reductions in the proportion of the population using solid fuels in these locations between 2010 and 2017 may partially explain these differences. In China and India, two previous studies found that solid biofuel combustion for residential heating and cooking contributed to 15% in China in 2013<sup>86</sup> and 24% in India in 2015<sup>87</sup>. These fractional contributions were similar to those of 12.7% and 22.5% for China and India in 2017 and suggest that these relative contributions have been relatively constant in recent

years. Due to such persistent contributions, however, previous studies have also shown the potential for significant air quality benefits by addressing the fuels and combustion efficiencies of sources used for residential heating and cooking in China<sup>89,90</sup>. For 2017, we estimate a total of nearly 250,000 (95% CI: 189,500-305,500) deaths avoidable by eliminating both solid biofuel and coal use in the residential sector in China.

### *Sectors*

For the residential sector, previous studies for India estimated PM<sub>2.5</sub> disease burden contributions between 27% and 50% in 2010 and 2015<sup>87,91</sup>. Contributions in 2017 were comparable but slightly lower at between 23%-35% when comparable sub-sectors (e.g., residential + waste) were considered. In China, previous residential estimates ranged from 25%-32% in 2010<sup>91,92</sup> and ~19%-22% in 2013<sup>86,93</sup>, both consistent with 26% here in 2017 (Supplementary Data 1). Fig. 2 and Fig. 3 in the main text show that the fractional residential contributions were generally smaller in Canada and the U.S. than in Asia, also consistent with multiple previous studies<sup>91,94-98</sup>. Emissions estimates from the residential sector, however, are particularly uncertain in emission inventories compared to those from other large anthropogenic emission sources<sup>54,99-101</sup>.

For the energy and industry sectors, 2017 contributions were 10.2% and 11.7%, respectively. These sectors have been studied relatively extensively in past work compared to other PM<sub>2.5</sub> sources, however, differences may arise due to differences in the detailed sub-sectoral categories used here, or recent emission changes. The more detailed sectors such as commercial, AFCID, and waste examined here isolate sources that may have either been lumped into the industry sector in prior work or neglected altogether. Over recent years, industrial and energy emissions have been decreasing in China, while these emission sources have been simultaneously increasing throughout other parts of Asia, Latin America, and Africa<sup>54</sup>. Previous studies have specifically investigated these source contributions at the national level in China<sup>86,91-93</sup>, India<sup>87</sup>, Canada<sup>94</sup>, the U.S.<sup>98</sup>, and throughout Africa<sup>82,83</sup>. In Canada, combined fractional energy and industry contributions in this work were similar to previous results<sup>94</sup>. In China, previous energy contributions were consistent with this work, however industrial emissions in 2017 were close to half those previously reported for 2010 and 2013<sup>86,92,93</sup>. In Africa, two recent studies found the greatest contributions from the energy sector in Egypt and Southern Sub-Saharan Africa<sup>82,83</sup>, also consistent with this work (Fig. 3).

Two additional fuel and sector specific simulations for 2017 revealed that 91% of these energy contributions in South Africa were from coal, while only 46% were from coal in Egypt (Fig. 3, Supplementary Data 1). One additional study predicted a much smaller (3%) contribution from combined energy and industry sources in Egypt in 2010, predicting instead a 92% contribution from natural sources<sup>91</sup>. More detailed assessments of these differences between industry, energy, and other source contributions are largely limited by a lack of more detailed emission sector descriptions.

For dust, agriculture, transportation, and fires, agreement with previous national-level results were variable. For example, national-level fractional dust estimates in 2017 were much larger for North Africa, the Middle East<sup>102</sup>, and China<sup>93</sup>, and smaller in India<sup>87</sup> compared to previous studies. For India specifically, updates to the model deposition<sup>29</sup> and dust size distribution schemes<sup>14</sup>, as well as interannual variability in dust emission fluxes and removal rates, likely contribute to the smaller total contribution from fine dust (< 2.5  $\mu\text{m}$  diameter) in this work (~14.9%) relative to previous estimates (~38%), derived using an older version of the GEOS-Chem model. As shown in Supplementary Figure 5, the model updates in this work improved the agreement with surface dust observations, however, the measured PWM dust concentrations at surface monitors were < 1  $\mu\text{g}/\text{m}^3$ , indicating that current surface monitor locations may not provide an accurate characterization of the total population exposure to dust. These uncertainties highlight the need for increased monitoring and continued improvement to the model treatment of dust to improve the accuracy of contribution estimates from this source.

For non-combustion agriculture, 2017 estimates were generally smaller than previous regional-level studies<sup>103,104</sup>. For example, 2017 contributions in Europe, North America, and South and East Asia were less than 22%, 11%, and 12%, respectively, while the same source was estimated to contribute to 34%, 17%, and 10% in 2010<sup>103</sup>. Global and regional  $\text{NH}_3$  emissions have been increasing between 2010 and 2017<sup>54</sup>, indicating that differences here are methodological (e.g., differences in emissions or chemical production), rather than real temporal trends. Our mechanistic updates to the ammonium nitrate simulation (Supplementary Text 3) both improved the agreement with observations and reduced the agricultural sources of  $\text{PM}_{2.5}$  in this work.

For the transportation sector, relative contributions have also been previously investigated at the national scales<sup>105-107</sup>. Consistent with previous studies, total transportation contributions in this work were generally greater than the global average in North America, Europe, parts of Asia, Australia, and Latin America<sup>105-107</sup>. Comparisons with additional national-level results<sup>86,87,91-93,98,107</sup> show that differences in fractional contributions generally follow recent trends in transportation emissions, with recent decreases in China and the U.S. and increases in India.

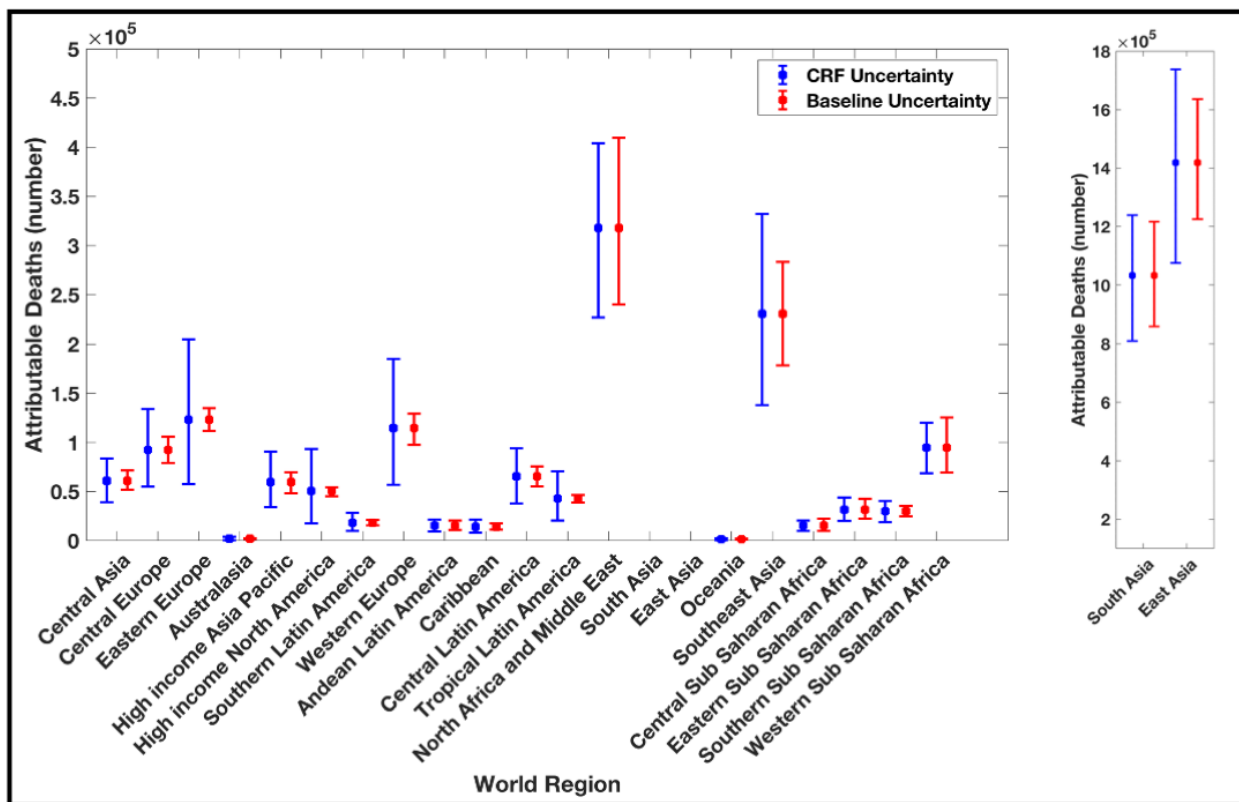
For fire emissions, comparisons to previous global and national level estimates are discussed in the main text.

Waste, solvent use, and international shipping sectors have relatively small contributions on the global scale but can significantly contribute to national and sub-national PM<sub>2.5</sub> variation (e.g., up to 18% in Sri Lanka; Fig. 5). Contributions from waste combustion to the ambient PM<sub>2.5</sub> disease burden have not been previously reported. The relative contribution from the solvent sector has only been reported in one previous national-level study<sup>86</sup>. As a result of non-linear PM<sub>2.5</sub> mass production, solvent emission reductions can result in an increase in total PM<sub>2.5</sub> mass. This was shown previously for a study in China<sup>86</sup>. Solvent emission reductions in 2017, however, resulted in a total mass decrease in this same country. As the solvent sector primarily emits NMVOCs (Supplementary Figure 6), this variable sign response demonstrates that decreases in these emissions can increase the availability of atmospheric oxidants, leading to increases in inorganic aerosol mass in NO<sub>x</sub>-limited/VOC-saturated chemical regimes<sup>108</sup>. Therefore, this negative response may be important to consider when developing air pollution reduction strategies in regions with large VOC/NO<sub>x</sub> emission ratios. Solvent emissions, however, are also highly uncertain as NMVOCs may be underestimated in U.S. emissions inventories by a factor of 2-3<sup>109</sup>. Relative national contributions from international shipping are generally consistent with previous studies<sup>110,111</sup>, where the largest relative contributions are predicted in coastal countries such as Ireland, Portugal, and the Bahamas (more than 12% each in 2017).

### **Supplementary Text 7. Uncertainty Sensitivity Study**

We conduct an additional sensitivity test to account for potential uncertainties in the PM<sub>2.5</sub> disease burden associated with the age- and disease-specific baseline mortality data from the

2019 GBD. The 95% uncertainty ranges are calculated by applying lower and upper estimates of the baseline mortality data to the PAF in Equation 2, derived from the mean CRF. The resulting 95% confidence intervals for 21 world regions are shown in Supplementary Figure 7, compared to the 95% CIs derived from uncertainties in the mean CRFs (reported in the Main Text). As the upper and lower limits in the baseline and CRF datasets are both estimated from multiple draws of underlying distributions, propagating the uncertainties from these two input variables likely leads to an overestimate in the 95% CI for the total attributable disease burden. Supplementary Figure 7 shows that for most regions, the 95% CI associated with uncertainties in the CRFs encompass the 95% CIs associated with uncertainties in the baseline mortality estimates. Additional uncertainties in the PM<sub>2.5</sub> exposure estimates and modeled fractional source contributions are not considered here to due computational limitations.



**Supplementary Figure 7. Total disease burden estimates and confidence intervals for 21 world regions, derived from uncertainties in CRFs and baseline mortality data.** Total disease burden estimates are from Supplementary Data 1. Uncertainty ranges illustrate the 95% CI derived from uncertainty estimates in the CRFs (blue) and baseline mortality data (red). The bounds for South and East Asia are shown on an expanded scale to the right.



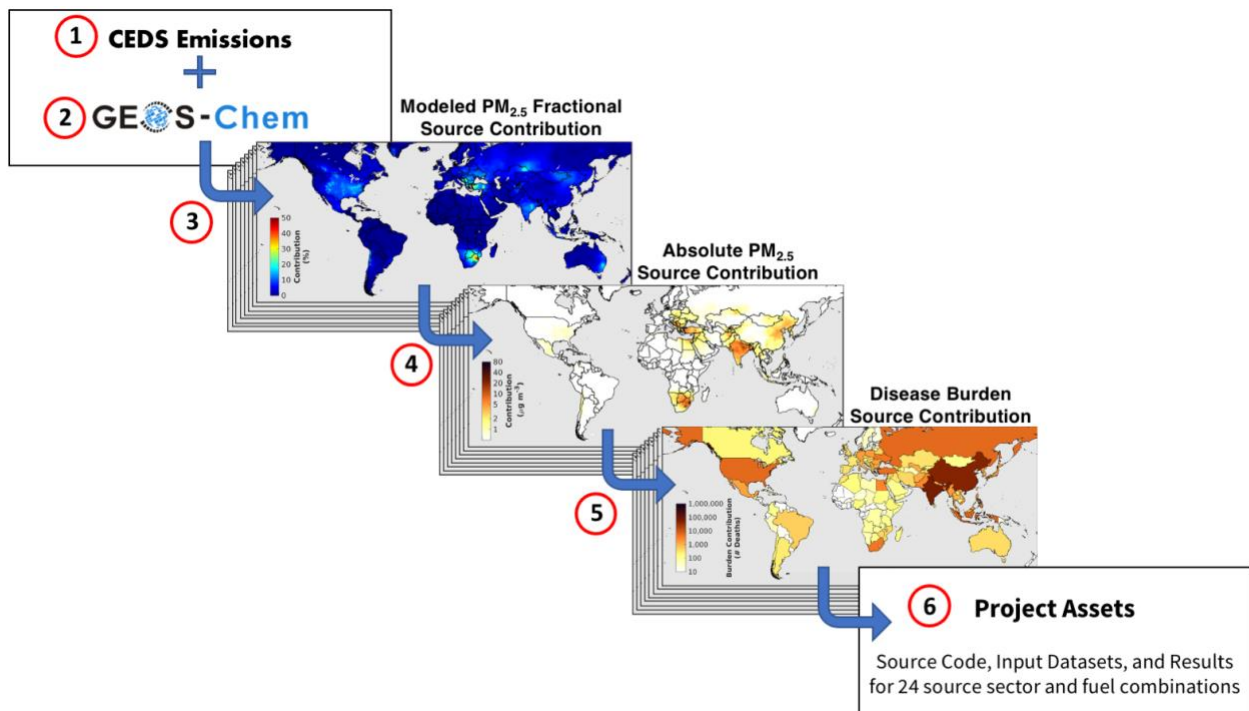
### **Supplementary Text 8. Consideration of the Zero-Out (Brute Force) Method**

Similar to many other analyses of this type of work, our analysis uses a zero-out or brute force approach for model sensitivity simulations. This widely used approach is designed to quantify source contributions to the total PM<sub>2.5</sub> disease burden under complete elimination of emissions from individual sources. As discussed in previous zeroing-out studies<sup>35,91,92,103</sup>, the non-linear chemical production of PM<sub>2.5</sub> will result in the sum of individual PM<sub>2.5</sub> simulations to exceed the total PM<sub>2.5</sub> mass predicted in the base simulation. By implementing Eq. (5) in the Main Text, we ensure that fractional contributions from individual source sectors sum to 100% in this work. Using this approach, the final fractional PM<sub>2.5</sub> source contributions will be sensitive to the number of individual source sensitivity simulations that are included in the calculation, resulting in further differences between the detailed simulations in this work and previous similar studies. Due to this non-linearity, fractional and absolute contributions predicted from this method may not be consistent with simulations that implement more moderate reduction strategies (i.e., < 20-50% emission reductions), or strategies that simultaneously target multiple emission sectors (e.g., simultaneous reductions in both energy and industry sources).

### **Supplementary Text 9. Methodological Schematic**

As described in the main text, results in this study are derived by integrating high-resolution satellite-derived PM<sub>2.5</sub> exposure estimates, CRFs from the 2019 GBD, and fractional source contribution results from 24 emission sensitivity simulations with the GEOS-Chem chemical transport model. Supplementary Figure 8 illustrates the overall workflow of this methodology. In Step 1, gridded global emissions of PM<sub>2.5</sub> precursors are developed as a function of source sector and fuel-type (Supplementary Table 5; anthropogenic emissions largely from the CEDS<sub>GBD-MAPS</sub> inventory), as described in McDuffie, et al.<sup>54</sup>. In Step 2, emissions are used as input in an updated version of the GEOS-Chem 3D chemical transport model (described in Supplementary Text 3), with the simulated PM<sub>2.5</sub> concentrations validated against available mass and composition surface observations (described in Supplementary Text 4). In Step 3, a series of zero-out emission sensitivity simulations are conducted (Supplementary Table 2) with the GEOS-Chem model and emission inputs. The resulting PM<sub>2.5</sub> concentrations from each simulation are compared to the base simulation (with all emission sources) to quantify the modeled fractional PM<sub>2.5</sub> contributions (reported in Data Files 1 (sectors) and 2 (fuel-types)). In

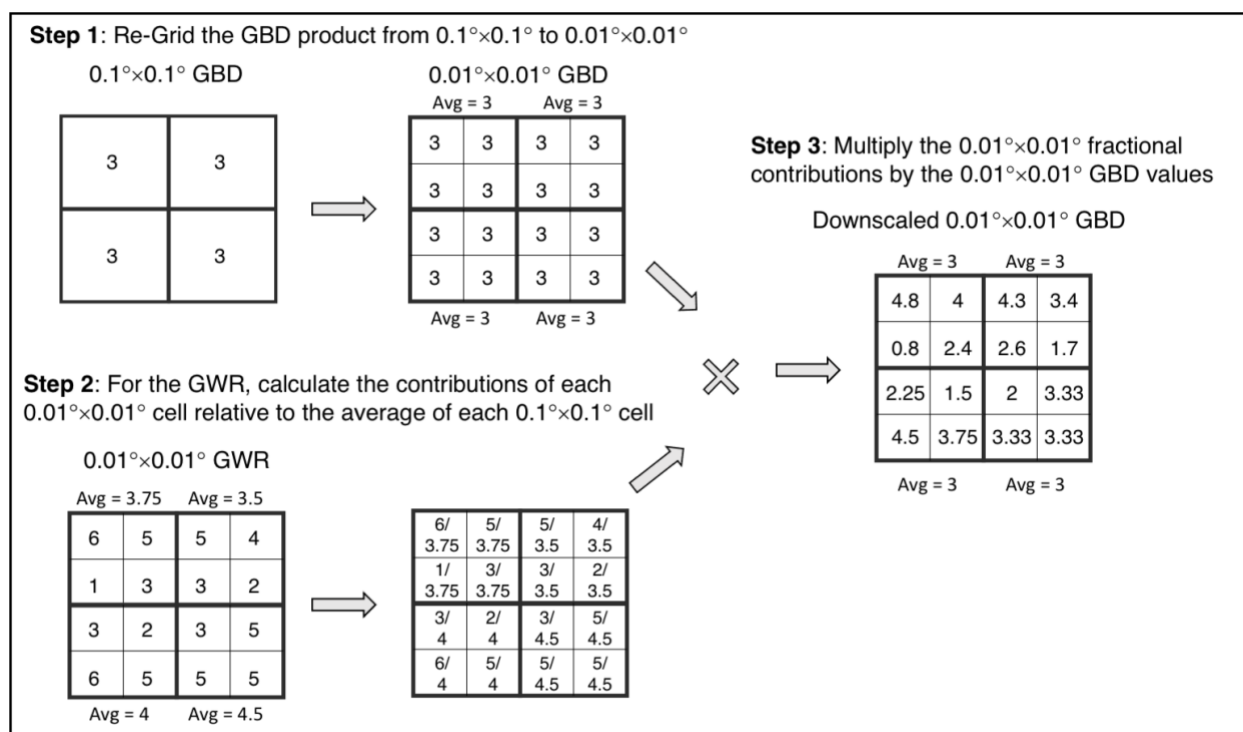
Step 4, high-resolution PM<sub>2.5</sub> exposure estimates are derived by downscaling exposure estimates from the 2019 GBD (described in Supplementary Text 10; reported in Supplementary Data 1 and 2) and are applied to the fractional model source contributions from Step 2 to quantify absolute source-specific contributions to ambient PM<sub>2.5</sub> mass. In Step 5, CRFs from the GBD2019 (Supplementary Figure 2) are combined with downscaled PM<sub>2.5</sub> exposure estimates from Step 4 to calculate the total ambient PM<sub>2.5</sub> disease burden (reported in Supplementary Data 1 and 2). The total burden is combined with modeled fractional source contributions from Step 3 to calculate source-specific burden contributions reported throughout the manuscript. Lastly, Step 6 highlights the data assets that are associated with this analysis and manuscript, including the analysis scripts, model source code, input emissions, CRFs, baseline burden and exposure estimate datasets (<https://github.com/emcduffie/GBD-MAPS-Global>), and the global, regional, national, and subnational source sector and fuel contribution results (Supplementary Data 1 and 2).



**Supplementary Figure 8: Overall methodological workflow schematic.** The relevant equations and data from Supplementary Text 9 are indicated in each step.

## Supplementary Text 10. PM<sub>2.5</sub> Exposure Estimates - Spatial Downscaling Procedural Details

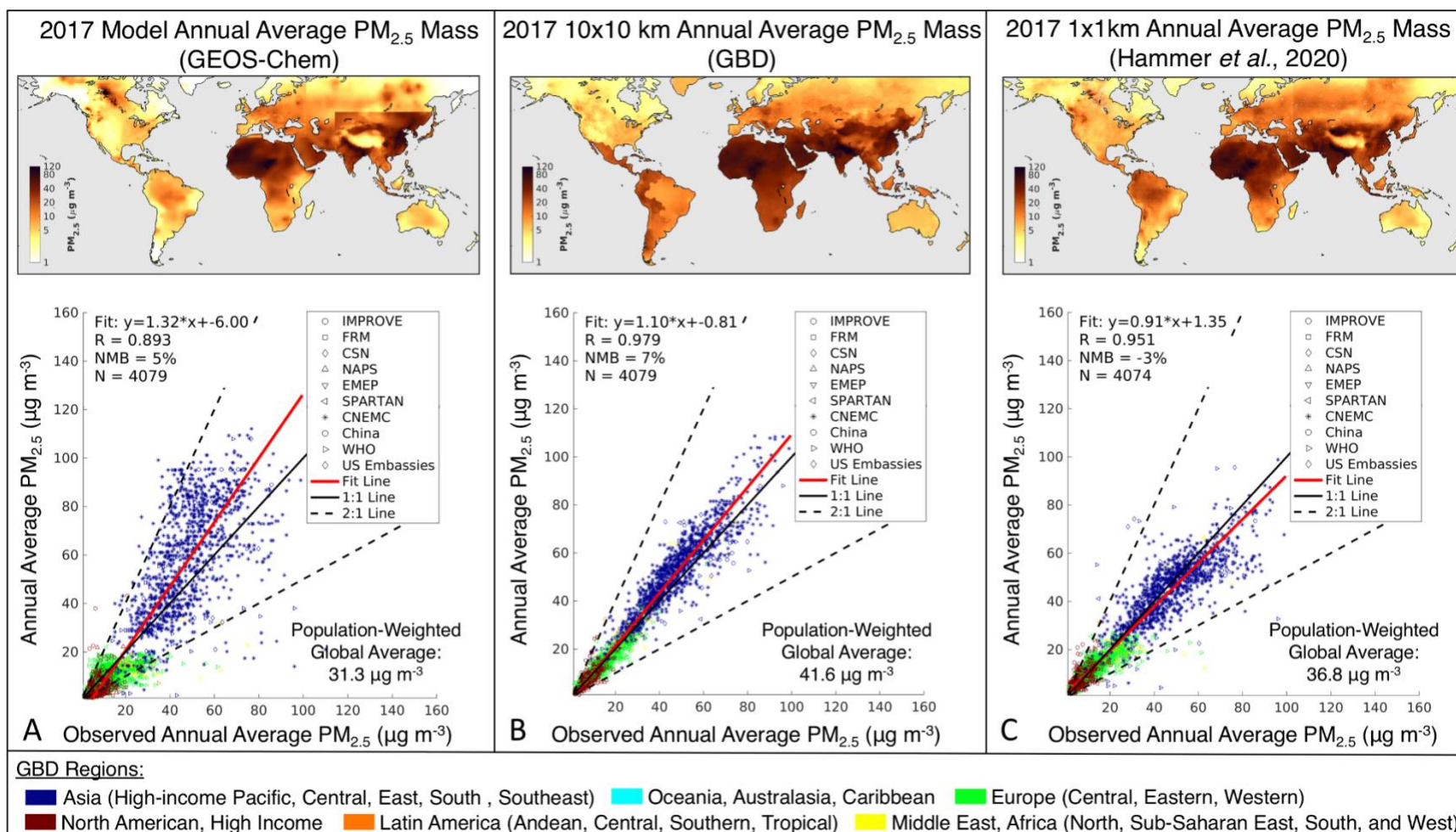
The process of spatially downscaling GBD PM<sub>2.5</sub> exposure estimates using a newly available high-resolution product from Hammer, et al. <sup>5</sup> involves three steps, illustrated in Supplementary Figure 9. First, the 0.1°×0.1° GBD product is re-gridded to a 0.01°×0.01° global grid, by setting each value in the new fine-resolution grid boxes (100 boxes) to the value from the corresponding coarser grid box in the original GBD product. Second, the fractional contribution of each grid-box in the 0.01°×0.01° Hammer, et al. <sup>5</sup>, product is calculated relative to the average PM<sub>2.5</sub> across the surrounding 100 grid boxes. In the event that the Hammer, et al. <sup>5</sup> product does not report data for a particular grid box, the spatial fraction in that box is set to 1. Third, these resulting fractional contributions are multiplied by the GBD values from the 0.01°×0.01° PM<sub>2.5</sub> product from Step 1. This process is independent of the GEOS-Chem emission sensitivity simulations.



**Supplementary Figure 9: Simplified schematic of the spatial downscaling procedure.** Values in each example grid box represent example PM<sub>2.5</sub> mass concentrations in units of  $\mu\text{g m}^{-3}$ . In actuality, one of the 0.1°×0.1° grid boxes in Step 1 above corresponds to 100 grid boxes of

0.01°×0.01° resolution, not the four as shown here. In this figure ‘GWR’ refers to the high-resolution PM<sub>2.5</sub> estimates from Hammer, et al. <sup>5</sup>.

To assess the sensitivity of PM<sub>2.5</sub> exposure estimates to the downscaling process, Supplementary Figure 10 shows maps of the gridded exposure estimates, as well as their correlations against observations for (A) the raw GEOS-Chem simulated concentrations, (B) original 0.1°×0.1° GBD PM<sub>2.5</sub> product, and (C) 0.01°×0.01° Hammer, et al. <sup>5</sup> product. Fig. 1 and Supplementary Figure 10 illustrate similarly good agreement between each of the exposure estimates and the total PM<sub>2.5</sub> mass observations, with correlation coefficients (r) and NMBs ranging from 0.89 to 0.979 and -3% to +11%, respectively. The added spatial information from the downscaling procedure slightly increases the NMB from +7% (Supplementary Figure 10b) to +11% (Fig. 1), but maintains a slightly higher correlation coefficient (r) than the high-resolution Hammer, et al. <sup>5</sup> product (0.977 vs 0.951). Across all four products, the 2017 global annual PWM PM<sub>2.5</sub> mass ranges between 31.3 μg m<sup>-3</sup> to 41.7 μg m<sup>-3</sup>. Differences between the GBD and Hammer, et al. <sup>5</sup> products are largely due to different methods used to calibrate geophysical estimates to surface observations.



**Supplementary Figure 10: Comparison of three PM<sub>2.5</sub> exposure estimates against surface observations for the year 2017.** (A) GEOS-Chem annual average PM<sub>2.5</sub> mass concentrations, (B) 0.1°×0.1° GBD annual average PM<sub>2.5</sub> exposure estimates, (C) 0.01°×0.01° Hammer, et al. <sup>5</sup> annual average exposure estimates. Each column contains a map of the PM<sub>2.5</sub> concentrations and a scatter plot comparing each product against 2017 surface observations. Colors represent world regions (Supplementary Table 1) and symbols represent observation networks (Supplementary Text 4). Red lines: correlation slope, solid black lines: 1:1 line, and dashed lines: 2:1 and 1:2 lines. The fit slope, intercept, correlation coefficient, normalized mean bias (NMB), number of observation points (N), and PWM PM<sub>2.5</sub> concentrations are also provided.

## Supplementary References

- 1 CIESIN (Center for International Earth Science Information Network). Gridded Population of the World Version 4. (*Palisades, NY.*), doi:doi.org/10.1128/AAC.03728-14 (2017).
- 2 Burnett, R. *et al.* Global estimates of mortality associated with long-term exposure to outdoor fine particulate matter. *P. Natl. Acad. Sci.* **115**, 9592, doi:10.1073/pnas.1803222115 (2018).
- 3 Yin, P. *et al.* Long-term Fine Particulate Matter Exposure and Nonaccidental and Cause-specific Mortality in a Large National Cohort of Chinese Men. *Environmental Health Perspectives* **125**, 117002, doi:10.1289/EHP1673.
- 4 Hystad, P., Yusuf, S. & Brauer, M. Air pollution health impacts: the knowns and unknowns for reliable global burden calculations. *Cardiovascular Research*, doi:10.1093/cvr/cvaa092 (2020).
- 5 Hammer, M. S. *et al.* Global Estimates and Long-Term Trends of Fine Particulate Matter Concentrations (1998-2018). *Environ. Sci. Technol.*, doi:10.1021/acs.est.0c01764 (2020).
- 6 Bey, I. *et al.* Global modeling of tropospheric chemistry with assimilated meteorology: Model description and evaluation. *J. Geophys. Res. Atmos.* **106**, 23073-23095, doi:10.1029/2001JD000807 (2001).
- 7 Wang, Y. X., McElroy, M. B., Jacob, D. J. & Yantosca, R. M. A nested grid formulation for chemical transport over Asia: Applications to CO. *J. Geophys. Res. Atmos.* **109**, doi:10.1029/2004JD005237 (2004).
- 8 Philip, S., Martin, R. V. & Keller, C. A. Sensitivity of chemistry-transport model simulations to the duration of chemical and transport operators: a case study with GEOS-Chem v10-01. *Geosci. Model Dev.* **9**, 1683-1695, doi:10.5194/gmd-9-1683-2016 (2016).
- 9 Park, R. J., Jacob, D. J., Field, B. D., Yantosca, R. M. & Chin, M. Natural and transboundary pollution influences on sulfate-nitrate-ammonium aerosols in the United States: Implications for policy. *J. Geophys. Res. Atmos.* **109**, doi:10.1029/2003JD004473 (2004).
- 10 Wang, Q. *et al.* Global budget and radiative forcing of black carbon aerosol: Constraints from pole-to-pole (HIPPO) observations across the Pacific. *J. Geophys. Res. Atmos.* **119**, 195-206, doi:10.1002/2013JD020824 (2014).
- 11 Kim, P. S. *et al.* Sources, seasonality, and trends of southeast US aerosol: an integrated analysis of surface, aircraft, and satellite observations with the GEOS-Chem chemical transport model. *Atmos. Chem. Phys.* **15**, 10411-10433, doi:10.5194/acp-15-10411-2015 (2015).
- 12 Jaeglé, L., Quinn, P. K., Bates, T. S., Alexander, B. & Lin, J. T. Global distribution of sea salt aerosols: new constraints from in situ and remote sensing observations. *Atmos. Chem. Phys.* **11**, 3137-3157, doi:10.5194/acp-11-3137-2011 (2011).
- 13 Duncan Fairlie, T., Jacob, D. J. & Park, R. J. The impact of transpacific transport of mineral dust in the United States. *Atmos. Environ.* **41**, 1251-1266, doi:<https://doi.org/10.1016/j.atmosenv.2006.09.048> (2007).
- 14 Zhang, L., Kok, J. F., Henze, D. K., Li, Q. & Zhao, C. Improving simulations of fine dust surface concentrations over the western United States by optimizing the particle size distribution. *Geophysical Research Letters* **40**, 3270-3275, doi:<https://doi.org/10.1002/grl.50591> (2013).
- 15 Martin, R. V., Jacob, D. J., Yantosca, R. M., Chin, M. & Ginoux, P. Global and regional decreases in tropospheric oxidants from photochemical effects of aerosols. *J. Geophys. Res. Atmos.* **108**, doi:<https://doi.org/10.1029/2002JD002622> (2003).

- 16 Koepke, P., Hess, M., Schult, I. & Shettle, E. P. Global Aerosol Dataset. (Max-Planck Institute for Meteorology, Hamburg, Germany, 1997).
- 17 Drury, E. *et al.* Synthesis of satellite (MODIS), aircraft (ICARTT), and surface (IMPROVE, EPA-AQS, AERONET) aerosol observations over eastern North America to improve MODIS aerosol retrievals and constrain surface aerosol concentrations and sources. *J. Geophys. Res. Atmos.* **115**, doi:<https://doi.org/10.1029/2009JD012629> (2010).
- 18 Latimer, R. N. C. & Martin, R. V. Interpretation of measured aerosol mass scattering efficiency over North America using a chemical transport model. *Atmos. Chem. Phys.* **19**, 2635-2653, doi:10.5194/acp-19-2635-2019 (2019).
- 19 Lee, C. *et al.* Retrieval of vertical columns of sulfur dioxide from SCIAMACHY and OMI: Air mass factor algorithm development, validation, and error analysis. *J. Geophys. Res. Atmos.* **114**, doi:<https://doi.org/10.1029/2009JD012123> (2009).
- 20 Ridley, D. A., Heald, C. L. & Ford, B. North African dust export and deposition: A satellite and model perspective. *J. Geophys. Res. Atmos.* **117**, doi:<https://doi.org/10.1029/2011JD016794> (2012).
- 21 Hammer, M. S. *et al.* Interpreting the ultraviolet aerosol index observed with the OMI satellite instrument to understand absorption by organic aerosols: implications for atmospheric oxidation and direct radiative effects. *Atmos. Chem. Phys.* **16**, 2507-2523, doi:10.5194/acp-16-2507-2016 (2016).
- 22 Fountoukis, C. & Nenes, A. ISORROPIA II: a computationally efficient thermodynamic equilibrium model for  $K^+$  - $Ca^{2+}$  - $Mg^{2+}$  - $NH_4^+$  - $Na^+$  - $SO_4^{2-}$  - $NO_3^-$  - $Cl^-$  - $H_2O$  aerosols. *Atmos. Chem. Phys.* **7**, 4639-4659, doi:10.5194/acp-7-4639-2007 (2007).
- 23 Pai, S. J. *et al.* An evaluation of global organic aerosol schemes using airborne observations. *Atmos. Chem. Phys. Discuss.* **2019**, 1-39, doi:10.5194/acp-2019-331 (2019).
- 24 Lin, S.-J. & Rood, R. B. Multidimensional Flux-Form Semi-Lagrangian Transport Schemes. *Monthly Weather Review* **124**, 2046-2070, doi:10.1175/1520-0493(1996)124<2046:Mffslt>2.0.Co;2 (1996).
- 25 Wu, S. *et al.* Why are there large differences between models in global budgets of tropospheric ozone? *J. Geophys. Res. Atmos.* **112**, doi:10.1029/2006jd007801 (2007).
- 26 Lin, J.-T. & McElroy, M. B. Impacts of boundary layer mixing on pollutant vertical profiles in the lower troposphere: Implications to satellite remote sensing. *Atmos. Environ.* **44**, 1726-1739, doi:<https://doi.org/10.1016/j.atmosenv.2010.02.009> (2010).
- 27 The International GEOS-Chem User Community. GEOS-Chem 12.1.0 (Version 12.1.0). Zenodo., doi:<http://doi.org/10.5281/zenodo.1553349> (2018, November 26).
- 28 Heald, C. L. *et al.* Atmospheric ammonia and particulate inorganic nitrogen over the United States. *Atmos. Chem. Phys.* **12**, 10295-10312, doi:10.5194/acp-12-10295-2012 (2012).
- 29 Luo, G., Yu, F. & Schwab, J. Revised treatment of wet scavenging processes dramatically improves GEOS-Chem 12.0.0 simulations of nitric acid, nitrate, and ammonium over the United States. *Geosci. Model Dev. Discuss.* **2019**, 1-18, doi:10.5194/gmd-2019-58 (2019).
- 30 McDuffie, E. E. *et al.* Heterogeneous  $N_2O_5$  Uptake During Winter: Aircraft Measurements During the 2015 WINTER Campaign and Critical Evaluation of Current Parameterizations. *J. Geophys. Res. Atmos.* **123**, 4345-4372, doi:10.1002/2018JD028336 (2018).
- 31 Shah, V. *et al.* Chemical feedbacks weaken the wintertime response of particulate sulfate and nitrate to emissions reductions over the eastern United States. *P. Natl. Acad. Sci.* **115**, 8110-8115 (2018).

- 32 McDuffie, E. E. *et al.* ClNO<sub>2</sub> Yields From Aircraft Measurements During the 2015 WINTER Campaign and Critical Evaluation of the Current Parameterization. *J. Geophys. Res. Atmos.* **123**, 12,994-913,015, doi:10.1029/2018JD029358 (2018).
- 33 Luo, G., Yu, F. & Moch, J. M. Further improvement of wet process treatments in GEOS-Chem v12.6.0: Impact on global distributions of aerosol precursors and aerosols. *Geosci. Model Dev. Discuss.* **2020**, 1-39, doi:10.5194/gmd-2020-11 (2020).
- 34 Snider, G. *et al.* SPARTAN: a global network to evaluate and enhance satellite-based estimates of ground-level particulate matter for global health applications. *Atmos. Meas. Tech.* **8**, 505-521, doi:10.5194/amt-8-505-2015 (2015).
- 35 Weagle, C. L. *et al.* Global Sources of Fine Particulate Matter: Interpretation of PM<sub>2.5</sub> Chemical Composition Observed by SPARTAN using a Global Chemical Transport Model. *Environ. Sci. Technol.* **52**, 11670-11681, doi:10.1021/acs.est.8b01658 (2018).
- 36 Wu, H. *et al.* Probabilistic Automatic Outlier Detection for Surface Air Quality Measurements from the China National Environmental Monitoring Network. *Advances in Atmospheric Sciences* **35**, 1522-1532, doi:10.1007/s00376-018-8067-9 (2018).
- 37 Sofowote, U., Su, Y., Bitzos, M. M. & Munoz, A. Improving the correlations of ambient tapered element oscillating microbalance PM<sub>2.5</sub> data and SHARP 5030 Federal Equivalent Method in Ontario: A multiple linear regression analysis. *Journal of the Air & Waste Management Association* **64**, 104-114, doi:10.1080/10962247.2013.833145 (2014).
- 38 Tortajada-Genaro, L.-A. & Borrás, E. Temperature effect of tapered element oscillating microbalance (TEOM) system measuring semi-volatile organic particulate matter. *Journal of Environmental Monitoring* **13**, 1017-1026, doi:10.1039/C0EM00451K (2011).
- 39 Rizzo, M., Scheff, P. A. & Kaldy, W. Adjusting Tapered Element Oscillating Microbalance Data for Comparison with Federal Reference Method PM<sub>2.5</sub> Measurements in Region 5. *Journal of the Air & Waste Management Association* **53**, 596-607, doi:10.1080/10473289.2003.10466196 (2003).
- 40 Hand, J. L., Prenni, A. J., Schichtel, B. A., Malm, W. C. & Chow, J. C. Trends in remote PM<sub>2.5</sub> residual mass across the United States: Implications for aerosol mass reconstruction in the IMPROVE network. *Atmos. Environ.* **203**, 141-152, doi:<https://doi.org/10.1016/j.atmosenv.2019.01.049> (2019).
- 41 White, W. H. Chemical markers for sea salt in IMPROVE aerosol data. *Atmos. Environ.* **42**, 261-274, doi:<https://doi.org/10.1016/j.atmosenv.2007.09.040> (2008).
- 42 Solomon, P. A. *et al.* U.S. National PM<sub>2.5</sub> Chemical Speciation Monitoring Networks—CSN and IMPROVE: Description of networks. *Journal of the Air & Waste Management Association* **64**, 1410-1438, doi:10.1080/10962247.2014.956904 (2014).
- 43 Li, C. *et al.* Trends in Chemical Composition of Global and Regional Population-Weighted Fine Particulate Matter Estimated for 25 Years. *Environ. Sci. Technol.* **51**, 11185-11195, doi:10.1021/acs.est.7b02530 (2017).
- 44 Xu, Q. *et al.* Nitrate dominates the chemical composition of PM<sub>2.5</sub> during haze event in Beijing, China. *Science of The Total Environment* **689**, 1293-1303, doi:<https://doi.org/10.1016/j.scitotenv.2019.06.294> (2019).
- 45 Zhao, L. *et al.* Changes of chemical composition and source apportionment of PM<sub>2.5</sub> during 2013–2017 in urban Handan, China. *Atmos. Environ.* **206**, 119-131, doi:<https://doi.org/10.1016/j.atmosenv.2019.02.034> (2019).



- 46 Huang, F. *et al.* Chemical characteristics and source apportionment of PM<sub>2.5</sub> in Wuhan, China. *Journal of Atmospheric Chemistry* **76**, 245-262, doi:10.1007/s10874-019-09395-0 (2019).
- 47 Zhang, H.-T. *et al.* [Spatial Temporal Characteristics and Cluster Analysis of Chemical Components for Ambient PM<sub>2.5</sub> in Wuhan]. *Huan Jing Ke Xue* **40**, 4764-4773, doi:10.13227/j.hjcx.201904069 (2019).
- 48 Zhang, Q. *et al.* Drivers of improved PM<sub>2.5</sub> air quality in China from 2013 to 2017. *P. Natl. Acad. Sci.* **116**, 24463, doi:10.1073/pnas.1907956116 (2019).
- 49 McNeill, J. *et al.* Large global variations in measured airborne metal concentrations driven by anthropogenic sources. *Scientific Reports* **10**, 21817, doi:10.1038/s41598-020-78789-y (2020).
- 50 Pandey, A., Shetty, N. J. & Chakrabarty, R. K. Aerosol light absorption from optical measurements of PTFE membrane filter samples: sensitivity analysis of optical depth measures. *Atmos. Meas. Tech.* **12**, 1365-1373, doi:10.5194/amt-12-1365-2019 (2019).
- 51 Dillner, A. M. & Takahama, S. Predicting ambient aerosol thermal-optical reflectance (TOR) measurements from infrared spectra: organic carbon. *Atmos. Meas. Tech.* **8**, 1097-1109, doi:10.5194/amt-8-1097-2015 (2015).
- 52 O'Brien, R. E. *et al.* Ultrasonic nebulization for the elemental analysis of microgram-level samples with offline aerosol mass spectrometry. *Atmos. Meas. Tech.* **12**, 1659-1671, doi:10.5194/amt-12-1659-2019 (2019).
- 53 Hoesly, R. M. *et al.* Historical (1750–2014) anthropogenic emissions of reactive gases and aerosols from the Community Emissions Data System (CEDS). *Geosci. Model Dev.* **11**, 369-408, doi:10.5194/gmd-11-369-2018 (2018).
- 54 McDuffie, E. E. *et al.* A global anthropogenic emission inventory of atmospheric pollutants from sector- and fuel-specific sources (1970–2017): an application of the Community Emissions Data System (CEDS). *Earth Syst. Sci. Data* **12**, 3413-3442, doi:10.5194/essd-12-3413-2020 (2020).
- 55 McDuffie, E. E. *et al.* *CEDS\_GBD-MAPS\_SourceCode\_2020\_v1.0*, (2020).
- 56 McDuffie, E. E. *et al.* CEDS\_GBD-MAPS: Global Anthropogenic Emission Inventory of NO<sub>x</sub>, SO<sub>2</sub>, CO, NH<sub>3</sub>, NMVOCs, BC, and OC from 1970-2017 (Version 2020\_v1.0). doi:<https://doi.org/10.5281/zenodo.3754964> (2020).
- 57 Crippa, M. *et al.* Gridded emissions of air pollutants for the period 1970–2012 within EDGAR v4.3.2. *Earth Syst. Sci. Data* **10**, 1987-2013, doi:10.5194/essd-10-1987-2018 (2018).
- 58 Amann, M. *et al.* Cost-effective control of air quality and greenhouse gases in Europe: Modeling and policy applications. *Environmental Modelling & Software* **26**, 1489-1501, doi:<https://doi.org/10.1016/j.envsoft.2011.07.012> (2011).
- 59 Klimont, Z. *et al.* Global anthropogenic emissions of particulate matter including black carbon. *Atmos. Chem. Phys.* **17**, 8681-8723, doi:10.5194/acp-17-8681-2017 (2017).
- 60 Keller, C. A. *et al.* HEMCO v1.0: a versatile, ESMF-compliant component for calculating emissions in atmospheric models. *Geosci. Model Dev.* **7**, 1409-1417, doi:10.5194/gmd-7-1409-2014 (2014).
- 61 Travis, K. R. *et al.* Why do models overestimate surface ozone in the Southeast United States? *Atmos. Chem. Phys.* **16**, 13561-13577, doi:10.5194/acp-16-13561-2016 (2016).

- 62 Vinken, G. C. M., Boersma, K. F., Jacob, D. J. & Meijer, E. W. Accounting for non-linear chemistry of ship plumes in the GEOS-Chem global chemistry transport model. *Atmos. Chem. Phys.* **11**, 11707-11722, doi:10.5194/acp-11-11707-2011 (2011).
- 63 Holmes, C. D., Prather, M. J. & Vinken, G. C. M. The climate impact of ship NO<sub>x</sub> emissions: an improved estimate accounting for plume chemistry. *Atmos. Chem. Phys.* **14**, 6801-6812, doi:10.5194/acp-14-6801-2014 (2014).
- 64 van der Werf, G. R. *et al.* Global fire emissions estimates during 1997–2016. *Earth Syst. Sci. Data* **9**, 697-720, doi:10.5194/essd-9-697-2017 (2017).
- 65 Mu, M. *et al.* Daily and 3-hourly variability in global fire emissions and consequences for atmospheric model predictions of carbon monoxide. *J. Geophys. Res. Atmos.* **116**, doi:10.1029/2011JD016245 (2011).
- 66 Philip, S. *et al.* Anthropogenic fugitive, combustion and industrial dust is a significant, underrepresented fine particulate matter source in global atmospheric models. *Environmental Research Letters* **12**, 044018, doi:10.1088/1748-9326/aa65a4 (2017).
- 67 Fairlie, D. T., Jacob, D. J. & Park, R. J. The impact of transpacific transport of mineral dust in the United States. *Atmos. Environ.* **41**, 1251-1266, doi:<https://doi.org/10.1016/j.atmosenv.2006.09.048> (2007).
- 68 Fairlie, T. D. *et al.* Impact of mineral dust on nitrate, sulfate, and ozone in transpacific Asian pollution plumes. *Atmos. Chem. Phys.* **10**, 3999-4012, doi:10.5194/acp-10-3999-2010 (2010).
- 69 Stettler, M. E. J., Eastham, S. & Barrett, S. R. H. Air quality and public health impacts of UK airports. Part I: Emissions. *Atmos. Environ.* **45**, 5415-5424, doi:<https://doi.org/10.1016/j.atmosenv.2011.07.012> (2011).
- 70 Murray, L. T., Jacob, D. J., Logan, J. A., Hudman, R. C. & Koshak, W. J. Optimized regional and interannual variability of lightning in a global chemical transport model constrained by LIS/OTD satellite data. *J. Geophys. Res. Atmos.* **117**, doi:10.1029/2012JD017934 (2012).
- 71 Hudman, R. C. *et al.* Steps towards a mechanistic model of global soil nitric oxide emissions: implementation and space based-constraints. *Atmos. Chem. Phys.* **12**, 7779-7795, doi:10.5194/acp-12-7779-2012 (2012).
- 72 Fischer, E. V., Jacob, D. J., Millet, D. B., Yantosca, R. M. & Mao, J. The role of the ocean in the global atmospheric budget of acetone. *Geophysical Research Letters* **39**, doi:10.1029/2011GL050086 (2012).
- 73 Millet, D. B. *et al.* Global atmospheric budget of acetaldehyde: 3-D model analysis and constraints from in-situ and satellite observations. *Atmos. Chem. Phys.* **10**, 3405-3425, doi:10.5194/acp-10-3405-2010 (2010).
- 74 Breider, T. J. *et al.* Multidecadal trends in aerosol radiative forcing over the Arctic: Contribution of changes in anthropogenic aerosol to Arctic warming since 1980. *J. Geophys. Res. Atmos.* **122**, 3573-3594, doi:10.1002/2016JD025321 (2017).
- 75 Riddick, S. N. *et al.* Global ammonia emissions from seabirds (NERC Environmental Information Data Centre). doi:<https://doi.org/10.5285/c9e802b3-43c8-4b36-a3a3-8861d9da8ea9> (2012).
- 76 Croft, B. *et al.* Contribution of Arctic seabird-colony ammonia to atmospheric particles and cloud-albedo radiative effect. *Nature Communications* **7**, 13444, doi:10.1038/ncomms13444 <https://www.nature.com/articles/ncomms13444#supplementary-information> (2016).

- 77 Carpenter, L. J. *et al.* Atmospheric iodine levels influenced by sea surface emissions of inorganic iodine. *Nature Geoscience* **6**, 108-111, doi:10.1038/ngeo1687 (2013).
- 78 Guenther, A. B. *et al.* The Model of Emissions of Gases and Aerosols from Nature version 2.1 (MEGAN2.1): an extended and updated framework for modeling biogenic emissions. *Geosci. Model Dev.* **5**, 1471-1492, doi:10.5194/gmd-5-1471-2012 (2012).
- 79 Liang, Q. *et al.* Finding the missing stratospheric Br<sub>y</sub>: a global modeling study of CHBr<sub>3</sub> and CH<sub>2</sub>Br<sub>2</sub>. *Atmos. Chem. Phys.* **10**, 2269-2286, doi:10.5194/acp-10-2269-2010 (2010).
- 80 Ordóñez, C. *et al.* Bromine and iodine chemistry in a global chemistry-climate model: description and evaluation of very short-lived oceanic sources. *Atmos. Chem. Phys.* **12**, 1423-1447, doi:10.5194/acp-12-1423-2012 (2012).
- 81 Lelieveld, J. *et al.* Effects of fossil fuel and total anthropogenic emission removal on public health and climate. *P. Natl. Acad. Sci.* **116**, 7192, doi:10.1073/pnas.1819989116 (2019).
- 82 Marais, E. A. *et al.* Air Quality and Health Impact of Future Fossil Fuel Use for Electricity Generation and Transport in Africa. *Environ. Sci. Technol.* **53**, 13524-13534, doi:10.1021/acs.est.9b04958 (2019).
- 83 Lacey, F. G. *et al.* Improving present day and future estimates of anthropogenic sectoral emissions and the resulting air quality impacts in Africa. *Faraday Discussions* **200**, 397-412, doi:10.1039/C7FD00011A (2017).
- 84 Chafe, Z. A. *et al.* Household Cooking with Solid Fuels Contributes to Ambient PM<sub>2.5</sub> Air Pollution and the Burden of Disease. *Environmental Health Perspectives* **122**, 1314-1320, doi:10.1289/ehp.1206340 (2014).
- 85 Wu, R. *et al.* Air quality and health benefits of China's emission control policies on coal-fired power plants during 2005–2020. *Environmental Research Letters* **14**, 094016, doi:10.1088/1748-9326/ab3bae (2019).
- 86 GBD MAPS Working Group. *Burden of Disease Attributable to Coal-Burning and Other Major Sources of Air Pollution in China. Special Report 20.* (Health Effects Institute [Available at: <https://www.healtheffects.org/publication/burden-disease-attributable-coal-burning-and-other-air-pollution-sources-china>], 2016).
- 87 GBD MAPS Working Group. *Burden of Disease Attributable to Major Air Pollution Sources in India. Special Report 21.*, (Health Effects Institute [Available at: <https://www.healtheffects.org/publication/gbd-air-pollution-india>], 2018).
- 88 Zheng, B. *et al.* Trends in China's anthropogenic emissions since 2010 as the consequence of clean air actions. *Atmos. Chem. Phys.* **18**, 14095-14111, doi:10.5194/acp-18-14095-2018 (2018).
- 89 Zhang, Z. *et al.* The contribution of residential coal combustion to PM<sub>2.5</sub> pollution over China's Beijing-Tianjin-Hebei region in winter. *Atmos. Environ.* **159**, 147-161, doi:<https://doi.org/10.1016/j.atmosenv.2017.03.054> (2017).
- 90 Liu, J. *et al.* Air pollutant emissions from Chinese households: A major and underappreciated ambient pollution source. *P. Natl. Acad. Sci.* **113**, 7756, doi:10.1073/pnas.1604537113 (2016).
- 91 Lelieveld, J., Evans, J. S., Fnais, M., Giannadaki, D. & Pozzer, A. The contribution of outdoor air pollution sources to premature mortality on a global scale. *Nature* **525**, 367, doi:10.1038/nature15371 (2015).
- 92 Gu, Y. *et al.* Impacts of sectoral emissions in China and the implications: air quality, public health, crop production, and economic costs. *Environmental Research Letters* **13**, 084008, doi:10.1088/1748-9326/aad138 (2018).

- 93 Hu, J. *et al.* Premature Mortality Attributable to Particulate Matter in China: Source Contributions and Responses to Reductions. *Environ. Sci. Technol.* **51**, 9950-9959, doi:10.1021/acs.est.7b03193 (2017).
- 94 Meng, J. *et al.* Source Contributions to Ambient Fine Particulate Matter for Canada. *Environ. Sci. Technol.* **53**, 10269-10278, doi:10.1021/acs.est.9b02461 (2019).
- 95 Caiazzo, F., Ashok, A., Waitz, I. A., Yim, S. H. L. & Barrett, S. R. H. Air pollution and early deaths in the United States. Part I: Quantifying the impact of major sectors in 2005. *Atmos. Environ.* **79**, 198-208, doi:<https://doi.org/10.1016/j.atmosenv.2013.05.081> (2013).
- 96 Fann, N., Fulcher, C. M. & Baker, K. The Recent and Future Health Burden of Air Pollution Apportioned Across U.S. Sectors. *Environ. Sci. Technol.* **47**, 3580-3589, doi:10.1021/es304831q (2013).
- 97 Penn Stefani, L. *et al.* Estimating State-Specific Contributions to PM<sub>2.5</sub>- and O<sub>3</sub>-Related Health Burden from Residential Combustion and Electricity Generating Unit Emissions in the United States. *Environmental Health Perspectives* **125**, 324-332, doi:10.1289/EHP550 (2017).
- 98 Thakrar, S. K. *et al.* Reducing Mortality from Air Pollution in the United States by Targeting Specific Emission Sources. *Environ. Sci. Tech. Lett.*, doi:10.1021/acs.estlett.0c00424 (2020).
- 99 Bond, T. C. *et al.* A technology-based global inventory of black and organic carbon emissions from combustion. *J. Geophys. Res. Atmos.* **109**, doi:10.1029/2003JD003697 (2004).
- 100 Butt, E. W. *et al.* The impact of residential combustion emissions on atmospheric aerosol, human health, and climate. *Atmos. Chem. Phys.* **16**, 873-905, doi:10.5194/acp-16-873-2016 (2016).
- 101 Crippa, M., Janssens-Maenhout, G., Guizzardi, D., Van Dingenen, R. & Dentener, F. Contribution and uncertainty of sectorial and regional emissions to regional and global PM<sub>2.5</sub> health impacts. *Atmos. Chem. Phys.* **19**, 5165-5186, doi:10.5194/acp-19-5165-2019 (2019).
- 102 Giannadaki, D., Pozzer, A. & Lelieveld, J. Modeled global effects of airborne desert dust on air quality and premature mortality. *Atmos. Chem. Phys.* **14**, 957-968, doi:10.5194/acp-14-957-2014 (2014).
- 103 Pozzer, A., Tsimpidi, A. P., Karydis, V. A., de Meij, A. & Lelieveld, J. Impact of agricultural emission reductions on fine-particulate matter and public health. *Atmos. Chem. Phys.* **17**, 12813-12826, doi:10.5194/acp-17-12813-2017 (2017).
- 104 Guo, H. *et al.* Effectiveness of ammonia reduction on control of fine particle nitrate. *Atmos. Chem. Phys.* **18**, 12241-12256, doi:10.5194/acp-18-12241-2018 (2018).
- 105 Anenberg, S., Miller, J., Henze, D. & Minjares, R. A global snapshot of the air pollution-related health impacts of transportation sector emissions in 2010 and 2015. *The International Council on Clean Transportation (ICCT)*. [Available at: <https://theicct.org/publications/health-impacts-transport-emissions-2010-2015> ] (2019).
- 106 Chambliss, S. E., Silva, R., West, J. J., Zeinali, M. & Minjares, R. Estimating source-attributable health impacts of ambient fine particulate matter exposure: global premature mortality from surface transportation emissions in 2005. *Environmental Research Letters* **9**, 104009, doi:10.1088/1748-9326/9/10/104009 (2014).
- 107 Silva Raquel, A., Adelman, Z., Fry Meridith, M. & West, J. J. The Impact of Individual Anthropogenic Emissions Sectors on the Global Burden of Human Mortality due to Ambient

- Air Pollution. *Environmental Health Perspectives* **124**, 1776-1784, doi:10.1289/EHP177 (2016).
- 108 Tsimpidi, A. P., Karydis, V. A. & Pandis, S. N. Response of Fine Particulate Matter to Emission Changes of Oxides of Nitrogen and Anthropogenic Volatile Organic Compounds in the Eastern United States. *Journal of the Air & Waste Management Association* **58**, 1463-1473, doi:10.3155/1047-3289.58.11.1463 (2008).
- 109 McDonald, B. C. *et al.* Volatile chemical products emerging as largest petrochemical source of urban organic emissions. *Science* **359**, 760, doi:10.1126/science.aag0524 (2018).
- 110 Corbett, J. J. *et al.* Mortality from Ship Emissions: A Global Assessment. *Environ. Sci. Technol.* **41**, 8512-8518, doi:10.1021/es071686z (2007).
- 111 Sofiev, M. *et al.* Cleaner fuels for ships provide public health benefits with climate tradeoffs. *Nature Communications* **9**, 406, doi:10.1038/s41467-017-02774-9 (2018).

## **Description of Additional Supplementary Data Files**

**File Name:** Supplementary Data 1

**Description:** Global, regional, national, and sub-national PM<sub>2.5</sub> exposure estimates and sector and disease-specific fractional contributions. Provides downscaled population weighted mean (PWM) national-level PM<sub>2.5</sub> exposure estimates for 200 sub-national areas, 204 countries and territories, and 21 world regions. This table also provides the total attributable deaths and the number of neonatal incidences associated with PWM PM<sub>2.5</sub> exposure levels in each country and region. Burden results are provided from both the 2019 Global Burden of Disease (GBD2019) concentration response relationships and the Global Exposure Mortality Model (GEMM). Also includes the fractional contributions (units of percent) of each source sector and disease to the total GBD2019 and GEMM disease burden estimates.

**File Name:** Supplementary Data 2

**Description:** Global, regional, national, and sub-national PM<sub>2.5</sub> exposure estimates and combustion fuel-type fractional contributions. Includes relative fuel-type contributions from the combustion of coal, solid biofuel, and the sum of oil and gas.

**File Name:** Supplementary Data 3

**Description:** Global, regional, national, and sub-national PM<sub>2.5</sub> exposure estimates for the year 2019.

**Data File 1: PM<sub>2.5</sub> Exposure Estimates, Sectoral Source Contributions, Total Attributable Mort**  
 McDuffie et al., 2021 -  
 Last Updated: March 23, 2021

Name Legend:

**Regions** Countries *Sub-national regions*

<b>Country Name</b>	<b>Population Weighted Annual Average PM<sub>2.5</sub> (<math>\mu\text{g m}^{-3}</math>)</b>	<b>Agriculture Contribution (%)</b>	<b>Energy Coal Contribution (%)</b>
<b>Central_Asia</b>	<b>27.5</b>	<b>5.1</b>	<b>6.1</b>
Armenia	31.9	12.8	5.2
Azerbaijan	23.9	8	3.2
<i>Baku</i>	<i>31.5</i>	<i>5.4</i>	<i>2.7</i>
Georgia	17.8	8.4	5.7
Kazakhstan	19	4.5	5.3
<i>Shymkent</i>	<i>38.1</i>	<i>3.4</i>	<i>4.3</i>
Kyrgyzstan	22.9	3.9	7.4
Mongolia	36.7	13.1	10.5
<i>Ulaanbaatar</i>	<i>81.4</i>	<i>13.5</i>	<i>12.8</i>
Tajikistan	35.9	3.6	6.2
Turkmenistan	25.5	4.2	2.3
Uzbekistan	32.5	3.6	7.1
<i>Bukhara</i>	<i>26.6</i>	<i>2.8</i>	<i>4.5</i>
<i>Tashkent</i>	<i>50.8</i>	<i>3.6</i>	<i>6.9</i>
<b>Central_Europe</b>	<b>20.5</b>	<b>18.6</b>	<b>10.7</b>
Albania	19.8	12.8	11.6
Bosnia_and_Herzegovina	29.8	16	17.8
Bulgaria	19.7	12.7	13.6
Croatia	18	15.4	8.6
Czech_Republic	16.8	23.3	7.9
Hungary	16.5	16.1	8.2
<i>Budapest</i>	<i>19.5</i>	<i>14.8</i>	<i>7.4</i>
Macedonia	31.6	13.2	18.4
Montenegro	21.6	10.5	14.5
Poland	22.7	24.6	8
<i>Warsaw</i>	<i>24.3</i>	<i>24.7</i>	<i>7.4</i>
Romania	15.9	12.8	11.2
Serbia	26.5	10.9	19.7
<i>Belgrade</i>	<i>25.7</i>	<i>10.6</i>	<i>26.3</i>
Slovakia	18.4	20.1	7.7
Slovenia	16.9	17.4	5

<b>Eastern_Europe</b>	<b>11.8</b>	<b>11.5</b>	<b>7.4</b>
Belarus	16.3	21.2	6.7
<i>Gomel</i>	<i>20.9</i>	<i>19.2</i>	<i>8</i>
Estonia	5.7	12.5	2.9
Latvia	11.7	15.3	3.8
Lithuania	10.2	18.8	4.7
<i>Kaunas</i>	<i>12</i>	<i>17.3</i>	<i>4.6</i>
Moldova	13.1	14.2	9.8
Russian_Federation	10.9	9	6.2
<i>Saint_Petersburg</i>	<i>8.2</i>	<i>9.2</i>	<i>3.3</i>
<i>Astrakhan</i>	<i>12.1</i>	<i>4.4</i>	<i>5.6</i>
<i>Moscow</i>	<i>13.8</i>	<i>7.8</i>	<i>5.2</i>
<i>Tyumen</i>	<i>13.4</i>	<i>9.9</i>	<i>4.7</i>
<i>Berezniki</i>	<i>13.9</i>	<i>9.6</i>	<i>5.4</i>
<i>Dzerzhinsk</i>	<i>11.6</i>	<i>10.7</i>	<i>5.5</i>
Ukraine	14	14.8	10.5
<i>Nikolaev</i>	<i>14.2</i>	<i>13.5</i>	<i>10.8</i>
<i>Rovno</i>	<i>19.9</i>	<i>19.5</i>	<i>8.4</i>
<b>Australasia</b>	<b>6.9</b>	<b>9.3</b>	<b>7</b>
Australia	7	8.8	8.1
<i>Sydney</i>	<i>7.6</i>	<i>12.6</i>	<i>14.4</i>
New_Zealand	6.6	12.5	0.7
<i>Auckland</i>	<i>6.5</i>	<i>10.5</i>	<i>0.6</i>
<b>High_income_Asia_Pacific</b>	<b>17.3</b>	<b>18.6</b>	<b>5.3</b>
Brunei	7.6	2.9	4
Japan	13.5	19.5	4
<i>Tokyo</i>	<i>15.1</i>	<i>20.4</i>	<i>3.1</i>
<i>Osaka</i>	<i>15.1</i>	<i>19</i>	<i>4.2</i>
<i>Fukuoka</i>	<i>17.7</i>	<i>18.1</i>	<i>5.1</i>
<i>Okayama</i>	<i>13.3</i>	<i>20.5</i>	<i>4.7</i>
<i>Yamaguchi</i>	<i>12.6</i>	<i>18.2</i>	<i>5</i>
South_Korea	26.6	18.5	6.1
<i>Seoul</i>	<i>27.4</i>	<i>17.5</i>	<i>6</i>
<i>Busan</i>	<i>24.3</i>	<i>18.9</i>	<i>5.6</i>
<i>Cheonan</i>	<i>28.6</i>	<i>19.3</i>	<i>6.5</i>
<i>Gwangju</i>	<i>27</i>	<i>19.8</i>	<i>6.3</i>
<i>Jinju</i>	<i>27.7</i>	<i>19.7</i>	<i>6.1</i>
<i>Pyongyang</i>	<i>52.9</i>	<i>16.4</i>	<i>5.8</i>
Singapore	18.5	4.2	16.9
<b>High_income_North_America</b>	<b>7.8</b>	<b>10.2</b>	<b>6.6</b>
Canada	7.3	12	3.1



<i>Montreal</i>	9.1	10.9	1.6
<i>Victoria</i>	6.3	6.5	0.6
Greenland	5.3	13.1	4
United_States	7.8	10	7
<i>Raleigh</i>	7.6	11.7	13
<i>New_York</i>	7.7	6.4	4.2
<i>Philadelphia</i>	8.6	10.5	5.8
<i>Houston</i>	9.9	6.9	7.7
<i>Minneapolis</i>	7.4	13.3	8.1
<i>Portland</i>	8	10.5	1.6
<i>Los_Angeles</i>	10.6	3.4	1.2
<i>Cleveland</i>	8.8	14.8	8.6
<i>Chicago</i>	9	12.3	7.9
<i>Springfield</i>	6.5	8.3	3.9
<i>Gainesville</i>	6.5	5.9	7.4
<i>Killeen</i>	7.4	11.7	8.9
<i>Modesto</i>	12.1	11.3	1
<b>Southern_Latin_America</b>	<b>15.3</b>	<b>5.8</b>	<b>2.7</b>
Argentina	13	5.7	1.6
<i>Buenos_Aires</i>	11.5	8.2	1.2
<i>Cordoba</i>	13.9	3	1.5
Chile	21.9	5.8	4.5
<i>Santiago</i>	28.9	4.6	4.7
Uruguay	9.8	7.5	1.7
<b>Western_Europe</b>	<b>11.7</b>	<b>21.7</b>	<b>3.7</b>
Andorra	8.8	16.3	2.6
Austria	12.1	20.7	5.1
<i>Vienna</i>	14.5	19.9	5.8
Belgium	12.8	29.2	2.4
<i>Antwerp</i>	14.1	28.4	2.7
Cyprus	15.2	7.8	16.6
Denmark	10.2	26.1	3.2
Finland	5.2	11.8	2.4
France	11.6	21.4	1.8
<i>Paris</i>	14	18.7	1.3
<i>Le_Mans</i>	13.6	25.5	1.4
Germany	11.9	28.5	4.9
<i>Berlin</i>	16	29.7	5.3
<i>Halle</i>	14.6	28.7	5.9
<i>Oldenburg</i>	13.2	33.3	3.7
Greece	14.6	9.8	14.7

<i>Thessaloniki</i>	15.9	13.8	16.5
Iceland	5.6	13.6	0.3
Ireland	7.7	25.6	1.4
Israel	19.7	9.9	10.2
<i>Tel_Aviv</i>	21.6	9.9	10.6
Italy	15.6	18.4	3.7
<i>Palermo</i>	15	5.7	5
<i>Milan</i>	23.4	21.6	1.9
Luxembourg	9.9	29	2.9
Malta	12.4	5.8	4.3
Netherlands	12.4	29.3	3.2
<i>Zwolle</i>	11.8	31.5	3.5
Norway	6.5	10.2	1.6
Portugal	8.6	14.2	1.8
Spain	9.9	13.5	2.7
<i>Madrid</i>	10.1	9.9	2.1
<i>Toledo</i>	8.5	14.8	8.1
Sweden	5.7	16.2	2.4
Switzerland	10.2	20.1	2.4
<i>Lausanne</i>	12.3	19.2	2.2
United_Kingdom	10.5	26.6	1.8
<i>Sheffield</i>	11.6	27.5	2.2
<i>London</i>	13	25.3	1.6
<i>Manchester</i>	11	26.8	1.8
Monaco	11.4	23.5	2.3
San_Marino	9.8	20.6	4.4
<b>Andean_Latin_America</b>	<b>25.9</b>	<b>7.5</b>	<b>0.4</b>
Bolivia	26	2.5	0.4
<i>Cochabamba</i>	26.2	1.7	0.3
Ecuador	18.8	8.7	0.1
<i>Quito</i>	17.6	8.6	0
Peru	29.6	8.7	0.5
<b>Caribbean</b>	<b>16.5</b>	<b>2.8</b>	<b>1.5</b>
Antigua_and_Barbuda	16.2	1.2	0.7
The_Bahamas	13.9	1.4	2.5
Barbados	19.6	0.1	0
Belize	19.3	1.5	0.8
Bermuda	7	0.8	3.3
Cuba	17.5	2.2	1.2
<i>Holguin</i>	15.5	2.7	0.9
Dominica	16.8	1.3	0.9

Dominican_Republic	16.8	4.1	2.2
Grenada	19.4	0.1	0
Guyana	20.5	0.1	0
Haiti	17.8	3.2	1.8
Jamaica	15.2	2.6	1
Puerto_Rico	7	2.4	0.6
Saint_Lucia	19.4	0.1	0.1
Saint_Vincent_and_the_Grenadines	19.4	0.1	0
Suriname	21.9	0	0
Trinidad_and_Tobago	19.5	0.1	0
Virgin_Islands_US	8.8	1	0.6
Saint_Kitts_and_Nevis	8.4	1.4	0.7
<b>Central_Latin_America</b>	<b>20.8</b>	<b>5.8</b>	<b>2.3</b>
Colombia	21.3	2.7	1.2
<i>Bogota</i>	<i>30.5</i>	<i>3.7</i>	<i>1.6</i>
<i>Valledupar</i>	<i>22.2</i>	<i>3.2</i>	<i>0.4</i>
Costa_Rica	17.3	6.2	0.2
El_Salvador	22.6	5.6	2.7
<i>San_Salvador</i>	<i>22.9</i>	<i>5.6</i>	<i>3</i>
Guatemala	27.3	3.1	1.3
<i>Guatemala_City</i>	<i>33.5</i>	<i>4.2</i>	<i>1.6</i>
Honduras	22.3	4.3	0.8
Mexico	20.1	8.5	3.6
<i>Culiacan</i>	<i>18.6</i>	<i>1.1</i>	<i>2.7</i>
<i>Guadalajara</i>	<i>18.9</i>	<i>9.1</i>	<i>3.2</i>
<i>Mexico_City</i>	<i>24.3</i>	<i>9.7</i>	<i>3</i>
<i>Reynosa</i>	<i>20.2</i>	<i>5.6</i>	<i>6.4</i>
<i>Tijuana</i>	<i>17.6</i>	<i>4.8</i>	<i>1.2</i>
Nicaragua	19.1	5	0.3
<i>Leon</i>	<i>19.9</i>	<i>4.9</i>	<i>0.2</i>
Panama	13.7	3.6	0.3
Venezuela	20.3	2.5	0.1
<i>Caracas</i>	<i>19.4</i>	<i>3.2</i>	<i>0</i>
<i>Cabimas</i>	<i>21.6</i>	<i>3.1</i>	<i>0.1</i>
<b>Tropical_Latin_America</b>	<b>11.8</b>	<b>4.1</b>	<b>1</b>
Brazil	11.8	4.2	1
<i>Sao_Paulo</i>	<i>15.3</i>	<i>5.5</i>	<i>1</i>
<i>Curitiba</i>	<i>8.9</i>	<i>5.8</i>	<i>0.8</i>
<i>Florianopolis</i>	<i>12.8</i>	<i>8.9</i>	<i>5.4</i>
<i>Belo_Horizonte</i>	<i>13.2</i>	<i>8.2</i>	<i>0.7</i>
<i>Palmas</i>	<i>10.4</i>	<i>0.3</i>	<i>0.1</i>

<i>Ilheus</i>	13.6	1.1	0.2
<i>Jequie</i>	13.3	1.8	0.3
<i>Ribeirao_Preto</i>	14.5	6.2	1
Paraguay	12.5	1.4	0.5
<b>North_Africa_and_Middle_East</b>	<b>44.1</b>	<b>5.7</b>	<b>4.4</b>
Afghanistan	50.8	5.2	6.6
<i>Kabul</i>	64.5	5.9	11.9
Algeria	31.6	4.6	1.6
<i>Algiers</i>	34	4.1	1.8
<i>Tebessa</i>	33.3	6.6	1.8
Bahrain	60.8	2.9	1.1
Egypt	65.8	5.6	5.4
<i>Cairo</i>	80.9	6.3	5.3
<i>Alexandria</i>	56.7	6.5	7.4
Iran	38.3	8.1	1.7
<i>Tehran</i>	36.3	11.4	1.4
<i>Ahvaz</i>	71.1	5.3	1.8
<i>Gorgan</i>	39.6	11.8	1.8
<i>Qom</i>	41.6	10.3	1.5
Iraq	48.6	5.1	3.4
<i>Baghdad</i>	58.2	4.9	3.3
Jordan	32.1	8.9	8.9
Kuwait	63.1	3.5	1.5
Lebanon	28.5	8.7	9.2
Libya	36.2	1.5	2.1
Morocco	34	3.4	1.8
<i>Marrakesh</i>	44	1.7	1.1
Palestine	32.6	9.8	9.7
Oman	42.6	1.7	0.9
Qatar	71.6	2.8	1
Saudi_Arabia	61.5	2.7	1.6
<i>Riyadh</i>	67.7	2.6	1.2
Sudan	50	0.7	1.1
<i>Khartoum</i>	61.2	0.5	1.1
Syria	31.1	8.9	9.1
Tunisia	29.3	3.8	2.2
<i>Kairouan</i>	35.4	4.5	2.1
Turkey	26.1	15.3	14.7
<i>Istanbul</i>	26	14.7	13.3
<i>Malatya</i>	32.7	15.2	16
<i>Kayseri</i>	37.5	16.2	12.5

United_Arab_Emirates	42.7	2.8	0.7
Yemen	44.1	2.2	1.5
<i>Sana</i>	44.7	2.2	1.5
<b>South_Asia</b>	<b>76.1</b>	<b>9.5</b>	<b>6.5</b>
Bangladesh	61.9	11.8	6.4
<i>Rajshahi</i>	55.8	11.8	8.2
<i>Dhaka</i>	69.6	11.9	6.2
<i>Saidpur</i>	61.4	12.2	6.1
Bhutan	38.8	10.2	4.7
India	80.2	9.4	7
<i>Jaipur</i>	102.8	8.7	5.3
<i>Ahmedabad</i>	131.5	6.1	7.5
<i>Kanpur</i>	152.3	9.4	6.8
<i>Kolkata</i>	85.8	8.9	7.4
<i>Mumbai</i>	60	7	7.6
<i>Pune</i>	57	9.4	6.5
<i>Hyderabad</i>	47.6	6.6	8.5
<i>Belgaum</i>	44.6	6.7	8.4
<i>Coimbatore</i>	41.2	6.2	6.3
<i>Hindupur</i>	41.3	6.3	9.2
<i>Jalna</i>	52.8	8.4	10.1
<i>Kozhikode</i>	34.8	3.7	5.1
<i>Malegaon</i>	57	7.8	10.3
<i>Parbhani</i>	41.7	8.3	10.6
<i>Singrauli</i>	153.2	11.6	13.9
<i>Sitapur</i>	136.5	10.9	6.5
<i>Vijayawada</i>	56.2	6.4	9.4
Nepal	79.3	9.2	4.4
<i>Pokhara</i>	74.6	8.1	3.8
Pakistan	59.7	8.5	2.8
<i>Karachi</i>	70.8	3.9	2.4
<i>Lahore</i>	72.5	9.1	2.2
<i>Sialkot</i>	66	10.7	2.9
<b>East_Asia</b>	<b>49.3</b>	<b>11.1</b>	<b>4.7</b>
China	49.8	11	4.7
<i>Chengdu</i>	63.9	10.4	2
<i>Qingdao</i>	46.8	13.5	5.9
<i>Taipei</i>	22	10.4	4
<i>Shanghai</i>	46.2	9.4	3.5
<i>Wuhan</i>	64.6	10.4	3.3
<i>Hangzhou</i>	54.1	9.9	3.5

<i>Guangzhou</i>	39.9	6.2	3.7
<i>Beijing</i>	71.8	13.7	5.4
<i>Tangshan</i>	73.4	14.2	6
<i>Tianjin</i>	71.7	12.4	5.5
<i>Jinan</i>	70.4	12.9	5.8
<i>Zhengzhou</i>	82.7	11	4.7
<i>Hong_Kong</i>	23.5	4.3	4.2
<i>Anqing</i>	55.4	11.1	4
<i>Bicheng</i>	54.4	8.9	3.1
<i>Changzhi</i>	72.2	13	6.2
<i>Changzhou</i>	56.1	9.4	3.9
<i>Chengguan</i>	37.3	10.4	6.6
<i>Gaoyou</i>	54.7	12.1	4.6
<i>Guixi</i>	48.9	7.9	2.8
<i>Haikou</i>	22.4	4.9	4.3
<i>Kaiping</i>	39	8.1	4.5
<i>Leshan</i>	58.8	10.2	2.4
<i>Pingxiang</i>	54.3	9.1	3.3
<i>Shenzhen</i>	32.4	4.4	4.1
<i>Suining</i>	51.2	8.2	3.4
<i>Xingping</i>	68.4	8.8	4.6
<i>Xucheng</i>	56.1	13	4.7
<i>Yanggu</i>	73.6	12.7	5.8
<i>Yiyang</i>	51.1	9.9	3.5
<i>Yucheng</i>	34.9	10.4	4.6
<i>Zhuji</i>	49.4	9.6	3.3
<i>Zunyi</i>	45.4	10.6	3.9
<i>Yulin</i>	40.7	7.6	3.3
North_Korea	41.8	16.7	6.4
Taiwan	23.9	11.5	4.1
<b>Oceania</b>	<b>12.7</b>	<b>0.6</b>	<b>0.4</b>
American_Samoa	6.1	0.2	0
Federated_States_of_Micronesia	9.1	0	0.1
Fiji	9.8	1.9	0.2
<i>Suva</i>	-	-	-
Guam	7.6	0	0.1
Kiribati	7.6	0	0
Marshall_Islands	8.6	0	0.1
Northern_Mariana_Islands	7.8	0.1	0.2
Papua_New_Guinea	13.3	0.6	0.4
Samoa	9.6	0.3	0

Solomon_Islands	10.7	0.2	0.3
Tonga	9.6	0.2	0.2
Vanuatu	11.1	0.9	0.8
Niue	6.4	0	0.1
Cook_Islands	6.1	0.1	0.1
Nauru	5.6	0	0
Palau	6.7	0.4	3.3
Tokelau	7	0	0
Tuvalu	5.7	0	0
<b>Southeast_Asia</b>	<b>20.1</b>	<b>4.5</b>	<b>5.9</b>
Cambodia	21.2	1.3	2.3
Indonesia	18	6.6	8.3
<i>Medan</i>	<i>34.6</i>	<i>2.5</i>	<i>3.1</i>
<i>Palembang</i>	<i>25.6</i>	<i>2.3</i>	<i>8.6</i>
<i>Cirebon</i>	<i>21.4</i>	<i>8.7</i>	<i>12.1</i>
<i>Parepare</i>	<i>14.4</i>	<i>1.3</i>	<i>2.5</i>
<i>Pematangsiantar</i>	<i>25.2</i>	<i>3.3</i>	<i>3.7</i>
Laos	18.5	4.9	3.8
Malaysia	16.2	3.3	7.6
<i>Ipoh</i>	<i>17.5</i>	<i>7.1</i>	<i>8</i>
<i>Rawang</i>	<i>17.2</i>	<i>4.5</i>	<i>6.6</i>
Maldives	9.9	2.6	5
Mauritius	14.7	0.8	2.6
Myanmar	28.5	3.6	5.4
<i>Myeik</i>	<i>22.7</i>	<i>2.2</i>	<i>3.3</i>
Philippines	18.4	3.4	5.8
<i>Manila</i>	<i>27.4</i>	<i>4</i>	<i>5.1</i>
<i>Bacolod</i>	<i>19.7</i>	<i>1.5</i>	<i>5.8</i>
<i>Cebu_City</i>	<i>22.4</i>	<i>2.6</i>	<i>7</i>
Sri_Lanka	19.6	2.4	4.5
Seychelles	15.4	0.2	1.2
Thailand	26.4	2.7	3.6
<i>Bangkok</i>	<i>30.4</i>	<i>1.7</i>	<i>2.7</i>
Timor_Leste	15.3	2.2	0.8
Vietnam	20	4.3	3.7
<i>Vinh_Long</i>	<i>23.7</i>	<i>2.3</i>	<i>2.5</i>
<i>Ho_Chi_Minh_City</i>	<i>27.1</i>	<i>1.9</i>	<i>2.7</i>
<b>Central_Sub_Saharan_Africa</b>	<b>32.2</b>	<b>0.2</b>	<b>0.4</b>
Angola	27	0.3	1.3
<i>Luanda</i>	<i>31.2</i>	<i>0.2</i>	<i>0.8</i>
Central_African_Republic	41.3	0.5	0.2

Congo	35.2	0.1	0.2
Democratic_Republic_of_the_Congo	33	0.2	0.3
<i>Kinshasa</i>	<i>39.4</i>	<i>0.1</i>	<i>0.2</i>
<i>Lubumbashi</i>	<i>27.4</i>	<i>0.8</i>	<i>0.7</i>
Equatorial_Guinea	41.3	0	0.1
Gabon	33.3	0	0.1
<b>Eastern_Sub_Saharan_Africa</b>	<b>28.5</b>	<b>0.5</b>	<b>1.2</b>
Burundi	31.5	0.1	0.2
Comoros	16.1	0.4	1.7
Djibouti	41.1	2.2	1.5
Eritrea	41.6	1.9	1.3
Ethiopia	32.6	0.9	0.8
<i>Addis_Ababa</i>	<i>31.5</i>	<i>0.6</i>	<i>0.7</i>
Kenya	24.4	0.2	0.6
<i>Nakuru</i>	<i>23.8</i>	<i>0.1</i>	<i>0.5</i>
Madagascar	17.5	0.4	1.9
Malawi	23.1	0.7	2.5
Mozambique	21.4	0.9	7
<i>Beira</i>	<i>24.2</i>	<i>0.6</i>	<i>7.8</i>
Rwanda	33.8	0.2	0.2
<i>Kigali</i>	<i>34.8</i>	<i>0.2</i>	<i>0.2</i>
Somalia	28.8	0.8	1.2
South_Sudan	36.4	0.3	0.4
Tanzania	24.6	0.2	0.9
<i>Arusha</i>	<i>23.1</i>	<i>0.1</i>	<i>0.9</i>
Uganda	36.7	0.2	0.3
<i>Kampala</i>	<i>48.5</i>	<i>0.1</i>	<i>0.2</i>
Zambia	24.9	0.8	2.4
<i>Ndola</i>	<i>26</i>	<i>0.9</i>	<i>1.4</i>
<b>Southern_Sub_Saharan_Africa</b>	<b>27</b>	<b>4.6</b>	<b>18.3</b>
Botswana	24.3	3.4	21.1
Lesotho	29.4	5.5	15.6
Namibia	24.4	1.1	7.5
South_Africa	28.8	5.5	20.5
<i>Port_Elizabeth</i>	<i>23.9</i>	<i>3.1</i>	<i>5.9</i>
<i>Johannesburg</i>	<i>40.2</i>	<i>6.7</i>	<i>26.1</i>
Eswatini	23.1	6.5	32.4
Zimbabwe	21.7	1.1	8.9
<b>Western_Sub_Saharan_Africa</b>	<b>59.4</b>	<b>0.1</b>	<b>0.2</b>
Benin	42.6	0.1	0.1
Burkina_Faso	50.4	0	0.2



Cameroon	58.9	0.1	0.2
Cape_Verde	46.4	0.1	0.1
Chad	55.3	0.2	0.5
Cote_d'Ivoire	52.1	0.1	0.1
The_Gambia	58.6	0.1	0.1
Ghana	54	0.1	0.1
<i>Accra</i>	<i>64.3</i>	<i>0.1</i>	<i>0.1</i>
Guinea	50.4	0.1	0.1
Guinea_Bissau	54.6	0.1	0.1
Liberia	46.5	0.1	0.1
Mali	56.5	0	0.2
<i>Bamako</i>	<i>56.3</i>	<i>0</i>	<i>0.2</i>
Mauritania	64.3	0	0.1
Niger	70.9	0.1	0.2
Nigeria	64.2	0.1	0.2
<i>Ibadan</i>	<i>38.9</i>	<i>0.2</i>	<i>0.1</i>
<i>Lagos</i>	<i>34.2</i>	<i>0.1</i>	<i>0.1</i>
<i>Gombe</i>	<i>79.1</i>	<i>0.1</i>	<i>0.2</i>
<i>Oyo</i>	<i>41.1</i>	<i>0.2</i>	<i>0.1</i>
Sao_Tome_and_Principe	29.5	0	0.3
Senegal	60.5	0.1	0.1
Sierra_Leone	48.2	0.1	0.1
Togo	44.4	0.1	0.1
<b>Global</b>	<b>41.7</b>	<b>8.3</b>	<b>5.1</b>

**mortality Estimates, and Fractional Disease Contributions**

<b>Energy NonCoal Contribution (%)</b>	<b>Industry Coal Contribution (%)</b>	<b>Industry NonCoal Contribution (%)</b>	<b>NonRoad Transport Contribution (%)</b>	<b>Road Transport Contribution (%)</b>
<b>4.8</b>	<b>2.1</b>	<b>4.8</b>	<b>0.2</b>	<b>5.3</b>
4.6	1.3	8.2	0.2	9
5.4	0.7	4.9	0.2	7.2
4.9	0.5	3.6	0.2	5.5
3.3	2.1	5.2	0.2	7.4
5	3	6	0.2	5.1
4.8	2.4	3.9	0.2	4.9
4.2	2.7	5.1	0.2	6.6
4.7	5.3	4.7	0.7	3.7
4.7	5.9	4.9	0.7	3.5
4.3	1.3	3.4	0.1	4.5
4.3	0.4	3.7	0.1	5.1
5	2.2	4.7	0.2	4.8
5.4	0.7	2.8	0.1	3.5
5	4.3	7.2	0.2	5.6
<b>5.7</b>	<b>1.7</b>	<b>4.8</b>	<b>0.7</b>	<b>7.7</b>
2.5	1.4	4.2	0.9	6.6
4.2	1.1	3.5	0.6	6.6
3.4	1.3	5.7	0.5	6.1
5	1	5.1	1	9.8
7.8	1.9	5.6	0.9	8.8
7.4	1.4	4.9	0.7	8.8
7.4	1.4	4.9	0.7	8.3
2.4	1	4	0.4	4.6
2.6	0.8	3	0.5	5
6.9	2.1	4.8	0.8	8.5
5.3	2.5	4.6	0.7	8.8
4.8	1.4	4.9	0.6	6.8
3.1	1.1	3.7	0.4	5
3.2	1.3	3.9	0.3	4.5
7.8	2	5.2	0.7	8.3
6	0.9	6.6	1.2	12.6

<b>8.8</b>	<b>1.3</b>	<b>5.5</b>	<b>0.6</b>	<b>6</b>
10.7	2.7	4.4	1.1	8.3
8.4	2.3	5	1	7.8
14.2	0.8	6.7	0.8	5.7
12.9	1	5.4	1.1	7.1
17.6	1.3	4.1	1.1	8
24.5	1.3	3.7	0.9	7.5
5.6	1.6	3.9	0.7	7.3
8.7	1	6.2	0.5	5.4
13.8	0.8	9.3	0.8	6.6
5	0.8	3.2	0.2	3
12.2	0.4	9.6	0.3	4.6
8.7	0.9	7.2	0.3	6.1
9.1	0.6	6.1	0.3	5.5
7.5	0.5	4.9	0.7	7.3
8	1.7	4	0.6	6.6
8.3	1.6	3.9	0.8	5.9
5.8	2.1	4.2	0.7	8.6
<b>1.1</b>	<b>1.2</b>	<b>6.2</b>	<b>0.4</b>	<b>4.3</b>
1.1	1	6.6	0.4	4
1.6	1	7.6	0.3	3.7
1	2.9	3.8	0.3	6.5
1.6	2.8	4.4	0.3	6
<b>6</b>	<b>7.3</b>	<b>8.4</b>	<b>1.5</b>	<b>8.9</b>
4.2	1.5	3.4	0.6	12.5
6.3	6.1	7.8	1.7	8
6.8	5.2	8.9	1.5	8.3
6.3	6.6	8.8	1.7	7.9
5.5	7.6	7.1	1.9	7.1
6.7	7	6.9	1.7	8.3
5.9	7.5	7.3	1.6	7.4
5.4	9.2	9.4	1.4	9.3
5.3	9.7	9.8	1.2	9
5.7	8.4	10.9	1.7	8.9
5.6	8.9	9.1	1.3	9.7
5.6	8.9	8.5	1.5	10.8
5.4	8.7	7.8	1.6	10.7
5	15.1	8	1.2	7.6
9.3	1.5	3.5	0.2	18.3
<b>5.1</b>	<b>2</b>	<b>9.1</b>	<b>3.2</b>	<b>11.7</b>
7.5	0.6	10.2	2.2	7.6

8.7	0.7	13.8	1.8	7.4
5.8	0.7	12.3	2.9	7.2
2.3	0.8	2.5	2.1	7.6
4.9	2.1	9	3.3	12.1
4.6	2	6.5	3.6	14
4.4	2.4	15.9	2.8	10.5
6.3	1.9	11.2	3.3	11.7
10.4	2	8.1	2.8	11.8
5.7	1.4	7.1	5.4	14.6
1.6	2.1	13	2.8	10.1
3.2	3.9	18.3	1.4	8.6
5.7	1.7	8	4	11.7
5.8	2	10.7	4.9	12.6
4	1.5	10.2	2.9	12.8
3.5	1.8	6.8	3.1	11.9
7.1	2.1	6.5	3.2	15.3
2.6	4.2	10.3	1.9	8.5
<b>3.1</b>	<b>0.3</b>	<b>11.6</b>	<b>0.3</b>	<b>7.7</b>
3.7	0.2	11.1	0.4	9
5.5	0.2	17.7	0.4	10.5
2.5	0.2	6.8	0.2	10.2
2.1	0.2	11.7	0.3	5.6
2.6	0.3	16.8	0.1	5.7
5.6	0.4	18.3	0.3	10
<b>6.3</b>	<b>1.1</b>	<b>7.1</b>	<b>1.5</b>	<b>10.4</b>
4.1	0.7	6.7	1.5	11.6
8.4	1.5	8.2	1.1	12
8	1.4	8.1	0.9	10.2
9.1	1.3	8.1	1.5	9.6
11.8	1.2	7.7	1.5	9.2
3.3	2.3	4.4	0.5	5.4
7.1	0.8	5.7	2.3	8.4
9.8	1	9.8	0.7	5.4
5	1.2	7.2	1.4	11.8
4.2	1.6	9.4	1.1	9.9
4.2	0.9	5.5	2	12.4
7.9	1.7	8.7	1.5	10.7
6.5	1.8	9.3	1.7	9.5
8.6	1.7	8.2	1.6	11.3
7.8	1.1	6	1.7	8.5
3.3	1.4	5.1	1.1	5.6

3.4	1.2	4.8	0.8	6.1
0.7	0.5	6	0.3	1.6
2.7	0.4	3.8	1.3	6.2
9.7	1.1	4.5	0.3	7.1
9.6	1.1	4.6	0.4	7.2
5	0.6	4.9	1.6	12.8
3.3	0.7	3.7	1.2	7
4.5	0.5	5.5	1.3	14.3
6	1.8	8.8	1.4	13.3
2.7	0.5	2.8	0.8	5.7
7.6	1.2	7.6	1.8	10.6
6.8	1.1	7	1.9	10.7
5	1	8.3	1.1	4.4
3.8	0.2	7.1	0.7	6.8
4.9	0.5	9.5	2	9.4
4.3	0.8	16.5	1.2	9.5
6.1	1.5	8.1	4.9	12.4
10	0.8	8.8	1.4	6.5
6.9	1.5	8.2	1.3	14.7
10.7	1.3	7.5	1.2	14.2
6.8	1.1	6.8	1.7	8.9
8.6	1.3	7	1.4	8.4
6.1	1.2	8.2	1.6	9.6
7.7	1.2	6.3	1.5	8.3
4.2	0.7	5.1	1.2	12.5
5	0.7	5.2	2.3	12.3
<b>3.5</b>	<b>0.4</b>	<b>22.5</b>	<b>0.1</b>	<b>8.2</b>
0.5	0.1	12.7	0	3.1
0.4	0	11.4	0	2.8
11.8	0.2	8.8	0.2	17.9
12.7	0.2	8	0.6	18.7
1.7	0.5	30.1	0.1	6.5
<b>9.7</b>	<b>0.4</b>	<b>9.1</b>	<b>0.4</b>	<b>5.5</b>
3.6	-0.1	1.5	0.1	5.5
6.1	1	5.1	1	6.3
0.5	0	0.2	0	0.8
5.2	0.5	4.1	0.3	6.3
2.7	0.8	3.3	1.1	5.9
9.9	0.5	19.7	0.6	5.7
16.7	0.3	11.6	0.4	4.8
3.8	-0.1	1.7	0.1	5.7

9.6	0.5	7.8	0.6	6.5
0.5	0	0.2	0	1
0.6	0	0.4	0.1	0.8
13	0.3	4	0.4	5.6
15.3	0.4	7.1	0.2	8.1
3	-0.2	2.1	0.1	4.5
0.8	0	0.3	0.1	1
0.7	0	0.3	0.1	1
0.6	0	0.4	0.1	0.8
0.7	0	0.3	0	1.4
3.3	-0.2	1.5	0.1	4.9
3.7	-0.1	1.6	0.1	5.5
<b>8.5</b>	<b>2.4</b>	<b>7.1</b>	<b>0.3</b>	<b>9.8</b>
3.4	7.9	9.1	0	9.1
2.8	12.3	12.4	0	8.5
5.5	0.8	6.5	0	10.8
2.8	0.1	5.6	0.1	6.9
11.2	0.1	4.3	0.1	6.5
11.1	0.1	4.4	0	6.5
5.4	0.1	4.2	0	5.5
4.6	0.1	7.1	0	5
8.8	0.4	4.8	0.1	7.8
12.4	1.6	8.1	0.5	12.3
5	0.9	3.5	1	17.2
9.1	1.9	10.3	0.2	15.8
10.9	1.8	12.1	0.2	12.2
11.7	1.6	5	2.6	12
2.9	2.9	11.7	2	11
7.1	0.1	2.1	0.2	5.5
8.3	0.1	1.9	0.3	5.9
3.4	0.2	2.6	0	8
4	0.4	4.6	0	6.6
4.3	0.2	5.1	0	4.9
5.4	0.3	5.9	0	10.7
<b>4.6</b>	<b>1.7</b>	<b>25.2</b>	<b>0.2</b>	<b>6.3</b>
4.6	1.8	25.6	0.2	6.3
8.4	2.3	42.1	0.2	6.8
6.9	2.6	35.8	0.3	8.2
8.3	1.7	24.6	0.3	7.9
3.6	3.6	40.7	0.2	5.5
0.6	0.5	3.6	0.1	2.4

1.1	0.6	6.5	0	3.6
1.5	1.3	12.6	0.1	5
4.9	2.3	30.7	0.3	10.3
2.8	0.6	13.4	0.2	7.5
<b>7.4</b>	<b>0.8</b>	<b>4.4</b>	<b>0.3</b>	<b>7</b>
5	2.2	2.7	0.1	6.2
4.8	2.8	2.3	0.1	6.7
3	0.2	3.9	0.6	17.1
3.4	0.2	6	0.8	23.3
2.7	0.2	3.5	0.5	14.3
22.9	0.4	5.7	0	6.9
6.3	0.6	4.7	0.5	5.8
6.9	0.6	5.2	0.5	6.3
6.7	0.8	4.5	0.6	5
9.8	0.4	5.2	0.1	11
7.8	0.4	6.7	0.1	14.4
15.9	0.3	4.1	0.1	8.6
7.5	0.4	6.2	0.1	12.2
8.8	0.4	6	0.1	13.8
11.1	0.6	3.7	0.1	9
11.4	0.5	3.9	0.1	8.9
9.4	1	4.4	0.3	6.8
15.2	0.3	3.6	0	6.1
11.6	1.4	4.2	0.3	6
1.2	0.2	1.1	0.2	3.3
1.6	0.1	2.7	0.3	5.4
0.8	0	1.8	0.1	3.5
9.4	1	4.5	0.3	7.1
8.5	0.8	4.4	0	3.6
20.9	0.4	5.4	0	6.4
13.8	0.4	6.8	0.1	5.1
13.6	0.3	6.9	0	5.8
4.4	0.2	2.4	0.1	2.4
4.3	0.2	2.6	0.1	2.4
8.3	1.7	4.2	0.3	6.7
3.4	0.3	4.1	0.5	9.6
3.2	0.3	3.8	0.5	10.6
3.2	3	5.2	0.5	7.4
3.1	4.4	7.5	0.7	6.8
3.5	1.9	3.3	0.4	7.9
2.7	2.8	4.5	0.3	8.1

14.6	1	5.9	0	5.3
11.7	0.8	5	0.1	3.9
12.5	0.8	5.1	0.1	4
<b>5.5</b>	<b>8</b>	<b>6.3</b>	<b>1</b>	<b>6</b>
6	6.7	5.6	1.6	7.2
6.2	7.8	7.3	1.1	5.2
5.6	6.2	5.2	2	7.5
4.4	7.8	6.7	1	6.1
3.5	8.2	5.7	1.1	4.3
5.5	8.2	6.6	1	5.7
4.8	7.4	4.8	1.3	8
6.1	6.2	5.5	0.8	6
4.7	8.1	6.1	1.2	6
6.3	10.7	12	0.6	3.4
5.6	10.2	9.9	1	4.3
4.2	9.8	10.1	1	4.5
4.6	8.5	6.6	1.3	5
5	7.6	5	1.6	7.6
4	8.5	7.5	0.7	5.4
5.7	7.5	4.7	1.6	6
5.2	7.6	5.2	1.4	5.5
4.1	8.8	7.1	1	5.1
6.1	7.3	5.2	1.2	5.3
5.5	7.8	5.2	1.5	5.4
12.4	5.5	4.2	0.9	3.9
4.5	7.4	5.1	1	6.6
6.5	8.7	7	1.4	4.5
3.3	8.3	4.5	0.7	5.3
2.8	6	3	0.7	5.4
5.7	7.5	4.1	0.7	8.6
6.6	7.7	6.9	0.5	6.5
5.2	9.1	6.5	0.9	9.5
4.9	8.6	4.4	1	9.9
<b>4.9</b>	<b>9.1</b>	<b>5.2</b>	<b>1.4</b>	<b>6.2</b>
4.8	9.1	5.2	1.4	6.2
2.3	13.5	4.8	0.9	5.5
4.1	11.2	4.6	1.4	7.1
7.6	8.1	6.3	0.8	8.1
7.5	11.3	10.1	0.6	5.4
6.2	11.3	5.7	1.6	6
4.2	8.7	7.3	0.6	6.9



3.3	9	4.8	1.5	6.9
6.3	9.8	4.4	1.2	8.8
5	9.1	4.1	1.2	7.9
4.6	8.8	4.2	1.4	8.7
4.1	10.5	4.4	1.5	6.1
4.9	8.8	4.5	1.1	5.5
3.2	9.1	6.1	0.8	6.8
4.6	9.3	5.9	1.7	5.8
3.5	10.4	3.4	1.8	6.9
9	7.2	4	1	5.2
3.8	8.5	6.6	1	6.4
4.1	6.5	3.7	1.5	4.3
4	9.9	5.8	1.8	6.8
3.2	7.7	3.3	2.7	6.3
4.5	8.7	4.4	1.4	6.6
3.6	8.4	4.6	1.8	8.4
2.9	12.8	4.2	1.2	6.2
5.6	11.2	4.8	1.7	5
3.1	9.3	5.1	0.8	6.1
3	9.3	3.4	1.4	6.2
3.5	7.1	4.9	0.8	6.8
4	10.2	5.7	1.8	6.7
4.1	10.3	4.2	1.8	5.8
4.6	10.2	4.5	3	5.2
3.7	7.4	7.1	0.3	5.1
4	9.1	7.2	0.6	7.3
5	8.3	3.6	1.7	5.3
4	10.8	5.3	2.3	5.5
5.6	12.2	7.1	1.3	7
12.6	7.8	5.6	0.9	8.4
<b>1.5</b>	<b>0.2</b>	<b>0.6</b>	<b>0.2</b>	<b>2.4</b>
0.4	0	0.2	0.1	0.3
0.4	0.1	0.1	0.1	0.5
2.2	0.1	1.1	0.2	0.6
-	-	-	-	-
0.5	0.3	0.4	0.1	0.8
0.2	0	0.1	0	0.5
0.3	0.1	0.1	0.1	0.5
0.7	0.5	0.6	0.2	1
1.6	0.2	0.7	0.2	2.6
0.5	0	0.2	0.1	0.4

1	0.1	0.3	0.1	0.7
0.5	0	0.3	0.1	0.4
0.8	0.3	0.4	0.1	0.7
0.3	0	0.1	0	0.3
0.4	0	0.2	0	0.3
0.3	0	0.1	0	0.4
2.3	1.2	1.9	0.4	11.8
0.3	0	0.1	0	0.3
0.2	0	0.1	0	0.4
<b>4.1</b>	<b>4.6</b>	<b>7.5</b>	<b>0.6</b>	<b>8.4</b>
4.6	2.8	2.9	0.5	5
1.5	2.8	6.7	0.3	12.1
1.9	3.2	7.4	0.5	14.5
2.1	2.3	4.5	0.6	10.8
1.6	3.4	8.4	0.1	10.7
0.3	1	1.8	0.1	18.1
1	1.7	6	0.1	13.2
4.5	4.4	6.7	0.9	5.7
4.5	1.7	3.2	0.3	16.6
2.8	2	4.5	0.3	14.9
6.6	1.6	4.5	0.2	21.3
6.7	6.4	4.3	1.8	5.7
4.8	0.2	0.9	0.1	1.7
4.9	5.4	5	1	4.4
10.3	6	10.1	1	6.8
4	8.2	8.9	0.7	5
5.9	15.6	16.3	0.4	4
2.1	3.9	5.1	1.1	5.6
2.7	5.2	6.5	2.3	5
5	3.3	15.8	0.4	5.8
2.9	1.6	2.4	0	2.7
11.8	5.8	14.4	0.8	8.3
18	7.2	29.2	0.6	8.6
0.2	0.3	1.7	0.3	9.1
2.6	5.3	4.2	0.7	5.5
1.5	3.1	2.3	0.3	4.4
1.5	4.4	3.6	0.2	4.7
<b>1.8</b>	<b>0.1</b>	<b>4.5</b>	<b>0</b>	<b>1.5</b>
2.5	0.1	5.7	0	1.8
3.8	0.1	5.5	0	1.9
1.8	0.1	0.9	0	1.2

2.3	0	4.6	0	2.3
1.5	0.1	4.3	0	1.4
2.4	0	7.8	0	2.5
2.3	0.1	21.7	0.2	0.9
3	0	4.5	0	1.9
1.9	0	10.3	0	1.6
<b>5.7</b>	<b>0.8</b>	<b>3.3</b>	<b>0</b>	<b>3.5</b>
2.6	0.2	2.5	0	3.4
2.2	0.6	1.3	0	1.9
10.7	0.8	4.8	0.1	3.6
9.1	0.5	4.4	0.1	3.3
9.3	0.8	3.7	0	3.3
11.1	0.9	4.1	0	3.5
7.3	1.7	2.9	0	6.1
7.9	1.9	2.5	0	7.2
2.2	1.7	2.5	0	2.3
1.2	0.4	2	0	2.3
1.3	0.7	1.9	0	2.8
1.1	0.7	1.9	0	2.6
3	0.3	3.1	0	3.8
3.2	0.3	3.2	0	4.1
4.9	1.1	2.6	0	2.3
3.9	0.3	1.5	0	2.4
3.9	0.9	3.5	0	3.2
6.6	2	4.4	0	4.3
4.8	0.6	2.2	0	4.5
6.7	0.8	3	0	5.7
1.9	0.3	10.7	0.1	1.8
1.9	0.2	15	0.1	1.3
<b>1.8</b>	<b>2.3</b>	<b>4.1</b>	<b>0</b>	<b>6.1</b>
1.5	2.2	4.9	0	6.7
1.7	3.1	3.8	0	7.7
0.9	0.8	8.2	0	3
2	2.7	4.1	0	6.5
1.3	2.1	2.9	0.1	7.2
2.6	3.1	5.1	0	6.9
1.7	1.6	2.8	0	4.9
1	1	3.6	0.1	4.4
<b>1.5</b>	<b>0</b>	<b>1</b>	<b>0</b>	<b>2.2</b>
1.9	0	1.4	0	3.9
0.8	0	0.5	0	1.7

2	0	1.2	0	1.7
0.1	0	0.1	0	0.4
1.7	0.1	0.9	0	1.4
1.7	0	0.6	0	2.4
0.7	0.1	0.2	0	0.9
2.1	0	1.2	0	3.1
2.5	0	1.6	0	3.4
0.8	0	0.4	0	1.2
0.7	0	0.3	0	1
1	0	0.5	0	1.7
0.6	0	0.4	0	1.1
0.7	0	0.4	0	1.2
0.2	0	0.2	0	0.5
0.7	0	0.4	0	1.2
1.7	0	1.3	0	2.6
2.3	0	2	0	4.6
2.6	0.1	2.1	0	4.4
1	0	0.6	0	2.1
2.1	0	2	0	4.8
1.5	0	2.3	0	1.4
0.6	0.1	0.2	0	0.7
0.9	0	0.5	0	1.3
2	0	1.4	0	3.6
<b>5.1</b>	<b>6</b>	<b>5.7</b>	<b>0.9</b>	<b>6</b>

<b>Residential Coal Combustion Contribution (%)</b>	<b>Residential Biofuel Combustion Contribution (%)</b>	<b>Residential Other Combustion Contribution (%)</b>	<b>Commercial Combustion Contribution (%)</b>	<b>Other Combustion Contribution (%)</b>
<b>0.5</b>	<b>9.2</b>	<b>0.3</b>	<b>0.4</b>	<b>0.4</b>
1	5.1	0.3	1.3	0.8
0.4	7.3	0.4	0.6	0.7
0.2	6.7	0.3	0.4	0.5
0.8	8.3	0.2	1	0.6
0.4	3.8	0.7	0.4	0.3
0.6	6.5	0.9	0.4	0.3
0.6	10.7	0.2	0.3	0.2
2.8	8.6	-1.2	0.8	1.3
3.1	8.9	-1.3	0.7	1.3
0.5	24	0.1	0.1	0.3
0.1	2	0.2	0.3	0.2
0.4	8.1	0.4	0.3	0.3
0.1	2.2	0.2	0.2	0.2
0.4	6.2	0.6	0.3	0.3
<b>3.6</b>	<b>15.8</b>	<b>0.5</b>	<b>1.6</b>	<b>2.1</b>
0.9	10.4	0.6	2.6	1.4
2.4	15	0.4	1.4	1.2
1.8	15.5	0.3	1.2	1.1
1.7	23.1	0.7	1.3	2.1
4.2	16.7	0.6	1.7	2.1
3	21.8	0.8	1.4	2.2
3.2	25.6	0.8	1.5	2.2
1.4	12.7	0.3	2.1	0.8
1.6	12.9	0.3	1.6	0.9
5.7	12.2	0.5	1.7	3
7.1	12.4	0.5	1.8	3.5
1.8	21.7	0.5	0.9	1.4
2.5	16.4	0.4	1.9	1
2.7	15.4	0.4	1.3	0.9
3.8	16.4	0.7	1.6	2.3
0.9	22	0.9	1.3	2.5

<b>1.4</b>	<b>8.4</b>	<b>0.6</b>	<b>1.4</b>	<b>1.3</b>
3.2	8.2	0.6	1.8	2.7
2.6	7.4	0.6	1.6	2.3
1.6	16.8	0.1	1.5	2.1
2.1	17.1	0.5	2.5	2.4
2.7	12.3	0.5	1.6	2.1
2.7	11.7	0.4	1.5	1.9
2.3	16.3	0.5	1.1	1.7
0.8	7.9	0.6	1.4	0.9
0.9	14.5	1	2.6	1.6
0.4	2.9	0.2	0.5	0.4
0.6	15.3	1.4	3	1.3
0.3	5.3	0.8	1	0.5
0.3	6.2	0.8	1.1	0.6
0.8	10.7	1	1.9	1.4
2.2	8.4	0.6	1	1.7
1.6	7.8	0.5	0.9	1.4
3.8	9.5	0.6	1.4	2.3
<b>0</b>	<b>2.5</b>	<b>0.1</b>	<b>0.3</b>	<b>0.9</b>
0	2.7	0.1	0.2	0.8
0	3.3	0.1	0.3	0.9
0.1	1.6	0	0.4	1.4
0.1	1.9	0	0.4	1.4
<b>3.1</b>	<b>6.9</b>	<b>-0.6</b>	<b>1.6</b>	<b>1.5</b>
0.6	10.5	-0.4	1	0.8
3	6.7	-1	1.4	1.4
2.1	4.9	-0.5	1.5	1.3
3	7.1	-0.9	1.4	1.3
4.1	8.5	-1.4	1.3	1.3
3.2	7.3	-1	1.2	1.3
3.8	8.4	-1.3	1.2	1.3
3.4	6.8	-0.2	1.9	1.9
3.3	6.6	-0.1	2	1.9
3.4	7.1	-0.4	1.7	1.8
3.2	6.4	0.1	2	2
3.4	7	-0.5	1.5	1.7
3.6	7.2	-0.5	1.7	1.8
3.4	7.5	-1	1	1.4
0.4	12.1	-0.2	0.3	0.3
<b>0.3</b>	<b>7.5</b>	<b>1.4</b>	<b>2.3</b>	<b>5.7</b>
0.8	14	0.1	0.8	4.3

0.8	22.7	0	1	5.2
0.5	14.6	2	1.6	5.6
6.1	2.2	-6.1	0.6	1.8
0.2	6.8	1.5	2.4	5.9
0.1	6	1.4	2.8	6.1
0.3	13.6	2.9	4.5	9.1
0.3	10.2	2.2	3.4	7.8
0.1	7	0.7	2.5	5.1
0.6	5.3	0.9	2.1	4
0.3	5.6	1.9	2.2	4.1
0.1	14.8	2.5	4.8	11.2
0.4	6	1.6	1.8	5.4
0.4	6.9	1.6	2.5	5.8
0.5	9.8	2.1	2.7	7.9
0	5	0.7	1.9	5.2
0.1	5.7	0.2	2	4.8
0.2	5.2	2	2.6	5.8
<b>0</b>	<b>7.6</b>	<b>0.3</b>	<b>0.6</b>	<b>2.2</b>
0	5	0.4	0.5	2.9
0	5.6	0.6	0.7	4.6
0	3.5	0.2	0.4	2.1
0	11.4	0.2	0.7	1.1
0	15	0.2	0.9	1.5
0	5.8	0.4	0.5	3.6
<b>1</b>	<b>9.9</b>	<b>1</b>	<b>2</b>	<b>2.3</b>
0.5	8	1.1	1.8	2.3
1.8	15	1.1	2	2.5
2.5	18.6	0.9	1.7	2.8
0.9	7.2	1.1	2.1	2.1
0.9	6.8	0.9	2.1	2.2
0.9	2.4	0.4	1.3	0.7
1.3	9.4	0.5	1.5	2.5
1.4	14.1	0.1	1.7	3.7
0.7	12.5	1.4	2.5	2.6
0.6	20.5	1.7	3.3	3.2
0.7	8.6	1.2	2.1	2.7
1.2	8.1	1	2.8	1.4
1.8	8.2	0.8	2.6	1.4
1.4	7.7	1	2.6	1.3
1.1	4.8	0.6	1.7	1.4
1.1	8	0.6	1	0.9

1.2	9.3	0.6	1.1	0.9
1.7	1.1	-1.4	0.2	2.4
2.9	1.9	0.2	1.2	1.3
0.4	1.7	0.2	0.5	0.3
0.4	1.7	0.2	0.6	0.3
0.5	16.7	1.4	1.3	3
0.6	9.7	0.7	0.7	1.3
0.3	23	2	2	4.7
0.8	6.7	1.3	2.2	1.9
0.3	5.3	0.7	0.6	0.8
1.1	6.2	0.8	2.1	2.4
1.2	5.4	0.7	1.9	2.1
1.4	10	-0.6	1.3	2.3
0.3	6.7	0.2	0.7	1.5
0.4	8	1	1.6	2.7
0.5	14.3	1.6	2.6	4.2
0.4	6.1	1.4	1.9	5.1
1.5	10.2	0	1.5	2.6
0.6	11.8	2.2	5.2	2.5
0.5	10.6	2.1	4.7	2.5
2.4	5.6	0.7	1.9	2.8
2.9	5.7	0.7	2	2.8
2.5	7.5	0.9	2.3	3.2
2.8	5.2	0.5	1.9	2.6
0.4	14.6	1.3	1.6	2.7
0.8	13.6	1.1	1.1	2.4
<b>0</b>	<b>6.4</b>	<b>0.1</b>	<b>0.5</b>	<b>0.5</b>
0	2.1	0.1	0.1	1.1
0	1.9	0.1	0	1.2
0	4.1	0.2	1.2	0.2
0	3.9	0.2	1.3	0.2
0	8.5	0	0.4	0.4
<b>0.5</b>	<b>15.1</b>	<b>-0.4</b>	<b>0.4</b>	<b>0.6</b>
1.9	14.5	-1.6	0.3	0.2
0.6	4.8	-0.4	0.8	2.5
0	0.9	0	0.1	0.1
0.5	6.6	-0.3	0.5	0.7
0.1	4	0	0.6	3
0.4	5.1	-0.2	0.5	1.5
0.5	7.4	-0.5	0.3	1
1.8	15.6	-1.7	0.2	0.1



0.8	13	-0.7	0.2	0.4
0	1	0	0.1	0.1
0	1.7	0	0.1	0.2
0.5	34	-0.4	0.4	0.3
0.6	14.4	-0.7	1.6	0.3
1.8	10.8	-1.6	0.1	0.2
0	0.9	0	0.1	0.1
0	0.9	0	0.1	0.1
0	1.5	0	0.1	0.2
0	1.1	0	0.1	0.1
1.9	11.9	-1.6	0.1	0.2
1.8	13.9	-1.6	0.2	0.2
<b>0.1</b>	<b>15.4</b>	<b>0.1</b>	<b>0.4</b>	<b>1.2</b>
0.3	11	0.1	0.1	0.7
0.4	13.6	0.1	0	0.9
0.1	4	0.1	0.2	0.2
0	4.7	0	0.6	0.3
0	29.2	0	0.9	0.1
0	30.3	0	0.9	0.1
0.1	46.1	0	1.2	0.2
0.1	54.2	0	1.4	0.1
0.2	23	-0.2	1.2	0.2
0	14.6	0.2	0.3	2
0	12.7	0.3	0	1.9
0	18.1	0.2	0.1	2
0	25.3	0.2	0.2	2.4
0.1	7.1	0.4	1.4	3.2
0.1	12.5	1.3	2.8	8.6
0	11.5	0	0.6	0.3
0	12.1	0	0.6	0.3
0	3.8	0	0.2	0.1
0	1.8	0.1	0.2	0.1
0	1.5	0.1	0.2	0
0	2	0.1	0.2	0.1
<b>0</b>	<b>4.4</b>	<b>0.1</b>	<b>0.1</b>	<b>2.6</b>
0	4.2	0.1	0.1	2.6
0	5	0.1	0.1	3.2
0	4.9	0.1	0.1	3.3
0	4	0.1	0.1	2.6
0	3.8	0.1	0.1	2.5
0	1.4	0	0	0.8

0	3.4	0.1	0.1	2.1
0	4.7	0.1	0.1	3.2
0	4.7	0.1	0.1	3.2
0	8.3	0.1	0.2	2.1
<b>0.3</b>	<b>2.6</b>	<b>0.3</b>	<b>0.5</b>	<b>0.4</b>
0	7.3	0.2	0.2	0.1
-0.1	8.7	0.2	0.1	0.1
0.1	2.5	0.4	0.4	0.5
0.2	3.1	0.4	0.5	0.5
0.2	3.2	0.5	0.4	0.6
0.1	0.4	0.1	0.1	0.1
0.2	3.5	0.3	0.3	0.5
0.2	4	0.3	0.3	0.5
0.3	3.4	0.3	0.4	0.5
0.1	1	0.4	0.4	0.6
0.1	1.1	0.7	0.6	0.9
0.1	0.5	0.2	0.2	0.3
0.1	1.3	0.9	0.6	0.8
0.1	0.9	0.6	0.5	0.7
0.2	0.7	0.3	0.3	0.3
0.2	0.7	0.2	0.3	0.2
0.3	1.5	0.2	0.5	0.3
0.1	0.4	0.1	0.2	0.1
0.5	1.8	0.2	0.6	0.4
0.2	1.6	0.7	0.2	0.2
0	2.6	0.1	1.4	0.5
0	1.9	0.1	1.1	0.3
0.3	1.7	0.2	0.5	0.3
0.1	1.4	0.1	0.1	0.1
0.1	0.4	0.1	0.1	0.1
0.1	0.9	0.1	0.1	0.1
0.1	0.6	0.1	0.1	0.1
0.1	2.3	0.1	0.5	0.1
0.1	1.8	0.1	0.6	0.1
0.7	1.7	0.4	0.9	0.6
0.2	5.3	1	0.5	1
0.2	5.4	1.1	0.5	1.1
1.8	4.1	0.5	2.1	1.2
2.5	7.4	0.9	2.5	1.6
1.6	2.6	0.5	1.9	1
1.8	2.9	0.4	2.2	1.2

0	0.7	0.1	0.1	0.1
0.1	2	0.1	0.2	0.1
0.1	1.8	0.1	0.2	0.1
<b>1.2</b>	<b>23.4</b>	<b>1.7</b>	<b>1.8</b>	<b>2.9</b>
0.9	25.9	1.4	0.9	3.4
1.1	23.2	1.5	1	3.5
0.7	27.5	1.3	0.7	3.4
1.2	27.4	1.8	1.2	4
1.3	30.1	1.4	1.3	2.6
1.4	22.5	1.8	2	3.1
1.4	22.3	1.8	2.2	2.9
1.4	21.6	1.5	1.9	2.2
1.6	24.5	2.2	2.3	3.8
1.5	22.7	1.7	1.8	3
1.2	18.9	1.5	2	2.3
1.3	19.4	1.6	2.2	2.4
1.5	18.8	1.7	2.4	2.5
1.5	18.6	1.8	2.5	2.7
1.8	21.3	1.3	2.2	1.9
1.6	18.4	1.7	2.6	2.6
1.4	18.9	1.8	2.4	2.8
1.7	22.2	1.5	2.6	1.9
1.3	19.2	1.7	2.1	2.5
1.4	18.2	1.8	2.3	2.8
0.9	15.1	1.5	1.5	2.5
1.4	24.4	2.1	2	3.8
1.4	18.1	1.7	2.2	2.6
1	36.6	1.4	1.6	2.7
0.7	37.6	1.2	1.4	2.2
0.2	26.9	0.9	1	0.9
0.1	27.4	0.5	0.6	0.5
0.3	33.9	1.2	1.2	1.2
0.8	27.3	1.7	1.7	2
<b>5.3</b>	<b>12.6</b>	<b>-0.1</b>	<b>1.8</b>	<b>1.3</b>
5.3	12.7	0	1.8	1.3
6.7	14.7	0.4	2.5	1.5
4.9	11.4	-0.2	1.7	1.4
5.3	10	-2.1	1.5	1
4.2	10.8	-0.3	1.3	0.8
5.4	13.6	0.3	1.8	1.2
4.8	12.1	-0.2	1.4	0.9

6.4	14.7	0.1	2.2	1.3
5.2	12.4	-0.1	1.6	1.3
4.7	11.1	-0.2	1.5	1.3
5.4	12.9	0	1.9	1.5
5.5	13.1	0.2	1.9	1.4
5.3	13.1	0.4	1.8	1.1
6.7	15.3	-0.1	2.2	1.2
5.2	13	0	1.7	1.1
7.1	15.7	0.6	2.8	1.8
3.5	8.8	0.2	1.2	0.9
4.7	11.5	-0.2	1.5	1
6.5	13.4	0.4	2.6	1.8
5.2	12.6	-0.1	1.8	1.3
8	17	0.5	3.1	2
7.1	16.3	0.3	2.6	1.6
6	14.2	0.3	2.1	1.3
6.8	14.9	0.4	2.5	1.6
5.8	13.9	0.2	2	1.3
7.2	16.4	0	2.5	1.4
7.8	16.7	0.5	2.9	1.9
5.6	14	0.3	1.9	1
5.2	12.8	0	1.8	1.3
5.6	13.4	0.4	2.1	1.5
5.7	14.2	0.4	2.1	1.4
5.7	13.5	-0.9	1.4	0.7
4.9	12.3	-0.2	1.4	0.9
6.7	13.9	0.5	2.8	1.9
6.8	15.6	0.4	2.4	1.5
3.9	8.6	-1.3	1.1	1.5
4.4	8.4	-1.6	1.4	0.9
<b>1</b>	<b>7.7</b>	<b>-0.9</b>	<b>0</b>	<b>0.2</b>
0	0.4	0	0	0
0.1	0.6	0	0	0
0	2	0	0	0.1
-	-	-	-	-
0.3	1.6	0	0.1	0.1
0	0.5	0	0	0
0.1	0.5	0	0	0.1
0.5	1.9	0	0.2	0.1
1.1	8.6	-1	0	0.2
0	0.6	0	0	0

0	1.5	0	0	0
0	0.3	0	0	0
0	0.7	0	0	0.1
0	0.2	0	0	0
0	0.2	0	0	0
0	0.4	0	0	0
2.5	17.4	-1.9	0.5	0.5
0	0.2	0	0	0
0	0.3	0	0	0
<b>1.9</b>	<b>25</b>	<b>0.1</b>	<b>1.3</b>	<b>1.2</b>
3.2	24.7	0	1.1	1.1
0.3	32.7	0.1	0.4	0.5
0.5	39	0.6	0.8	0.9
0.4	31.3	0	0.5	0.5
0	35.7	0.2	0.3	0.5
0.8	39.7	-0.5	0.4	0.6
0.3	44.9	0.2	0.4	0.6
3.8	15.8	0.3	1.6	1.6
0.6	13.4	0.2	0.7	0.9
0.4	11.3	0.4	0.9	1.2
0.2	11.9	0.1	0.6	0.9
1.4	16.5	1.9	2.6	2.2
0.1	0.7	0.1	0.1	0.1
2	28.1	0.5	1.6	1.9
2.2	14	0.9	1.5	1.6
1	15.5	-0.4	2.8	0.4
0.7	16.8	-0.2	3.1	0.4
1	16.7	-0.5	3.1	0.3
0.8	15.3	-0.3	2.4	0.4
0.9	19.5	0.4	1.2	0.6
0.6	9.2	0.2	0.5	0.2
2.5	11.8	0.4	1.3	1.5
1.2	7.3	0.3	0.7	1.1
0	8.9	0	0.1	0.1
6.6	30.2	0.2	2.3	3
6.7	37	0.2	2.3	3.5
7.7	41.4	0.1	2.6	4
<b>0.1</b>	<b>9.6</b>	<b>0.2</b>	<b>0.3</b>	<b>0.3</b>
0.2	4.9	0.1	0.3	0.2
0.1	4.9	0.1	0.3	0.1
0	3.6	0.1	0.2	0.1

0	7.6	0.2	0.7	0.1
0	11.5	0.2	0.3	0.4
0	10.6	0.3	1.3	0.2
0.1	8	0	0.2	0.2
0	8	0.3	1	0.1
0	5.8	0.2	0.4	0.1
<b>0.2</b>	<b>19.3</b>	<b>1</b>	<b>0.6</b>	<b>0.8</b>
0	29.5	0.6	0.8	2
0.3	7.2	0.2	0.4	0.5
0.1	3.9	0.2	0.3	0.2
0.1	4	0.2	0.4	0.1
0.1	21.3	0.6	0.6	0.2
0.1	28.1	0.8	0.6	0.2
0.1	23	3.6	0.3	0.7
0.1	27.2	5	0.2	0.6
0.3	7.8	0.7	0.9	1.2
0.3	9.7	0.1	1.1	0.9
1.1	7.9	0.2	1.2	0.7
1.1	6.7	0.2	1.1	0.6
0	34.2	0.8	1	2.3
0	36.1	0.9	1.1	2.5
0.2	5.5	0.2	0.3	0.3
0.1	7.6	0.2	0.3	0.2
0.2	19.1	0.9	0.3	1.8
0.2	20.6	2.1	0.2	1.8
0.1	28.3	1.5	0.7	1.3
0.1	34.2	2.1	0.8	1.6
0.3	9.5	0.1	0.4	0.5
0.2	8.3	0	0.3	0.3
<b>5.4</b>	<b>9.6</b>	<b>0.6</b>	<b>2.3</b>	<b>1.2</b>
4.1	8.5	0.4	1.7	1
6.4	9.6	0.6	2.7	1.1
0.9	5.1	0.1	0.5	0.7
6.5	8.8	0.7	2.7	1
5.2	5.5	0.4	2.1	0.8
7	9.6	0.9	2.9	1.1
4.1	8	0.5	1.9	0.7
1.1	13.9	0.5	0.8	1.9
<b>0</b>	<b>7.5</b>	<b>0.3</b>	<b>0.7</b>	<b>0.1</b>
0	8.9	0.5	0.9	0
0	3.7	0.1	0.3	0.1

0	8.1	0.4	1.4	0.1
0	0.3	0	0	0
0	2.3	0.1	0.3	0.1
0	6.2	0.3	0.7	0.1
0	1.4	0.1	0.1	0.1
0	6.3	0.3	0.6	0.1
0	6.8	0.4	0.6	0.1
0	3.5	0.1	0.2	0.2
0	2.2	0.1	0.1	0.1
0	5	0.2	0.4	0.2
0	2.3	0.1	0.2	0.1
0	2.5	0.1	0.2	0.1
0	0.6	0	0.1	0
0	3	0.1	0.2	0
0	10.4	0.5	0.9	0
0	12.7	0.7	1.2	0
0	12.5	0.7	1.2	0
0	5.5	0.2	0.6	0
0	12.6	0.6	1.2	0
0.1	5.1	0.1	0.3	0.1
0	1	0.1	0.1	0.1
0	4.4	0.2	0.3	0.2
0	8	0.5	0.8	0
<b>2</b>	<b>16.4</b>	<b>0.8</b>	<b>1.5</b>	<b>1.8</b>

<b>Solvent Contribution (%)</b>	<b>Waste Contribution (%)</b>	<b>International Shipping Contribution (%)</b>	<b>Agricultural Waste Burning Contribution (%)</b>	<b>Other Open Fire Contribution (%)</b>	<b>AFCID Dust Contribution (%)</b>
<b>0</b>	<b>6.1</b>	<b>0.2</b>	<b>0.4</b>	<b>1.8</b>	<b>4</b>
-0.2	2.2	0.3	0.7	1.1	6.3
-0.1	2.4	0.2	0.6	1	5
-0.1	2.3	0.1	0.4	0.9	4.2
-0.1	2.8	0.4	1.4	2.2	6.6
0	4.3	0.3	1	3.8	5.7
0.1	6.4	0.4	0.3	1.5	5.3
-0.1	7.8	0.1	0.2	1.4	2.9
0.2	3	0.4	0.8	10.4	6.2
0.2	3.4	0.4	0.7	8.2	6.4
-0.1	7.1	0.2	0	0.5	2.5
-0.1	2.1	0.1	0.2	0.9	2.3
0	8.5	0.3	0.2	1	3.4
-0.1	4.6	0.1	0.2	1	2.6
0.2	11.2	0.4	0.3	1.1	4.2
<b>-0.1</b>	<b>1.5</b>	<b>1.1</b>	<b>1</b>	<b>0.8</b>	<b>6.9</b>
-0.2	2.8	1.5	2	2.1	7.1
-0.2	2.4	0.9	1.3	1.7	4.9
-0.2	2	0.6	3	1.2	8
-0.3	1	1.4	1	1.3	5.3
-0.1	0.5	1.2	0.2	0.5	5.4
-0.2	0.9	0.8	0.5	0.6	6.8
-0.1	0.8	0.8	0.4	0.5	6.3
-0.2	2.7	0.7	1.9	1.6	8.6
-0.2	3.6	0.9	2.7	3.8	6.5
-0.1	0.9	1.5	0.2	0.4	7
0	1	1.3	0.2	0.4	7.4
-0.2	1.8	0.6	2	0.7	8.1
-0.1	3.9	0.5	2	1.1	6.2
-0.1	3.7	0.4	2.4	0.6	5.1
-0.2	0.8	0.8	0.4	0.7	7.6
-0.3	0.5	1.5	0.4	1.4	5.2



<b>-0.2</b>	<b>3.2</b>	<b>0.6</b>	<b>2.3</b>	<b>3.2</b>	<b>14.6</b>
-0.3	1.5	1	0.7	0.7	9.9
-0.4	1.9	0.8	1.4	1.1	11.5
-0.2	1.1	1.7	0.2	0.7	11.3
-0.3	1.7	1.7	0.3	0.6	8.1
-0.3	1.4	1.6	0.4	0.5	7.5
-0.2	1.4	1.3	0.4	0.4	6.9
-0.4	2.8	0.7	2.7	0.8	11.8
-0.1	3.6	0.4	2.1	4.5	15.9
0	4.2	0.7	0.2	0.6	15.5
-0.1	1.5	0.1	1.5	3.2	7.2
0.1	4	0.4	0.4	0.4	18.8
-0.1	5	0.1	1.5	5.8	19.3
-0.1	3.5	0.1	0.9	4.7	17.4
-0.2	4.2	0.9	1	0.9	17.5
-0.3	2.8	0.7	3.3	0.8	13.5
-0.3	3	1	4.9	0.8	13
-0.4	2.2	0.8	1.1	0.6	12.6
<b>0</b>	<b>0.4</b>	<b>3.2</b>	<b>1.1</b>	<b>10.8</b>	<b>2.6</b>
0	0.4	3	1.3	12.1	2.9
0	0.7	1.7	0.5	9.1	2.4
-0.1	0.3	4.2	0.2	2.9	1
-0.1	0.4	4.2	0.1	1.9	0.8
<b>0.2</b>	<b>4.2</b>	<b>1.6</b>	<b>0.9</b>	<b>1.9</b>	<b>9.5</b>
0.4	3.4	2.7	0.6	4	11.9
0.4	3.7	2.1	1.1	2.4	9.5
0.8	2.7	2.4	1.1	2.1	11.7
0.3	4.5	1.9	1.1	2.3	7.8
-0.1	5.3	2.5	0.7	1.4	8.5
0	4.3	1.5	1.2	2.4	7.8
-0.1	5.2	1.7	0.8	1.8	8.6
0.1	4.7	1	0.6	1.2	9.6
0.1	4.8	0.8	0.6	1.1	11
0	4.9	1.4	0.7	1.3	7
0.2	4.2	1	0.6	1.1	9.2
-0.1	4.3	1.4	0.6	1.1	7.3
-0.1	4.4	1.2	0.7	1.4	7.4
0	6.8	0.5	0.6	1	10.9
0.1	5.9	3.1	0.1	2.6	7.1
<b>0.1</b>	<b>2.9</b>	<b>1.5</b>	<b>1.2</b>	<b>12.2</b>	<b>2.7</b>
0.1	1.3	2.3	0.4	18.5	3.1

0.1	1.3	3.4	0.3	7.2	2.6
0.1	2.2	1.5	0.2	19	4.1
-0.2	1	9.4	0.7	19.6	2.7
0.1	3.1	1.4	1.3	11.6	2.7
0	3.7	1.1	0.6	6	2.1
0.4	3.4	1.3	0.2	4.8	2.9
0.4	3.8	1.3	0.2	5.2	3.9
-0.1	3.2	2.6	1.2	5.3	1.3
0	2.2	0.6	0.6	13.9	3.5
0	3.3	1.2	0.5	24.2	2
0.4	4.8	0.7	1.2	8.7	4.6
0.1	2.7	3.4	0.3	9.7	2.6
0.2	2.5	1.9	0.6	7.8	2.5
0.1	3.8	1.1	0.2	8.9	4.4
-0.2	3.2	2.3	1.4	12.6	2.6
-0.1	3	1.1	0.9	6	3.3
0.2	3.5	1.2	3.3	25.9	2.8
<b>0</b>	<b>2.6</b>	<b>0.7</b>	<b>1.3</b>	<b>19.4</b>	<b>4.5</b>
0	2.8	0.8	0.9	12.9	4.5
0	3.3	1.7	0.4	6	5.4
0	2.9	0.2	1.1	16.8	4.3
0	2.5	0.5	2.1	30	4.3
-0.1	3	0.4	2	27.5	5.4
-0.1	2.2	1.9	0.4	7	5.6
<b>-0.1</b>	<b>0.9</b>	<b>4.5</b>	<b>0.4</b>	<b>1.5</b>	<b>5.1</b>
-0.5	0.8	3.8	0.9	4.3	6.2
-0.3	0.5	1.3	0.2	0.6	5.6
-0.1	0.5	1.1	0.3	0.5	5.6
0.3	0.4	5	0.1	0.6	5
0.4	0.4	4.9	0.1	0.6	5
-0.2	1.6	1.4	0.5	0.3	6.6
0	0.5	8.5	0.1	0.6	4.4
-0.2	0.9	1.8	0.1	0.9	12.1
-0.1	0.7	5.1	0.5	1.5	5.5
0.1	0.7	3.6	0.1	0.6	5.2
-0.2	0.6	6.8	0.1	0.9	5.1
0	0.3	3.7	0.1	0.6	4.6
0	0.4	4.4	0.1	0.5	4.4
0	0.3	2.8	0.1	0.5	4.6
0.3	0.3	11.6	0.1	0.6	3.2
-0.2	1.2	1.6	1.7	1.4	6.4

-0.2	1.4	1	2	4.1	8.8
0	0.2	7.7	0.1	2.2	2.4
-0.1	0.3	16.5	0.1	1	2.1
-0.2	3.8	1.2	0.3	0.1	5.2
-0.2	3.9	1.2	0.3	0.1	5.3
-0.3	1	2.9	0.9	1.6	4.8
-0.4	1.2	4	1.2	1.6	5.7
-0.1	0.8	1.8	0.5	2.1	4.1
0.1	0.4	3.2	0.1	0.6	5.9
-0.3	1	6.4	1.2	1.3	4.6
0.3	0.4	5.4	0.1	0.6	4.9
0.3	0.3	6.1	0.1	0.6	4.5
-0.1	0.6	5.3	0.2	1.4	10.6
0	0.7	12.6	0.7	15.9	5.6
-0.2	0.9	6.4	0.5	3.7	5
0.1	0.7	3.5	0.3	2.8	4.4
0.1	2.6	2.6	0.4	9.5	2.7
-0.2	0.8	4.4	0.1	1.1	9.2
-0.4	0.7	1.8	0.2	0.9	5.8
-0.4	0.7	2.1	0.2	0.8	5.5
0	1.5	6.1	0.1	0.7	4.3
0.1	1.6	4.8	0.1	0.7	4.1
0.1	2	4.9	0.1	0.7	5
0	1.4	5.9	0.1	0.7	4.4
-0.2	1	9.2	0.5	1.8	4.3
-0.4	1	3.9	0.7	1	5.2
<b>-0.1</b>	<b>3.7</b>	<b>1</b>	<b>0.3</b>	<b>14.2</b>	<b>2.9</b>
0	1.2	0	0.5	37.1	3
0	1	0	0.5	41.2	3
0	4.8	1.9	0.5	7.4	3.7
0	4.8	1.6	0.4	6.5	4.1
-0.1	4.1	0.9	0.2	9.4	2.6
<b>-0.1</b>	<b>5.4</b>	<b>4.9</b>	<b>1</b>	<b>2.6</b>	<b>1.7</b>
0	2.6	2.4	0	3.4	1.3
-0.1	2.4	12.2	0.9	4.1	1.5
0	0.4	1.5	0.2	1.6	0.5
0	2.8	5.6	1.6	16.9	2
0	1.4	8.9	-0.5	4.6	1.5
-0.2	3.5	7.1	3	3.7	2.5
-0.1	3.9	7.4	1.2	2.4	2.1
0	2.8	1.9	0.3	2.7	1.2

-0.1	7.3	4.6	0	1.9	1.6
0	0.4	1.8	0.2	1.8	0.5
0	1.1	1	0.6	4.3	0.8
0	8.1	3.5	0.2	1.3	1.3
-0.1	4.5	6.3	0.3	1.8	1.5
0	3.3	4.3	-0.3	3.4	1.2
0	0.5	1.5	0.2	1.4	0.5
0	0.5	1.6	0.2	1.5	0.5
0	0.5	0.8	0.4	4.9	0.6
0	1.4	1.7	0.4	3.4	0.6
0	2.6	3.8	-0.2	3.5	1.3
0	2.9	2.7	0	3.4	1.3
<b>-0.1</b>	<b>4.8</b>	<b>1.4</b>	<b>1.1</b>	<b>7.4</b>	<b>3.6</b>
0	3.6	1	0.3	6.4	4.2
0	4	0.2	0.2	6.8	4.8
0	3	2.4	0.4	3.8	2.4
0	3.8	4.1	0.7	2.1	2
0	6	1	0.6	3.9	2.1
0	6.1	1	0.6	3.7	2.1
0	6.8	0.9	0.8	6.4	1.9
0	6.7	0.5	0.3	3.1	1.3
0	5.3	2.8	1.1	6.3	2.1
-0.2	5.3	1.3	1.7	9.1	4.3
-0.1	4.3	1.6	3	13	3.5
-0.3	4.7	0.3	1.4	11.7	3.5
-0.3	7.3	0.4	0.9	3.2	4
-0.1	3.9	2.9	1.6	7	4.3
0.3	7	2	0.8	9.6	4.3
0	3.2	2.6	0.5	3.1	1.5
0	3.3	2.5	0.5	3.1	1.5
0	2.3	6.2	0.3	1.9	1.3
0	3.2	1.7	0.6	5.9	2.2
0	3.4	1.9	0.5	5.3	2.3
0	3.5	2	0.8	5.2	2.6
<b>0</b>	<b>2.6</b>	<b>2</b>	<b>0.6</b>	<b>11.4</b>	<b>7.7</b>
0	2.6	2	0.6	10.7	7.7
-0.1	3	1.4	0.4	3.4	8.9
-0.1	3	1.8	0.5	5.6	9.1
-0.1	2.6	2.2	0.4	5.5	7.9
0	2.8	1	0.1	6.6	7.9
0	0.7	0.5	0.6	57.4	3.4

0	1.8	6.7	0.2	7.1	7.6
0	2.6	5.4	0.2	6.7	10.7
-0.1	3.4	0.6	2.1	9.7	8.8
0	1.6	0.2	0.9	30.3	5.5
<b>-0.1</b>	<b>3.4</b>	<b>1.3</b>	<b>0.3</b>	<b>0.5</b>	<b>6.4</b>
-0.2	3.9	0.1	0	0.5	5.1
-0.2	5.7	0.1	0	0.4	7.3
-0.2	4.7	5.5	0.5	2.4	13.1
-0.2	4.9	7.1	0.5	2.4	14.8
-0.2	3.8	3.7	0.4	1.6	17.4
-0.1	1.1	0.1	0	0	1.3
-0.2	5.8	1.9	0.3	0.1	11.8
-0.2	6.5	2	0.3	0.1	14
-0.2	4.8	2.4	0.3	0.1	10.5
0	2.6	0.3	0.2	0.5	3.8
0.1	3.6	0.3	0.2	0.7	5.5
-0.1	2.6	0.2	0.1	0.2	2.7
0	2.1	0.2	0.3	0.8	4.4
0	2.9	0.3	0.2	0.5	4.2
-0.1	3.8	0.3	0.2	0.2	4.3
-0.1	4.2	0.3	0.1	0.1	4.6
-0.2	3.4	0.9	0.2	0.1	4.6
-0.1	2.2	0.2	0.1	0.1	1.6
-0.1	3.9	0.9	0.3	0.1	4.9
-0.1	0.6	0.9	0.3	0.5	1.9
-0.1	2	3.3	0.1	0.6	3.3
-0.1	1.5	1.1	0.1	0.4	2.2
-0.2	3.9	1.2	0.3	0.1	5.6
-0.1	0.7	0.9	0	0.1	1.3
-0.1	1	0.1	0	0	1.3
-0.1	1.3	0.5	0.1	0.1	1.6
-0.1	1.1	0.2	0.1	0.1	1.2
0	1.1	0.4	0.2	1.3	2.1
0	1.1	0.3	0.1	0.3	2.2
-0.2	4.5	0.8	0.5	0.2	6.9
-0.2	2.8	4.9	0.4	1.1	16.4
-0.2	3.3	4.4	0.4	1	24.5
-0.1	2.6	1.1	0.9	0.5	7.9
-0.1	3.9	1.5	1.4	0.6	7.7
-0.2	2.2	0.5	0.4	0.3	6.9
-0.2	2	0.6	0.5	0.4	9.4

-0.1	0.8	0.5	0	0.1	1.4
-0.1	2.2	1.1	0.1	0.2	2.1
-0.1	2.3	0.9	0.1	0.2	2
<b>0.4</b>	<b>4.4</b>	<b>0.6</b>	<b>0.9</b>	<b>0.9</b>	<b>10.9</b>
-0.2	6.1	0.1	0.2	0.6	9
-0.2	4.6	0	0.1	0.1	12.1
-0.3	6	0.1	0.1	0.2	9.2
-0.4	5.2	-0.1	0.1	0.3	8.9
-0.2	3.8	0	0.2	3.5	10.6
0.4	4.2	0.7	1	1	11.5
0.6	4.9	0.9	1.1	0.8	10.8
0.3	4.9	0.7	0.5	0.4	14.7
0.5	4	0.7	1	0.7	9.9
0.1	2.9	0.1	0.2	0.3	11.8
0.6	4.8	1.1	0.8	0.7	10.2
0.6	5	1.4	0.9	0.9	11.4
0.9	4.4	1.1	1.1	1.2	16.9
0.9	4.9	1.5	1.2	1.3	12.7
0.4	5.3	1.2	0.6	1.4	17.1
1.2	4.7	1.5	1.4	1.6	14.5
0.8	5.3	1.2	1.1	1	11.3
0.8	4.8	2.5	0.9	1.5	13.3
0.6	5.4	1	0.9	0.8	12.4
0.9	4.9	1.1	1.2	1.1	11.7
0.5	3.5	0.6	0.7	0.6	14.6
0.4	4.1	0.6	1.3	1.7	9.8
0.8	4.3	1	1.1	1.3	15.7
0.2	3.1	0.4	0.8	2.7	7.6
0.3	2.4	0.5	0.8	3.5	11.1
0.4	5.3	0.7	0.9	0.7	8.6
0.2	4.3	1	0.4	0.4	9.4
0.6	4.2	0.7	1.5	0.8	5.1
0.5	5.1	0.8	1	1	7
<b>0.2</b>	<b>8.8</b>	<b>0.4</b>	<b>0.5</b>	<b>0.9</b>	<b>12.7</b>
0.2	8.9	0.3	0.5	0.9	12.8
0.4	8.3	0.2	0.5	0.5	11.5
0.3	7.7	0.6	0.6	0.8	14.8
-0.3	4.8	3.5	0.4	1.3	13.3
0.2	7.2	0.8	0.4	0.5	18.7
0.4	11.9	0.2	0.4	0.5	11.4
0.2	10.1	0.3	0.6	1.1	19.7

0.6	8.1	0.7	0.4	1.2	22.2
0.6	6	0.1	0.3	0.6	11.4
0.5	6.7	0.3	0.5	0.7	16.2
0.7	7	0.4	0.6	0.8	14.1
0.5	8.1	0.3	0.5	0.6	13.4
0.6	8	0.2	0.3	0.4	18.5
0	7.9	1.3	0.2	0.9	21.7
0.2	13.4	0.2	0.6	0.6	12.9
0.5	10.1	0.4	0.8	0.8	10.6
0.1	7.1	0.1	0.3	0.5	16
0.4	8.1	0.4	0.6	0.6	24.2
0	10.8	0.4	0.5	1.5	11.2
0.4	10.3	0.6	0.8	0.7	12.8
0	11.2	0.4	0.6	0.8	8.4
0.1	10.3	1.1	0.6	1.8	13.9
0.6	10.7	0.8	0.4	1.2	15.9
0.2	9.8	0.2	0.5	0.6	10.4
-0.1	12.8	0.2	0.4	0.9	14.1
0.2	8	1.1	0.3	1.1	22.2
-0.2	10.4	0.3	0.6	0.6	7.7
0.1	9.2	0	0.1	0.3	9.2
0.4	11	0.5	0.6	0.7	11.2
0.6	8	0.4	0.6	0.7	11.3
0.2	14	0.3	0.6	0.7	10.8
-0.3	12.1	1.5	0.2	0.6	17.3
0.2	11.3	0.3	0.8	2	16.8
0	10.2	0.5	0.6	1.1	10.9
-0.1	12	0.5	0.5	1.8	12.1
0	6.5	0.5	0.7	1.3	10.4
-0.3	4	4.1	0.3	1.2	13.2
<b>0</b>	<b>5.8</b>	<b>2.8</b>	<b>1.5</b>	<b>14.7</b>	<b>0.6</b>
0	0.4	2.4	0	0.4	0.1
0.1	0.2	1.3	0	0.5	0.4
0	2	2	0	1.2	0.1
-	-	-	-	-	-
0.1	0.3	7	0	0.6	1.9
0	0.1	2	0	0.9	0.4
0.1	0.1	1	0	0.5	0.5
0.1	0.4	6.1	0.1	0.7	2.5
0	6.4	2.8	1.6	16.5	0.7
0	0.7	2.3	0	0.4	0.1

0.1	0.5	3.1	0.1	0.9	0.1
0	0.1	2.4	0	1	0.1
0	0.6	2.7	0.1	1.9	0.1
0	0.1	2.7	0	0.7	0.1
0	0.1	2.7	0	0.8	0.1
0.1	0.1	1	0	0.5	0.2
0.2	1.9	3.6	0.4	3.6	6.4
0	0.1	2	0	0.4	0.1
0	0.1	1.1	0	0.4	0.2
<b>0.1</b>	<b>5.3</b>	<b>1.2</b>	<b>0.7</b>	<b>4.9</b>	<b>8.9</b>
0.1	5.4	0.9	1.3	22.2	10
0	3.2	1	0.2	4	4.7
0	3.9	4.8	0.4	1.9	6.1
0	3.1	1.1	0.4	13.3	5.1
-0.2	3	0.4	0.1	1.9	4.8
0	4.3	0.8	0.4	4.1	4.5
-0.1	5.5	3.5	0.1	1.5	5.6
0.5	5.8	0.7	1	13.4	13.1
0.1	5.8	2.6	0.5	4	16.8
0.2	6.7	1.6	0.6	3.1	20.7
0	6.1	1.6	0.5	3.9	19.4
1.5	3.4	3.1	1.8	2.6	12.1
0	1.7	5	0	1.7	1.6
0.6	4	0.8	1.2	9.1	9.2
0.7	4.4	1.1	1.6	8.2	11
-0.1	5.5	2.2	0.4	1.4	13.6
-0.2	4.1	1.6	0.4	1	10.2
-0.1	7.5	2.1	0.2	1.1	14.7
-0.1	6.9	2.2	0.1	1	12.3
0.2	18.3	2.4	0.4	1.1	7
0	1.5	2.9	0.1	1	7.2
0.4	6	0.9	1.6	5.9	11.3
0.3	4.1	0.5	1.5	2.5	7.5
0	1.3	1.4	0.2	21.1	2.2
0.2	8.1	1	1	3.2	10.2
0.1	8.7	1.3	3.7	3.1	10.5
0	7.5	1	0.8	2.3	7.6
<b>0</b>	<b>1.1</b>	<b>0.1</b>	<b>1.8</b>	<b>55</b>	<b>2.5</b>
0	0.9	0.2	1.1	67.6	1.7
0	0.9	0.4	0.9	64.2	2
0	0.7	0.1	1	41.8	1.5



0	0.8	0.2	2.4	49.5	2.3
0	1.2	0.1	2	53.9	2.7
0	1	0.1	3	53.2	2.7
0	2.1	0.1	0.4	54	1
0	0.9	0.4	1.2	22.1	3.2
0	0.5	0.3	1.6	37.5	3.1
<b>0</b>	<b>2</b>	<b>0.6</b>	<b>0.7</b>	<b>19.3</b>	<b>4.6</b>
0	3	0	1.1	32.8	5.6
0	2.1	3.3	0.4	18	2.8
-0.1	1.7	1.5	0.1	0.3	2.3
-0.1	1.6	1	0.1	0.5	2.4
0	1.9	0.6	0.3	5	4.2
0	2.2	0.6	0.2	2.1	4.9
0	2.1	0.5	0.3	6	7
0	2.4	0.3	0.2	5.3	8.2
0	3.4	1.4	0.5	31.2	3.8
0	1.9	0.4	0.5	57.6	3
0	1.6	1.5	0.5	43.9	3.1
0	1.2	2	0.4	40.8	2.7
0	3.9	0	1.2	22.8	6.9
0	4.2	0.1	1.2	20.2	7.2
0	1.1	1.3	0.1	0.9	3.4
0	1	0.3	1.5	27.4	2.6
0	1.6	0.5	0.8	27	5.2
0	1.6	0.5	0.4	9.3	6.8
0	2.1	0.1	1.6	20.6	5.5
0	2.1	0.1	1.1	11.9	5.9
0	1.5	0.2	0.6	55.2	2.4
0	1.8	0.1	0.5	56.3	1.5
<b>-0.1</b>	<b>3.4</b>	<b>0.8</b>	<b>0.6</b>	<b>14.7</b>	<b>7</b>
-0.1	2.7	0.3	0.3	17.4	5.8
-0.1	3.8	0.5	0.6	11.4	5.6
0	0.9	0.3	0.4	42.5	2.7
-0.1	3.9	0.9	0.7	8.6	7.5
-0.1	2.4	3.2	0.3	9.6	5.3
-0.1	4.1	0.2	0.6	6.2	8.6
-0.1	3.9	1	0.9	10	4.1
0	1.7	0.5	0.4	37.9	6.1
<b>0</b>	<b>0.9</b>	<b>0.2</b>	<b>1</b>	<b>5.9</b>	<b>1.7</b>
0	0.9	0.2	1.3	6.5	1.9
0	0.5	0.1	0.5	2.3	0.9

0	1.1	0.2	1.2	16	2.4
0	0.1	0.7	0	0.3	0.2
0	0.6	0.1	0.5	6.7	1.1
0	0.7	0.4	1.1	9.8	1.7
0	0.4	0.5	0.6	2.6	0.5
0	0.7	0.3	1.7	9.7	2.2
0	0.7	0.5	2	9.8	2.6
0	0.5	0.3	0.6	11.2	0.7
0	0.4	0.4	0.6	5.4	0.5
0	0.7	0.8	0.9	12	1.1
0	0.4	0.1	0.4	2.3	0.6
0	0.4	0.1	0.5	3	0.7
0	0.1	0.2	0.1	0.6	0.2
0	0.4	0.1	0.2	0.6	0.7
0	1.1	0.1	1.2	4.8	2.2
0	1.4	0.2	1.6	7.5	2.6
0	1.2	0.3	1.7	8.1	2.5
0	0.7	0.1	0.7	1.7	1.4
0	1.4	0.2	1.6	7	2.7
0	0.5	0.7	1.1	35.5	2
0	0.3	0.4	0.5	1.7	0.4
0	0.6	0.6	0.8	12.2	0.9
0	0.8	0.2	1.7	8.1	1.9
<b>0.2</b>	<b>4.8</b>	<b>0.7</b>	<b>0.7</b>	<b>3.4</b>	<b>9.3</b>

Windblown Dust Contribution (%)	Remaining Sources Contribution (%)	Total Attributable Mortality (Deaths)		
		GBD2019 CRF	Lower 95% Confidence Interval (CRF)	Upper 95% Confidence Interval (CRF)
<b>44.3</b>	<b>3.9</b>	<b>60999</b>	<b>38899</b>	<b>83661</b>
35.7	4.2	3037	2012	4034
49.1	2.9	7590	4617	10689
58.5	2.6	-	-	-
38.2	5.1	3162	1792	4737
43.2	7	9606	5643	14051
48.8	4.7	-	-	-
41.7	4.1	2378	1442	3374
17.8	6.3	1989	1418	2532
15	6.8	-	-	-
37.9	3.5	4459	3049	5822
70.2	1.3	3462	2164	4806
46.5	3.2	25316	16762	33617
67.3	1.7	-	-	-
38.2	4	-	-	-
<b>8.4</b>	<b>6.8</b>	<b>92306</b>	<b>54865</b>	<b>133818</b>
20.7	8.3	1580	938	2310
11.4	7.5	3666	2440	4874
14	8.2	9265	5472	13561
8.9	6.5	3024	1726	4502
5	6	6263	3414	9521
7.7	6.2	7200	3958	10902
7.1	5.9	-	-	-
15.1	8	2845	1957	3718
20.4	8.2	599	370	850
4.5	6.5	27725	16919	39238
4.1	6.3	-	-	-
11.3	6.8	14936	8195	23045
12.6	7.7	10974	7110	14947
9	8	-	-	-
7.1	6.4	3420	1909	5135
8	6	808	457	1215

<b>12.7</b>	<b>9.6</b>	<b>123227</b>	<b>57686</b>	<b>205136</b>
6.7	8.3	8681	4578	13454
8.5	9	-	-	-
9.3	10.3	136	9	323
7.8	8.9	1100	513	1849
5.8	8.4	1274	534	2229
4.7	7.1	-	-	-
9.4	7.2	2074	1009	3377
14.5	10.4	68482	30672	117145
6.9	7.5	-	-	-
55.3	4.7	-	-	-
5.8	8.3	-	-	-
9.5	13.2	-	-	-
13.7	14.1	-	-	-
11	11.7	-	-	-
10.7	8.4	41480	20371	66759
12.1	8.7	-	-	-
8.6	7.6	-	-	-
<b>15.1</b>	<b>33.6</b>	<b>2147</b>	<b>597</b>	<b>4218</b>
16.6	30	1802	516	3516
15.3	24.5	-	-	-
5.8	54.5	346	81	702
5.5	57.3	-	-	-
<b>6.6</b>	<b>6.8</b>	<b>59889</b>	<b>34089</b>	<b>90490</b>
1	34.4	35	11	68
7.9	8.2	38942	20649	61823
6.3	9.5	-	-	-
8	7.8	-	-	-
9.5	6.1	-	-	-
8.5	6.6	-	-	-
9.6	6	-	-	-
5.5	4.4	19685	12741	26753
4.8	4.3	-	-	-
6.6	4.5	-	-	-
5	4.6	-	-	-
6	4.7	-	-	-
6.7	4.5	-	-	-
4.8	4	-	-	-
0.4	13.8	1226	688	1846
<b>2.2</b>	<b>11.9</b>	<b>50594</b>	<b>17329</b>	<b>93521</b>
0.9	10.4	3686	1157	6967

0.5	10.1	-	-	-
1.5	11	-	-	-
8.9	21	3	0	8
2.4	12.1	46904	16172	86546
0.6	14.2	-	-	-
0.4	9.6	-	-	-
0.4	10.1	-	-	-
1.1	20	-	-	-
0.9	9.8	-	-	-
1.4	11.5	-	-	-
3.8	2.3	-	-	-
0.6	11.1	-	-	-
0.6	10.5	-	-	-
0.7	13.7	-	-	-
1.1	23.8	-	-	-
1.7	16.5	-	-	-
1.3	6.4	-	-	-
<b>9</b>	<b>20.2</b>	<b>18377</b>	<b>9779</b>	<b>28513</b>
13.2	24.4	12197	6138	19540
8.5	19.7	-	-	-
13.6	30.5	-	-	-
3.2	14.1	5409	3295	7651
2.5	6.9	-	-	-
7.2	21.6	772	345	1322
<b>10.1</b>	<b>9.4</b>	<b>114536</b>	<b>56831</b>	<b>185059</b>
15.4	11.9	10	4	17
6.8	6.2	2358	1136	3824
5.5	5.9	-	-	-
4.9	8.8	3458	1798	5471
4.9	8.5	-	-	-
35.8	8.1	378	201	577
5.7	11.4	1348	633	2236
12	10.5	280	6	741
7.5	9.8	13251	6545	21491
5.5	8.5	-	-	-
8.7	10.8	-	-	-
4.6	7.6	26869	13026	43657
4.2	7.5	-	-	-
4.6	7.2	-	-	-
3.7	8.6	-	-	-
25.2	10.2	5592	3019	8723

14.4	8.9	-	-	-
20.7	39.5	14	1	32
11.5	19.8	496	171	922
38.1	5.5	2161	1263	3119
37.1	5.8	-	-	-
10.7	8.4	24366	13450	37014
28.1	18.8	-	-	-
4	5.1	-	-	-
5.7	8	85	38	144
39.1	16.4	135	65	220
5.1	9.5	4574	2378	7212
4.5	9.7	-	-	-
18	18	384	90	783
8.6	11.9	2202	884	3989
16.9	10.5	9026	4145	15201
13	7.8	-	-	-
0.6	10.5	-	-	-
10.5	12.1	614	51	1445
6.2	7.1	1398	627	2367
6.7	7.6	-	-	-
8.2	11.9	15518	7290	25840
7.7	10.6	-	-	-
6.6	10.5	-	-	-
8.9	12	-	-	-
5.9	7.3	15	7	24
11.3	7.7	5	2	9
<b>6.1</b>	<b>21.7</b>	<b>15247</b>	<b>9354</b>	<b>21463</b>
7.8	27.8	3393	2108	4722
5.7	28.8	-	-	-
8.6	19.7	3853	2181	5678
10.8	17.5	-	-	-
4.7	20.6	8000	5064	11064
<b>10.8</b>	<b>28.1</b>	<b>14258</b>	<b>7804</b>	<b>21590</b>
13.1	49.5	28	15	42
4.9	42.4	84	43	132
72.4	20.6	155	89	225
2.4	42.1	76	43	110
4.7	53.8	8	2	15
3.5	29.7	5918	3323	8889
4.7	32.2	-	-	-
11.8	49.9	29	16	44

6	33.6	3453	1883	5241
70.8	21.5	47	27	68
68.3	19.8	402	235	577
3.2	19.3	1504	846	2248
4.4	30.3	893	479	1356
11.8	52.4	430	104	857
69.8	22.6	71	42	103
70.1	22.3	57	32	83
70.9	18.3	253	153	357
69.5	19.1	813	459	1173
12.5	52.7	30	11	54
12.8	49.4	8	3	16
<b>13.9</b>	<b>14.8</b>	<b>65630</b>	<b>38150</b>	<b>94095</b>
23.2	15.8	11818	7074	16861
16.7	11.1	-	-	-
40.3	16	-	-	-
26.8	33	888	494	1331
10.7	15	1803	1064	2571
10	14.4	-	-	-
1.8	14.2	3338	2051	4644
0.6	9.3	-	-	-
7.8	23.1	1581	976	2221
2.7	11.8	34259	19616	49136
9	19.7	-	-	-
0.5	8.2	-	-	-
0.2	6.2	-	-	-
1.9	21.5	-	-	-
8.7	5.4	-	-	-
25.5	30.8	863	487	1264
23.3	31.2	-	-	-
35	30.9	643	328	1013
49.3	16.6	10436	6060	15054
50.7	16.3	-	-	-
43	15	-	-	-
<b>4.8</b>	<b>20.8</b>	<b>42973</b>	<b>20585</b>	<b>70359</b>
4.9	20.8	41992	20110	68776
0.6	7.5	-	-	-
1.3	10	-	-	-
1.9	15.7	-	-	-
0.8	12.1	-	-	-
3.6	23.8	-	-	-

2.8	54.8	-	-	-
2.6	41.1	-	-	-
1	10.5	-	-	-
3	21.3	981	475	1583
<b>50.8</b>	<b>3.5</b>	<b>317861</b>	<b>227116</b>	<b>404247</b>
51.8	2.8	7110	5208	8918
39.5	3.8	-	-	-
30.9	8.3	19437	12897	25909
15.8	10.4	-	-	-
28.9	10.1	-	-	-
55.7	1.1	551	412	671
42	4.7	87957	67883	106168
36.1	4.6	-	-	-
39.8	5.9	-	-	-
52.9	0.9	40870	28535	52551
41.2	2.5	-	-	-
58.3	-1.5	-	-	-
46.3	2.2	-	-	-
46.9	1.4	-	-	-
56.6	-0.1	22830	16961	28159
56.5	-0.4	-	-	-
44	4.6	2622	1745	3466
66.2	-1.4	1370	1046	1666
39.3	5.7	3240	2037	4445
77.4	6.1	3030	2093	3925
66.3	4.5	25152	17055	32982
80.2	2.4	-	-	-
38.9	5.3	1695	1132	2234
73.5	2	1617	1149	2053
58.8	1.1	459	354	552
63.7	1.1	16992	13138	20453
66.8	-0.7	-	-	-
78	2.8	13005	9667	16117
80.4	1.9	-	-	-
38.9	4.9	10039	6572	13454
33	9.7	6946	4507	9394
24	9.4	-	-	-
21.9	6.3	41149	26190	56294
11.8	7.7	-	-	-
29.5	4.7	-	-	-
26.2	5.6	-	-	-



65	1	2783	2019	3475
63.2	3.6	9006	6517	11362
62.9	3.3	-	-	-
<b>4.1</b>	<b>3.8</b>	<b>1032907</b>	<b>810092</b>	<b>1238344</b>
1.5	4.8	63718	49507	76737
1.2	4.4	-	-	-
1.4	5	-	-	-
1.5	4.6	-	-	-
3.6	3.9	240	170	306
3.4	3.8	866566	682014	1036734
6.4	3.6	-	-	-
7.3	4.3	-	-	-
3	3.5	-	-	-
0.9	3.8	-	-	-
5.3	5.2	-	-	-
3.7	3.5	-	-	-
2.9	3.4	-	-	-
4.2	4.2	-	-	-
3.1	3.7	-	-	-
3.4	3.8	-	-	-
4.9	3.6	-	-	-
6.4	5	-	-	-
5.3	3.6	-	-	-
4.4	3.9	-	-	-
2.1	3.5	-	-	-
2.7	3.8	-	-	-
2.5	3.3	-	-	-
3	3.3	15905	12615	19009
4.9	3.6	-	-	-
13	2.6	86477	65786	105558
17.9	2.9	-	-	-
3.8	3	-	-	-
6	2.9	-	-	-
<b>9.2</b>	<b>3.9</b>	<b>1418337</b>	<b>1075605</b>	<b>1738024</b>
9.2	3.8	1386689	1053525	1696981
10.7	2.8	-	-	-
4.3	3.8	-	-	-
8	7.6	-	-	-
4.3	3.5	-	-	-
4.8	3.6	-	-	-
4.1	3.9	-	-	-

2.6	4	-	-	-
6.5	4.4	-	-	-
5	4.2	-	-	-
4.8	4.2	-	-	-
5	4.1	-	-	-
6.3	3.7	-	-	-
3.8	4.3	-	-	-
5.1	3.7	-	-	-
8.2	2.8	-	-	-
11.9	3.6	-	-	-
3.8	3.7	-	-	-
11.8	2.2	-	-	-
4.6	4	-	-	-
11.8	2.3	-	-	-
4.6	5	-	-	-
2.9	4.3	-	-	-
9.9	2.4	-	-	-
5	2.7	-	-	-
3	3.7	-	-	-
13.3	2.5	-	-	-
18.4	3.3	-	-	-
4.7	4	-	-	-
6.7	4.1	-	-	-
5.4	3.1	-	-	-
5.7	4.2	-	-	-
4.1	4	-	-	-
10.5	2	-	-	-
4.2	3.3	-	-	-
5.8	4.5	20110	14907	25011
6.5	6.9	11539	7172	16032
<b>2.5</b>	<b>58.1</b>	<b>1381</b>	<b>631</b>	<b>2286</b>
0.7	94.3	7	1	16
0.8	94.8	25	9	45
3.6	82.5	273	104	476
-	-	-	-	-
1.7	83.9	25	7	48
2	93.1	11	3	23
1	94.9	10	4	19
2.1	82.1	9	3	17
2.6	54.2	841	424	1330
0.7	93.6	32	13	56

1.6	89.5	80	35	137
3.5	90.8	18	7	30
4	85.7	42	19	70
2.3	93	0	0	1
2.8	92.1	2	0	4
1	95.6	1	0	2
1.3	42.3	4	1	9
0.9	95.5	0	0	0
1	96.1	1	0	3
<b>2.8</b>	<b>10.6</b>	<b>230616</b>	<b>138209</b>	<b>332098</b>
2.6	8	2975	1788	4291
2.4	12.2	93807	54694	137546
1.1	6.9	-	-	-
0.4	12.5	-	-	-
2.4	6	-	-	-
1.3	18.5	-	-	-
0.7	8	-	-	-
4.9	6.5	1087	631	1604
0.9	16.2	9619	5179	14843
1	12.3	-	-	-
0.3	9.1	-	-	-
7.5	10.9	37	16	64
3.3	74.8	574	293	879
4.7	6.6	21691	14555	28851
4.1	9.2	-	-	-
1.4	20.2	29306	16666	43512
0.9	9.9	-	-	-
1.3	27.5	-	-	-
1.1	26.7	-	-	-
4.8	6.4	6940	3979	10055
12.9	52.6	33	18	52
3.2	5.8	29501	18954	40308
1.6	3.4	-	-	-
15.7	34.4	183	100	283
2.8	5	34862	21336	49809
1.3	5.2	-	-	-
1	4.9	-	-	-
<b>11.6</b>	<b>9</b>	<b>15279</b>	<b>10064</b>	<b>20591</b>
4	7.1	3851	2425	5351
5	8.7	-	-	-
37.9	8.2	738	508	967

15.3	11.4	1367	932	1790
10.6	9.3	8344	5536	11198
6.9	7.7	-	-	-
2.4	4.8	-	-	-
44.1	9.2	288	201	371
23.4	13.1	691	462	913
<b>24.4</b>	<b>11.5</b>	<b>31529</b>	<b>20012</b>	<b>43791</b>
7.2	8.2	731	480	989
12.2	44.5	75	41	116
60.9	5	343	239	445
64.6	4.5	1078	747	1403
38.3	8	6473	4239	8765
32.2	7	-	-	-
25.1	12.4	5029	3101	7115
20.9	9.3	-	-	-
3.5	34.4	1768	1006	2664
4.2	11.1	1070	644	1539
5.2	18.8	1506	906	2175
4.7	23.8	-	-	-
7.5	8.7	1325	890	1762
7.2	8.2	-	-	-
61	12.9	583	365	817
42	8.2	1084	712	1469
15	15.2	4856	2961	6929
23.2	15	-	-	-
16.2	9.6	3430	2317	4545
14.7	8.8	-	-	-
3.7	7.8	2179	1363	3058
3	7	-	-	-
<b>8</b>	<b>9.2</b>	<b>29840</b>	<b>18964</b>	<b>40735</b>
9.2	9	803	492	1125
12.8	7.5	781	506	1056
15.8	8.6	697	429	979
8.5	8.9	25035	16073	33892
22.5	20.2	-	-	-
3.7	4.7	-	-	-
4.9	10.3	303	182	427
4.2	10.9	2221	1282	3256
<b>74.1</b>	<b>2.7</b>	<b>94736</b>	<b>68733</b>	<b>119976</b>
68.6	2.6	1686	1158	2216
86.2	2.1	2666	1855	3479

58.9	5.1	7777	5708	9754
93.4	4	244	175	310
80.5	2.9	1979	1396	2567
69.3	4.9	4970	3553	6359
89.4	2.3	407	302	508
67.6	3.8	10734	7908	13427
64.8	4	-	-	-
76.5	3.5	2084	1468	2698
85.1	3	291	213	365
69.7	5.7	506	360	646
89	2.1	2176	1574	2769
87.4	2.4	-	-	-
95.6	1.3	1117	835	1382
90.9	1.2	2232	1632	2812
70.6	2.3	50577	36761	63987
59.8	2.9	-	-	-
59.1	3.1	-	-	-
83.4	1.7	-	-	-
60.6	2.8	-	-	-
36.8	11.9	45	29	61
91.7	2	2732	2034	3391
72.2	4.6	1236	868	1601
67.8	2.9	1278	903	1644
<b>16.1</b>	<b>5.2</b>	<b>3832670</b>	<b>2715393</b>	<b>4972016</b>

GEMM	COPD Contribution (%)		DM Contribution (%)		LRI Contribution (%)	
	GBD2019 CRF	GEMM	GBD2019 CRF	GEMM	GBD2019 CRF	GEMM
<b>75492</b>	<b>4.2</b>	<b>4.9</b>	<b>5</b>	<b>5.8</b>	<b>5.7</b>	<b>8.8</b>
3644	8.1	9.3	8.1	9.5	3.1	4.5
8630	3.1	3.8	4.6	5.2	4.3	6.8
-						
3543	3.5	4.4	6	6.7	2.1	3.5
10602	11.6	14.1	4.7	5.1	4.2	6.7
-						
3228	7	8.6	1.8	2	3.1	5
2885	2.6	3.1	0.9	1.2	4.1	6.2
-						
7288	4.3	4.9	5.4	6.7	10.3	14.8
3728	1.7	2	3.6	4.1	5.4	8.5
31945	1.6	1.9	5.4	6.6	7	10.3
-						
-						
<b>100703</b>	<b>5.5</b>	<b>6.6</b>	<b>5</b>	<b>5.6</b>	<b>3.4</b>	<b>5.3</b>
1774	4.5	5.6	1.4	1.6	2.6	4.3
4710	5.3	6.2	11.3	13.3	1.5	2.3
9724	4	5	3.6	4.1	2.1	3.5
3134	7.1	8.8	5.7	6.2	1.6	2.7
6572	6.8	8.2	8.3	8.6	4.6	7.3
7529	8.8	10.8	5.1	5.3	1.4	2.3
-						
3380	4	4.8	7.2	8.8	1	1.5
652	1.9	2.4	4	4.6	1.3	2.1
31196	5.5	6.4	5	5.4	5	7.7
-						
14974	5	6.4	2.3	2.4	3.5	5.8
12615	5.3	6.4	6.1	7.1	1.9	2.9
-						
3586	3.7	4.5	3.6	3.8	5.1	8.1
857	7.7	9.1	6.3	6.4	7	10.9

<b>117852</b>	<b>3</b>	<b>3.9</b>	<b>2</b>	<b>2.1</b>	<b>1.9</b>	<b>3.2</b>
8560	2.8	3.5	0.6	0.7	1.1	1.8
-						
98	3.9	5.3	3.4	3.4	2.5	4.1
1023	2.5	3.3	3.3	3.5	1.7	2.9
1168	3.4	4.5	1.7	1.8	1.9	3.2
-						
2024	3.6	4.7	1.6	1.7	2.8	4.7
64298	3.4	4.5	2.9	3.1	2.3	3.8
-						
-						
-						
-						
-						
40682	2.3	3	0.7	0.8	1.4	2.4
-						
-						
<b>2090</b>	<b>14.2</b>	<b>17.9</b>	<b>10.1</b>	<b>9.6</b>	<b>4.7</b>	<b>7.3</b>
1757	14.2	17.8	10.5	10	4.8	7.4
-						
333	14.2	18	7.5	7.2	4.5	7
-						
<b>67774</b>	<b>8.3</b>	<b>9.3</b>	<b>5.8</b>	<b>6.1</b>	<b>15.8</b>	<b>22.8</b>
33	6.3	8.2	25.5	25.2	5.7	9.2
42858	8.1	9.1	2.7	2.5	18.2	26.7
-						
-						
-						
-						
-						
23414	8.9	9.7	12.2	13	10.4	15
-						
-						
-						
-						
-						
1469	5.7	6	2	1.9	24.7	34.7
<b>49670</b>	<b>14.4</b>	<b>18</b>	<b>9.1</b>	<b>8.6</b>	<b>4.5</b>	<b>7</b>
3632	12.6	15.6	9.1	8.6	5.4	8.2

-						
-						
3	11.8	15.4	4	3.9	3.8	6
46035	14.6	18.2	9.1	8.6	4.4	6.8
-						
-						
-						
-						
-						
-						
-						
-						
-						
-						
-						
<b>20581</b>	<b>11.3</b>	<b>12.8</b>	<b>10.6</b>	<b>10.2</b>	<b>15.6</b>	<b>22.8</b>
13619	11.2	12.5	10	9.3	18.9	27.6
-						
-						
6199	11.3	12.9	11.9	12.4	9	13.6
-						
763	13.7	16.7	10	9.5	8.5	13.2
<b>118698</b>	<b>12.6</b>	<b>15.1</b>	<b>8.9</b>	<b>8.7</b>	<b>6.8</b>	<b>10.4</b>
10	15.6	18.7	6.3	5.9	6.9	10.5
2368	10	12.3	10.9	10.8	2.8	4.4
-						
3717	15.2	17.6	5.6	5.2	10.6	15.8
-						
392	10.8	13	16.9	17.2	3.1	4.9
1403	18.3	21.6	9.1	8.5	7.8	11.7
254	6.6	8.9	3.4	3.4	2.1	3.5
13733	9.1	10.8	9.6	9.2	8.6	13.2
-						
-						
27266	10.8	13.2	8.8	8.6	4.9	7.7
-						
-						
-						
5806	9.6	11.5	3.2	3.2	7.3	11.5



-						
13	11	13.7	4.8	4.4	8.1	12.4
499	15.1	18.4	5.5	5.1	8.4	12.7
2436	10.1	11.4	19.4	19.6	7.9	11.8
-						
25517	11.6	13.8	12.1	12.3	3.8	6
-						
-						
85	12.5	15.2	6.5	6.2	6.3	9.7
138	6.8	8.2	10	9.9	7.8	12.2
4847	16.4	19.2	7.7	7.3	7.5	11.3
-						
385	15.7	19.2	6.7	6.1	9.3	13.9
2202	12.1	14.7	13.5	12.7	12	18.3
9163	19.1	22.9	9.5	9	6.3	9.5
-						
-						
583	10.2	13.1	9.4	9	5.5	8.7
1404	10.8	13.3	8.6	8.4	5.7	8.9
-						
16453	16.9	19.6	3.6	3.3	11.8	17.4
-						
-						
-						
15	7.8	9.3	2.9	2.8	8.7	13.2
5	9	11.2	6.5	6.3	5.6	8.9
<b>21966</b>	<b>7.5</b>	<b>7.9</b>	<b>13.9</b>	<b>13.8</b>	<b>23.5</b>	<b>32.3</b>
5522	9.2	9.7	15.5	15.9	20	27.8
-						
4518	8.5	9.6	19.6	19.6	13.1	19.6
-						
11927	6.4	6.4	10.5	10.6	30.1	39.2
<b>19138</b>	<b>6.1</b>	<b>7</b>	<b>13.2</b>	<b>13.5</b>	<b>8.1</b>	<b>13.9</b>
29	2.7	3.3	27.8	28.6	8.6	13.6
86	3.2	4	19.5	20.2	6.9	11.2
172	3.2	3.7	30.6	31.5	10	15.3
100	6.6	7.5	25.2	25.5	11.5	17.3
7	4.8	6.2	15.6	15.4	5	8.1
6639	8.4	9.7	5.1	5.1	10.5	16
-						
33	5.6	6.6	27.1	27.6	8.1	12.7

3951	3.9	4.9	10.7	11.5	4.6	7.6
54	3.6	4.2	24.4	25.4	9.6	14.9
472	2.4	2.9	20.6	22.3	6.3	10
4860	5.1	6	13	13.4	13.1	20.4
967	5.4	6.7	33.2	34.7	3.6	5.8
415	9.9	12.6	35.3	33.8	5.8	9.1
81	7.5	8.8	27.2	28.5	7	10.9
65	3	3.5	28.1	29.7	6.4	10.1
302	4.4	5.3	16.2	17.7	6.5	10.3
870	2.8	3.4	35.7	37.9	3.3	5.1
28	3.1	4.1	19	19.4	2.8	4.6
8	3.6	4.8	22.2	22.8	6.9	11.5
<b>85241</b>	<b>11.1</b>	<b>12.6</b>	<b>22.4</b>	<b>23.1</b>	<b>7.1</b>	<b>11.3</b>
14390	17.2	19.7	8.9	9.3	6.6	10
-						
-						
974	14.7	17.2	9.3	9.5	6.4	10
2502	8.4	9.3	18.6	19.1	12.5	18.2
-						
7029	5.7	5.8	22.8	22.9	24.5	32.7
-						
3250	14.1	16.7	6.3	6.8	4.3	6.8
43465	10.7	12.2	30.4	31.2	5.9	9
-						
-						
-						
-						
-						
1616	10.1	11.7	20.2	20.8	7	10.7
-						
694	9	10.9	21.6	21.6	8	12.5
11322	7.2	8.4	15.8	16.8	5.2	8.2
-						
-						
<b>45750</b>	<b>10.7</b>	<b>12.9</b>	<b>15.3</b>	<b>14.9</b>	<b>10.8</b>	<b>16.7</b>
44559	10.8	13.1	15.1	14.7	10.9	16.8
-						
-						
-						
-						
-						

-						
-						
-						
1192	6.4	8	22.7	22.9	7.1	11.4
<b>419282</b>	<b>6.1</b>	<b>6.8</b>	<b>6</b>	<b>7.7</b>	<b>6.1</b>	<b>9.6</b>
29383	4.9	5.3	4.2	5.7	20.9	27.2
-						
22018	4.9	5.8	5.1	6.2	4.7	7.1
-						
-						
776	5.9	5.9	26.7	36.1	3.8	4.4
110679	5.4	6	5	7.9	7.4	9.6
-						
-						
48441	7.3	8.3	7.6	9.5	4.8	6.8
-						
-						
-						
27431	1.9	2.2	8.2	11.6	3.4	4.7
-						
3077	3.8	4.3	14.4	16.8	6.2	9
1754	3.3	3.7	5.3	8	12.8	16.4
3693	5	5.7	5.2	6	4.1	6.2
3535	5.3	6.2	5.7	7.1	4.8	6.9
30306	4.8	5.6	4.9	6	4.2	6.3
-						
1992	3.4	3.8	15.2	18	4.8	7
1951	3.7	4.2	9.9	12.9	5.9	8.2
625	3.4	3.5	14.9	22.7	4.4	5.2
20827	4	4.6	3.6	5.6	7.3	9.8
-						
25334	5.9	6.8	2.7	3.8	8.6	11.9
-						
11249	3.6	4.3	3.3	3.9	3.8	5.8
7808	5	5.9	5	5.8	4	6
-						
47245	12.7	14.4	9	9.9	4.9	7.3
-						
-						
-						

3331	9.1	10.4	8.4	11	4	5.6
17827	5.7	6.6	2.3	3.2	9.4	13.2
-						
<b>2146883</b>	<b>24.4</b>	<b>25.5</b>	<b>4.7</b>	<b>7.5</b>	<b>10.9</b>	<b>13.1</b>
158987	14.1	15.6	5.2	7.9	8.3	10.8
-						
-						
-						
524	26.7	29	7.5	9.1	7.7	10.5
1752666	26	27.2	4.5	7.2	10.8	12.9
-						
-						
-						
-						
-						
-						
-						
-						
-						
-						
-						
-						
-						
-						
-						
39195	41.2	42.8	2.5	4	10.4	12.3
-						
195510	13.8	14.8	6.8	9.8	13.6	17.1
-						
-						
-						
<b>2049784</b>	<b>18.3</b>	<b>20.6</b>	<b>2.4</b>	<b>3.3</b>	<b>2.8</b>	<b>3.7</b>
1992762	18.4	20.6	2.3	3.2	2.6	3.6
-						
-						
-						
-						
-						

-						
-						
-						
-						
-						
-						
-						
-						
-						
-						
-						
-						
-						
-						
-						
-						
-						
-						
-						
-						
-						
-						
-						
-						
-						
43106	21.1	24.1	2.4	3.2	4	5.6
13916	11.6	12.5	16.5	16.7	13.8	19.6
<b>3812</b>	<b>9.8</b>	<b>13.5</b>	<b>23.6</b>	<b>20</b>	<b>10.5</b>	<b>19</b>
5	6.4	8.7	29.1	29.5	3.4	5.6
30	5.6	7.4	25.4	26.1	4.3	7.1
311	2.4	3.1	44	45.2	2.7	4.4
-						
22	5.1	6.8	10.3	10.4	3.5	5.8
23	3.6	4.9	28.4	29.9	3.4	5.8
12	5.6	7.4	18.4	19	5.1	8.5
8	5.6	7.5	18.4	18.8	3.3	5.5
2977	13.5	15.6	18.7	17.8	14.5	21.9
46	7.9	10.2	20.6	21	5.2	8.5

260	5.2	6.6	14.4	14.7	8.5	13.9
21	7.6	9.6	32.4	31.8	6.4	10.2
90	7.6	9.8	12.6	13	5.9	9.7
0	5.7	7.6	33.1	33.2	3.8	6.3
2	4.9	6.4	39.8	39	6.1	9.8
1	3.4	4.8	20.5	21.4	5.3	9.1
4	6.2	8.1	23.5	23.1	8	12.9
0	7.3	9.7	22.7	22.9	4.7	7.7
1	6.2	8.5	24.2	24.7	4.1	6.9
<b>326462</b>	<b>8.3</b>	<b>10.2</b>	<b>11.7</b>	<b>12.5</b>	<b>7.6</b>	<b>12</b>
7983	6.9	7.7	8.1	8.2	19.4	28.5
119054	7.3	9.1	13.1	14.3	3.5	5.8
-						
-						
-						
-						
-						
2831	8.1	9.5	8.5	8.8	12.9	20
10569	6.1	7	4.3	4.3	17.5	26.4
-						
-						
37	12.2	15.7	9.9	10.1	3.5	5.7
595	4.6	5.6	41.5	42.7	3.5	5.6
46930	14.6	16.6	10.3	11.7	8.2	12.1
-						
43218	6.5	7.5	10.4	10.6	14.2	21.7
-						
-						
-						
9675	7.5	8.8	24.3	25.6	5.3	8.2
37	6.8	7.8	10	9.7	17.6	26.4
38193	9.9	10.9	10.7	11.5	12.6	18.2
-						
386	9.4	11.2	6.5	6.6	12.4	19.4
46955	8.4	10.3	10.1	11.1	5	8.1
-						
-						
<b>53321</b>	<b>7.4</b>	<b>8</b>	<b>8.9</b>	<b>8.8</b>	<b>26.6</b>	<b>36.7</b>
8764	5.4	5.7	9.8	10	26.6	36.4
-						
4423	6.1	6.1	6.4	7.3	37.4	46.3

2589	6.5	7	10.9	12.6	17.4	23.7
36180	8.6	8.9	7.6	8.1	28.2	37.1
-						
-						
439	7.5	7.7	13.5	15.9	22.3	28.4
927	5.9	6.3	16.7	18.7	16	21.8
<b>131540</b>	<b>6.4</b>	<b>6.5</b>	<b>9.3</b>	<b>9.4</b>	<b>29.7</b>	<b>40.7</b>
4539	7.9	8.2	7.6	8.1	28.5	37.9
205	6.2	7	11.9	11.5	20.9	31
592	4.5	4.6	8.8	10.4	27.6	35.3
3668	5.7	5.8	7.6	8.8	33.6	42.1
33633	7.4	7.5	9.5	10	31.9	41.2
-						
12872	7.6	8	9.9	9.9	26.2	36.5
-						
6616	6.1	6.9	6.4	6.4	21.1	31.8
4842	5.5	5.8	10.5	10.2	29.1	40.2
8492	4.2	4.7	10.3	10.4	23.3	34
-						
4827	8.7	9	9.4	10.3	26	34.4
-						
9549	5	4.9	6.5	6.3	42.6	53.9
4609	5.1	4.9	6.8	7.1	46.2	55.7
18021	4.7	4.8	9.8	9.6	31.8	43.1
-						
13648	7.1	7.2	9.5	10.4	31.6	40.3
-						
5427	5.2	5.6	9.6	9.8	24.8	35
-						
<b>45500</b>	<b>8.3</b>	<b>8.5</b>	<b>21.3</b>	<b>21.6</b>	<b>17.7</b>	<b>25.5</b>
1213	6.4	6.9	18.9	19.2	19	27
1800	9.9	10.4	18.1	19	20.9	28.4
1128	9.4	10.1	15.4	15.7	20	28.4
34898	8.7	9.2	22.3	23.5	16.2	22.3
-						
-						
561	6.4	6.8	26.3	26.2	19.1	27.1
5900	3.7	3.8	12.5	11.7	31.3	42.5
<b>320839</b>	<b>5</b>	<b>4.9</b>	<b>5.8</b>	<b>7.3</b>	<b>43.4</b>	<b>51.5</b>
7039	5	4.9	6.1	7	40.1	48.9
16949	3.3	3.1	5.1	6.1	49.5	57.5

19088	5.4	5.4	8	10.8	34.7	40.9
393	5.7	6	8.7	11.1	18.9	24.3
13333	4.6	4.4	3.9	4.9	54	61.3
16003	4.9	4.9	6.3	8	38.6	46
1538	6.7	6.9	6.2	8.5	29.3	35.6
22565	5.9	6.1	7.9	10.6	25.5	31.7
-						
11118	5.6	5.4	5.5	6.8	44.1	52
1400	5.8	5.9	6.5	8.7	29.4	36.1
2170	4.8	5	7.9	9.9	27.3	34.4
14124	7.6	7.5	5.7	7.4	41	48
-						
2501	6	6.1	7.6	10.7	29.3	34.7
19482	4.6	4.4	3.3	4.6	57	62.9
152639	4.6	4.4	5	6.8	49.9	56.4
-						
-						
-						
-						
98	12	12.8	3.3	3.5	21.6	29.8
9924	7	7.2	7.6	10.6	27.5	33.1
6034	5	5	5.1	6.2	40.9	49.2
4440	5.5	5.7	6.3	7.6	28.9	36.7
<b>6222380</b>	<b>16.1</b>	<b>18.2</b>	<b>5.2</b>	<b>6.7</b>	<b>7.7</b>	<b>12.3</b>



LC Contribution (%)		IHD Contribution (%)		Stroke Contribution (%)		Pre-Term Birt
GBD2019 CRF	GEMM	GBD2019 CRF	GEMM	GBD2019 CRF	GEMM	GBD2019 CRF
3.4	3.8	54.3	52.8	27.5	23.9	17558
8.6	9.7	54.5	51.7	17.6	15.2	504
4.6	5.2	57.7	56.7	25.7	22.3	1411
6.5	7.5	44.8	45.4	37.1	32.5	323
4.8	5.4	39.9	39.1	34.8	29.6	1351
2.8	3.2	57.5	57.1	27.7	24.2	1082
5.3	6.5	42.1	41.8	45	41.3	907
2	2.3	51.7	48.6	26.2	22.7	2453
1.9	2.2	55.3	54.8	32.2	28.4	1164
1.8	2.1	60.8	58.6	23.3	20.5	8362
<b>12.6</b>	<b>14.1</b>	<b>43.7</b>	<b>42.6</b>	<b>29.8</b>	<b>25.7</b>	<b>7243</b>
9.1	10.4	42.1	42.6	40.3	35.5	219
11.2	12.9	36	34.9	34.6	30.4	192
7.1	8.1	43.7	44.3	39.6	34.9	432
12.5	14	44.7	44.2	28.3	24.1	130
12	13	50	47.9	18.2	15	575
15	16.5	50	48.7	19.6	16.4	494
8.5	10.1	31.9	31.8	47.4	43	222
13	15.1	34.5	35.2	45.5	40.7	48
17.5	19.1	43.9	41.9	23.2	19.5	2429
8.5	9.6	44.5	44.6	36.3	31.2	1012
11.6	13.3	37.3	36.9	37.7	33.3	1010
9.7	10.7	56.5	54.9	21.4	18	382
19	20.3	34.9	33	25.1	20.4	97

<b>5</b>	<b>5.7</b>	<b>60.4</b>	<b>61.3</b>	<b>27.8</b>	<b>23.8</b>	<b>8485</b>
4.7	5.4	67.9	68.7	22.9	19.9	308
12.9	14.4	59.7	58.3	17.5	14.5	10
7	8	54.7	55.6	30.8	26.6	49
7.1	8	62.8	62.9	23.1	19.6	56
4.7	5.3	61.2	61.4	26.2	22.3	147
5.6	6.5	53.9	54.6	32	27.5	5955

3.9	4.5	69.6	70.3	22	19	1960
-----	-----	------	------	----	----	------

<b>17.3</b>	<b>18.2</b>	<b>36.8</b>	<b>33.8</b>	<b>16.8</b>	<b>13.2</b>	<b>524</b>
17.7	18.5	36.1	33.1	16.7	13.1	457

15.7	16.6	40.8	37.6	17.4	13.7	67
------	------	------	------	------	------	----

<b>20.3</b>	<b>20.6</b>	<b>23.3</b>	<b>20.7</b>	<b>26.5</b>	<b>20.6</b>	<b>6093</b>
10.9	11.8	33.7	31.4	17.9	14.2	14
20.7	20.5	24.7	21.8	25.7	19.4	2761

19.9	21	19.8	17.9	28.8	23.3	2880
------	----	------	------	------	------	------

15.5	14.9	37.3	31.6	14.8	10.9	439
<b>17.7</b>	<b>18.6</b>	<b>40.5</b>	<b>37.1</b>	<b>13.8</b>	<b>10.7</b>	<b>8634</b>
22.5	23.5	37.1	33.7	13.3	10.4	593

26.4	28.4	31	28.3	22.9	18	1
17.4	18.2	40.8	37.3	13.8	10.8	8041

<b>10.5</b>	<b>10.6</b>	<b>30.1</b>	<b>26.7</b>	<b>21.9</b>	<b>16.8</b>	<b>4440</b>
10.1	10	30.5	26.5	19.2	14.2	2780

10.8	11.4	29.5	27.3	27.4	22.3	1521
------	------	------	------	------	------	------

14.2	14.8	28.9	26.5	24.8	19.3	140
<b>18.1</b>	<b>18.8</b>	<b>34.3</b>	<b>31.7</b>	<b>19.4</b>	<b>15.3</b>	<b>14863</b>
24.3	24.8	31.6	28.4	15.3	11.7	1
15.1	16.2	46.8	44.5	14.5	11.7	310

20.6	20.8	29.5	26.4	18.5	14.1	585
------	------	------	------	------	------	-----

12.9	13.8	39.1	37	17.4	14.2	163
21	21.3	26.3	23.5	17.6	13.4	154
12.8	14.2	54.3	52.7	20.8	17.3	21
24.2	25	29.1	26.6	19.5	15.2	2556

16.2	17.2	42.1	39.5	17.1	13.7	2929
------	------	------	------	------	------	------

16	17.1	36.8	34.7	27.1	22	595
----	------	------	------	------	----	-----

18.8	19.5	43.2	39	14.2	11	3
17.3	17.7	38.5	34.5	15.1	11.6	87
15.6	16.2	29.6	27	17.5	13.9	1253
16.9	18.1	33.1	31.4	22.5	18.3	2191
20.7	21.7	34.6	31.9	19.5	15.3	20
12.1	12.8	46.7	43.7	16.7	13.3	14
24.3	24.8	25.7	23.2	18.4	14.1	596
17.2	17.5	33.6	29.9	17.5	13.3	49
10.9	11.3	22.9	20.8	28.6	22.1	175
17.6	18.1	28.6	25.9	19	14.7	868
13.3	14.2	42.7	39.9	18.8	15.1	68
17.9	18.8	40.4	37.5	16.5	13.1	220
18.4	18.3	32.7	28.8	16.7	12.5	2002
31.1	32	31.8	29	17.7	13.8	1
23.2	24.7	31.2	29.3	24.5	19.6	1
<b>5.9</b>	<b>6</b>	<b>29</b>	<b>24.7</b>	<b>20.1</b>	<b>15.4</b>	<b>9906</b>
4.5	4.6	28	24.4	22.8	17.7	2353
4.9	5.1	32.8	29.7	21.1	16.5	1949
7	6.9	27.5	22.9	18.5	14	5604
<b>8</b>	<b>7.5</b>	<b>39.2</b>	<b>36.3</b>	<b>25.3</b>	<b>21.8</b>	<b>3143</b>
3.8	4	29.8	28.3	27.3	22.2	6
6	6.6	37.6	36.1	26.7	21.9	21
3.9	4.2	25.7	23.8	26.6	21.5	22
5.1	5.3	29.9	27.2	21.8	17.2	46
14.4	15.7	42.1	40	18	14.6	1
13.6	14.2	40.7	37.5	21.8	17.3	445
6.1	6.5	27.8	26.1	25.3	20.4	5

4.3	4.9	48.2	47.3	28.3	23.9	1294
4.3	4.6	30.3	28.4	27.7	22.5	10
1.8	1.9	37.3	36	31.8	26.8	103
2.1	2.3	33.7	31.4	32.8	26.4	723
6.4	7	20.8	20.2	30.6	25.5	198
6.4	6.8	30.9	28.5	11.8	9.2	44
4.7	5	22.3	21.1	31.3	25.7	13
3.1	3.4	33.5	31.9	25.9	21.4	11
4.9	5.5	33.4	32.1	34.4	29.1	71
3.2	3.5	34.9	33.4	20.1	16.8	124
7.8	8.8	50.1	49	17.1	14.2	4
3.4	3.8	28.3	27.7	35.6	29.5	2
<b>5</b>	<b>5.1</b>	<b>37.9</b>	<b>34.5</b>	<b>16.5</b>	<b>13.4</b>	<b>28834</b>
7.1	7.5	41.4	38.4	18.8	15.2	9034

6.3	6.7	45	42	18.4	14.8	446
4.5	4.6	40.5	36.4	15.5	12.3	815
2.8	2.7	28	23.6	16.3	12.3	2494
6.9	7.6	37.3	35.8	31.1	26.3	1018
3.7	3.9	35.5	32.6	13.8	11	10363

3.2	3.4	41.8	39	17.8	14.4	567
6.1	6.5	31.5	29.5	23.7	19	373
7.1	7.8	44.1	41.8	20.5	17	3723

<b>6.6</b>	<b>6.9</b>	<b>32.2</b>	<b>29.5</b>	<b>24.5</b>	<b>19.1</b>	<b>15130</b>
6.6	6.9	32.1	29.4	24.5	19.1	14740

6.1	6.6	33.2	31.4	24.5	19.8	390
<b>4.5</b>	<b>4.8</b>	<b>54.3</b>	<b>50.7</b>	<b>23</b>	<b>20.4</b>	<b>177440</b>
1.6	1.9	43.8	39.2	24.6	20.8	7496
3.3	3.8	55.8	54.1	26.1	23.1	14103
6.1	6.9	42.8	35.3	14.6	11.4	283
1.9	2.5	62.1	58	18.2	16.1	58393
4.7	5.5	52.1	49.3	23.6	20.6	12173
4.4	5.4	49.3	46.9	32.8	29.3	16200
6.4	7.1	43.9	41	25.3	21.6	4901
4.3	5.3	54.2	49.3	20.1	17.4	1224
8.4	9.4	67.4	64.2	9.8	8.4	1070
6.4	7.5	54.2	51.6	23.6	20.8	1512
4.1	4.8	56.5	54.7	25.5	22.7	10153
5.9	6.7	45.2	42.5	25.4	21.9	1416
2.3	2.7	58.2	54.5	20	17.5	1094
6.6	8	54.6	47.3	16.1	13.3	257
2.3	3	55.1	52.1	27.7	24.9	3525
1.8	2.3	53.2	50.5	27.8	24.8	16343
2.7	3.1	66.7	65.1	19.9	17.7	2820
6.7	7.7	54.8	53.1	24.5	21.4	2645
12.8	13.9	39.4	36.8	21.3	17.7	12340

3.8	4.6	48.9	45.7	25.8	22.7	552
2.1	2.6	53.6	50.8	26.8	23.7	8942

<b>2.1</b>	<b>2.7</b>	<b>36</b>	<b>32.2</b>	<b>21.9</b>	<b>19.2</b>	<b>589379</b>
2.1	2.6	28.8	26.7	41.5	36.4	51595

2.3	2.6	35.3	31.8	20.5	17.1	119
2	2.5	36.5	32.8	20.3	17.4	474772

1.9	2.3	24.8	22.1	19.2	16.4	3935
-----	-----	------	------	------	------	------

3.4	4	37.6	33.4	24.9	21	58958
-----	---	------	------	------	----	-------

<b>11.6</b>	<b>13.9</b>	<b>26.5</b>	<b>24.7</b>	<b>38.4</b>	<b>33.7</b>	<b>178666</b>
11.6	14	26.6	24.9	38.5	33.7	174361

6	7.1	22.9	21.7	43.5	38.4	3040
16.6	16.9	20.6	18.2	20.7	16.1	1265
<b>2.9</b>	<b>3.1</b>	<b>32.4</b>	<b>27.9</b>	<b>20.8</b>	<b>16.6</b>	<b>576</b>
5.7	6.4	34.1	32.5	21.3	17.3	2
3.5	4	37.8	36.2	23.4	19.1	4
1.3	1.5	35.8	34.4	13.9	11.4	49
9.6	10.7	55	52.8	16.6	13.5	6
1.9	2.2	32.3	31.7	30.4	25.4	3
3.7	4.2	41.1	39.5	26.2	21.4	2
10.3	11.6	39	37.4	23.5	19.2	1
3.1	3.1	28.5	25.2	21.8	16.4	459
2	2.2	39.1	37.5	25.3	20.6	8



2.5	2.7	42.5	40.2	27	21.8	22
6.4	6.9	30.2	28	17	13.5	6
3.2	3.5	42.6	41	28.1	23	13
4.9	5.4	33.9	32.3	18.7	15.2	0
7.3	8	26.3	24.4	15.6	12.4	0
3.1	3.6	43.2	41.2	24.5	19.9	0
6.2	6.8	36.9	34	19.1	14.9	0
4.8	5.3	37.1	35.4	23.5	19	0
3.7	4.2	38	36.4	23.8	19.4	0
<b>6.2</b>	<b>6.7</b>	<b>28.2</b>	<b>26.4</b>	<b>38</b>	<b>32.2</b>	<b>67696</b>
6	6.2	24.8	22.2	34.7	27.3	1356
5.1	5.8	29.5	29.2	41.6	35.8	23142

4.7	5	29.9	27.8	35.9	29	525
5.9	6.1	41.1	36.9	25	19.4	3304

3.9	4.3	46.4	44.6	24.2	19.7	17
3.5	3.8	28.2	26.9	18.7	15.3	87
4.7	5.2	19	17.9	43.2	36.5	6259

4.4	4.6	35.5	32.5	29.1	23.1	18547
-----	-----	------	------	------	------	-------

3.8	4.1	36.7	34.7	22.5	18.6	1289
5.9	6	35.3	31.4	24.3	18.6	11
12	12.7	24.9	22.6	29.8	24.1	7418

4.8	5.1	30.3	28.3	36.7	29.4	111
7.4	8.4	21.8	21.5	47.2	40.6	5631

<b>3.4</b>	<b>3.2</b>	<b>24.7</b>	<b>20.7</b>	<b>29</b>	<b>22.5</b>	<b>20528</b>
3.8	3.8	24.8	21.3	29.6	22.8	7075

2.1	2.2	21	17.3	27	20.9	720
-----	-----	----	------	----	------	-----

4.1	4.5	29.8	26.5	31.3	25.8	1467
3	3	24	20.5	28.7	22.4	10131
5.3	5.7	23.5	20.1	27.9	22.2	563
5.5	5.9	27.9	24.7	28	22.7	573
<b>2</b>	<b>1.9</b>	<b>21.3</b>	<b>18</b>	<b>31.3</b>	<b>23.5</b>	<b>48729</b>
1.7	1.8	23.7	20.3	30.6	23.8	1243
2.3	2.3	27.7	24.6	31	23.6	50
3	3.2	26	22.3	30.1	24.1	458
1.9	2	21.1	17.7	30.2	23.7	1324
1.7	1.8	22.1	18.6	27.4	21	12659
1.9	1.9	21.9	18.9	32.5	24.8	5106
1.3	1.4	24.7	22.2	40.4	31.4	1965
1.7	1.6	23.2	19.7	30.1	22.6	1337
1.8	1.8	20	17.7	40.4	31.5	2155
2.5	2.6	19.9	17.2	33.4	26.4	1771
1	0.9	19	15.2	25.9	18.7	841
2.2	2.1	16.7	13.2	23	16.9	1677
2.5	2.4	21.3	17.9	29.9	22.3	10517
2.1	2.1	20.1	16.9	29.6	23	4383
2.5	2.6	19.3	16.8	38.6	30.1	3244
<b>5.7</b>	<b>5.6</b>	<b>22.9</b>	<b>20.2</b>	<b>24.1</b>	<b>18.7</b>	<b>16252</b>
4.7	4.8	25	21.9	26	20.2	432
3.2	3.3	19	16.4	28.8	22.5	333
1.9	2	24.3	21.4	28.9	22.5	513
6.2	6.3	22.3	19.5	24.2	19.1	12668
3.6	3.6	20.7	18	24	18.4	207
3.2	3	29.8	24.7	19.5	14.2	2099
<b>2</b>	<b>2.2</b>	<b>20.3</b>	<b>16.4</b>	<b>23.5</b>	<b>17.7</b>	<b>137091</b>
2.3	2.4	20.6	16.9	26	19.9	2150
1.9	2	20.9	16.7	19.3	14.6	3902

3.1	3.5	21.6	18	27.2	21.5	11120
5.3	5.9	35.6	31.3	25.9	21.3	169
1.9	2	15.8	12.6	19.9	14.9	3278
2.9	3.1	22.9	18.9	24.5	19.1	7652
1.7	2	28.4	24.5	27.7	22.5	553
2.1	2.5	24.9	21.6	33.6	27.5	11057
1.9	2	19.5	15.9	23.4	17.9	2406
2.4	2.7	26.3	22.5	29.7	24	362
2.7	2.9	28.4	24.4	28.9	23.3	779
1.6	1.8	19.7	16.2	24.4	19	4112
3.5	4.1	27	23	26.7	21.5	1564
1.5	1.6	14.9	12.1	18.8	14.4	4305
1.7	1.9	18.4	14.9	20.5	15.7	76712
4.5	4.7	29.3	25.9	29.3	23.3	35
3.5	4	26.5	22.6	27.9	22.5	3846
2.1	2.2	22.6	18.6	24.2	18.8	1456
2.8	3	27.8	23.9	28.8	23.1	1635
<b>7.6</b>	<b>7.7</b>	<b>33.9</b>	<b>30.2</b>	<b>29.5</b>	<b>24.8</b>	<b>1361207</b>

hs (Incidences)	Low Birth Weight (Incidences)	
GEMM	GBD2019 CRF	GEMM
<b>24545</b>	<b>4811</b>	<b>6861</b>
639	196	267
1775	504	613
419	108	124
1664	786	877
1641	298	432
1457	196	361
4203	563	1092
1397	274	325
11351	1886	2772
<b>8747</b>	<b>3193</b>	<b>3516</b>
282	63	74
267	45	65
521	251	277
152	75	78
660	343	345
575	285	290
292	104	147
60	16	19
2933	1035	1190
1168	562	559
1283	187	238
442	180	187
111	48	48

<b>9659</b>	<b>3879</b>	<b>3455</b>
353	214	212
9	7	4
54	27	24
61	33	27
169	54	50
6752	2759	2386

2261	786	753
------	-----	-----

<b>580</b>	<b>332</b>	<b>236</b>
505	289	205
74	44	30

<b>7107</b>	<b>4361</b>	<b>4402</b>
15	11	8
3114	2907	2691

3470	1216	1465
------	------	------

508	227	237
<b>9552</b>	<b>5752</b>	<b>4257</b>
656	380	275

1	1	0
8895	5371	3982

<b>5132</b>	<b>2274</b>	<b>2216</b>
3159	1558	1435

1821	631	712
------	-----	-----

152	85	68
<b>16717</b>	<b>8533</b>	<b>7598</b>

1	1	1
347	168	149

657	271	246
-----	-----	-----

186	36	35
171	81	67
24	14	9
2858	1510	1317

3279	1453	1280
------	------	------

675	279	266
-----	-----	-----

4	2	1
96	64	47
1461	623	665
2499	1166	1141
22	10	8
16	8	7
669	321	287
54	33	23
193	154	118
955	796	644
76	25	17
244	140	116
2228	1379	1155
1	1	0
1	0	0
<b>13871</b>	<b>5160</b>	<b>7036</b>
3740	853	1346
2358	1512	1653
7774	2795	4037
<b>5546</b>	<b>1965</b>	<b>2889</b>
7	3	3
25	18	17
26	11	11
63	22	28
1	1	1
526	223	234
6	3	3

1677	861	978
12	5	6
133	88	106
2507	363	1121
241	177	183
49	34	24
16	7	7
14	5	6
92	56	68
144	86	91
4	2	2
2	1	1
<b>40086</b>	<b>14630</b>	<b>19242</b>
11518	3289	3922

524	195	202
1147	455	610
4961	1344	2700
2270	591	1248
13743	6290	7677

1127	341	614
440	240	233
4357	1886	2036
<b>17596</b>	<b>7602</b>	<b>6952</b>
17066	7349	6676



531	254	276
<b>267499</b>	<b>71840</b>	<b>149526</b>
30910	6693	36613
17287	3450	4523
368	110	201
76699	15651	29574
15168	9012	13109
20561	6202	10254
6016	1706	2254
1597	386	718
1299	520	647
1875	519	732
13204	5709	8200
1750	573	767
1374	485	749
343	136	265
4583	3255	5989
33593	5735	15538
3452	1347	1751
3219	691	872
14839	5585	6676

694  
18670

494  
3581

763  
9332

**1257195**  
132821

**383815**  
25072

**1191054**  
91494

260  
982038

54  
291840

139  
886289

9811  
132266

5242  
61606

19193  
193939

**267456**  
259102

**46334**  
44965

**90948**  
87927

6846	909	2490
1509	460	531
<b>1939</b>	<b>302</b>	<b>804</b>
1	1	1
6	3	3
66	28	28
6	5	3
7	2	3
3	2	2
1	1	1
1709	231	702
13	4	5

84	12	35
8	4	4
33	10	19
0	0	0
0	0	0
0	0	0
0	0	0
0	0	0
0	0	0
<b>106133</b>	<b>43901</b>	<b>63644</b>
3696	842	2144
33523	12533	16215

1460	489	1224
3780	2116	2100

20	23	20
100	75	73
14245	3512	8200
28838	15781	22051

1935	1608	2208
12	6	6
9765	3012	3956

253	51	99
8504	3854	5349

<b>65759</b>	<b>10828</b>	<b>36436</b>
15555	4382	9688
3980	346	2310

2766	610	1291
41883	4946	22282

816	245	431
758	300	434
<b>198691</b>	<b>25250</b>	<b>107062</b>

7385	712	4517
140	58	141
754	197	392
4221	568	2197
61602	6142	32395

12701	3427	8292
-------	------	------

7639	1606	5535
5809	953	3964
12261	1322	7043

6207	509	1967
------	-----	------

12421	433	6581
6321	770	3306
36897	3356	11484

16347	3619	15443
-------	------	-------

7988	1578	3805
------	------	------

<b>25094</b>	<b>8910</b>	<b>13882</b>
--------------	-------------	--------------

646	286	416
743	190	441
821	337	524
17266	6834	9593

377	92	161
5242	1171	2748
<b>435067</b>	<b>54595</b>	<b>242053</b>

8200	1518	7107
22051	1541	11514

25314	3774	12008
266	70	140
19509	1256	10230
22647	3508	13908
1994	263	1325
22366	4578	12572
11590	956	6086
1660	222	1389
3195	320	1681
24419	1563	12802
3319	572	1738
34082	1546	17839
209187	29421	114778
76	9	20
13267	1998	9710
6501	643	3728
5424	837	3477
<b>2783970</b>	<b>708266</b>	<b>1964067</b>

**Data File 2: PM<sub>2.5</sub> Exposure Estimates, Combustion Fuel-Type Source Contributions, and To**

McDuffie et al., 2021 -

Last Updated: March 23, 2021

Name Legend:

**Regions** Countries *Sub-national regions*

<b>Country Name</b>	<b>Population Weighted Annual Average PM<sub>2.5</sub> (<math>\mu\text{g m}^{-3}</math>)</b>	<b>Total Biofuel Contribution (%)</b>	<b>Total Coal Contribution (%)</b>
<b>Central_Asia</b>	<b>27.5</b>	<b>9.9</b>	<b>9</b>
Armenia	31.9	5.4	8.6
Azerbaijan	23.9	7.8	4.6
<i>Baku</i>	<i>31.5</i>	<i>7.2</i>	<i>3.7</i>
Georgia	17.8	8.8	9.5
Kazakhstan	19	4.8	9.2
<i>Shymkent</i>	<i>38.1</i>	<i>7.6</i>	<i>7.3</i>
Kyrgyzstan	22.9	11.2	11.1
Mongolia	36.7	11.4	18.2
<i>Ulaanbaatar</i>	<i>81.4</i>	<i>11.7</i>	<i>21.6</i>
Tajikistan	35.9	24.4	8.2
Turkmenistan	25.5	2.2	2.9
Uzbekistan	32.5	8.7	9.9
<i>Bukhara</i>	<i>26.6</i>	<i>2.3</i>	<i>5.4</i>
<i>Tashkent</i>	<i>50.8</i>	<i>7.1</i>	<i>11.7</i>
<b>Central_Europe</b>	<b>20.5</b>	<b>20.8</b>	<b>18.7</b>
Albania	19.8	12.5	15.5
Bosnia_and_Herzegovina	29.8	18	23.8
Bulgaria	19.7	18.1	18.5
Croatia	18	26.8	12.4
Czech_Republic	16.8	23.4	16.4
Hungary	16.5	28.2	14.4
<i>Budapest</i>	<i>19.5</i>	<i>32.4</i>	<i>13.7</i>
Macedonia	31.6	14.7	23.3
Montenegro	21.6	15.1	19
Poland	22.7	18.7	19.5
<i>Warsaw</i>	<i>24.3</i>	<i>18.9</i>	<i>21.7</i>
Romania	15.9	24.6	15.8
Serbia	26.5	19.4	25.8
<i>Belgrade</i>	<i>25.7</i>	<i>18.9</i>	<i>32.2</i>

Slovakia	18.4	23.2	16.5
Slovenia	16.9	27.4	7.2
<b>Eastern_Europe</b>	<b>11.8</b>	<b>12.5</b>	<b>11.2</b>
Belarus	16.3	14.7	15
<i>Gomel</i>	20.9	11.2	14.8
Estonia	5.7	30.8	5.6
Latvia	11.7	30.4	7.9
Lithuania	10.2	26.7	10.5
<i>Kaunas</i>	12	33	10.6
Moldova	13.1	19.2	15.3
Russian_Federation	10.9	11.7	8.5
<i>Saint_Petersburg</i>	8.2	25.3	5.3
<i>Astrakhan</i>	12.1	4.2	7.2
<i>Moscow</i>	13.8	24.5	6.5
<i>Tyumen</i>	13.4	7.5	6.4
<i>Berezniki</i>	13.9	8.5	6.8
<i>Dzerzhinsk</i>	11.6	14.3	7.1
Ukraine	14	11.7	16.7
<i>Nikolaev</i>	14.2	10.8	15.8
<i>Rovno</i>	19.9	13.2	17
<b>Australasia</b>	<b>6.9</b>	<b>3.5</b>	<b>8.6</b>
Australia	7	3.6	9.4
<i>Sydney</i>	7.6	4.8	16.2
New_Zealand	6.6	2.8	4.2
<i>Auckland</i>	6.5	3.7	4
<b>High_income_Asia_Pacific</b>	<b>17.3</b>	<b>11</b>	<b>15.3</b>
Brunei	7.6	10.9	5.6
Japan	13.5	9.2	12.4
<i>Tokyo</i>	15.1	7.4	9.5
<i>Osaka</i>	15.1	10	13.6
<i>Fukuoka</i>	17.7	11.6	16.7
<i>Okayama</i>	13.3	9.7	14.7
<i>Yamaguchi</i>	12.6	11.4	16.2
South_Korea	26.6	13	18.7
<i>Seoul</i>	27.4	13.2	19.1
<i>Busan</i>	24.3	14.1	17.4
<i>Cheonan</i>	28.6	12.8	18.6
<i>Gwangju</i>	27	12.3	18.8
<i>Jinju</i>	27.7	11.8	18.4
<i>Pyongyang</i>	52.9	11.2	24.3
Singapore	18.5	14.5	19.1



<b>High_income_North_America</b>	<b>7.8</b>	<b>13.2</b>	<b>9.1</b>
Canada	7.3	17.1	3.9
<i>Montreal</i>	9.1	26.4	2.5
<i>Victoria</i>	6.3	20.5	1.6
Greenland	5.3	3.1	5.1
United_States	7.8	12.8	9.7
<i>Raleigh</i>	7.6	11.4	15.6
<i>New_York</i>	7.7	23.7	7.4
<i>Philadelphia</i>	8.6	17.4	8.4
<i>Houston</i>	9.9	12.6	10.2
<i>Minneapolis</i>	7.4	10.2	10.2
<i>Portland</i>	8	11.9	4.1
<i>Los_Angeles</i>	10.6	27.2	5.8
<i>Cleveland</i>	8.8	10.8	11.1
<i>Chicago</i>	9	13.3	10.7
<i>Springfield</i>	6.5	15.6	6
<i>Gainesville</i>	6.5	9.2	9.5
<i>Killeen</i>	7.4	9.2	11.3
<i>Modesto</i>	12.1	12.8	5.6
<b>Southern_Latin_America</b>	<b>15.3</b>	<b>15.5</b>	<b>3</b>
Argentina	13	13	1.9
<i>Buenos_Aires</i>	11.5	19.3	1.4
<i>Cordoba</i>	13.9	7.7	1.6
Chile	21.9	18.5	4.8
<i>Santiago</i>	28.9	25.6	5.2
Uruguay	9.8	21	2.1
<b>Western_Europe</b>	<b>11.7</b>	<b>14.3</b>	<b>6</b>
Andorra	8.8	10.4	3.6
Austria	12.1	22.8	9.1
<i>Vienna</i>	14.5	26.8	10.9
Belgium	12.8	13.5	4.6
<i>Antwerp</i>	14.1	14	4.7
Cyprus	15.2	3.2	21.9
Denmark	10.2	15.7	5.4
Finland	5.2	28.2	5.2
France	11.6	16.8	3.6
<i>Paris</i>	14	25.6	3.5
<i>Le_Mans</i>	13.6	11.4	2.9
Germany	11.9	14.1	8.1
<i>Berlin</i>	16	13.5	9.5
<i>Halle</i>	14.6	13.3	9.5

<i>Oldenburg</i>	13.2	8.9	6
Greece	14.6	9.7	18.5
<i>Thessaloniki</i>	15.9	11.1	20.4
Iceland	5.6	1.7	1
Ireland	7.7	4.1	4.1
Israel	19.7	2.1	12.3
<i>Tel_Aviv</i>	21.6	2.1	12.8
Italy	15.6	19.4	5.1
<i>Palermo</i>	15	11.6	6.7
<i>Milan</i>	23.4	25.7	2.8
Luxembourg	9.9	11.3	5.6
Malta	12.4	6.5	5.5
Netherlands	12.4	11.6	5.5
<i>Zwolle</i>	11.8	10	5.9
Norway	6.5	15.5	3.3
Portugal	8.6	9.6	2.1
Spain	9.9	10.5	3.5
<i>Madrid</i>	10.1	17.9	3.2
<i>Toledo</i>	8.5	10.9	10.4
Sweden	5.7	22.7	4.6
Switzerland	10.2	20.9	4.6
<i>Lausanne</i>	12.3	22.6	4.1
United_Kingdom	10.5	10.3	5.4
<i>Sheffield</i>	11.6	11.7	6.6
<i>London</i>	13	12.7	5.5
<i>Manchester</i>	11	9.7	5.7
Monaco	11.4	17.2	3.4
San_Marino	9.8	16.4	6.4
<b>Andean_Latin_America</b>	<b>25.9</b>	<b>8.5</b>	<b>0.8</b>
Bolivia	26	5.1	0.5
<i>Cochabamba</i>	26.2	4.9	0.3
Ecuador	18.8	6.1	0.3
<i>Quito</i>	17.6	6.2	0.3
Peru	29.6	10.3	1.1
<b>Caribbean</b>	<b>16.5</b>	<b>20.6</b>	<b>1.9</b>
Antigua_and_Barbuda	16.2	17.3	0.6
The_Bahamas	13.9	7.5	3.5
Barbados	19.6	1.2	0.1
Belize	19.3	9.1	1.3
Bermuda	7	5.7	4.1
Cuba	17.5	14.5	1.7

<i>Holguin</i>	15.5	15.1	1.2
Dominica	16.8	18.5	0.8
Dominican_Republic	16.8	19.6	2.7
Grenada	19.4	1.2	0.1
Guyana	20.5	2.2	0.1
Haiti	17.8	36.5	2.1
Jamaica	15.2	19.5	1.5
Puerto_Rico	7	13.6	0.4
Saint_Lucia	19.4	1.2	0.1
Saint_Vincent_and_the_Grenadines	19.4	1.2	0.1
Suriname	21.9	1.9	0.1
Trinidad_and_Tobago	19.5	1.3	0.1
Virgin_Islands_US	8.8	14.2	0.4
Saint_Kitts_and_Nevis	8.4	16.7	0.6
<b>Central_Latin_America</b>	<b>20.8</b>	<b>19.2</b>	<b>4.8</b>
Colombia	21.3	16.2	9.5
<i>Bogota</i>	30.5	20.9	14.3
<i>Valledupar</i>	22.2	5.8	1.3
Costa_Rica	17.3	9.6	0.3
El_Salvador	22.6	35.4	2.9
<i>San_Salvador</i>	22.9	36.6	3.1
Guatemala	27.3	50.2	1.5
<i>Guatemala_City</i>	33.5	59	1.6
Honduras	22.3	29.3	1.2
Mexico	20.1	18.1	5.3
<i>Culiacan</i>	18.6	14.3	3.6
<i>Guadalajara</i>	18.9	21.5	5.2
<i>Mexico_City</i>	24.3	30	4.9
<i>Reynosa</i>	20.2	11.5	8.2
<i>Tijuana</i>	17.6	20.2	4.6
Nicaragua	19.1	15.3	0.4
<i>Leon</i>	19.9	16.8	0.4
Panama	13.7	5.4	0.5
Venezuela	20.3	2.9	0.5
<i>Caracas</i>	19.4	2.6	0.2
<i>Cabimas</i>	21.6	3	0.4
<b>Tropical_Latin_America</b>	<b>11.8</b>	<b>23</b>	<b>2.8</b>
Brazil	11.8	23.1	2.8
<i>Sao_Paulo</i>	15.3	37	3.5
<i>Curitiba</i>	8.9	29.8	3.5
<i>Florianopolis</i>	12.8	21.5	7.2

<i>Belo_Horizonte</i>	13.2	29.7	4.4
<i>Palmas</i>	10.4	3.7	0.5
<i>Ilheus</i>	13.6	8.7	0.9
<i>Jequie</i>	13.3	14.1	1.6
<i>Ribeirao_Preto</i>	14.5	25.4	3.5
Paraguay	12.5	19.4	1.1
<b>North_Africa_and_Middle_East</b>	<b>44.1</b>	<b>3.3</b>	<b>6</b>
Afghanistan	50.8	7.9	9.2
<i>Kabul</i>	64.5	9.3	15.5
Algeria	31.6	3.2	1.9
<i>Algiers</i>	34	4	2.2
<i>Tebessa</i>	33.3	3.9	2.2
Bahrain	60.8	0.5	1.6
Egypt	65.8	4.8	6.6
Cairo	80.9	5.5	6.5
<i>Alexandria</i>	56.7	4.7	9.1
Iran	38.3	1.2	2.4
<i>Tehran</i>	36.3	1.5	2.1
<i>Ahvaz</i>	71.1	0.7	2.4
<i>Gorgan</i>	39.6	1.6	2.4
<i>Qom</i>	41.6	1.2	2.1
Iraq	48.6	0.9	4.5
<i>Baghdad</i>	58.2	0.9	4.3
Jordan	32.1	1.9	10.7
Kuwait	63.1	0.5	2
Lebanon	28.5	2.2	11.9
Libya	36.2	1.9	2.6
Morocco	34	4.2	1.9
<i>Marrakesh</i>	44	3	1.2
Palestine	32.6	2.3	11.6
Oman	42.6	1.6	1.8
Qatar	71.6	0.5	1.5
Saudi_Arabia	61.5	1.1	2.1
<i>Riyadh</i>	67.7	0.7	1.7
Sudan	50	3.1	1.4
<i>Khartoum</i>	61.2	2.9	1.4
Syria	31.1	2	12.7
Tunisia	29.3	6.1	2.8
<i>Kairouan</i>	35.4	6.2	2.6
Turkey	26.1	4.7	23
<i>Istanbul</i>	26	8.4	24.1

<i>Malatya</i>	32.7	2.9	22.4
<i>Kayseri</i>	37.5	3.3	20.8
United_Arab_Emirates	42.7	0.8	1.8
Yemen	44.1	2.4	2.4
<i>Sana</i>	44.7	2.2	2.4
<b>South_Asia</b>	<b>76.1</b>	<b>29.2</b>	<b>16.2</b>
Bangladesh	61.9	29.5	14.7
<i>Rajshahi</i>	55.8	28.9	18
<i>Dhaka</i>	69.6	30.6	13.9
<i>Saidpur</i>	61.4	31.7	16.1
Bhutan	38.8	33.7	14.9
India	80.2	28.8	17.1
<i>Jaipur</i>	102.8	26.8	14
<i>Ahmedabad</i>	131.5	29	15.6
<i>Kanpur</i>	152.3	30.6	16.9
<i>Kolkata</i>	85.8	33	20.7
<i>Mumbai</i>	60	27.7	19.6
<i>Pune</i>	57	27	18.9
<i>Hyderabad</i>	47.6	24.8	18.7
<i>Belgaum</i>	44.6	23.3	17.7
<i>Coimbatore</i>	41.2	26.8	17.6
<i>Hindupur</i>	41.3	23.1	18.3
<i>Jalna</i>	52.8	24.1	19.6
<i>Kozhikode</i>	34.8	28.1	16.2
<i>Malegaon</i>	57	25.4	19.5
<i>Parbhani</i>	41.7	23.6	20.2
<i>Singrauli</i>	153.2	27.2	20.8
<i>Sitapur</i>	136.5	29.5	15.7
<i>Vijayawada</i>	56.2	24.5	19.5
Nepal	79.3	39.8	14.1
<i>Pokhara</i>	74.6	40.2	10.6
Pakistan	59.7	30.5	10.3
<i>Karachi</i>	70.8	34	10.1
<i>Lahore</i>	72.5	40.2	11.4
<i>Sialkot</i>	66	31.1	12.2
<b>East_Asia</b>	<b>49.3</b>	<b>13.3</b>	<b>22.7</b>
China	49.8	13.3	22.7
<i>Chengdu</i>	63.9	14.7	26.9
<i>Qingdao</i>	46.8	12.2	24.6
<i>Taipei</i>	22	11.1	17.6
<i>Shanghai</i>	46.2	11.3	22.4

<i>Wuhan</i>	64.6	14	24.4
<i>Hangzhou</i>	54.1	12.5	21.2
<i>Guangzhou</i>	39.9	15	23.4
<i>Beijing</i>	71.8	13.4	23.4
<i>Tangshan</i>	73.4	12.1	22.3
<i>Tianjin</i>	71.7	13.8	22.8
<i>Jinan</i>	70.4	13.8	25.8
<i>Zhengzhou</i>	82.7	13.5	23.5
<i>Hong_Kong</i>	23.5	15.7	24
<i>Anqing</i>	55.4	13.5	23
<i>Bicheng</i>	54.4	15.7	25.1
<i>Changzhi</i>	72.2	9.3	20.6
<i>Changzhou</i>	56.1	12	20.7
<i>Chengguan</i>	37.3	13.7	25
<i>Gaoyou</i>	54.7	13.2	23.4
<i>Guixi</i>	48.9	17.1	23.1
<i>Haikou</i>	22.4	17.2	23.4
<i>Kaiping</i>	39	14.6	23.2
<i>Leshan</i>	58.8	14.9	26.5
<i>Pingxiang</i>	54.3	14.3	24.4
<i>Shenzhen</i>	32.4	16.7	24.9
<i>Suining</i>	51.2	16.8	25
<i>Xingping</i>	68.4	14.2	22
<i>Xucheng</i>	56.1	13.3	24.1
<i>Yanggu</i>	73.6	14	25.7
<i>Yiyang</i>	51.1	14.6	23.9
<i>Yucheng</i>	34.9	14.2	22.3
<i>Zhuji</i>	49.4	12.8	21.6
<i>Zunyi</i>	45.4	14	23.8
<i>Yulin</i>	40.7	16.1	24.5
<i>North_Korea</i>	41.8	11.6	22.5
<i>Taiwan</i>	23.9	9.4	16.4
<b>Oceania</b>	<b>12.7</b>	<b>7.9</b>	<b>0.6</b>
<i>American_Samoa</i>	6.1	0.4	0.1
<i>Federated_States_of_Micronesia</i>	9.1	3.2	1.2
<i>Fiji</i>	9.8	2.2	0.3
<i>Suva</i>	-	-	-
<i>Guam</i>	7.6	1.8	0.9
<i>Kiribati</i>	7.6	0.6	0.1
<i>Marshall_Islands</i>	8.6	0.6	0.2
<i>Northern_Mariana_Islands</i>	7.8	2.1	1.3

Papua_New_Guinea	13.3	8.8	0.7
Samoa	9.6	0.7	0.1
Solomon_Islands	10.7	1.6	0.4
Tonga	9.6	0.4	0.2
Vanuatu	11.1	0.8	1.1
Niue	6.4	0.2	0.2
Cook_Islands	6.1	0.2	0.2
Nauru	5.6	0.5	0.1
Palau	6.7	19.1	5.3
Tokelau	7	0.3	0
Tuvalu	5.7	0.4	0.1
<b>Southeast_Asia</b>	<b>20.1</b>	<b>31.2</b>	<b>12.9</b>
Cambodia	21.2	28.3	8.8
Indonesia	18	36	11.5
<i>Medan</i>	<i>34.6</i>	<i>43.2</i>	<i>6.9</i>
<i>Palembang</i>	<i>25.6</i>	<i>33.9</i>	<i>11</i>
<i>Cirebon</i>	<i>21.4</i>	<i>39.8</i>	<i>16.4</i>
<i>Parepare</i>	<i>14.4</i>	<i>40.9</i>	<i>3.5</i>
<i>Pematangsiantar</i>	<i>25.2</i>	<i>47.3</i>	<i>5.9</i>
Laos	18.5	18.7	13
Malaysia	16.2	14.6	10
<i>Ipoh</i>	<i>17.5</i>	<i>12.1</i>	<i>10.7</i>
<i>Rawang</i>	<i>17.2</i>	<i>12.4</i>	<i>8.6</i>
Maldives	9.9	21.6	11.8
Mauritius	14.7	3.5	2.9
Myanmar	28.5	31.6	12.6
<i>Myeik</i>	<i>22.7</i>	<i>25.4</i>	<i>11.8</i>
Philippines	18.4	22.6	15.6
<i>Manila</i>	<i>27.4</i>	<i>30.3</i>	<i>23.2</i>
<i>Bacolod</i>	<i>19.7</i>	<i>19.6</i>	<i>10.4</i>
<i>Cebu_City</i>	<i>22.4</i>	<i>20.3</i>	<i>12.7</i>
Sri_Lanka	19.6	35.1	8.8
Seychelles	15.4	11.5	3.6
Thailand	26.4	29.8	12.3
<i>Bangkok</i>	<i>30.4</i>	<i>44.2</i>	<i>11.2</i>
Timor_Leste	15.3	9.4	1.2
Vietnam	20	34	17.4
<i>Vinh_Long</i>	<i>23.7</i>	<i>41.1</i>	<i>13.8</i>
<i>Ho_Chi_Minh_City</i>	<i>27.1</i>	<i>46.6</i>	<i>16.5</i>
<b>Central_Sub_Saharan_Africa</b>	<b>32.2</b>	<b>11.8</b>	<b>0.6</b>
Angola	27	5.7	1.7

<i>Luanda</i>	31.2	5.5	1.1
Central_African_Republic	41.3	4.2	0.3
Congo	35.2	11.2	0.3
Democratic_Republic_of_the_Cong	33	14	0.4
<i>Kinshasa</i>	39.4	17.4	0.2
<i>Lubumbashi</i>	27.4	12.8	1
Equatorial_Guinea	41.3	12.6	0.1
Gabon	33.3	14.8	0.2
<b>Eastern_Sub_Saharan_Africa</b>	<b>28.5</b>	<b>21.7</b>	<b>2.3</b>
Burundi	31.5	34.6	0.5
Comoros	16.1	8.9	2.7
Djibouti	41.1	4.5	2.5
Eritrea	41.6	4.7	2
Ethiopia	32.6	22.2	1.8
<i>Addis_Ababa</i>	31.5	29	1.8
Kenya	24.4	25.2	2.5
<i>Nakuru</i>	23.8	28.8	2.5
Madagascar	17.5	11.1	3.9
Malawi	23.1	12.2	3.3
Mozambique	21.4	9.5	9.4
<i>Beira</i>	24.2	8	10.2
Rwanda	33.8	40.2	0.5
<i>Kigali</i>	34.8	42.5	0.5
Somalia	28.8	6.7	2.7
South_Sudan	36.4	8.4	0.8
Tanzania	24.6	23.8	2
<i>Arusha</i>	23.1	25.4	3.2
Uganda	36.7	31.5	1
<i>Kampala</i>	48.5	38.4	1.2
Zambia	24.9	12.7	3.1
<i>Ndola</i>	26	11.6	1.9
<b>Southern_Sub_Saharan_Africa</b>	<b>27</b>	<b>11.7</b>	<b>31.4</b>
Botswana	24.3	10.2	31.2
Lesotho	29.4	11.2	31.6
Namibia	24.4	6.1	9.8
South_Africa	28.8	10.9	36.5
<i>Port_Elizabeth</i>	23.9	6.5	16.2
<i>Johannesburg</i>	40.2	12.6	44.1
Swaziland	23.1	9.4	43.7
Zimbabwe	21.7	16.7	11.8
<b>Western_Sub_Saharan_Africa</b>	<b>59.4</b>	<b>8.9</b>	<b>0.2</b>



Benin	42.6	10.9	0.2
Burkina_Faso	50.4	4.3	0.2
Cameroon	58.9	10.1	0.2
Cape_Verde	46.4	0.4	0.1
Chad	55.3	2.8	0.6
Cote_dIvoire	52.1	7.2	0.1
The_Gambia	58.6	1.7	0.2
Ghana	54	7.6	0.1
<i>Accra</i>	<i>64.3</i>	<i>8.4</i>	<i>0.1</i>
Guinea	50.4	4.1	0.1
Guinea_Bissau	54.6	2.5	0.2
Liberia	46.5	5.8	0.1
Mali	56.5	2.7	0.2
<i>Bamako</i>	<i>56.3</i>	<i>3.1</i>	<i>0.2</i>
Mauritania	64.3	0.7	0.1
Niger	70.9	3.3	0.3
Nigeria	64.2	12.3	0.2
<i>Ibadan</i>	<i>38.9</i>	<i>15.5</i>	<i>0.2</i>
<i>Lagos</i>	<i>34.2</i>	<i>15.5</i>	<i>0.2</i>
<i>Gombe</i>	<i>79.1</i>	<i>6.4</i>	<i>0.3</i>
<i>Oyo</i>	<i>41.1</i>	<i>15.4</i>	<i>0.2</i>
Sao_Tome_and_Principe	29.5	6.4	0.5
Senegal	60.5	1.2	0.2
Sierra_Leone	48.2	5.2	0.1
Togo	44.4	9.7	0.2
<b>Global</b>	<b>41.7</b>	<b>20</b>	<b>14.1</b>

## Total Attributable Mortality Estimates

Oil and Gas Contribution (%)	Total Attributable Mortality (Deaths)			
	GBD2019 CRF	Lower 95% Confidence Interval (CRF)	Upper 95% Confidence Interval (CRF)	GEMM
<b>10.7</b>	<b>60999</b>	<b>38899</b>	<b>83661</b>	<b>75492</b>
17.1	3037	2012	4034	3644
14.8	7590	4617	10689	8630
11.9	-	-	-	-
13.5	3162	1792	4737	3543
10.4	9606	5643	14051	10602
9.4	-	-	-	-
11.2	2378	1442	3374	3228
9.7	1989	1418	2532	2885
9.9	-	-	-	-
8.2	4459	3049	5822	7288
11.2	3462	2164	4806	3728
9.8	25316	16762	33617	31945
7.8	-	-	-	-
10.3	-	-	-	-
<b>14.7</b>	<b>92306</b>	<b>54865</b>	<b>133818</b>	<b>100703</b>
15.5	1580	938	2310	1774
12	3666	2440	4874	4710
11.9	9265	5472	13561	9724
18.4	3024	1726	4502	3134
16.3	6263	3414	9521	6572
16.4	7200	3958	10902	7529
16.2	-	-	-	-
10	2845	1957	3718	3380
10.1	599	370	850	652
16.2	27725	16919	39238	31196
16	-	-	-	-
13.6	14936	8195	23045	14974
9.9	10974	7110	14947	12615
8.9	-	-	-	-

15.4	3420	1909	5135	3586
22.2	808	457	1215	857
<b>14.3</b>	<b>123227</b>	<b>57686</b>	<b>205136</b>	<b>117852</b>
19.3	8681	4578	13454	8560
18.3	-	-	-	-
15.6	136	9	323	98
17.2	1100	513	1849	1023
17.9	1274	534	2229	1168
16.6	-	-	-	-
14.9	2074	1009	3377	2024
13.7	68482	30672	117145	64298
17.2	-	-	-	-
7.2	-	-	-	-
13.4	-	-	-	-
16.4	-	-	-	-
14.6	-	-	-	-
16.6	-	-	-	-
14.4	41480	20371	66759	40682
14.4	-	-	-	-
16.7	-	-	-	-
<b>12.6</b>	<b>2147</b>	<b>597</b>	<b>4218</b>	<b>2090</b>
12.2	1802	516	3516	1757
11	-	-	-	-
14.6	346	81	702	333
14.4	-	-	-	-
<b>18.7</b>	<b>59889</b>	<b>34089</b>	<b>90490</b>	<b>67774</b>
19.5	35	11	68	33
18.7	38942	20649	61823	42858
20.8	-	-	-	-
19.1	-	-	-	-
16.8	-	-	-	-
17.6	-	-	-	-
16.4	-	-	-	-
18	19685	12741	26753	23414
17.6	-	-	-	-
18.3	-	-	-	-
18.9	-	-	-	-
19.4	-	-	-	-
19.1	-	-	-	-
13	-	-	-	-
27.5	1226	688	1846	1469

<b>27.3</b>	<b>50594</b>	<b>17329</b>	<b>93521</b>	<b>49670</b>
21.3	3686	1157	6967	3632
23.6	-	-	-	-
21.4	-	-	-	-
24.1	3	0	8	3
27.9	46904	16172	86546	46035
28.3	-	-	-	-
31.8	-	-	-	-
31.1	-	-	-	-
27	-	-	-	-
28.6	-	-	-	-
21.9	-	-	-	-
28.5	-	-	-	-
31.1	-	-	-	-
31.6	-	-	-	-
30.8	-	-	-	-
26.2	-	-	-	-
29.8	-	-	-	-
22.1	-	-	-	-
<b>15.5</b>	<b>18377</b>	<b>9779</b>	<b>28513</b>	<b>20581</b>
17.1	12197	6138	19540	13619
23.2	-	-	-	-
15.3	-	-	-	-
12.7	5409	3295	7651	6199
15	-	-	-	-
21	772	345	1322	763
<b>25.5</b>	<b>114536</b>	<b>56831</b>	<b>185059</b>	<b>118698</b>
26.1	10	4	17	10
21.3	2358	1136	3824	2368
19.1	-	-	-	-
25.8	3458	1798	5471	3717
24.3	-	-	-	-
14.2	378	201	577	392
26.7	1348	633	2236	1403
15.1	280	6	741	254
28.4	13251	6545	21491	13733
27.7	-	-	-	-
29.9	-	-	-	-
23.7	26869	13026	43657	27266
22.4	-	-	-	-
23	-	-	-	-

29.3	-	-	-	-
14.1	5592	3019	8723	5806
13.4	-	-	-	-
14.4	14	1	32	13
30	496	171	922	499
20.6	2161	1263	3119	2436
20.6	-	-	-	-
25.4	24366	13450	37014	25517
17.7	-	-	-	-
29.1	-	-	-	-
28.5	85	38	144	85
18.1	135	65	220	138
27.5	4574	2378	7212	4847
28.1	-	-	-	-
17.1	384	90	783	385
26.4	2202	884	3989	2202
29.3	9026	4145	15201	9163
34.7	-	-	-	-
31	-	-	-	-
18.3	614	51	1445	583
28	1398	627	2367	1404
27.3	-	-	-	-
26.8	15518	7290	25840	16453
24.8	-	-	-	-
27.7	-	-	-	-
25	-	-	-	-
30.8	15	7	24	15
25.6	5	2	9	5
<b>15</b>	<b>15247</b>	<b>9354</b>	<b>21463</b>	<b>21966</b>
8.4	3393	2108	4722	5522
8.3	-	-	-	-
34	3853	2181	5678	4518
34.7	-	-	-	-
10.7	8000	5064	11064	11927
<b>22.3</b>	<b>14258</b>	<b>7804</b>	<b>21590</b>	<b>19138</b>
10.8	28	15	42	29
29.8	84	43	132	86
3.1	155	89	225	172
18.4	76	43	110	100
22.2	8	2	15	7
31.4	5918	3323	8889	6639

30.5	-	-	-	-
10.6	29	16	44	33
22.3	3453	1883	5241	3951
3.6	47	27	68	54
2.6	402	235	577	472
19.4	1504	846	2248	4860
29.3	893	479	1356	967
11.9	430	104	857	415
3.7	71	42	103	81
3.7	57	32	83	65
2.6	253	153	357	302
3.8	813	459	1173	870
11.8	30	11	54	28
11.5	8	3	16	8
<b>21.1</b>	<b>65630</b>	<b>38150</b>	<b>94095</b>	<b>85241</b>
15.7	11818	7074	16861	14390
15.2	-	-	-	-
19.7	-	-	-	-
15.7	888	494	1331	974
17.6	1803	1064	2571	2502
17.4	-	-	-	-
12	3338	2051	4644	7029
13.7	-	-	-	-
18.8	1581	976	2221	3250
27.7	34259	19616	49136	43465
27.5	-	-	-	-
30.3	-	-	-	-
29.5	-	-	-	-
28	-	-	-	-
29.5	-	-	-	-
14.5	863	487	1264	1616
15.4	-	-	-	-
19.2	643	328	1013	694
13.4	10436	6060	15054	11322
12.6	-	-	-	-
19.2	-	-	-	-
<b>16.8</b>	<b>42973</b>	<b>20585</b>	<b>70359</b>	<b>45750</b>
17	41992	20110	68776	44559
20.8	-	-	-	-
22.4	-	-	-	-
21	-	-	-	-

22.1	-	-	-	-
4.7	-	-	-	-
13.3	-	-	-	-
16.1	-	-	-	-
21.6	-	-	-	-
11.8	981	475	1583	1192
<b>18.1</b>	<b>317861</b>	<b>227116</b>	<b>404247</b>	<b>419282</b>
10.5	7110	5208	8918	29383
10.2	-	-	-	-
28.6	19437	12897	25909	22018
39.1	-	-	-	-
23.6	-	-	-	-
28.7	551	412	671	776
17.5	87957	67883	106168	110679
19.2	-	-	-	-
17.5	-	-	-	-
23.5	40870	28535	52551	48441
29.4	-	-	-	-
23.4	-	-	-	-
25.2	-	-	-	-
27	-	-	-	-
22.8	22830	16961	28159	27431
23.5	-	-	-	-
19.7	2622	1745	3466	3077
21.9	1370	1046	1666	1754
21.5	3240	2037	4445	3693
6.8	3030	2093	3925	3535
12.8	25152	17055	32982	30306
6.9	-	-	-	-
20.4	1695	1132	2234	1992
12.6	1617	1149	2053	1951
25.4	459	354	552	625
22.9	16992	13138	20453	20827
22.7	-	-	-	-
7.6	13005	9667	16117	25334
7.6	-	-	-	-
19.4	10039	6572	13454	11249
21.4	6946	4507	9394	7808
21.9	-	-	-	-
16.6	41149	26190	56294	47245
18.8	-	-	-	-

15.7	-	-	-	-
15.8	-	-	-	-
19.1	2783	2019	3475	3331
16.4	9006	6517	11362	17827
16.9	-	-	-	-
<b>14.6</b>	<b>1032907</b>	<b>810092</b>	<b>1238344</b>	<b>2146883</b>
19.2	63718	49507	76737	158987
16.8	-	-	-	-
19.7	-	-	-	-
17.6	-	-	-	-
13.2	240	170	306	524
14.2	866566	682014	1036734	1752666
15.4	-	-	-	-
12.8	-	-	-	-
15.8	-	-	-	-
13.8	-	-	-	-
12.1	-	-	-	-
12.3	-	-	-	-
11.6	-	-	-	-
14.4	-	-	-	-
12.6	-	-	-	-
11.5	-	-	-	-
12.7	-	-	-	-
12.3	-	-	-	-
12.5	-	-	-	-
12.5	-	-	-	-
10.5	-	-	-	-
15.9	-	-	-	-
11.5	-	-	-	-
12.3	15905	12615	19009	39195
10.9	-	-	-	-
14.5	86477	65786	105558	195510
12.7	-	-	-	-
15.7	-	-	-	-
16.6	-	-	-	-
<b>11.1</b>	<b>1418337</b>	<b>1075605</b>	<b>1738024</b>	<b>2049784</b>
11	1386689	1053525	1696981	1992762
9	-	-	-	-
12.2	-	-	-	-
15.9	-	-	-	-
9.6	-	-	-	-



10.5	-	-	-	-
11	-	-	-	-
11.7	-	-	-	-
14.3	-	-	-	-
13.1	-	-	-	-
13.8	-	-	-	-
11	-	-	-	-
9.6	-	-	-	-
12	-	-	-	-
10.6	-	-	-	-
11	-	-	-	-
8.9	-	-	-	-
10.5	-	-	-	-
7.4	-	-	-	-
12.1	-	-	-	-
10.8	-	-	-	-
10.4	-	-	-	-
13.7	-	-	-	-
10.2	-	-	-	-
9.3	-	-	-	-
10.6	-	-	-	-
10.1	-	-	-	-
10.7	-	-	-	-
12.1	-	-	-	-
10.8	-	-	-	-
11	-	-	-	-
10.5	-	-	-	-
11.4	-	-	-	-
8.5	-	-	-	-
10.4	-	-	-	-
12.8	20110	14907	25011	43106
16.6	11539	7172	16032	13916
<b>7.6</b>	<b>1381</b>	<b>631</b>	<b>2286</b>	<b>3812</b>
3.2	7	1	16	5
4.6	25	9	45	30
6.1	273	104	476	311
-	-	-	-	-
8.5	25	7	48	22
2.6	11	3	23	23
1.8	10	4	19	12
8	9	3	17	8

8	841	424	1330	2977
3.3	32	13	56	46
5.5	80	35	137	260
3.6	18	7	30	21
4.7	42	19	70	90
3.2	0	0	1	0
3.4	2	0	4	2
1.6	1	0	2	1
17.6	4	1	9	4
2.4	0	0	0	0
1.6	1	0	3	1
<b>13</b>	<b>230616</b>	<b>138209</b>	<b>332098</b>	<b>326462</b>
7.2	2975	1788	4291	7983
16.3	93807	54694	137546	119054
22.2	-	-	-	-
14.5	-	-	-	-
15.2	-	-	-	-
20.8	-	-	-	-
18.8	-	-	-	-
7.5	1087	631	1604	2831
23.6	9619	5179	14843	10569
22	-	-	-	-
29.2	-	-	-	-
11.1	37	16	64	37
9.8	574	293	879	595
8.9	21691	14555	28851	46930
9.6	-	-	-	-
12.9	29306	16666	43512	43218
12.7	-	-	-	-
13.8	-	-	-	-
14	-	-	-	-
12.4	6940	3979	10055	9675
8.2	33	18	52	37
11.4	29501	18954	40308	38193
12.4	-	-	-	-
11.7	183	100	283	386
9	34862	21336	49809	46955
7.8	-	-	-	-
8.4	-	-	-	-
<b>2.5</b>	<b>15279</b>	<b>10064</b>	<b>20591</b>	<b>53321</b>
3.3	3851	2425	5351	8764

4.3	-	-	-	-
2.7	738	508	967	4423
3.4	1367	932	1790	2589
2.2	8344	5536	11198	36180
3.5	-	-	-	-
1.6	-	-	-	-
3.7	288	201	371	439
3.3	691	462	913	927
<b>8.5</b>	<b>31529</b>	<b>20012</b>	<b>43791</b>	<b>131540</b>
4.7	731	480	989	4539
6.3	75	41	116	205
16	343	239	445	592
14.2	1078	747	1403	3668
11.3	6473	4239	8765	33633
11.9	-	-	-	-
13.4	5029	3101	7115	12872
15.7	-	-	-	-
6	1768	1006	2664	6616
3.5	1070	644	1539	4842
5.3	1506	906	2175	8492
5.5	-	-	-	-
5.6	1325	890	1762	4827
6	-	-	-	-
7.9	583	365	817	9549
5.5	1084	712	1469	4609
5.9	4856	2961	6929	18021
10.2	-	-	-	-
7.8	3430	2317	4545	13648
9.9	-	-	-	-
2.7	2179	1363	3058	5427
2	-	-	-	-
<b>9.2</b>	<b>29840</b>	<b>18964</b>	<b>40735</b>	<b>45500</b>
9	803	492	1125	1213
10.5	781	506	1056	1800
4.4	697	429	979	1128
10	25035	16073	33892	34898
12.4	-	-	-	-
10.1	-	-	-	-
7.6	303	182	427	561
6.3	2221	1282	3256	5900
<b>3.4</b>	<b>94736</b>	<b>68733</b>	<b>119976</b>	<b>320839</b>

5.3	1686	1158	2216	7039
2.4	2666	1855	3479	16949
3.3	7777	5708	9754	19088
1.4	244	175	310	393
3.2	1979	1396	2567	13333
3.7	4970	3553	6359	16003
1.9	407	302	508	1538
4.7	10734	7908	13427	22565
5.3	-	-	-	-
2.1	2084	1468	2698	11118
1.9	291	213	365	1400
3.1	506	360	646	2170
1.7	2176	1574	2769	14124
1.8	-	-	-	-
1	1117	835	1382	2501
1.9	2232	1632	2812	19482
3.8	50577	36761	63987	152639
6.2	-	-	-	-
6.1	-	-	-	-
3.1	-	-	-	-
6.3	-	-	-	-
2.7	45	29	61	98
1.6	2732	2034	3391	9924
2.6	1236	868	1601	6034
5	1278	903	1644	4440
<b>13.2</b>	<b>3832670</b>	<b>2715393</b>	<b>4972016</b>	<b>6222380</b>

### Data File 3: PM<sub>2.5</sub> Exposure Estimates for the year 2019

McDuffie et al., 2021 -

Last Updated: March 23, 2021

Name Legend:

**Regions** Countries *Sub-national regions*

---

Name	2019 Population Weighted Annual Average PM <sub>2.5</sub> (µg m <sup>-3</sup> )
<b>Central_Asia</b>	<b>24.5</b>
Armenia	30.7
Azerbaijan	24.3
<i>Baku</i>	<i>34.2</i>
Georgia	17.6
Kazakhstan	19.2
<i>Shymkent</i>	<i>37.8</i>
Kyrgyzstan	22.7
Mongolia	39
<i>Ulaanbaatar</i>	<i>86.2</i>
Tajikistan	35.6
Turkmenistan	24.6
Uzbekistan	32.3
<i>Bukhara</i>	<i>26</i>
<i>Tashkent</i>	<i>50</i>
<b>Central_Europe</b>	<b>20.2</b>
Albania	19.2
Bosnia_and_Herzegovina	29.3
Bulgaria	19.4
Croatia	18.1
Czech_Republic	16.8
Hungary	16.5
<i>Budapest</i>	<i>19.6</i>
Macedonia	30.3
Montenegro	20.9
Poland	22.6
<i>Warsaw</i>	<i>23.8</i>
Romania	15.8
Serbia	25.2
<i>Belgrade</i>	<i>24.3</i>
Slovakia	18.5
Slovenia	17.2
<b>Eastern_Europe</b>	<b>11.9</b>
Belarus	16.3

<i>Gomel</i>	20
Estonia	5.9
Latvia	11.9
Lithuania	10.3
<i>Kaunas</i>	12.1
Moldova	13.5
Russian_Federation	11
<i>Saint_Petersburg</i>	8.2
<i>Astrakhan</i>	12
<i>Moscow</i>	13.5
<i>Tyumen</i>	13.8
<i>Berezniki</i>	13.4
<i>Dzerzhinsk</i>	11.6
Ukraine	14
<i>Nikolaev</i>	14.7
<i>Rovno</i>	20.1
<b>Australasia</b>	<b>6.8</b>
Australia	6.9
<i>Sydney</i>	7.6
New_Zealand	6.6
<i>Auckland</i>	6.4
<b>High_income_Asia_Pacific</b>	<b>17.4</b>
Brunei	7.8
Japan	13.4
<i>Tokyo</i>	15
<i>Osaka</i>	15
<i>Fukuoka</i>	17.7
<i>Okayama</i>	13.1
<i>Yamaguchi</i>	12.9
South_Korea	27.2
<i>Seoul</i>	28.1
<i>Busan</i>	24.8
<i>Cheonan</i>	29.4
<i>Gwangju</i>	27.7
<i>Jinju</i>	28.4
<i>Pyongyang</i>	55.8
Singapore	18.7
<b>High_income_North_America</b>	<b>7.7</b>
Canada	7.1
<i>Montreal</i>	8.8
<i>Victoria</i>	5.9
Greenland	5.2
United_States	7.7

<i>Raleigh</i>	7.7
<i>New_York</i>	7.7
<i>Philadelphia</i>	8.4
<i>Houston</i>	9.7
<i>Minneapolis</i>	7.3
<i>Portland</i>	7.3
<i>Los_Angeles</i>	10.2
<i>Cleveland</i>	8.7
<i>Chicago</i>	9.2
<i>Springfield</i>	6.4
<i>Gainesville</i>	6.6
<i>Killeen</i>	7.3
<i>Modesto</i>	12
<b>Southern_Latin_America</b>	<b>15.5</b>
<i>Argentina</i>	12.9
<i>Buenos_Aires</i>	11.5
<i>Cordoba</i>	14.2
<i>Chile</i>	22.7
<i>Santiago</i>	30.2
<i>Uruguay</i>	9.7
<b>Western_Europe</b>	<b>11.6</b>
<i>Andorra</i>	8.7
<i>Austria</i>	12.3
<i>Vienna</i>	14.5
<i>Belgium</i>	12.7
<i>Antwerp</i>	13.9
<i>Cyprus</i>	15.6
<i>Denmark</i>	9.7
<i>Finland</i>	5.5
<i>France</i>	11.6
<i>Paris</i>	13.7
<i>Le_Mans</i>	13.5
<i>Germany</i>	11.8
<i>Berlin</i>	15.5
<i>Halle</i>	14.6
<i>Oldenburg</i>	12.7
<i>Greece</i>	14.3
<i>Thessaloniki</i>	15.2
<i>Iceland</i>	5.6
<i>Ireland</i>	7.9
<i>Israel</i>	19.3
<i>Tel_Aviv</i>	21.1
<i>Italy</i>	15.6

<i>Palermo</i>	15.1
<i>Milan</i>	23.1
Luxembourg	10.2
Malta	12.9
Netherlands	12
<i>Zwolle</i>	11.3
Norway	6.5
Portugal	8.4
Spain	9.9
<i>Madrid</i>	10.3
<i>Toledo</i>	8.9
Sweden	5.7
Switzerland	10.2
<i>Lausanne</i>	12.3
United_Kingdom	10.2
<i>Sheffield</i>	11.4
<i>London</i>	12.4
<i>Manchester</i>	10.9
Monaco	11.6
San_Marino	9.9
<b>Andean_Latin_America</b>	<b>26.3</b>
Bolivia	25.7
<i>Cochabamba</i>	26
Ecuador	19.6
<i>Quito</i>	18.4
Peru	30.1
<b>Caribbean</b>	<b>16.3</b>
Antigua_and_Barbuda	16.5
The_Bahamas	14.1
Barbados	20.1
Belize	19.5
Bermuda	6.9
Cuba	16.8
<i>Holguin</i>	15.7
Dominica	17.3
Dominican_Republic	16.8
Grenada	19.9
Guyana	18.9
Haiti	17.6
Jamaica	15
Puerto_Rico	7.1
Saint_Lucia	19.9
Saint_Vincent_and_the_Gren	19.8



Suriname	19.9
Trinidad_and_Tobago	20.1
Virgin_Islands_US	8.9
Saint_Kitts_and_Nevis	8.6
<b>Central_Latin_America</b>	<b>20.6</b>
Colombia	21.3
<i>Bogota</i>	29.6
<i>Valledupar</i>	22.7
Costa_Rica	17.2
El_Salvador	21.7
<i>San_Salvador</i>	21.9
Guatemala	27.1
<i>Guatemala_City</i>	32.8
Honduras	22.5
Mexico	19.8
<i>Culiacan</i>	18.2
<i>Guadalajara</i>	18.9
<i>Mexico_City</i>	24.1
<i>Reynosa</i>	19.5
<i>Tijuana</i>	18
Nicaragua	19.8
<i>Leon</i>	20
Panama	13
Venezuela	20.5
<i>Caracas</i>	19.8
<i>Cabimas</i>	22.3
<b>Tropical_Latin_America</b>	<b>11.8</b>
Brazil	11.7
<i>Sao_Paulo</i>	15.3
<i>Curitiba</i>	9.1
<i>Florianopolis</i>	13.3
<i>Belo_Horizonte</i>	13.3
<i>Palmas</i>	10.1
<i>Ilheus</i>	14.1
<i>Jequie</i>	14.4
<i>Ribeirao_Preto</i>	14.1
Paraguay	12.5
<b>North_Africa_and_Middle_E:</b>	<b>43.9</b>
Afghanistan	49.9
<i>Kabul</i>	62.6
Algeria	31.9
<i>Algiers</i>	33.9
<i>Tebessa</i>	34.8

Bahrain	58.4
Egypt	66.6
<i>Cairo</i>	<i>81.9</i>
<i>Alexandria</i>	<i>57.3</i>
Iran	37.4
<i>Tehran</i>	<i>35.1</i>
<i>Ahvaz</i>	<i>70.6</i>
<i>Gorgan</i>	<i>36.9</i>
<i>Qom</i>	<i>40.7</i>
Iraq	47.1
<i>Baghdad</i>	<i>57.4</i>
Jordan	30.3
Kuwait	60.7
Lebanon	28.3
Libya	36.9
Morocco	35.2
<i>Marrakesh</i>	<i>49.4</i>
Palestine	31.6
Oman	43
Qatar	67.8
Saudi_Arabia	59.3
<i>Riyadh</i>	<i>64.3</i>
Sudan	51
<i>Khartoum</i>	<i>63.4</i>
Syria	30.7
Tunisia	29.9
<i>Kairouan</i>	<i>34.7</i>
Turkey	25.9
<i>Istanbul</i>	<i>26.4</i>
<i>Malatya</i>	<i>29.1</i>
<i>Kayseri</i>	<i>32.1</i>
United_Arab_Emirates	42.5
Yemen	42.4
<i>Sana</i>	<i>42.3</i>
<b>South_Asia</b>	<b>77.3</b>
Bangladesh	62.6
<i>Rajshahi</i>	<i>54.5</i>
<i>Dhaka</i>	<i>69.1</i>
<i>Saidpur</i>	<i>66.4</i>
Bhutan	38.9
India	81.6
<i>Jaipur</i>	<i>102.4</i>
<i>Ahmedabad</i>	<i>134</i>

<i>Kanpur</i>	154.1
<i>Kolkata</i>	87
<i>Mumbai</i>	60
<i>Pune</i>	63.2
<i>Hyderabad</i>	50
<i>Belgaum</i>	46.1
<i>Coimbatore</i>	43
<i>Hindupur</i>	41.4
<i>Jalna</i>	55.3
<i>Kozhikode</i>	34.9
<i>Malegaon</i>	56.6
<i>Parbhani</i>	42.2
<i>Singrauli</i>	157.5
<i>Sitapur</i>	137.7
<i>Vijayawada</i>	56.8
<i>Nepal</i>	81.4
<i>Pokhara</i>	72.2
<i>Pakistan</i>	60.5
<i>Karachi</i>	70.9
<i>Lahore</i>	74.4
<i>Sialkot</i>	66.9
<b>East_Asia</b>	<b>47.1</b>
<i>China</i>	47.6
<i>Chengdu</i>	61.4
<i>Qingdao</i>	44
<i>Taipei</i>	20.8
<i>Shanghai</i>	44.9
<i>Wuhan</i>	61.4
<i>Hangzhou</i>	51.8
<i>Guangzhou</i>	38.1
<i>Beijing</i>	71.4
<i>Tangshan</i>	74.6
<i>Tianjin</i>	71.8
<i>Jinan</i>	67.9
<i>Zhengzhou</i>	75.2
<i>Hong_Kong</i>	23
<i>Anqing</i>	50.6
<i>Bicheng</i>	50.6
<i>Changzhi</i>	64.2
<i>Changzhou</i>	51.8
<i>Chengguan</i>	34.9
<i>Gaoyou</i>	50.9
<i>Guixi</i>	44.9

<i>Haikou</i>	21.7
<i>Kaiping</i>	37.8
<i>Leshan</i>	54.3
<i>Pingxiang</i>	51.3
<i>Shenzhen</i>	31.4
<i>Suining</i>	49.8
<i>Xingping</i>	60.1
<i>Xucheng</i>	51.5
<i>Yanggu</i>	70
<i>Yiyang</i>	47.1
<i>Yucheng</i>	33.4
<i>Zhuji</i>	47.2
<i>Zunyi</i>	43.5
<i>Yulin</i>	38.8
North_Korea	43.3
Taiwan	23.9
<b>Oceania</b>	<b>12.9</b>
American_Samoa	6.1
Federated_States_of_Micron	9.2
Fiji	9.7
<i>Suva</i>	-
Guam	8.1
Kiribati	7.5
Marshall_Islands	8.5
Northern_Mariana_Islands	8.1
Papua_New_Guinea	13.5
Samoa	9.7
Solomon_Islands	11.1
Tonga	9.5
Vanuatu	11.1
Niue	6.5
Cook_Islands	6.1
Nauru	5.6
Palau	6.6
Tokelau	7
Tuvalu	5.7
<b>Southeast_Asia</b>	<b>20.5</b>
Cambodia	21.3
Indonesia	18.7
<i>Medan</i>	33.2
<i>Palembang</i>	27.1
<i>Cirebon</i>	23
<i>Parepare</i>	15

<i>Pematangsiantar</i>	23.7
Laos	19.7
Malaysia	16.3
<i>Ipoh</i>	17
<i>Rawang</i>	17.5
Maldives	9.6
Mauritius	14.8
Myanmar	28.8
<i>Myeik</i>	23.5
Philippines	18.6
<i>Manila</i>	28.5
<i>Bacolod</i>	19.9
<i>Cebu_City</i>	21.2
Sri_Lanka	19.6
Seychelles	15
Thailand	26.9
<i>Bangkok</i>	30.2
Timor_Leste	15.2
Vietnam	20
<i>Vinh_Long</i>	23.7
<i>Ho_Chi_Minh_City</i>	27
<b>Central_Sub_Saharan_Africa</b>	<b>32.6</b>
Angola	27.4
<i>Luanda</i>	31.9
Central_African_Republic	43
Congo	36
Democratic_Republic_of_the_	33.3
<i>Kinshasa</i>	38.7
<i>Lubumbashi</i>	27.6
Equatorial_Guinea	43.6
Gabon	34.5
<b>Eastern_Sub_Saharan_Africa</b>	<b>27.4</b>
Burundi	32
Comoros	16.5
Djibouti	40.8
Eritrea	41.8
Ethiopia	32.5
<i>Addis_Ababa</i>	31.9
Kenya	21.1
<i>Nakuru</i>	20.1
Madagascar	17.3
Malawi	21.6
Mozambique	20.1

<i>Beira</i>	24.1
Rwanda	34.4
<i>Kigali</i>	35.2
Somalia	29
South_Sudan	35.4
Tanzania	24
<i>Arusha</i>	19.9
Uganda	33.6
<i>Kampala</i>	42
Zambia	24.7
<i>Ndola</i>	26.1
<b>Southern_Sub_Saharan_Afric</b>	<b>26.4</b>
Botswana	24.1
Lesotho	27.2
Namibia	23.4
South_Africa	28.6
<i>Port_Elizabeth</i>	23.9
<i>Johannesburg</i>	40.2
Eswatini	23
Zimbabwe	20.1
<b>Western_Sub_Saharan_Afric</b>	<b>59.9</b>
Benin	44
Burkina_Faso	50.6
Cameroon	61
Cape_Verde	45.2
Chad	55.1
Cote_dIvoire	52.5
The_Gambia	55.6
Ghana	52.2
<i>Accra</i>	61.7
Guinea	49.5
Guinea_Bissau	51.6
Liberia	48.6
Mali	55.7
<i>Bamako</i>	55.3
Mauritania	61.8
Niger	72.5
Nigeria	65.3
<i>Ibadan</i>	42.1
<i>Lagos</i>	35.7
<i>Gombe</i>	78.5
<i>Oyo</i>	45.2
Sao_Tome_and_Principe	30.5

Senegal	57.5
Sierra_Leone	49
Togo	44.1
<b>Global</b>	<b>41.7</b>